DESIGN, SYNTHESES AND BIOLOGICAL APPLICATIONS OF THROUGH-BOND ENERGY TRANSFER CASSETTES AND NOVEL NON-COVALENTLY CELL PENETRATING PEPTIDES

A Dissertation

by

JUNYAN HAN

Submitted to the Office of Graduate Studies of
Texas A&M University
in partial fulfillment of the requirements for the degree of

DOCTOR OF PHILOSOPHY

August 2009

Major Subject: Chemistry

DESIGN, SYNTHESES AND BIOLOGICAL APPLICATIONS OF THROUGH-BOND ENERGY TRANSFER CASSETTES AND NOVEL NON-COVALENTLY CELL PENETRATING PEPTIDES

A Dissertation

by

JUNYAN HAN

Submitted to the Office of Graduate Studies of
Texas A&M University
in partial fulfillment of the requirements for the degree of

DOCTOR OF PHILOSOPHY

Approved by:

Chair of Committee,	Kevin Burgess
Committee Members,	Jean-Philippe Pellois
	Daniel Romo
	Daniel Singleton
Head of Department,	David Russell

August 2009

Major Subject: Chemistry

ABSTRACT

Design, Syntheses and Biological Applications of Through-bond Energy Transfer Cassettes and Novel Non-covalently Cell Penetrating Peptides. (August 2009)

Junyan Han, B.S., Shandong University, P. R. China

Chair of Advisory Committee: Dr. Kevin Burgess

A xanthene-BODIPY cassette is used as a ratiometric intracellular pH reporter for imaging protein-dye conjugates in living cells. A model was hypothesized to explain the pH-dependent energy transfer efficiencies from the donor to the acceptor based on the electronic chemistry data.

Sulfonation conditions were developed for BODIPY dyes to give water-soluble functionalized monosulfonation and disulfonation donors. A water-soluble TBET cassette, which has good photophysical properties, was synthesized using a bissulfonated BODIPY dye as the donor, and their applications for *in vitro* protein labeling is achieved. Chemoselective cross-coupling reactions were demonstrated for *C-S* bonds in the BODIPY dye, and similar reactions were applied to make the acceptor of the water-soluble cassette.

Chemiluminescent energy transfer cassettes based on fluorescein and Nile Red were synthesized and their spectral properties were studied.

Pep-1 (also known as Chariot), R_8 (which is not often used as a non-covalent protein carrier), and a new synthesized compound, Azo-R_8, was used for the study of

non-covalent delivery of four different proteins into mammalian cells. Data from confocal spectroscopy revealed that all three carriers are effective for translocating protein cargos into live cells. At 37^{o}C, import into endocytic compartments dominates, but at 4°C weak, diffuse fluorescence is observed in the cytosol indicative of a favorable mode of action.

DEDICATION

To my wife, Guangqing Shan, my two sons, Daniel P. Han, and Gabriel P. Han

ACKNOWLEDGEMENTS

I would like to thank my committee chair, Dr. Kevin Burgess, my former advisor Dr. Gary Sulikowski, and my committee members, Dr. Daniel Romo, Dr. Daniel Singleton, Dr. Jean Philippe Pellois, and Dr. Jianrong Li, for their guidance and support throughout the course of this research and my graduate study.

Thanks to Ms. Jill Rutlegde, Ms. Jade Kennedy, and Ms. Angie Medina for their assistance throughout all these years.

Thanks to everyone in the Burgess group, especially the dyes group.

Thanks also go to my friends and colleagues and the department faculty and staff for making my time at Texas A&M University a great experience. I also especially want to thank Mr. Cliferson Thivierge and Dr. Aurore Loudet for their great encouragement and helpful discussions in my research.

Finally, thanks to my wife and my two sons, and my two sisters for their love, patience, and help.

TABLE OF CONTENTS

CHAPTER Page

LIST OF FIGURES

Page

Page

Page

Page

LIST OF TABLES

LIST OF SCHEMES

CHAPTER I

INTRODUCTION: THE IMPORTANCE AND CHALLENGES OF THE RESEARCH

My research focuses on the synthesis and biological applications of through-bond energy transfer cassettes. Intramolecular energy transfers have been studied using molecules containing two fluophores, i.e. D-A. When the donor (D) is brought to an excited state, emission is observed from the acceptor (A) portion of the molecule. The energy can be transferred via non-conjugated linkers (through-space), or a π-conjugated system (through-bond).

The efficiency of energy transfer through space, fluorescence resonance energy transfer (FRET), is dependent on the overlap of donor emission with the absorption of the acceptor. The smaller the overlap, the less efficient the energy transfer. However, there is no known requirement for Förster rule for through-bond energy transfer (TBET). This process seems to involve the physical contact of orbital of the donor and acceptor. Our group has proved that efficient energy transfer through bonds does not require the overlap of donor emission with acceptor absorbance. Therefore, TBET cassttes could process desired photophysical properties for cell imaging, e.g. large Stoke shifts, long-wavelength excitation and emission wavelengths. Our group focuses on the synthesis and biological applications of through-bond energy transfer cassettes. We are particularly interested in applying TBET cassettes for studying multiple proteins' interaction in vivo,

---

The dissertation follows the style of *Journal of American Chemical Society.*

determination of intracellular pH values, and detection of H_2O_2 in living cells. In order to study the protein interaction in water, we have to synthsize water-soluble TBET cassettes, which should have high quantum yields and a handle to attach to proteins. Please read the chapter II to chapter IV for detailed description of the study. I hope I will convince you that how useful the TBET cassettes in biological chemistry after knowing the advantages of TBET cassettes compared to regular dyes.

There are many exhisting methods for uptaking proteins into living cells, e.g. microinjection, electroporation. Conjugation of proteins to carrier peptides is also another commonly used method. The well-known carriers of this type are TAT and polyarginine derivatives. These to methods are either disruptive to cells or time consuming. We are interested in non-covalent proteins carries, which can translocate proteins in life cells relatively easy and noninvasive. The Pep-1, also called carrier peptide, is commercialized and widely used. However, it is very expensive and not easy to synthesize in large scale since it involved solid-state prepation. We are interested in developing novel non-covalent protein carriers for transferring cassette-labeled protein inside living cells. Please see the chapter V for the details of our discovery in this area.

CHAPTER II

AN RATIOMETRIC PH INDICATOR FOR IMAGING PROTEIN-DYE CONJUGATES IN LIVING CELLS BASED ON THROUGH-BOND ENERGY TRANSFER

A. INTRODUCTION: INTRACELLULAR PH INDICATORS

1. Introduction

Intracellular pH (pH_i) can influence many critical cell, enzyme and tissue activities, including apoptosis,[1-3] proliferation, multidrug resistance (MDR),[4] ion transport,[5,6] endocytosis,[3] and muscle contraction.[7,8] Changes of pH_i effect the nervous system too, by influencing synaptic transmission, neuronal excitability, cell-cell coupling via gap junctions, and signal cascades.[9,10] Abnormal pH_i values are associated with inappropriate cell function, growth, and division, and are observed in some common disease types such as cancer[11] and Alzheimer's.[12] Some organelles, *e.g.* endosomes[13] and plant vacuoles,[14] have intracompartmental pHs of 4 - 6. In cell biology, low intracompartmental pH values can serve to denature proteins, or to activate enzyme and protein functions that would be too slow around pH 7.0. For instance, the acidic environments in lysosomes (4.5 – 5.5)[15,16] can facilitate the degradation of proteins in cellular metabolism. Thus, cellular dysfunction is often associated with abnormal pH values in organelles.[13]

Intimate connections between the cell functions with intracellular pH means that precise measurement of intracellular pH can provide critical information for studying physiological and pathological processes down to a single organelle. Good resolution in the space and time dimensions, ie spatial and temporal, is highly desirable. Compared to other pH_i measurement methods (*e.g.* microelectrodes, NMR, and absorbance spectroscopy) fluorescence spectroscopy has advantages with respect to spatial and temporal observation of pH_i changes. Moreover fluorescence techniques have high sensitivities, they tend to be operationally simple, and they are in most cases non-destructive to cells.

Qualitative measurements of pH_i can be achieved using fluorescent indicators that switch on or off at sharply defined pH values. However, such measurements may be influenced by many factors, including optical pathlength, changes of temperature, altered excitation intensities, and varied emission collection efficiencies. The alternative is to use "ratiometric detection".

Ratiometric spectroscopic methods require fluorescent sensors that are differentially sensitive to the analyte (ie protons for pH probes) for at least two excitation or emission wavelengths (see Figure 2.1). For instance, for a suitable fluorescent dye, emission at one carefully chosen wavelength may be enhanced or diminished relative to the emission at another. Ratios between these signals then can be calibrated to indicate pH_i values. Advantages in using ratiometric methods are accrued because parameters such as optical pathlength, local probe concentration,

photobleaching, and leakage from the cells are irrelevant. This must be so since both signals come from the probe in exactly the same environment.

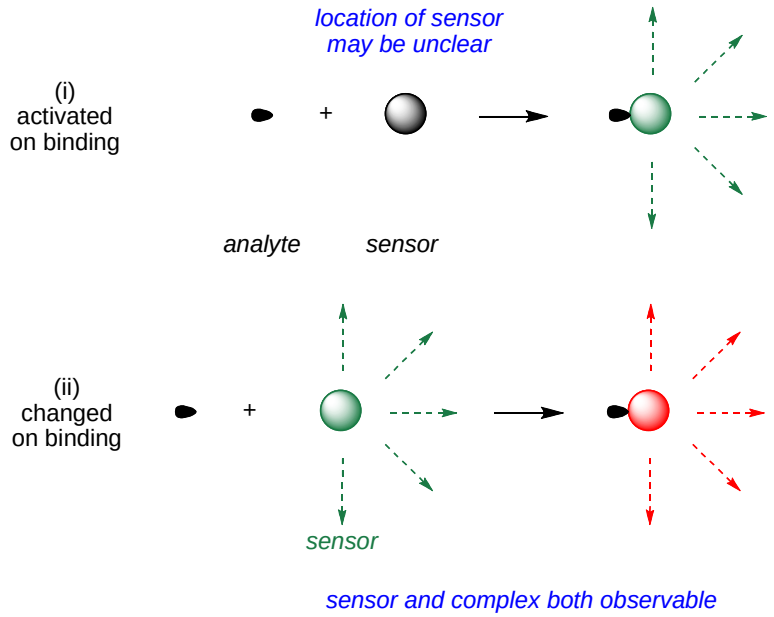

Figure 2.1 Fluorescent sensors may be activated (i) by analytes; Ratiometric ones (ii) which change wavelength of fluorescence emissions on binding.

A variety of methods can be used for importing highly charged fluorescent compounds into cells. These include microinjection,[17] scrape loading,[18] hypertonic lysis,[19] and carrier-mediated endocytosis.[20] All of these approaches perturb the cell resting state physiology.

Another strategy for import of fluorescent compounds into cells uses concepts similar to the "prodrug approach".[21] This strategy involves chemical modification of charged, non-cell-permeable dyes outside cells to neutral cell-permeable ones after import. Thus transport of masked forms into the cell allows endogenous cellular proteases to liberate the charged fluorescent form of these compounds. The archetypical

example of this is the use of non-fluorescent acetoxylmethyl (AM) or acetate esters of fluoresceins as pH_i indicators. These compounds diffuse into cells, and are then hydrolyzed by non-selective intracellular esterases to afford the free, charged, fluorescent dyes (Figure 2.2). In fact, conversion of non-fluorescent AM esters into fluorescent free dyes has been used for cell viability assays.[1] Application of this approach is probably less disruptive to the cells than the methods mentioned above, but it is not totally innocuous. Hydrolysis of AM esters yields acetic acid and methanol; both these by-products may induce abnormal cellular events. Moreover, the fluorescent dyes can localize in any cellular compartment, and in this approach the fluorescent compounds may particularly tend to accumulate in organelles having high concentrations of esterases. The AM ester and the liberated dye also may be cytotoxic to some extent. Nevertheless, these undesirable effects may be tolerable fro many applications.

AM esters are typically synthesized via the same strategy. This features reaction of hydroxyl and/or carboxylic acid groups on the free dye with freshly prepared bromomethyl acetate[22] in the presence of diisopropylethylamine in anhydrous chloroform (Figure 2.2).[23,24]

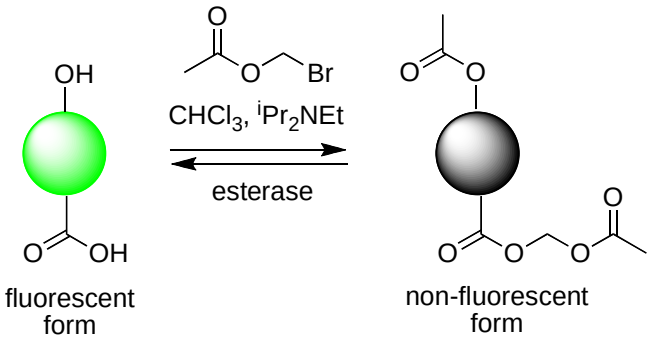

Figure 2.2 Synthesis and hydrolysis of AM and acetate esters.

Fluorescence intensities of the free pH indicators inside cells are reduced if the fluorescent molecules are somehow expelled from the cells. Rates of dye leakage from cells are related to the net charge on the dyes; more highly charged ones are expelled slower. For instance, fluorescein has a higher leakage rate relative to 5-(and 6)-carboxyfluorescein because the former has one less negative charge.[25] Dye-dextran (a complex, branched polyglucose with varying lengths from 10 to 150 kilodaltons), -biomolecule or -nanoparticle conjugates can circumvent the leakage problem because passage of the dyes from the inside to the outside of the cells is unfavorable, and the concentration decreases only due to cell division. Cells labled with pH indicator BCECF on dextran have been shown to produce much more stable fluorescent signals, reduced probe compartmentalization, and 10-fold greater resistance to light-induced damage when compared with dye AM–labeled cells.[26] Overall, pH indicators that are coupled to carrier molecules that do not cross the cell membrane may be particularly useful for long-term experiments where retention of the probe in cells is an issue.

Interactions of probes with biomolecules or organelles in cells can significantly change their spectral properties relative to aqueous saline solutions.[27,28] Consequently,

ex-vivo, calibration is required for more accurate pH_i measurements. Thomas et al in 1979 introduced the method that is most widely used for pH_i calibration.[29] In this approach, intracellular pH is assumed to be equal to extracellular pH when the cells are treated with the K^+/H^+ ionophore, nigericin (5μL/ml). Nigericin makes cells permeable to K^+ and H^+, thus equilibrating the intra and extracellular pH.

This review provides a brief overview of intracellular pH sensors, including small fluorescent organic molecules, nanoparticles, and fluorescent proteins *e.g.* GFP. It focuses on their preparations, photophysical properties, and advantages/disadvantages for intracellular pH measurements. The discussion is limited to fluorescent indicators that have been applied to measure intracellular pH values since 1970's; relatively few indictors were used to measure intracellular pH values before that date, and those that were are now largely redundant. [30]

2. Fluorescein-based pH_i Indicators

2.1 The Most Widely Used pH_i Indicator: BCECF

2',7'-bis-(2-Carboxyethyl)-5-(and-6-)carboxyfluorescein (BCECF; Figure 2) was introduced for measuring cytoplasmic pH by Roger Tsien and his coworkers in 1982.[25] Since then it has been widely used for mammalian or plant cells,[5,6] living tissues[31] and individual organelles, *e.g.* endoplasmic reticulum.[32]

BCECF is synthesized via condensation of ethyl 3-(2,4-dihydroxyphenyl)-propionate (from hydrogenation of commercially available 7-hydroxycoumarin in ethanol containing catalytic amount of trifluoroacetic anhydride) with trimellitic

anhydride in the presence of anhydrous $ZnCl_2$ at 180 ^oC (Scheme 2.1). The commercially available acetoxymethyl ester of BCECF is a mixture of three compounds BCECF AM I-III (Figure 2.3). Three regioisomeric BCECF AM esters could all be transformed into the free BCECF by nonselective esterase inside living cells.

Scheme 2.1 Synthesis of BCECF. TFAA: trifluoroacetic anhydride

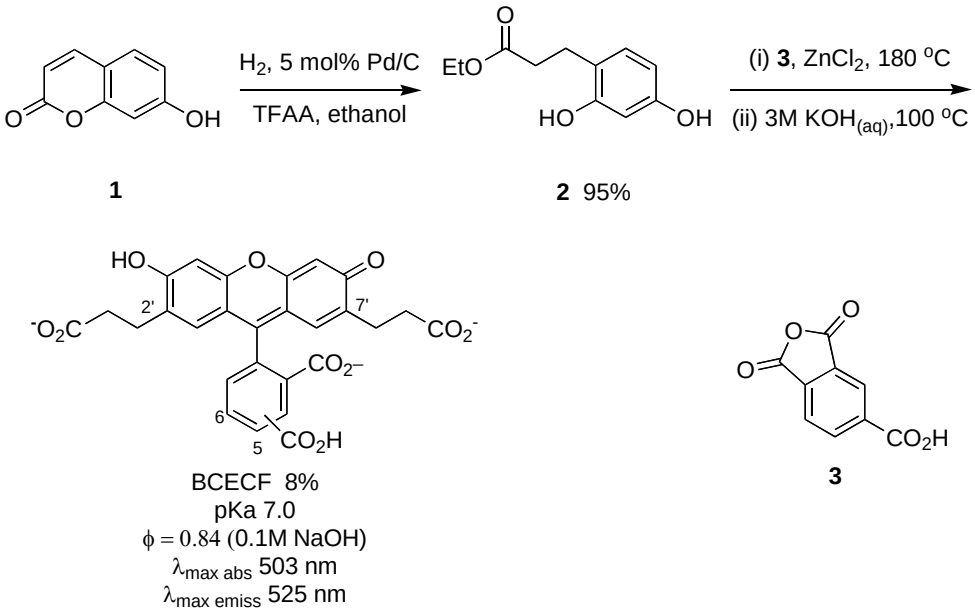

Just like fluorescein, carboxyfluorescein and fluorescein sulfonic acid, the absorbance of BCECF is sensitive to the pH. Absorption of BCECF red-shifts from pH 3.6 to 9.2, and its molar absorptivity is much larger in the phenolate anion form than in the phenolic form.[33] However, indicators based on fluorescence are far more sensitive than those that use absorption.

BCECF is often used as a ratiometric excitation (or dual excitation) pH indicator. In this approach fluorescence intensity ratios corresponding to excitation at two different

wavelengths are measured, and these data are correlated to pH via ex vivo calibration using Thomas's method.[29] The physical basis of this method is that the absorption profile for the dye changes significantly with pH.

An alternative to ratiometric excitation for pH measurements is the ratiometric emission method. This strategy involves measuring fluorescence intensities at two different wavelengths when the indicator is excited at one wavelength. BCECF is unsuitable for this approach since its relative emissions at any two different wavelengths are not significantly dependant on pH. An example of a dye that can be used in this mode is carboxy.SNARF, i.e. C.SNARF-1 (See below).

BCECF is widely applied in cell biology because of several attributes. First, the free dye is retained well inside cells because it posses 4-5 negative charges at physiological pH values (~7.4). Second, the pKa of BCECF (7.0) is ideal for sensing cytosolic pHs, which are normally in the range of 6.8 - 7.4. Third, BCECF AM esters are cell membrane permeable and this facilitates non-invasive loading of the dye into cells. Conversion of non-fluorescent BCECF AM esters into fluorescent BCECF acid forms is efficient, so much so that this transformation has been used for cell viability assays.[1] Fourth, ionic strengths of solutions surrounding BCECF do not have much influence on the spectral properties of the dye.[25]

There are also some problems associated with BCECF in measurements of pH_i values. For instance, even though the rate of leakage of this dye form cells is relatively slow, it can still be ca 10% over 10 - 20 min at 25 °C, and more at 37 °C.[25] To circumvent this issue, the BCECF-dextran conjugate might be used; this exhibits

excellent intracellular retention and much lower cytotoxicity effects, but it is not cell membrane permeable and has to be delivered into cells via relatively destructive techniques, *e.g.* microjection. Another disadvantage of BCECF is that it, like most fluorescein-based dyes, photobleaches relatively quickly hence erroneous pH_i measurements can result.[31] Simultaneously, such photobleaching reactions can damage cells. Free BCECF inside cells does not usually accumulate in any particular cellular compartment.

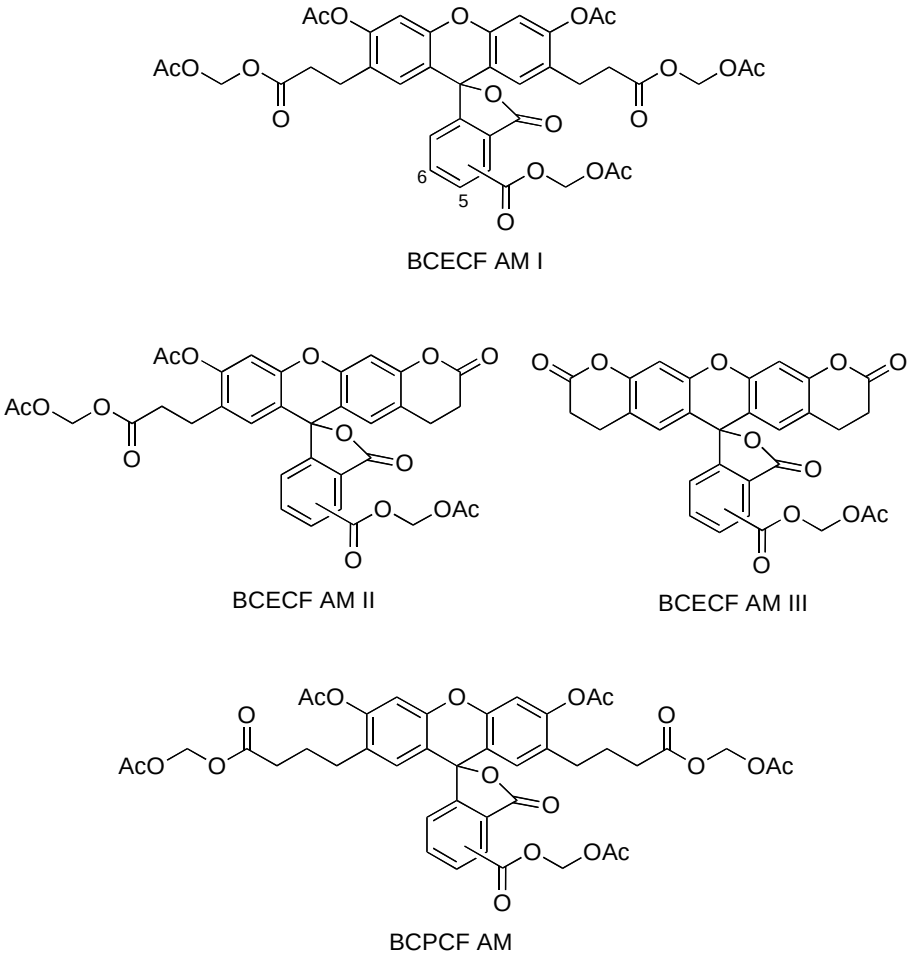

Figure 2.3. Structures of BCECF/BCPCF AM esters

2.2 BCPCF

BCPCF (structure in Scheme 2), 2',7'-bis-(2-carboxypropyl)-5-(and-6-)-carboxyfluorescein, is a homolog of BCECF. BCPCF has 2-carboxypropyl substituents at 2'- and 7'-xanthene positions whereas BCECF has 2-carboxyethyl groups there. The original synthesis of BCPCF is shown in Scheme 2. In this, 1,3-dimethoxybenzene is subjected to Friedel-Crafts acylation with succinic anhydride, followed by in situ demethylation and Fisher esterification to yield the ketone ester **4** in 40 % yield. The ketone group of the **4** was reduced to **6** which has a chain of three methylene groups. Condensation of this resorcinol derivative 6 with trimetallic acid anhydride **3** in methanesulfonic acid eventually gives BCPCF as a mixture of two regioisomers. In fact, the intermediate acid is esterified solely to facilitate chromatographic separation, then this ester is converted back to the carboxylic acid form.

Scheme 2.2. Synthesis of BCPCF.

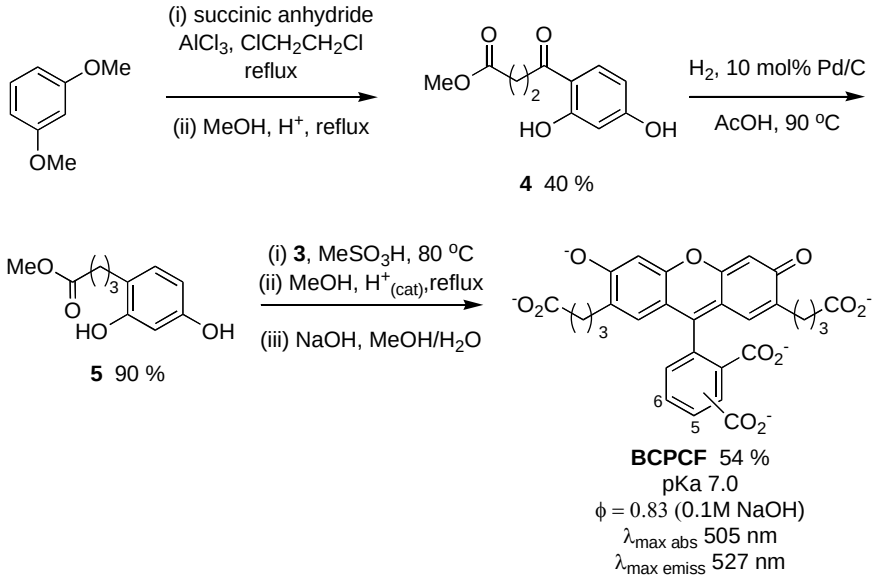

Commercial available BCPCF AM esters predominantly exists in a form shown in Figure 2.3. BCECF and BCPCF have very similar pKa values, absorption and emission maximum wavelengths, and quantum yields, just as expected for such structurally similar compounds. The previous section notes that ratiometric excitation pH_i measurements featuring BCECF are usually achieved by determination fluorescence intensity ratios at 535 nm corresponding to excitation at 503 nm and at 439 nm. The absorbance of BCECF at 439 nm corresponds to its isobestic point; this is generally ideal for ratiometric methods except that in this case the absorptivity of BCECF at 439 nm is quite weak. Application of BCPCF overcomes this disadvantage of BCECF. The isosbestic point of BCPCF is red-shifted to 454 nm compared with BCECF; this corresponds to a stronger absorbance hence BCPCF tends to be a better ratiometric excitation probe.

BCECF and BCPCF share a common disadvantage for pH_i measurements. Their fluorescence emission intensities are dependant on the concentration of the probes. Thus if the dyes accumulate in certain regions of the cell then they can indicate different pH_i values indicative of dye, not proton, concentration differences.[33,34]

2.3 Fluorescein, Carboxyfluorescein and Fluorescein Sulfonic Acid

BCECF and BCPCF are preferred for intracellular pH measurements, but fluorescein, fluorescein sulfonic acid, and, especially, carboxyfluorescein are still widely used for pH_i determination presumably because easy and cheap to prepare via standard condensation methods.[35] Condensation of resorcinol with trimetallic acid anhydride 3

and 4-sulfophthalic acid produced a mixture of 5(6)-carboxyfluorescein and 5(6)-sulfofluorescein respectively.[36,37] The two isomers exhibit essentially identical pH-dependent spectral properties with pKa of ~6.5, therefore the mixture is sufficiently good for pH_i determination. Fluorescein sulfonic acid moves through the paracellular space inside live cells since it is water-soluble and is cell membrane impermeant, it can be used for the denermination of barrier permeability.[38]

On rare occasions it may be desirable to use regioisomerically pure substituted-fluorescein probes. Fortunately, methods for the preparation of single isomers are available.[39,40] For instance, 5- and 6-carboxyfluorescein begins by condensation of trigllic anhydride **3** with resorcinol in the presence of methane sulfonic acid at 85 ºC. The reaction affords a 1:1 mixture of isomeric compounds **7** and **7'**. An insoluble salt of the 6-isomer (**7'**) is selectively precipitated with an isomeric purity over 98% when this mixture is recrysalized in methanol/hexane two times. The compounds left in the filtrate are recrystallized from ethanol/hexane two times to give the 5-isomer (**7**) also in greater than 98% purity. Hydrolysis of the isomerically pure pivalate esters **7** and **7'** under basic conditions affords 5-carboxyfluorescein and 6-carboxyfluorescein (Scheme 2.3a). Preparation of isomerically pure 5-sulfofluorescein and 6-sulfofluorescein can be achieved via a similar approach. The 5- and 6-isomers **8** and **8'** were produced as dipivaloyl esters, and their di-isopropylethylamine salts were separated via crystallization from dichloromethane and diethylether solution (Scheme 2.3b). Basic hydrolysis of these pivaloyl esters **8** and **8'** yields the isomerically pure 5-sulfofluorescein and 6-sulfofluorescein respectively.

Scheme 2.3. Synthesis of: **a** carboxyfluorescein; and, **b** sulfonofluorescein, regioisomers.

a

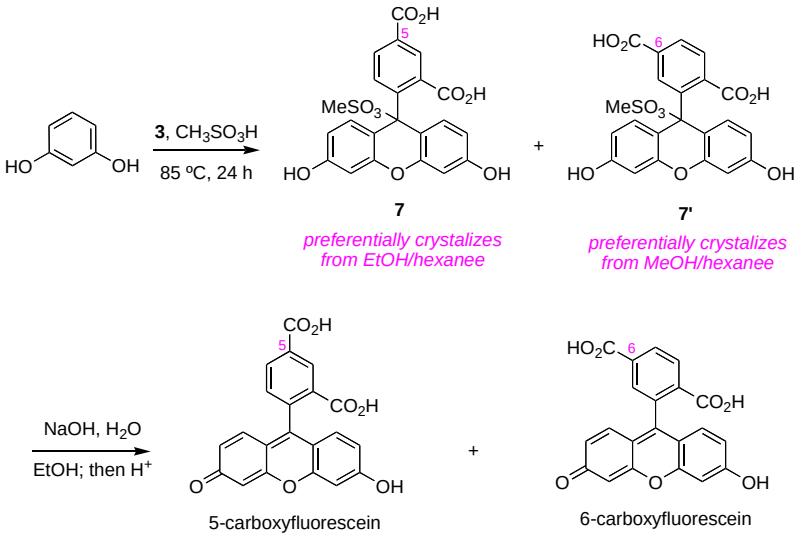

b

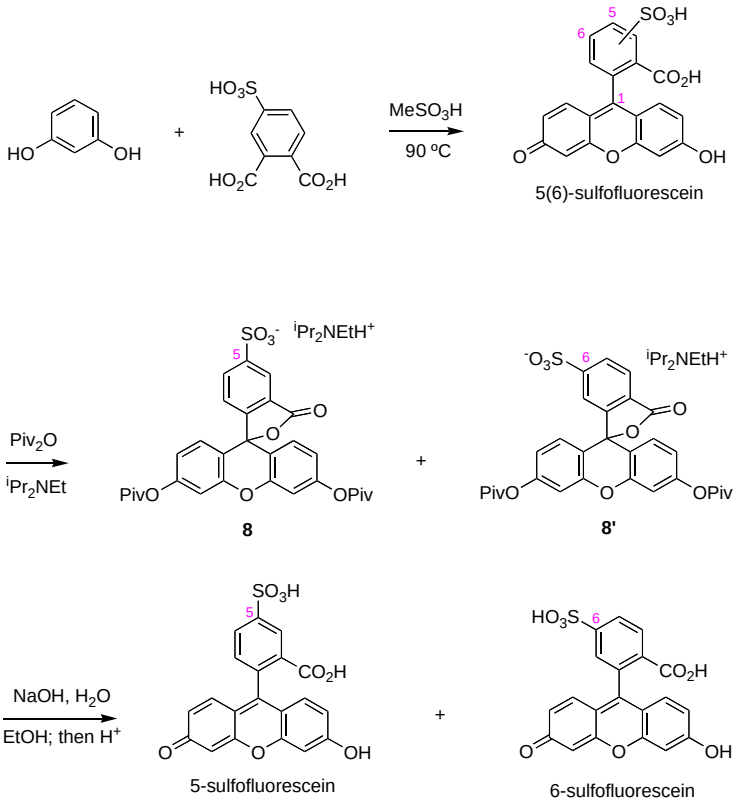

Fluorescein diacetate is occasionally used for measuring pH_i values;[41] the main disadvantage of this is that once fluorescein is liberated via intracellular hydrolysis it can rapidly leak out of cells, hence it is not easy to discern if fluorescence intensity decreases were induced by leakage or pH changes. The more charged derivatives, 5- and 6-carboxyfluorescein applied as cell-permeable carboxyfluorescein AM esters, is more often used for pH_i measurements because it can be better retained in living cells. Even so, at 37 ^{o}C, intracellular concentrations of 5- and 6-carboxyfluorescein have been observed to diminish by 30 – 40 % in the first 10 min after washing.[25] 5- and 6-Sulfonofluoresceins are more water soluble and even better retained inside cells or organelles when compared with carboxy-fluorescein. However, these sulfonic acid derivatives are not commonly used as pH_i indicators because their diacetate forms cannot easily diffuse into cells. Some other fluorescein derivatives (*e.g.* dimethylcarboxyfluorescein)[34] can be used as pH_i indicators, but many of these are not particularly photostable or well retained in living cells.

One approach to the problem of leakage of fluorescein derivatives from cells is to import some activated form that will non-specifically conjugate to intracellular biomolecules. For instance, fluorescein isothiocyanate[32,42] and 5-(6-)carboxyfluorescein diacetate succinimidyl ester,[43] have both been used in this way.

The xanthene parts of the pH_i indicators discussed above have very similar pKa values to fluorescein, ~ 6.4.[44] The detailed spectral properties of fluorescein, carboxy-fluorescein and fluorescein sulfonic acid can be obtained on the website of Invitrogen.[45]

2.4 Miscellaneous Fluorescein Derivatives

Some of fluorescein derivatives with longwave absorption and fluorescence are possible for pH_i measurements.[46] For instance, 5 (and 6)-carboxynaphthofluorecein is a dual emission ratiometric near neutral pH probe with a pKa of ~7.6.[47] The compound in acidic form absorbs and emits at 509 nm and 572 nm respectively. Its base form has a bathchromic shift in absorption and emission with maximum peak at 598 and 668 nm. The pH-sensitive long-wavelength dual emission spectra have been applied for determination of physiological pH_i.[47]

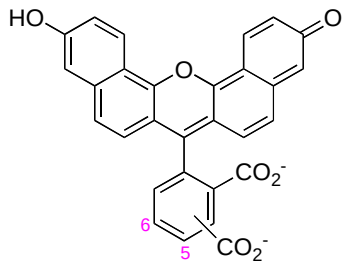

5 (and 6)-carboxynaphthofluorescein
pKa 7.6
ϕ = NA
$\lambda_{max\ abs}$ 509/598 nm
$\lambda_{max\ emiss}$ 572/668 nm

Fluorescein derivatives with different pKa values can be applied in similar ways to observe changes of proton concentrations that are centered around other pH values.[48] Electron withdrawing groups on xanthenes lower their pKa values. For instance, the halogenated fluoresceins Oregon green 488/514,[49] and carboxy-DCF[50] all have pKa's of ~ 4.7. Otherwise, the pH-dependent absorbance and fluorescence spectral characteristics of these dyes are similar to fluorescein, hence dual-excitation ratiometric measurements

of pHi are possible. Detailed information about applications of these dyes can be obtained through the Invitrogen website.[51]

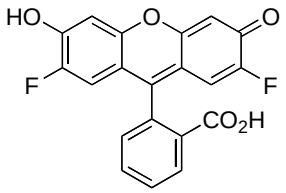

Oregon Green 488
pKa 4.8
$\phi = 0.97$
$\lambda_{max\ abs}$ 490 nm
$\lambda_{max\ emiss}$ 514 nm

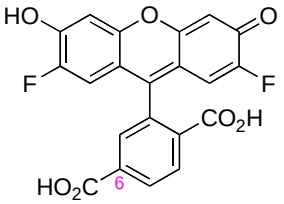

6-carboxyl
Oregon Green 488
pKa 4.8
$\phi = 0.92$
$\lambda_{max\ abs}$ 492 nm
$\lambda_{max\ emiss}$ 514 nm

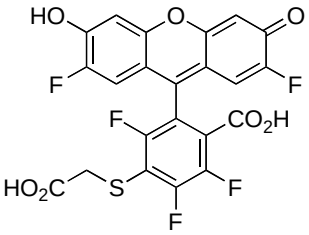

Oregon Green 514
pKa 4.8
ϕ = NA
$\lambda_{max\ abs}$ 506 nm
$\lambda_{max\ emiss}$ 529 nm

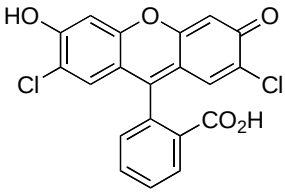

Dichlorofluorescein
pKa 4.7
$\phi = 0.86$
$\lambda_{max\ abs}$ 503 nm
$\lambda_{max\ emiss}$ 522 nm

Fluorescent rhodols, which is the hybrid of a rhodamine and a fluorescein molecules, have the same backbone as rhodamine and rosamine dyes with one of the NR_2 groups replaced by oxygen.[52-54] These fluorophores have high molar absorptivities in the visible region, high quantum yields in the range of 520-580 nm with appropriate N-substituents. The dyes are much more photostable comparing to fluorescein detivatives. The probes usually exhibit significant shift in absorbance spectra with variation of pH values, and are suitable for dual excitation ratiometric pH measurement.

Some of these compounds have lower pKa values between 4.5 - 6.5 and suitable for pH measurement in acidic environments.[49,54] For instance, the conjugate of rhodol **9** with ethylenediamino-ouabain has been used for probing the pH values in the microenvironment in the cardiac glycoside-binding site of Na^+/K^+-ATPase.[55]

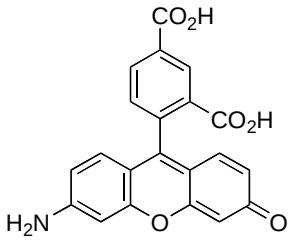

9
pKa 5.59
ϕ = 0.89
$\lambda_{max\ abs}$ = 494 nm
$\lambda_{max\ emiss}$ = 520 nm

3. SNAFLs, SNAFRs, and SNARFs

There are three possible isomers of benzoxanthene dyes that differ via their orientation of annulation (Figure 2.4a). Representatives of all three compounds types have been prepared, and their spectral and photophysical properties have been studied. Benzo[c]xanthenes were introduced by Molecular Probes in the early 1990s.[24] These dyes include the seminaphthofluorones (SNAFRs), seminaphthofluoresceins (SNAFLs), and seminaphthorhodafluors (SNARFs); all these dyes have one benzene and a naphthalene component in the fluorophore (Figure 2.4b). SNAFLs and SNAFRs, and SNARFs are long-wavelength fluorescent pH_i indicators with oxygen and nitrogen 10-substitutuents, respectively.[24,56]

The pnemonics for these compounds are so similar that it is bewildering to use them. The following are generalities that may make these abbreviations more user-friendly. Throughout, "SNA" stands for "SemiNAphtho-". SNAFRs and SNAFLs share similar molecular structures except that SNAFRs do not possess a carboxyl substituent at the 3' position (they are FluoRones), whereas SNAFLs are FLuorescein derivatives, and SNARFs are derived from RhodaFluors. Figure 2.4c delineates how these dyes are related to fluorescein and rhodamines. Consideration of this graphic also makes it evident that there are other permutations of the annulation structure and O/N-substitution patterns that correspond to compounds that are not used as pH indicators, and may even not have been prepared.

a

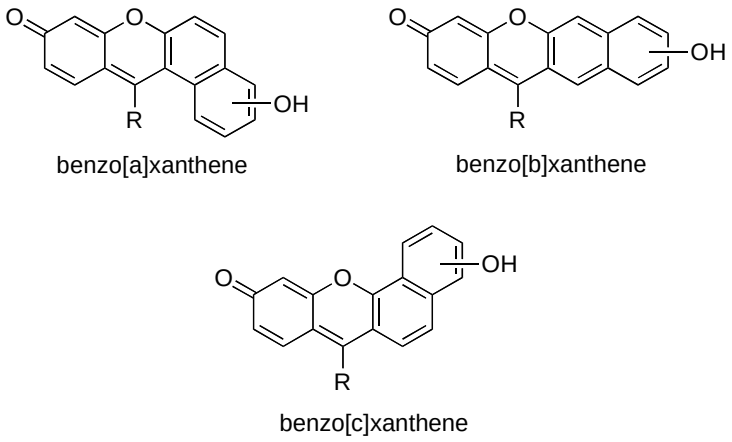

Figure 2.4. (a) Three types of benzoxanthenes; (b), three types of benzo[c]xanthenes that have different heterocyclic substituents; and (c), evolution of benzoxanthenes from fluorescein and rhodamine.

b

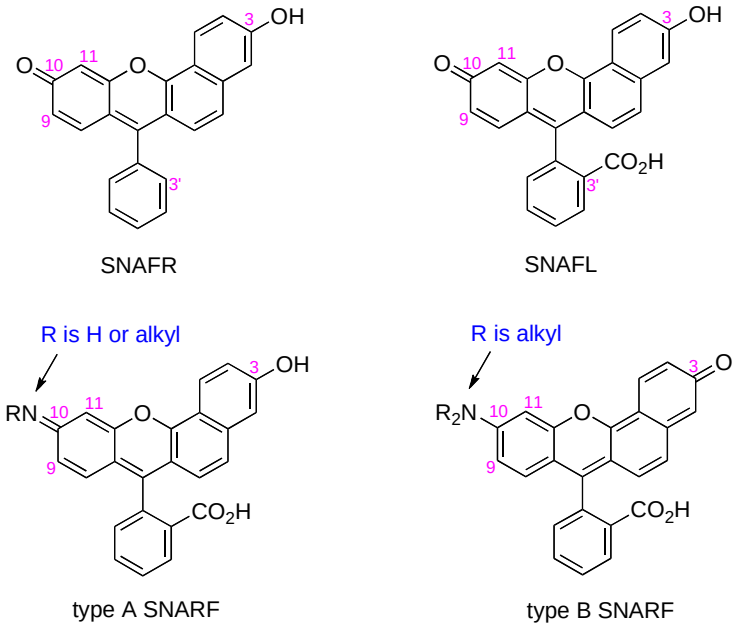

c

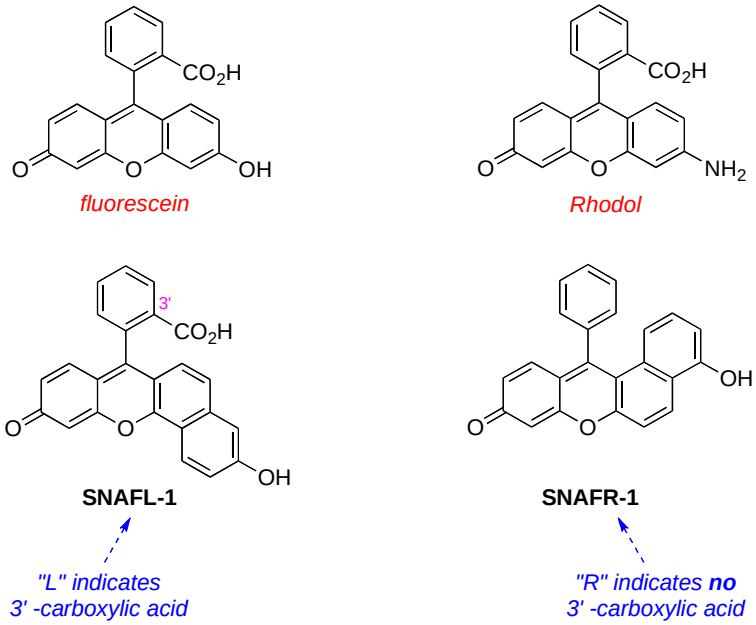

Figure 2.4. Continued.

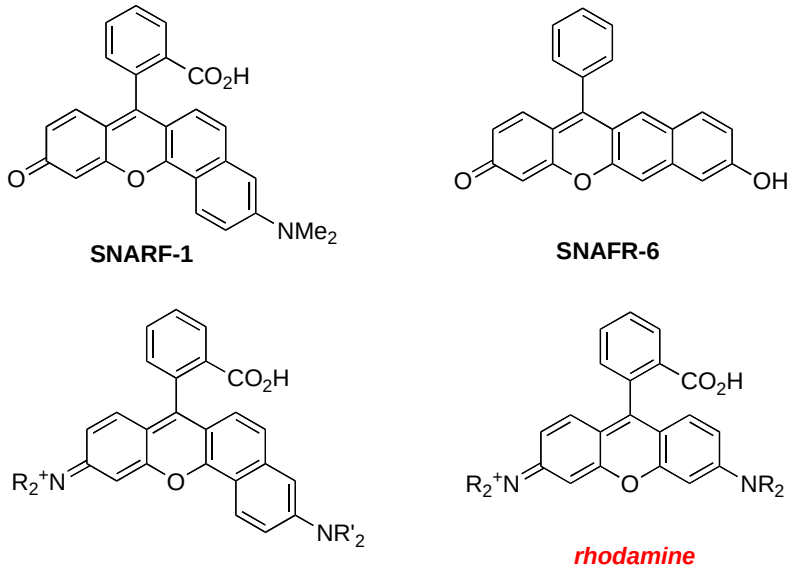

Figure 2.4. Continued.

Semiempirical computer calculations (AM1) have been used to predict that bathochromic shifts should be observed in the absorption and fluorescence spectra of the type [a] and [b] benzoxanthene isomers.[57] Some compounds in that series have recently been prepared, and they do indeed have red-shifted absorbance and emission maxima, but they have not yet been used for pH_i measurements.[56,58]

Scheme 2.5a shows syntheses of benzo[c]xanthene dyes, ie SNARFs and SNAFLs, via condensation of 1,6-dihydroxynaphthalenes with the appropriately substituted benzophenone derivatives 10; these in turn were made via coupling of resorcinol or 3-aminophenol with phthalic anhydride in toluene. For instance, carboxySNARF-4F was synthesized via acid catalyzed condensation of 5-fluoro-1,6-dihydroxynaphthalene with 2,4- (and 2,5)-dicarboxy-3'-dimethylamino-2'-hydroxybenzophenone.[59] Syntheses of benzo[a] and [c]xanthene dyes was only recently

achieved.[56,58] For instance, lithiated 1,6-dimethothynaphthelene was coupled with 2,4-dimethoxybenzophenone to produce compounds **11** and **12**. SNAFR-1 and SNAFR-6 were isolated in 55% and 15% yield after treatment with BBr_3.[58]

Molar absorptivities of SNARFs and SNAFLs are highest under basic conditions and their absorbance maxima shift to the red; this is true of most fluorescein derivatives. However, unlike most fluorescein-based pH indicators, their fluorescent emission spectra also show significant pH-dependent shifts. The protonated form emits in the yellow-orange region (540 ~ 580 nm), whereas deep red emissions (620 ~ 640 nm) are observed for the basic form. Both the absorbance and fluorescence spectra of SNARFs and SNAFLs show sharp, pH-independent, isosbestic points at ~530 nm and ~585 nm, respectively; these are desirable properties for dual-absorbance and dual-emission ratiometric measurements. SNARFs and SNAFLs have been used as dual-emission pH indicators[60] for determination of intracellular pH values via flow cytometry[61] and confocal spectroscopy.[60] N,N-Dialkyl SNARFs (ie type B SNARFs in Figure 2.4b) are more fluorescent in basic solutions where they exist predominantly as their anionic forms (quantum yields 0.05-0.20) than in their neutral forms (quantum yields of 0.02-0.07). Conversely, SNAFLs and type A SNARFs (Figure 2.4b) have higher quantum yields (up to 0.5) in the neutral form (ie under acidic conditions; Figure 2.5).

Scheme 2.4. (a) Original syntheses of SNARFs and SNAFLs; and (b), One example of syntheses of a benzo[a]xanthene and a benzo[b]xanthene.

a

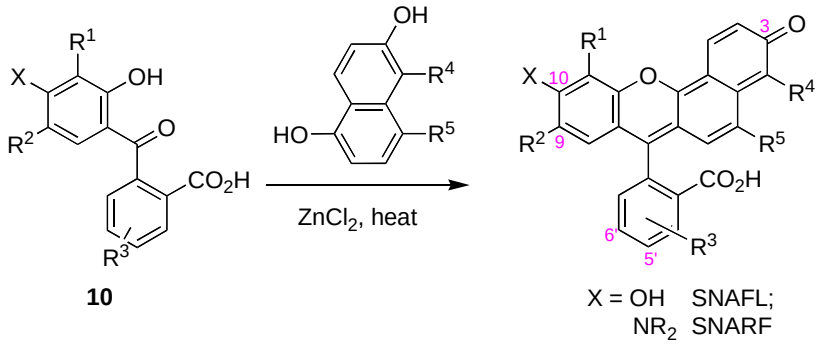

10

X = OH SNAFL;
NR_2 SNARF

b

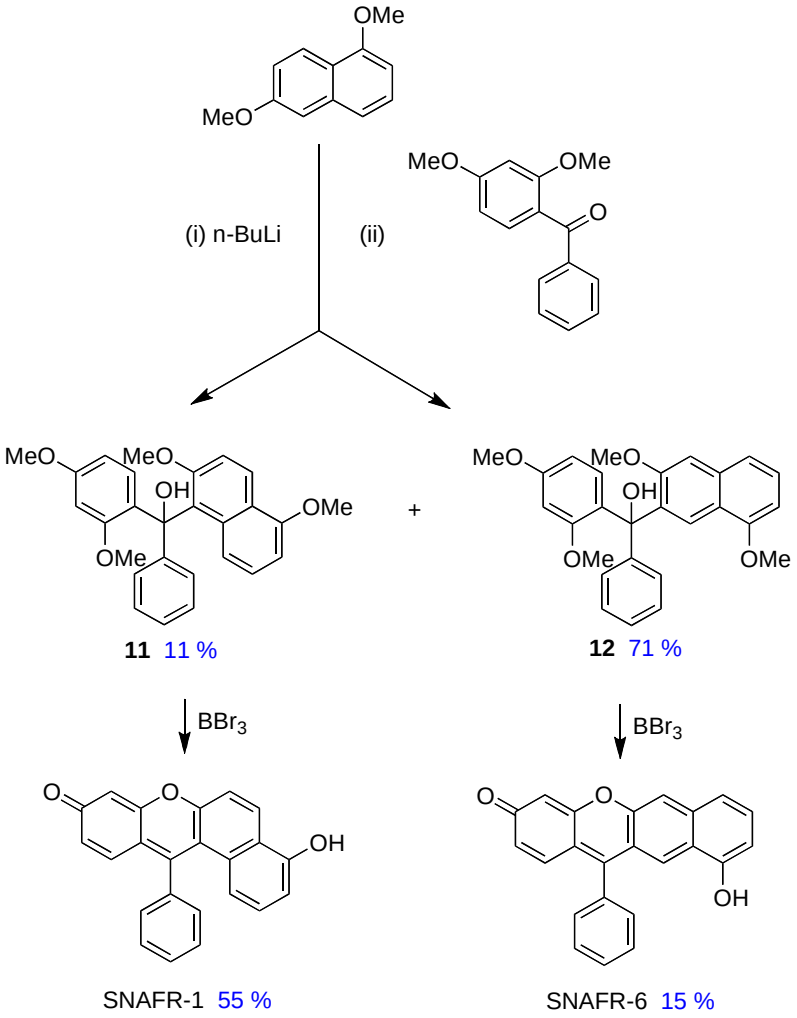

11 11 %

12 71 %

SNAFR-1 55 %

SNAFR-6 15 %

a

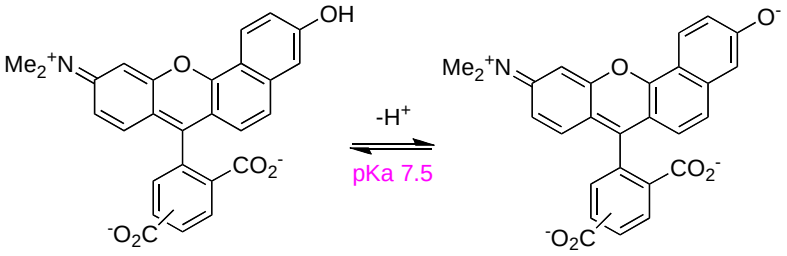

C.SNARF-1
acidic form
ϕ = 0.03
$\lambda_{max\ abs}$ 544 nm
$\lambda_{max\ emiss}$ 575 nm

basic form
ϕ = 0.09
$\lambda_{max\ abs}$ 583 nm
$\lambda_{max\ emiss}$ 631 nm

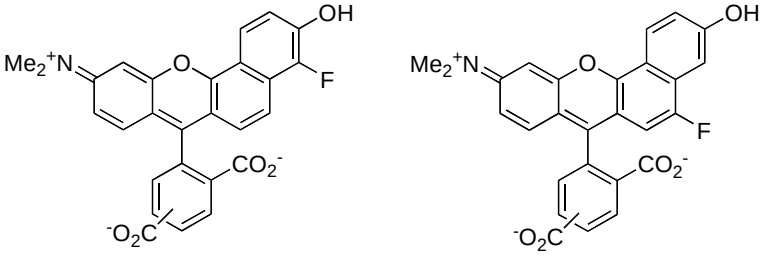

C.SNARF-4F
pKa 6.4
acidic/basic form
$\lambda_{max\ abs}$ 520/582 nm
$\lambda_{max\ emiss}$ 592/661 nm

C.SNARF-5F
pKa 7.2
acidic/basic form
$\lambda_{max\ abs}$ 560/575 nm
$\lambda_{max\ emiss}$ 580/628 nm

b

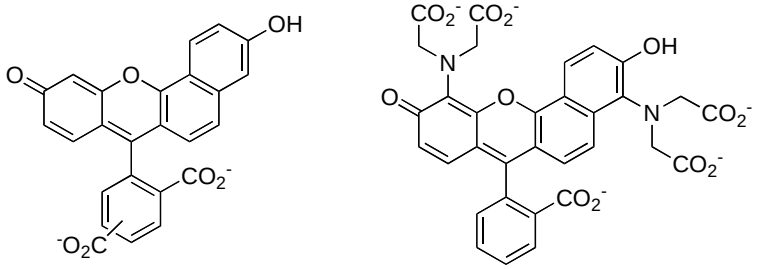

C. SNAFL-1
pKa 7.8
acidic/asic form
ϕ = 0.32/0.08
$\lambda_{max\ abs}$ 510/542 nm
$\lambda_{max\ emiss}$ 539/623 nm

SNAFL-calcein
pKa 7.0
acidic/asic form
ϕ = NA
$\lambda_{max\ abs}$ 492/535 nm
$\lambda_{max\ emiss}$ 540/625 nm

Figure 2.5. Spectral and photophysical properties of some commercially available benzo[c]xanthenes that have been used as pH indicators. (a) SNARF; and (b), SNAFL-1 derivatives.

Carboxy-SNARF-1 (or "C.SNARF-1")[62] is probably the second most widely used pH_i indicator behind BCECF (see above). It has been applied to determine absolute cytosolic, mitocontrial[60] and nuclear[63] pH values in living cells using flow cytometry,[61] microplate readers,[20] confocal imaging[60] or microspectrofluorometry.[27]

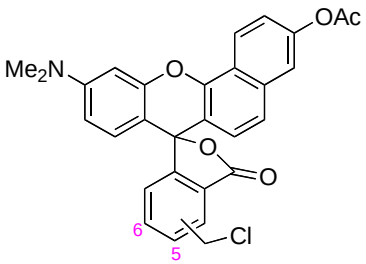

chloromethyl SNARF-1 acetate

Dyes like C.SNARF-1 have several attributes that may explain why they are so widely used. First, C.SNARF-1 can be temporarily shielded as an AM ester, facilitating import into living cells. Furthermore, the cell permeable chloromethyl SNARF-1 acetate slowly reacts with intracellular thiols forming conjugates that are retained inside cells and facilitate long-term pH studies. Second, the ratiometric properties of C.SNARF-1 are not significantly dependant on its concentration or on the ionic strength of the surrounding aqueous media; these are desirable properties for general-use pH_i indicators.[33] When C.SNARF-1 was irradiated to photobleach the compound, the ratio of the fluorescence intensities at 580 and 640 nm was shown to be essentially invariant; this makes the dye more suitable for extended experiments than it would otherwise be.[60] Furthermore, the fluorescence spectrum of C.SNARF-1 has been shown to be sufficiently different to the Ca^{2+} sensor fura-2[64] and to the Na+ sensor SBFI,[65]

facilitating simultaneous measurement of H^+, Ca^{2+} and Na^+ concentrations in cells. Finally, C.SNARF-1 can be excited at longer wavelengths (514 nm or 536 nm) than some other probes, reducing cell damage due to irradiation and circumventing some effects of intracellular autofluorescence.

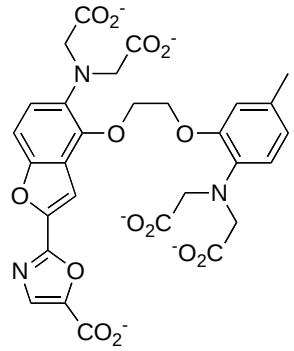

Fura-2

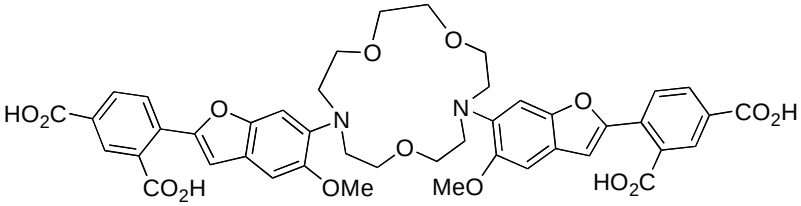

SBFI

There are also some drawbacks to using C.SNARF-1 as a pH indicator. It has a low quantum yield, especially under acidic conditions (neutral form; $\Phi = 0.03$). Intracellular pH values under 7.0 cannot be measured accurately using this dye because its pKa is too high (7.5). Moreover, the spectral properties of C.SNARF-1 are significantly influenced by temperatures and environments in living cells.[27] The quantum yield of the probe decreases by 25% when the temperature increases from 25

°C to 37 °C. Further, the brightness of the dye inside living cells is diminished probably because of its interaction with intracellular proteins. C.SNARF-4F[59] and C.SNARF-5F have lower pKa values, 6.4 and 7.2 respectively, and are recommended by Invitrogen (formerly Molecular Probes) as replacements for C.SNARF-1 to measure acidic or cytosolic pH_i.[66,67] Some other C.SNAFLs, *e.g.* C.SNAFL-1 and SNAFL-calcein have been used for measuring pH_i too, but their pKas are usually bigger than 7.6. Finally, the fast photobleaching rate of these dyes, especially at 37 ^oC, restricts the application of SNAFLs for the measurement of pH_i in the living systems.[68]

4. Miscellaneous Small Molecule pH_i Indicators

This section covers small molecule pH_i indicators that cannot be grouped into the categories discussed above. The first four considered in this subsection (europium complexes, a fluorene derivative **14**, 1,4-DHPN, and HPST) are indicators for near neutral environments. The rest of the dyes in this section are useful under more acidic conditions; they are based on anthracene, BODIPY, or cyanine structures to give emission maxima that occur at longer wavelengths.

4.1 Various Indicators for Near Neutral pH Values

Europium Complexes

Emissive europium(3+)[69] complexes such as **13** may be applied for measurement of pH_i.[70] In these molecular, the sensitizing group azathiaxanthone allows excitation in the range 360 to 405 nm. Fluorescence of this complex between 680 - 710 nm is hypersensitive to N-ligation of the sulfonamide which, unlike the sensitizing group,

dissociates from the metal as the pH is lowered. Thus the fluorescence intensity at 680 nm is quite strong in basic aqueous solutions (pH ~8) and diminished in acidic media (pH 4-5). This characteristic makes the complex suitable for ratiometric pH measurement based on fluorescence intensity ratios at 587 and 680 nmas a function of pH. The complex possesses a large Stoke shift ~200 nm and fluoresces in the near-IR region where cell autofluorescence is less problematic. Moreover, complex **13** is cell-permeable and non-toxic. When the dyes is used to stain cells, confocal fluorescence microscopy indicates that both the europium emission (ca 570 nm) and the azathiaxanthone fluorescence (450 nm) eminate mainly from the nucleus implying that the intact complex is localized there. A disadvantage of **13** is that, like most lanthanide complexes, it has a low quantum yield (0.06).

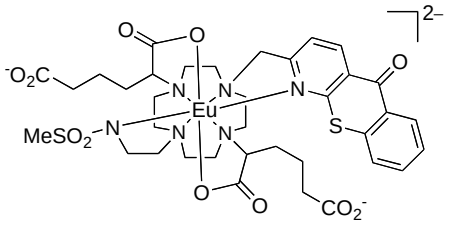

13

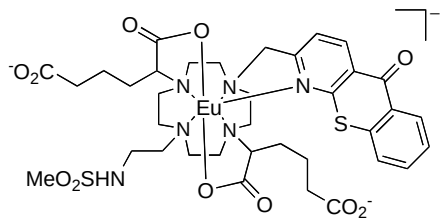

13'

Fluorene Derivative 14

The donor-π-acceptor fluorene derivative **14**[71] is a near-neutral pH_i indicator with pKa of ~ 7. It is water-soluble, cell permeable, and diffuses into the cytosol. Also it has low cytotoxicity (in the 0.1 – 100 μM concentration range)[71] as indicated by the Alamar Blue (AB) reduction analysis (a method to test cell viability).[72] Sharp isobestic points are observed in the absorbance and emission spectra of this dye (at 355 and 492 nm respectively); as we have already commented, isobestic points are highly desirable for ratiometric measurements because they are indicative of well proportioned spectral transformations between two {pH} states. Furthermore, this probe has been applied for imaging of with two-photon excitation with a relatively large 2PA cross section (100 GM at ~800 nm) in its neutral form **14'**.

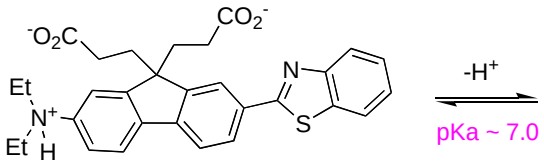

14
ϕ = 0.21
$\lambda_{max\ abs}$ = 341 nm
$\lambda_{max\ emiss}$ = 391 nm

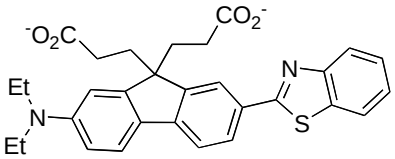

14'
ϕ = 0.56
$\lambda_{max\ abs}$ = 382 nm
$\lambda_{max\ emiss}$ = ~ 580 nm

1,4-Dihydroxyphthalonitrile (1,4-DHPN)

1,4-DHPN[73,74] was a commonly used pH_i indicator before it was largely superceded by BCECF and C.SNARF-1 in the early 1980s. The spectral properties of this compound are more desirable for intracellular pH_i measurements than fluorescein derivatives; this is because the fluorescence emission maximum for 1,4-DHPN shifts with pH whereas fluoresceins tend not to have this properties hence they are used to give a change of fluorescence intensity at one single wavelength.[29] The maximum fluorescence wavelengths in the emission spectra of 1,4-DHPN shift from 450 to 476 nm as pH is increased from 3 to 10, and this permits the dual emission ratiometric measurement. The ratio of the fluorescence intensities at 512 and 455 nm do not significantly change with dye concentration and the ionic strength of the medium. Further, the dye is also not toxic to cells (at least as assessed by monitoring oxygen consumption, an older method to test cell viability).[74] The parent dye is not especially cell permeable but the corresponding diacetate, 1,4-diacetoxyphthalonitrile (1,4-DAPN),[75] is and it can be hydrolyzed into 1,4-DHPN by the enzyme esterase. 1,4-DHPN has been used to sense the pH_i regulatory responses when A6 cells are incubated with acid and with base.[74]

There are, however, several drawbacks associated with applications of 1,4-DHPN in pH_i measurements. First the dye is rapidly cleared from living cells because it only has 1-2 negative charges at physiological pH values.[76] Second the low UV excitation wavelengths typically used for this dye (350-365 nm) might perturb the cells. Third, the emission spectrum does not have a well-behaved isobestic point hence this dyes is not ideal for ratiometric methods based on differences in emission wavelenghts.

Overall, dyes like the BCECF and SNARFs are more favorable with respect to these parameters hence they tend to be preferred over 1,4-DHPN for pH_i measurements.

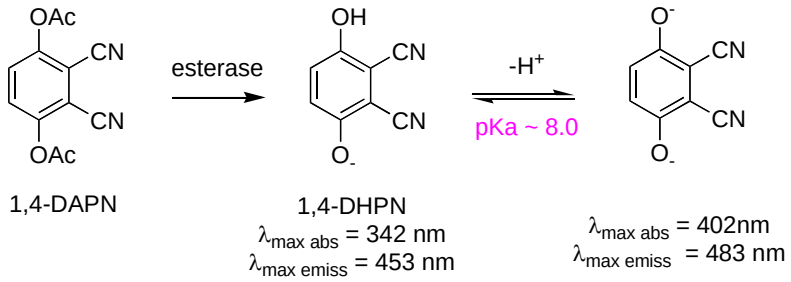

8-Hydroxypyrene-1,3,6-trisulfonic Acid (HPTS)

HPTS is a highly water-soluble dye compound[77] with low toxicity,[78] and it is also very cheap compared with most other indicators. It has been used for measurement of cytoplasmic pH[79] or acidic organelle pH[80] in many cell types. Excitation ratio imaging is possible using HPTS since it has absorbance maxima at 405 and 465 nm that increases and decreases, respectively, when the solution pH is varied from 5 to 8. Furthermore, this tri- or tetra-anionic dye is retained well inside living cells at physiological pH values. The main limitation to the use of HPTS as an intracellular indicator is its lack of cell permeability, and there is no convenient pro-drug like form to facilitate transport of this dye into cells. This accentuates the general need for sulfonic acid protecting groups that are cleaved by esterases. At present HPTS is only useful for pH_i measurements when loaded inside living cells via microinjection, electroporation,[81] and scrape-loading[79] which might damage the cells.

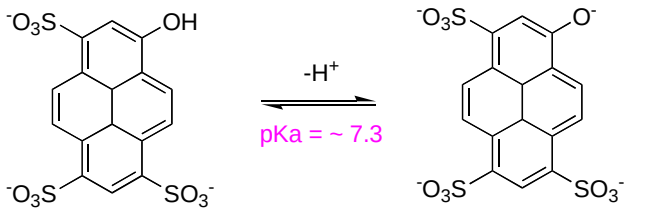

HPTS phenolic form
ϕ = 1.0
$\lambda_{max\ abs}$ = 405 nm
$\lambda_{max\ emiss}$= 514 nm

HPTS phenolate form
ϕ = 1.0
$\lambda_{max\ abs}$ = 465 nm
$\lambda_{max\ emiss}$= 514 nm

Cyanine-based pH Indicators

Near IR pH stains based on cyanine dyes tend to emit in the near IR region, hence minimizing cell damage on excitation and undesirable effects from cell autofluorescence.[82] A new near-infrared neutral pH fluorescent probe **15**[83] was recently introduced for measurement of near neutral pH_i values. This pH indicator consists of a near IR fluorescent tricarbocynine (Cy) fluorophore with high molar absorptivity and a 4'-(aminomethylphenyl)-2,2':6',2"-terpyridine(Tpy) receptor. In pH 10, the fluorescence of 15 was quenched (ϕ = 0.008) by the lone pair electrons of Tpy via PeT. Conversely, the protonation of N atoms stops PeT process and the dye fluoresces brightly (φ = 0.13) with a peak at 750 nm. Fluorimetric titration showed that the pKa of the probe in aqueous buffered solution is about 7.1. Compound **15** was applied to living HepG2 cells for observing pH-dependent changes of fluorescence brightness.[83] Confocal spectra revealed that dye **15** was more fluorescent at pH 7.0 than at pH 7.8, and it could monitor minor pH changes within the range of 6.7 – 7.9. Extensive studies showed that this probe has low toxicity, cell membrane permeability and good

photostability. All these advantages suggest that this probe could be widely used for monitoring minor pH changes in biological systems.

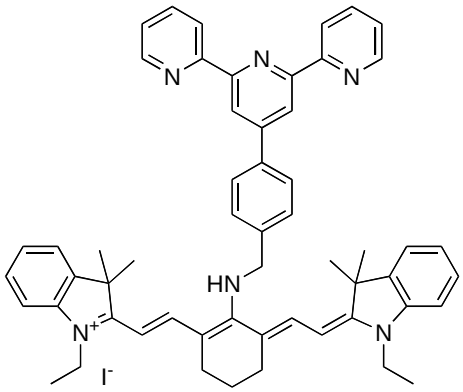

15
pKa ~ 7.1
ϕ = 0.13 (in acidic solution)
$\lambda_{max\ abs}$ = 648 nm
$\lambda_{max\ emiss}$ = 750 nm

4.2 Various pH Indicators for Acidic Environments

Commercialized Lysosensors

Many probes are available from Life Technologies (former name Invitrogen) for measurement of acidic pH_i values. A pyridyl Oxazol probe Yellow/Blue DND-160 PDMPO[84], the anthrathene-based sensor DND-167[85] and DND-153, and DND-189 (Figure 2.6) are dyes that work on the principle of that electronic excited states can be quenched before they fluoresce by electron transfer form amines; this is photoinduced electron transfer (PeT).[86,87] Dyes of this type become more emissive in acidic environments when proximal amine is protonated. Of all the Lysosensors shown in Figure 4, DND-160 is unique because it is brightly fluorescent at protonated and

deprotonated forms (Φ < 0.3 for both forms) and its absorbance and fluorescence spectra are significantly blue shifted with isosbestic points at 365 and 470 nm as the pH values are increased. Furthermore, it showed pH-dependent lifetime responses indicating a good probe for lifetime imaging to determine lysosomal pH.[87] The acidic form DND-160 fluoresces brightly in yellow light with a peak at 540 nm. The basic form emits strongly blue light with a maximum at 440 nm. The pKa of DND-160 is about 5.1. DND-160 has been applied for dual emission imaging for lysosomal pH. Advantages of the DND dyes, and of anthracene derivatives in particular, are that they tend to be very photostable, and cell permeable. Conversely, a disadvantage associated with that particular dye type is that that anthracene is a dye that absorbs and emits at relative short wavelengths (377 and 430 nm),[85] leading to cell damage and undesirable artifacts from autofluorescence. LysoSensor DND-189 is exceptional insofar as it remains fluorescent even when the pendant amine is not protonated, ie at pH values from 5.4 to 7.0.[88] DND-153 with a pKa of 7.5 is sensitive to neutral pH, but still has strongly emission in green light at pH 8.[87] We conclude that PeT does not quench the fluorescence of these dyes so effectively because the oxidation/reduction potentials of the fluorophore and the amine are not well matched for this.

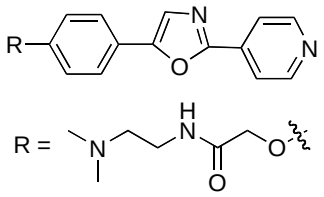

Yellow/Blue DND-160
(PDMPO)
pKa ~ 4.5
ϕ = 0.43/0.41
$\lambda_{max\ abs}$ = 385/329 nm
$\lambda_{max\ emiss}$ = 542/464 nm

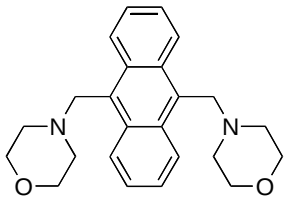

Blue DND-167
pKa ~ 5.1
ϕ = 0.80(at pH 3.0)
$\lambda_{max\ abs}$ = 373 nm
$\lambda_{max\ emiss}$= 425 nm

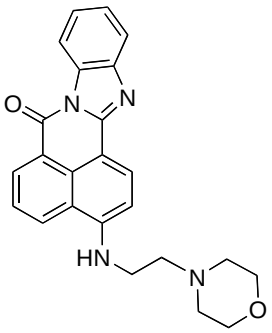

Green DND-189
pKa 5.2
ϕ = 0.48 (at pH 4.4)
$\lambda_{max\ abs}$ = 443 nm
$\lambda_{max\ emiss}$ = 505 nm

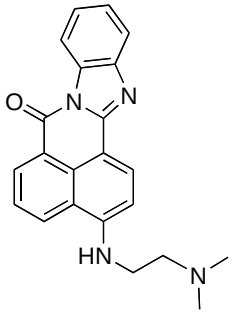

Green DND-153
pKa 7.5
ϕ = 0.34 (at pH 4.0)
$\lambda_{max\ abs}$ = 442 nm
$\lambda_{max\ emiss}$ = 505 nm

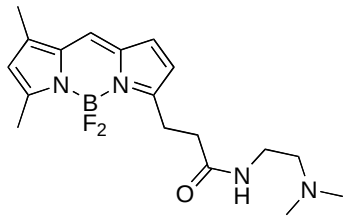

Green DND-26
pKa NA
ϕ = NA
$\lambda_{max\ abs}$ = 504 nm
$\lambda_{max\ emiss}$ = 511 nm

Figure 2.6. Commercialized Lysosensors for acidic environments.

A group of macrocyclic peptidomimetics FG-H503, FG-H504, FG-H506 and FG-H508 derived from 9,10-dimethylanthracene moiety were reported in 2005.[88] All of

these probes have very similar absorbance (at 377 nm) and fluorescence maxima (ca 430 nm) in aqueous solution but have tunable pH properties for the fluorescence imaging of acidic organelles in live cells. The peptidic parts differ only in the size of the cyclic systems they form around the anthracene (n changes from 3 to 8): this structural change modifies the pKa values of the amine parts from 5.06 to 5.43. Thus these peptidomimetics are useful in a pH region that is not covered effectively by lysosensors DND-167 and DND-189 (pKa of 5.1 and 5.2). It was concluded that FG-H503 localizes in acidic organelles after being taken up by macrophage Raw 264.3 cells, because it co-localized with lysosomal probes DND-189 and DND-26.

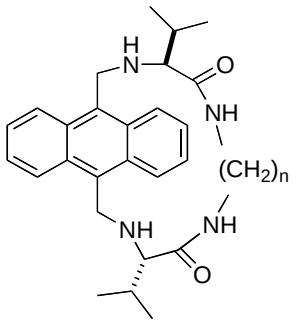

n	pKa
3	5.06
4	5.24
6	5.41
8	5.43

Acridine Dyes

One of the most commonly method to study the changing of pH in acidic organelle in live cell is based on the use of lipophilic weak bases, such as monoamine, 9-amino-6-chloro-2-methoxyacridine (ACMA), and diamine acridine orange (AO). These dyes are cell permeable in neutral form and much less permeable in protonated form. The alteration of absorbance and fluorescence spectra of AO is dependent upon its

concentration.[89] The monomeric form of AO absorbs at ~ 492 nm and emits green light at 530 nm. A red emission at 655 nm has been attributed to the dimmer or oligomers of AO, which has a blue shift absorbance at 465 nm.[90,91] The ratio in the green/red (530/655 nm) is dependent on the concentration in acidic compartments in living cells, which is harnessed by the pH gradient through membrane vesicles. Therefore, the relative acidity of acidic vesicles in sensitive or in muiltidrug-resistant living cancer cells has been appraised by determination of the red/green ratio of accumulated AO.[90] Limitations of using AO as a probe for measuring pH across membrane is that its spectral properties are significantly affected by temperature and the presence of anions.[91,92] For instance, NO3- anion can induce aggregation of AO. Therefore, AO can not be used for quantitatively determination of pH_i.

ACMA,[93] the nucleic acid stain, mainly exists in monocation form (pKa of 8.6) in physiological environments. This dye, unlike AO, does not dimerize in solution at concentration as high as 200 μM.[94] Its fluorescence is quenched by pH or potential gradients across cell membranes.[94,95]

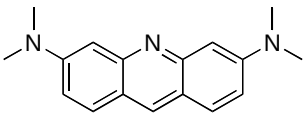

Acridine orange
ϕ = 0.46 EtOH, 0.01M HCl
monomer/dimer
$\lambda_{max\ abs}$ = 495/465nm
$\lambda_{max\ emiss}$ = 530/655 nm

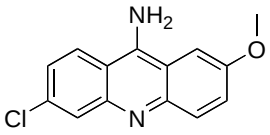

ACMA
pKa 8.6 (monocation)
ϕ = 0.66 (pH 7.2)
$\lambda_{max\ abs}$ = ~ 419nm
$\lambda_{max\ emiss}$ = 484 nm

BODIPY-based

Cell permeable LysoTracker Green DND-26, a BODIPY derivative (Figure 2.6), could also be used for imaging acidic compartments in live cells. This dye tends to absorb and emit at longer wavelengths than the anthracene derivatives, and it is a brighter probe because its molar absorptivity is higher.

A series of pH probes based on BODIPYs (ie NH2BDP, DiMeNBDP, EtMeNBDP and DiEtNBDP) were recently reported for imaging acidic endosomes in cancer cells.[96] These compounds are almost non-fluorescent in basic media (<0.002) due to PeT quenching by the meso-aminophenol substituent. However, these compounds are highly fluorescent in acidic environments (0.55 – 0.60) when the aniline amine is protonated. The pKa values of these BODIPY dyes range from 3.8 to 6.0; this range is possible by changing the alkyl group on the nitrogen. Monoclonal antibody trastuzumab labeled with these acidic pH-sensitive dyes selectively target the human epidermal growth factor type 2 (HER2) receptor, and are then internalized. Confocal spectroscopy revealed that the antibody-probe conjugates are not fluorescent outside cells at neutral pH values. However, 2 h after they are combined with appropriate cells, the pH probe-antibody conjugates fluoresce in endosomes. Only viable cells are visualized under these conditions because the acidic pH in lysosomes is maintained by energy-consuming proton pump; this factor can be an advantage for some analyses.

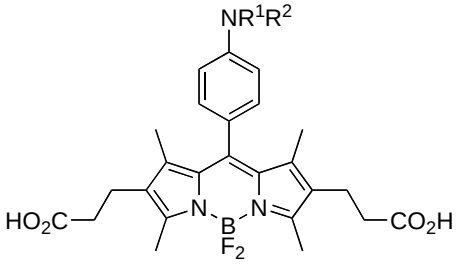

R^1	R^2	pKa
H	H	3.8
Me	Me	4.3
Me	Et	5.2
Et	Et	6.0

A Cyanine-based pH Indicator

The cyanine derivative 15 is cell permeable, and has an optimal pH response around ~5.1.[97] The aminophenol part is the modulator; when protonated, the dye has a maximum absorbance at 558 nm, and fluoresces at 615 nm. The fluorescence intensity increases about 10 times when the pH is decreased from 6.5 to 4.0. Indicator 15 has been applied for monitoring intracellular H^+ within HepG2 cells. One general disadvantage cyanine-based dyes is that they tend to photobleach faster than ones based on anthracene and BODIPY systems.

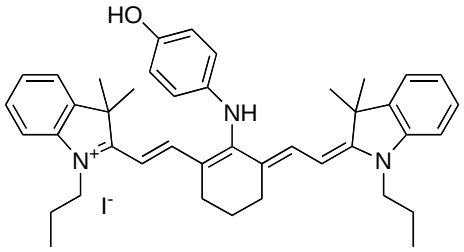

Ap-Cy
pKa ~ 5.1
ϕ = NA
$\lambda_{max\ abs}$ = 558nm
$\lambda_{max\ emiss}$ = 615 nm

5. An Energy Transfer Cassette

Compound **16** based on through-bond energy transfer cassettes[98-101] has been used for probing pH_i in cos-7 cells.[20] Probe **16** consists of two xanthene donors, one BODIPY acceptor, and a triethylene glycol carboxylic acid linker. The linker part is designed to increase the water solubility of the compound in aqueous solution, and to allow attachment to biomolecules. Energy transfer efficiency from the donors to the acceptor is modulated by the oxidative potentials of the xanthene part, which in turn depend on its protonation state. Thus when the system is excited at wavelengths that correspond to the donor then the fluorescence of the whole system is sensitive to the pH of the medium. At pH 5.5 or less, the xanthene donors exists the phenolic state, the oxidation potential of this is ideal for energy transfer, and the probe fluoresces via the acceptor, ie red, around 600 nm.[102] Conversely, the xanthene donors exists predominantly in the phenolate form under basic conditions pH > 7. In that state the donor and acceptor oxidation potentials are not well matched for energy transfer, and the sensor fluoresces almost exclusively from the donors parts (green, *ie* around 520 nm). If the pH is between 5.5 and 6.5, the cassette emits from donors as well as the acceptor. Overall, the cassette remains fluorescent as the pH is changed.

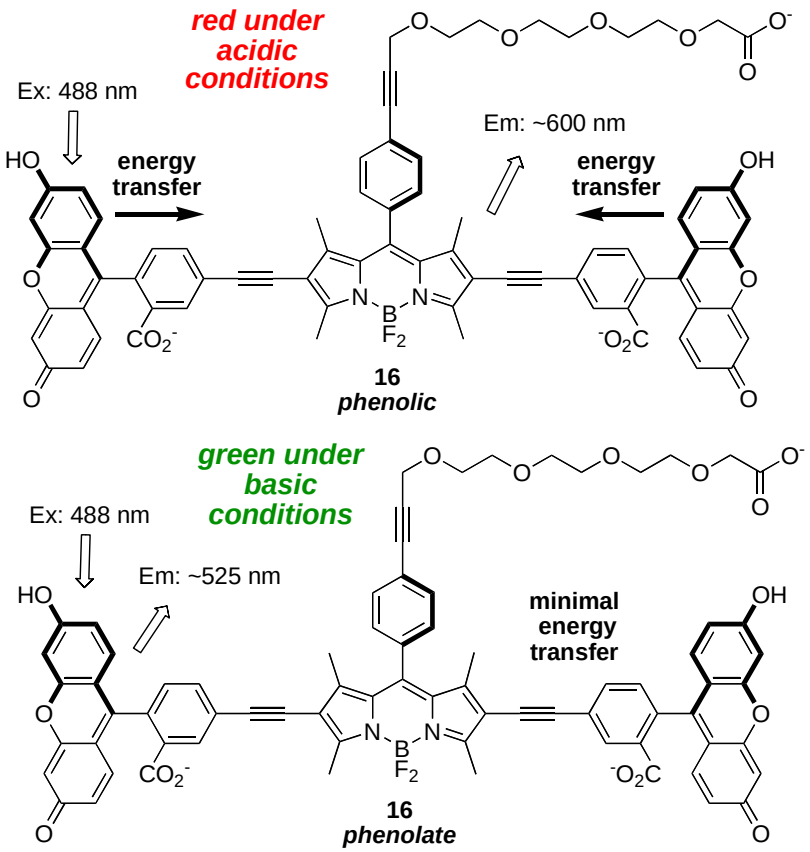

A recent discovery from our laboratories shows that Pep-1 mediated import into COS-7 cells tends to deposit the dye-labeled protein cargoes into the cytosol and ensosome when the experiment is performed at 4 and 37 °C respectively.[103] Thus, BSA-**16** under these conditions would be expected to fluoresce with different red-to-green ratios when BSA-**16** is distributed within the cytosol with pH at ~ 7.2, and the endosome with pH around 5-6. An ex-vivo calibration curve was generated for the cassette shown above (Figure 2.7); this facilitated its use to determine pH values for the endosomes and the cytosol. The pH values of endosome and cytosol, obtained from the red/green ratio

(R/G = 5.03 and 2.03), were 5.4 and 7.4 respectively; these data are consistent with those expected for such intracellular regions.

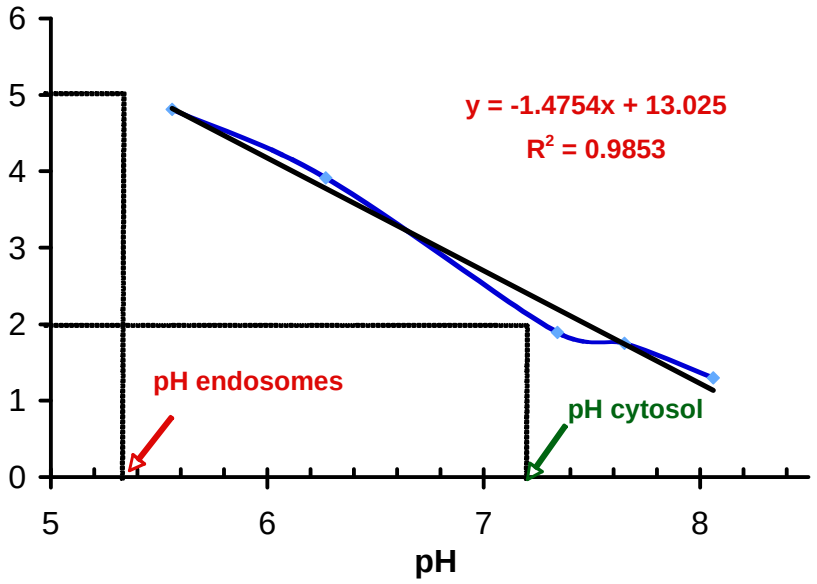

Figure 2.7. ex-vivo calibration curve with pH values corresponding to those observed within endosomes (red/green = 5.03; import at 37 °C) and the cytosol (red/green = 2.03; import at 4 °C).

Imaging of protein-**16** inside cells was possible using this probe. We favor reserving the word probe for labels that can be conjugated with biomolecules to track them within cells. This distinction is important when differentiating these from stains. We reserve the word stains for dyes like C.SNARF-1 that are usually used in solutions to bathe the cells and stain their interiors. Dyes like C.SNARF-1 are usually not attached ot biomolecules then imported into cells for several reasons. These reasons relate to their low quantum yields making them hard to visualize at low concentrations, and photobleaching effects.

6. pH Indicators Based on Nanoparticles, Lipobeads and Microspheres

Nanoparticles can have unique properties resulting from their large surface-to-volume ratios and their small sizes; consequently, they have some potential as sensors in medicine and biotechnology. Probes for pH based on a nanoscaffolds can possess several advantages over small molecule pH sensors. Firstly, multiple indicators can be attached to single particles, hence the localized brightness of the system is increased. Second, particles can simultaneously support pH-sensitive and -insensitive dyes to facilitate ratiometric measurements. Third, nanoparticles may be less vulnerable to leakage through cell membranes and to cellular compartmentalization. Fourth, some nanoparticles are more photostable than small organic dyes. Finally, the physical properties of the nanoparticles can be modulated and manipulated by adjusting their core structures, *e.g.* by choosing between bacteriophage, silica, and coated polystyrenes.

Fluorescein-loaded onto amino-functionalized polystyrene microspheres, ca 2μM diameter have been used for real-time detection of H^+ concentrations inside living cells.[104] These microsphere were shown to be cell permeable to varied cell lines, and non-toxic to cells at any concentration tested. These bead have an aminohexanoic acid linker between the bead and the fluorescent label {formed from 5(6)-carboxyfluorescein}.

Scheme 2.5. Synthesis of fluorescein-capped polystyrene microspheres.

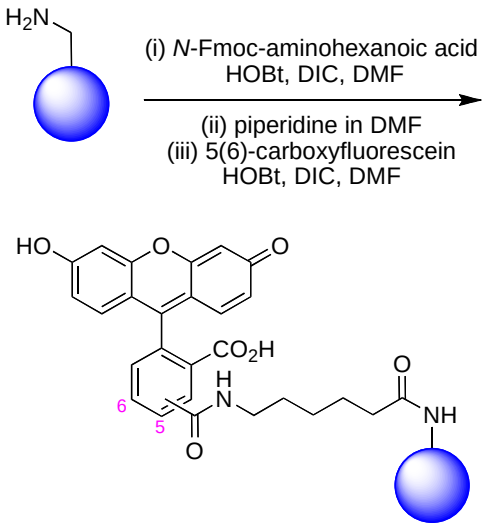

M13 bacteriophage particles functionalized with cyanine dyes have been used for determination of intracellular pH.[105] These particles provide a flexible heterofunctional platform that is approximately 880 x 6.6 nm in size. They contain ca 2700 copies of the p8 coat protein, hence the surface of the particle displays amine groups that may be used for conjugation to other molecules. In this particular case those amines were coupled with the cyanine dyes, HCyC-646 (pH-sensitive) and Cy-7 dyes (pH insensitive, Figure 2.8). When protonated, HCyc-646 absorbs at 646 nm and emits at 670 nm with a quantum yield of 0.08 in aqueous solution. In neutral or basic environments, the dye is deprotonated, there is an hypsochromic (blue) shift of the absorbance to 506 nm, and the near-IR fluorescence is lost. The pKa of HCyc-646 is 6.2, which is suitable for sensing acidic environments in live cells. The pH insensitive dye Cy-7 emits at 775 nm, and this fluorescence provides an in-built control on the nanoparticle that can be used to calibrate the fluorescence changes of the other dye. Typically 400-500 copies of HCyC-646 and

Cy-7 combined were attached to the bacteriophage. In one experiment, incubation of the labeled bacteriophage with RAW cells for 1 h gave internalization of the particles into acidic organelles where they indicated a pH of 5.0 - 6.5; such values are to be expected for intracellular vesicles such as lysosomes, endosomes and phagosomes. Imaging through tissue was also achieved using dye-labeled bacteriophage particles.[105] Good correlations were observed between ratiometric pH readings from these particles and the values measured via an electrode. However, a limitation of this system is that fluorescence emissions from HCyC-646 and Cy-7 at (670 and 775 nm respectively) penetrate tissue with different efficiencies hence a correction factor must be applied for accurate measurements of pH.

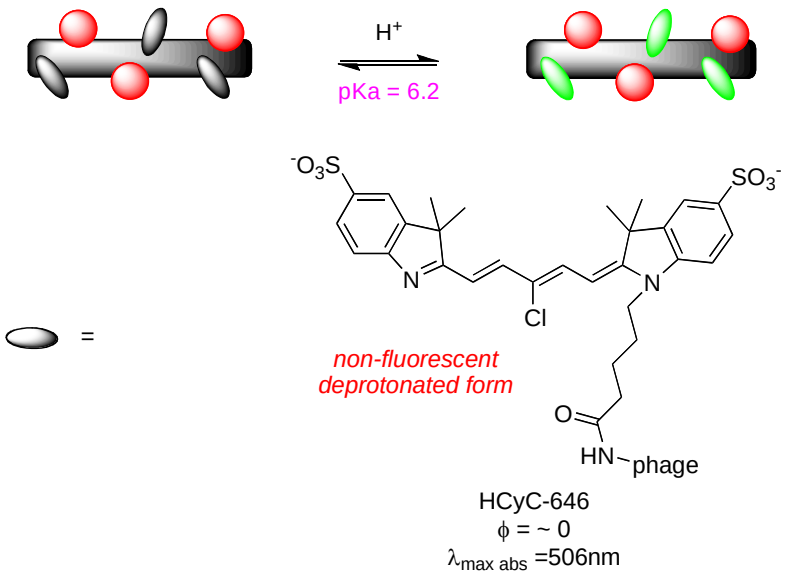

Figure 2.8. HCyC-646 and Cy-7 loaded onto bacteriophage particles.

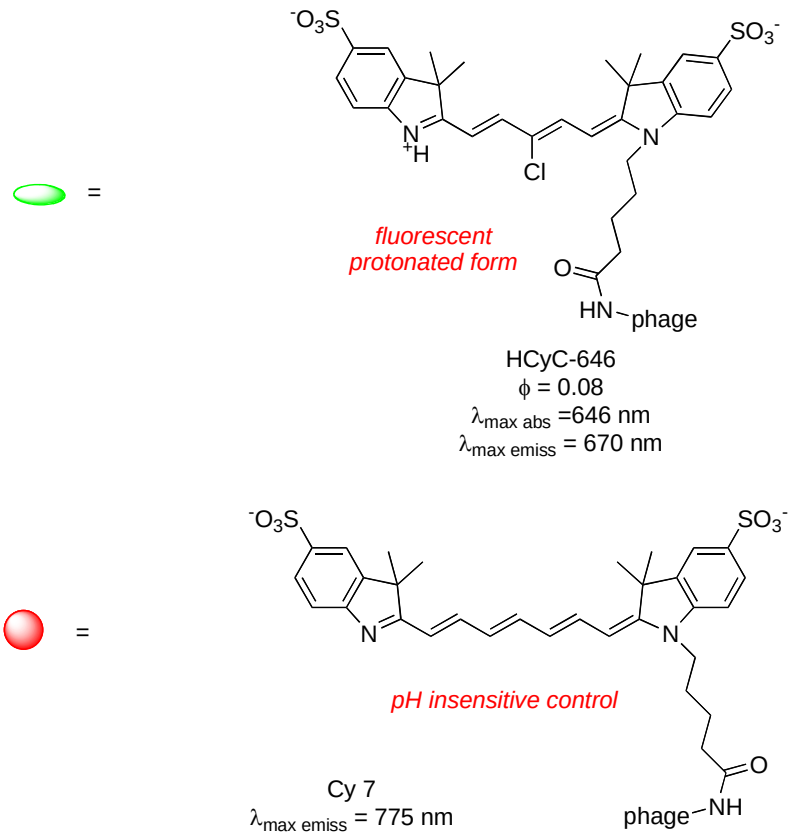

Figure 2.8. Continued.

Colloidal luminescent mercaptoacetic acid capped CdSe/ZnSe/ZnS quantum dots are pH-sensitive andhave been applied to sensing intracellular pH in human ovarian cancer cells.[106] The CdSe core emits visible light, and the two ZnSe/ZnS shells stabilize the photoluminescence properties of the quantum dots by preventing oxidation of the core. Capping the dots with mercaptoacetic acid also serves to increase their water solubilities. Fluorescence intensities of these quantum dots in cells increases monotonically with increasing pH, ie it is quenched in acidic solutions. In living cells these particles are around 10-fold less fluorescent at pH 4 than at pH 10. Further, their

high resistance to photobleaching facilitates long-term cell tracking and monitoring of the intracellular pH.

Fluorescent dyes encapsulated in silica nanoparticles, ”fluorescent core-shell silica nanoparticles”, have been produced for quantitative chemical sensing in live cells. The fluors encapsulated in these particles tend to be brighter and more photostable than the corresponding free dyes in solution.[107,108] Dual emission sensor nanoparticles can combine a pH-sensitive fluorescein dye and a pH-insensitive dye like tetramethylrhodamine. Such particles have been shown to be endocytosed by RBL mast cells upon the addition of the macropinocytosis stimulator, phorbol 12,13-dibutyrate. Following uptake, the particles were trapped in endosomes that later matured into lysosomes. The pH values of various intracellular locations indicated by confocal fluorescence images varied from 6.5 (endosome) to 5.0 - 5.5 (lysosome). The rhodamine internal standard for the pH_i measurements also acts as an indicator of the particle location even in acidic pH conditions where the fluorescein component is less emissive.

Micrometric phospholipid-coated polystyrene particles, also called “lipobeads”, have been used for determination of pH_i in murine macrophage cells.[109] Again, just as in the work described above, pH sensitive fluorescein and pH-insensitive tetramethylrhodamine were used for these ratiometric pH measurements; the liposome-encapsulated dyes display sensing properties similar to those observed in aqueous solution. In this case those fluors were covalently attached to the phospholipids coats on the polystyrene particles thus preventing leakage of dye molecules into the microenvironment. The lipobeads were shown to be non-invasively ingested by

macrophage cells and delivered into lysosomes. However, we note that use of macrophage cells is not a stringent test of the ability of particles to permeate cell walls or of their cytotoxic effects; this is because macrophage cells easily ingest foreign material, and they are relatively robust. Bright field images of the particles in these cells indicated they were not significantly aggregated. Lysosome pH values deduced using these lipobeads were 5.7 ± 0.1; this is a reasonable value.

7. Fluorescent Proteins

Green fluorescent protein (GFP) from the jellyfish Aequorea Victoria is a widely used as the reporter for gene expression[110] and as a marker for biomolecules.[111] GFP has a cylindrical 11-strand β-barrel structure encapsulating the chromophore p-hydroxybenzylideneimidazolidinone **17**. This fluorescent part is formed by autocatalytic condensation, cyclization and oxidation of three consecutive amino acids Ser-Tye-Gly from the 65-67 parent protein. The β-barrel forms a relatively rigid, hydrophobic environment which enhances the quantum yield of the chromophore.[112]

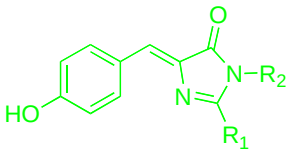

17
GFP chromophore

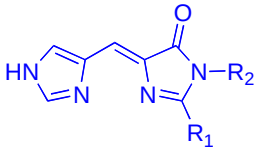

18
BFP chromophore

Photophysical properties of GFP and similar fluorescent proteins can be modified by mutagenesis.[113-115] For instance, the replacement of S66 tyrosine residue in GFP with histidine gives the blue fluorescent protein BFP that contains the chromophore 18. The spectral properties of both native GFP and its mutants are strongly pH dependent in aqueous solutions,[116] suggesting a pH sensing roles and applications in cell compartments. The S65T-GFP chromophore has a pKa of 6.0 and has absorbance maxima at ~382 and 490 nm. The intensities of these peaks change with solution pH; in acidic environments, absorbance at 382 nm predominates, but in basic media, the 490 nm peak predominates.

Two type GFP mutants S65T and F64L/S65T, also termed GFPmul1, have been used for measurement of cell compartments in living cells.[117,118] Similar pH_i values were deduced using GFPmul1 and pH_i indicator BCECF. Another pH sensitive GFP mutant, called enhanced yellow fluorescent protein (EYFP), has a pKa of 7.1, suggesting that this protein is suitable for pH_i measurements in pH range of 6.5 -7.5.

One advantage of fluorescent proteins is that they can be targeted to specific organelles (*e.g.* cytosol, nucleus, mitochondria, trans-Golgi and endoplasmic reticulum) by expressing them in conjugation with appropriate targeting peptides or proteins.[119,120] The fact that they are expressed in cells, rather than imported into them, can also be an advantage in some situations.

8. Conclusions

Probes for pH_i measurements can be used to study pH-dependent biological and

pathological processes, *e.g.* cell death, cancers, and cell proliferation. BCECF and carboxy-SNARF-1 are the two most widely used pH_i indicators since they have desirable photophysical properties for the determination of near neutral intracellular H^+ concentrations. Fluorescein and fluorescein derivatives, *e.g.* carboxyfluorescein, are common pH_i indicators; however, they rapidly leak from the cytosol through cell membranes and this can lead to erroneous pH measurements. HPTS, another widely used intracellular pH probe, tends to be retained inside living cells because it has three sulfonate groups, and it can be applied for measurements of acidic and near neutral pH values. However, HPTS is not cell permeable and must be injected into cells if it is to be observed there. Other organic fluors that have been used as stains in pH measurements have sub-optimal properties in terms of photostabilities or quantum yields. Figure 2.9 gives a "pH spectrum" for the most widely used cellular pH sensitive stains.

Most pH_i measurements are ratiometric. They can be dual excitation (changes at one fluorescent wavelength are observed) or dual emission. Methods based on a single excitation wavelength (dual emission) have a significant advantage insofar as they are most easily used on different equipment (*e.g.* confocal microscopes, plate readers, and flow cytometers) where only one or limited excitation wavelengths are available.

Fluorescent proteins can be used to measure the pH_i of specific cell organelles (*e.g.* the mitochondria, ER and Golgi) after fusing them to targeting entities. This is a big advantage when probing the pH of specific organelles, but it is a significant amount of work to construct suitably genetically encoded cells.

Other methods for pH_i determination are more futuristic. Nanoparticles, *e.g.*

CdSe quantum dots, dye-dopped silica nanoparticles, and dye-labeled bacteriophage can be more photostable and brilliant than small fluorescent organic dyes. However, they tend to be endocytosed into cells and thus they can be trapped in acidic vesicles or endosomes. Moreover, there are more convenient ways to *stain* cells, and the disadvantage of using these indicators as *probes* bioconjugated to proteins is that they tend to be as big or bigger than the protein itself.

In fact, most of the molecules used for measurements of intracellular pH_i values are *stains*, *ie* entities that color the whole cell. The xanthene-BODIPY cassette **16** has the potential to be used as a *probe*, *ie* it can be attached to proteins then imported into cells to track that protein. This is possible because **16** has a higher quantum yield than C.SNARF-1 both in acidic and basic environments, and because it has a functional group to allow bioconjugation. There is clearly an opportunity to devise other pH_i *probes* for tracking spatial and temporal protein function inside live cells and the way pH changes around them.

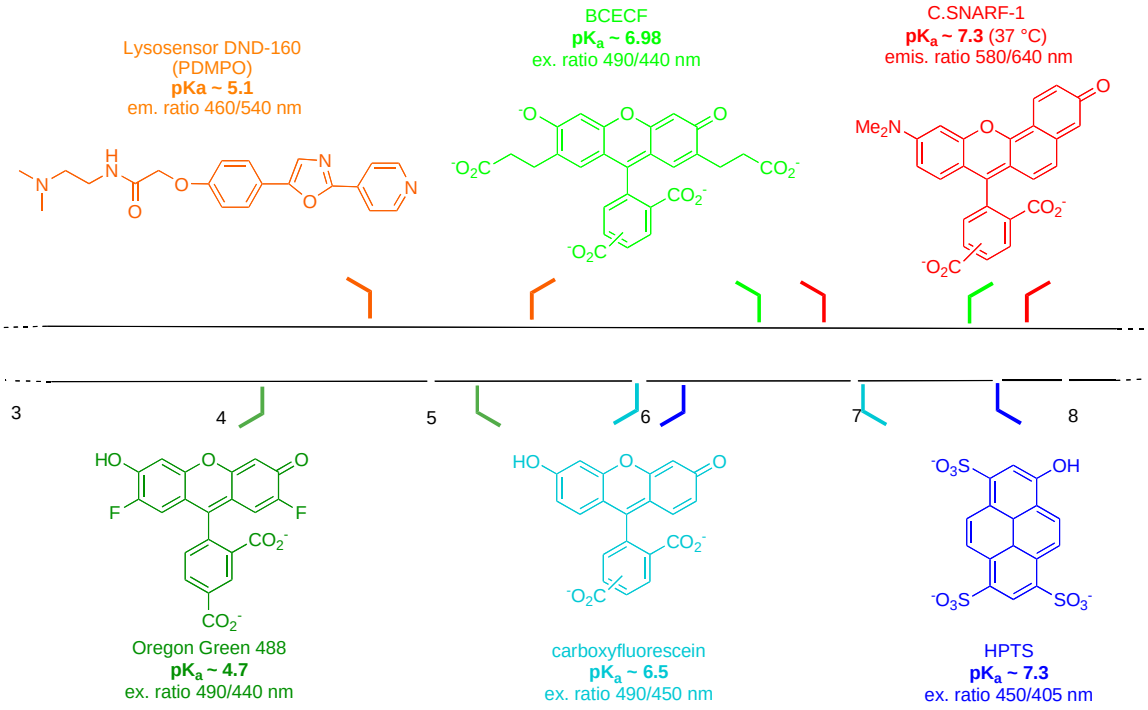

Figure 2.9. pH sensitive ranges of most widely used cellular pH sensitive stains.

B. AN RATIOMETRIC pH REPORTER FOR IMAGING PROTEIN-DYE CONJUGATE IN LIVING CELLS

Of the numerous fluorescent small molecule pH probes that have been reported, only a small number are practical for intracellular imaging of protein-dye conjugates. This is unfortunate because pH changes within cells are indicative of many cellular processes.[9-11,121,122] The most useful probes are the ratiometric ones that absorb UV excitation at a fixed wavelength, and emit at two different fluorescence wavelengths in a pH dependent manner. These probes do not give dark regions in the cell at extreme pH environments, and simply areas where the dye did not permeate are clear. A widely used, commercially available pH-sensitive probe of this type is C.SNARF-1 (Invitrogen Inc.). This communication focuses on the pH probe **16** based on a through-bond energy transfer cassette.[98-100] Data are presented to demonstrate that probe **16** tends to fluoresce with higher quantum yields than SNARF over a physiologically relevant pH range. The ideal pH ranges of operation for **16** and for C.SNARF-1 are complementary (4.0 – 6.5 and 7.0 – 8.0, respectively).

Xanthene (the fluorescent core of fluorescein) is highly emissive at pH values above 7 ($\phi = 0.9$); under those conditions it exists predominantly in the phenolate form. As the pH is lowered to around 6, it transforms into the phenolic state that is somewhat less emissive ($\phi = 0.4$).[51,102,123] The pH probe **16,** which has two xanthene donors and one BODIPY acceptor, was designed to harness changes in the oxidation potentials associated with these protonation states. We hypothesized that the efficiency of the energy transfer from the xanthene donors to the BODIPY core would be governed by

oxidation potentials which in turn depend on the protonation state of the xanthenes, making the whole cassette sensitive to pH changes in the range of cellular physiological processes. Perfect energy transfer, when the probe is excited near the fluorescein absorption maxima (*ca* 495 nm), would give red fluorescence (600 nm). Conversely, if the energy transfer was completely eliminated at certain pH values then the cassette would fluoresces from the xanthene core (*ie* around 520 nm). In either case, *the cassette would remain fluorescent as the cellular pH changes.*

1. Design and Synthesis of the pH Probe

Cassette **16** was prepared via Sonogashira coupling of two 5'-alkynyl fluorescein diacetate molecules **C**[98] with an appropriate diiodo-BODIPY **20**, followed by deprotection of t-butyl ester and acetate esters by pyrolysis and hydrolysis respectively. Compound **16** was designed to have a triethylene glycol linker that would somewhat separate the dye from the protein as well as increase solubility in polar solvents. Iodination of BODIPY **19**, which is synthesized by the Sonogashira coupling reaction of two known fragments BODIPY **B**[124] and terminal alkyne **A**[125], gave diiodo-BODIPY **20** in quantitative yield using conditions developed in Nagano's group.[Yogo, 2005 #10599 The final cassette is slightly water soluble at neutral pH, and more so at pH 8.

Scheme 2.6. Syntheses of pH indicator **16**

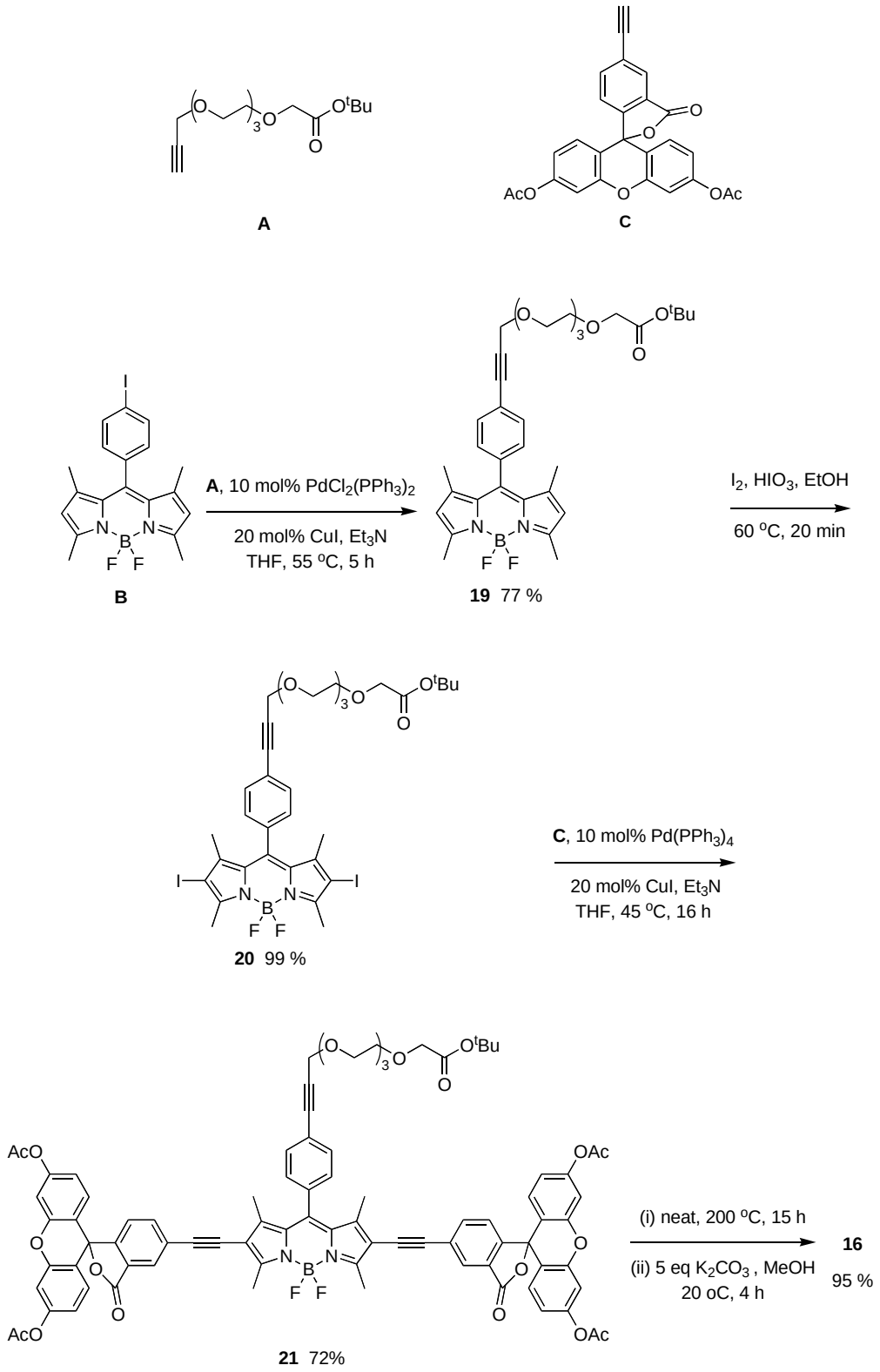

2. Results and Discussion

Absorbance spectra for the conjugate of this probe with bovine serum albumin, *ie* **BSA-16** were measured as a function of pH in aqueous media. The absorption maxima for the acceptor BODIPY part is around 576 nm, and is impervious to pH changes between 4.1 and 7.9. However, the extinction coefficient for the fluorescein part at around 495 nm diminishes markedly from pH 7.9 to 4.1. (Figure 2.10a)

Fluorescence spectra for **BSA-16** as a function of pH are shown in Figure 2.10b. Under neutral and basic conditions, pH 7.0 and 7.9, the probe emits almost exclusively at around 520 nm, *ie* green fluorescence. Conversely, at the acidic extreme, pH 4.1 and 5.0, the cassette fluoresces almost completely red, *ie* from the BODIPY acceptor. The inset of Figure 2.10b shows that the ratio of red-to-green fluorescence for **BSA-16** is highly sensitive to pH in the 4.0 – 6.5 range. A crossover occurs around pH 6.0 where significant red and green fluorescence are observed. If the measurement at pH 7.9 is excluded from consideration in Figure 2.10b (this is justifiable because we do not claim that the probe is sensitive above pH 7), then an isobestic point is apparent. Quantum yield measurements for **BSA-16** at the pH extremes of 4.1 and 8.8 were 0.18 and 0.14. By comparison, literature quantum yields for SNARF are 0.03 (pH 5 – 6) and 0.09 (pH 10 – 12).[Brasselet, 2000 #13204] The fluorescence response of **16** as the pH is cycled between acidic (3.4) and basic media (8.0) demonstrated that the probe is stable to this treatment as shown in Figure 2.11.

a

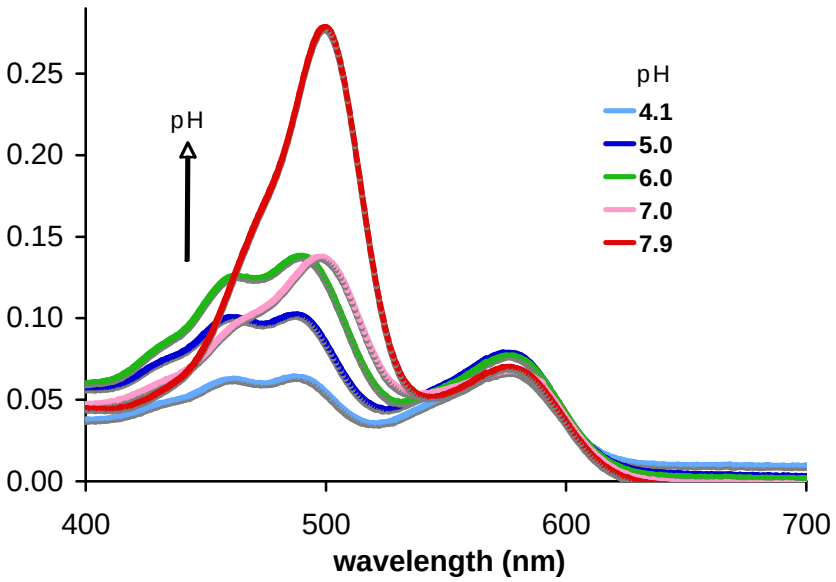

b

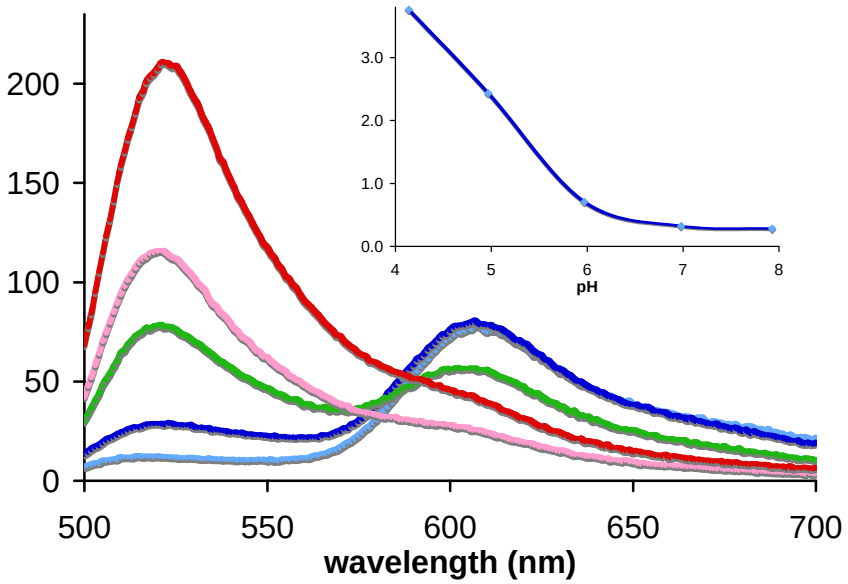

Figure 2.10. Spectroscopy and pH titration of **BSA-16** (0.75×10^{-6} M) in aqueous solutions containing 125 mM KCl, 20 mM NaCl, 0.5 mM $CaCl_2$, 0.5 mM $MgCl_2$, and 25 mM of one of the buffers, including acetate (4.1, 5.0), Mes (6.0), Mops (7.0) and HEPES (7.9). (a) Absorbance spectra; (b) emission spectra with excitation at 488 nm. Inset: Ratio of fluorescence integral for the red channel (575-625 nm) relative to the green channel (503–553 nm) at different pH values.

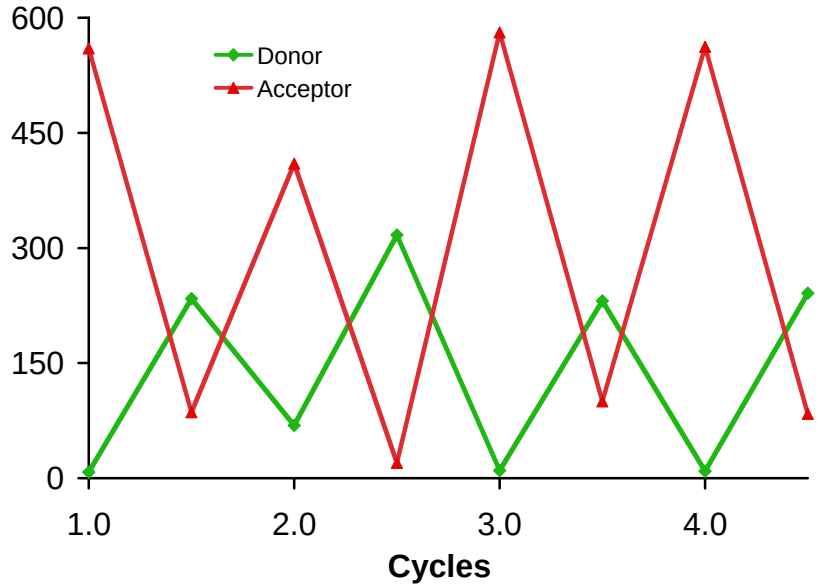

Figure 2.11. Fluorescence responses of **16** (8.0 x 10^{-7} M) to acid/base cycles in 1:1 water-ethanol solutions. The pH values used were 3.8 to 7.2, 6.0 to 8.0, 3.5 to 7.5, and 3.4 to 7.6, corresponding to cycles 1 to 4 respectively. The fluorescence intensities of the donor at 525 nm and acceptor at 600 nm were monitored with excitation at 488 and 565 nm respectively.

Endosomes within cells (pH 5.0 – 5.5) are markedly more acidic than the cytosol.[126] We have observed that when the non-covalently bound carrier peptide "Pep-1"[127] imports dye labeled proteins into COS-7 cells the protein-dye conjugates tend to be encapsulated in endosomes.[103] Consequently, we anticipated that when **BSA-16** was imported into cells using Pep-1, it would localize in endosomes and, in that acidic environment the probe would emit around 600 nm. When **BSA-16** was imported into COS-7 cells using Pep-1 (1 mM protein; 1:20 mol ratio protein:carrier, 37 ºC, 1h), irradiation at 488 nm resulted predominantly in red fluorescence localized in punctuate vesicular structures (Figure 2.12a).

a

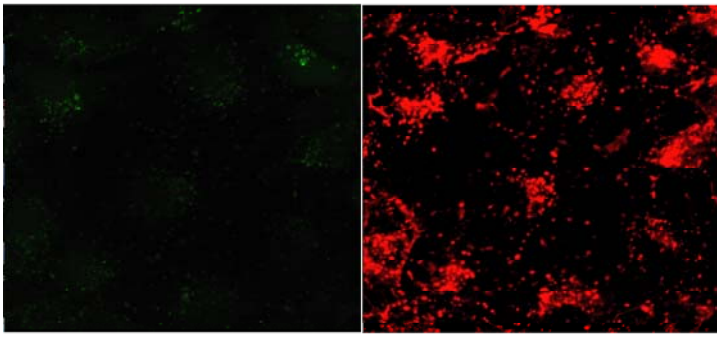

b

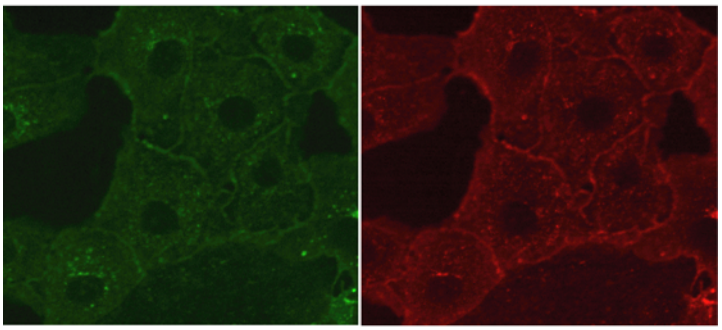

Figure 2.12. Pep-1 mediated cellular uptake of **BSA-16** (1 μM) into COS-7 cells after 1h incubation at (a) 37 °C and (b) 4 °C. The cells were irradiated at 488 nm and fluorescence from donor (503-553 nm) and acceptor (575-625 nm) was detected respectively.

A recent discovery from our laboratories shows that Pep-1 mediated import into COS-7 cells tends to deposit the dye-labeled protein cargoes *into the cytosol when the experiment is performed at 4 °C.*[103] Thus, **BSA-16** under these conditions would be expected to fluoresce with diminished red-to-green ratios. The fluorescence intensity for **BSA-16** is distributed within the cytosol, hence the images in Figure 2.12 appear to be deceptively weak relative to situations (*e.g.* Figure 2.12a) where the probe is concentrated in punctates. A better impression of the relative intensities in the red and green channels for both experiments (37 and 4 °C) after correction for autofluorescence and donor bleed through is shown in the Figure 2.13a.

Quantitative data for pH measurements in cells were obtained via a calibration experiment. Details of this are provided in the supporting information, but the salient feature is that the ionophore nigericin was used to produce "leaky cells" that were then bathed in buffers. This is a standard approach that has been used for the same purpose to calibrate other pH measurements *ex-vivo*.[27,29,61,119] A curve generated with the calibration experiment (Figure 2.13b) was used to determine pH values for the endosomes and the cytosol for the experiments shown in Figure 22. The pH values, obtained from the red/green ratio (R/G = 5.03 and 2.03 at 37 and 4 °C, respectively), were 5.4 and 7.4 and were in good agreement with those expected for such intracellular regions. When C.SNARF-1 AM (not protein conjugated) was imported into COS-7 cells (at 37 and 4 °C) as a lipophilic, hydrolysable form, a pH value of 7.1 was determined (see Figure 2.13c); this is very close to the value cited above for probe **16** (*ie* 7.4).

a

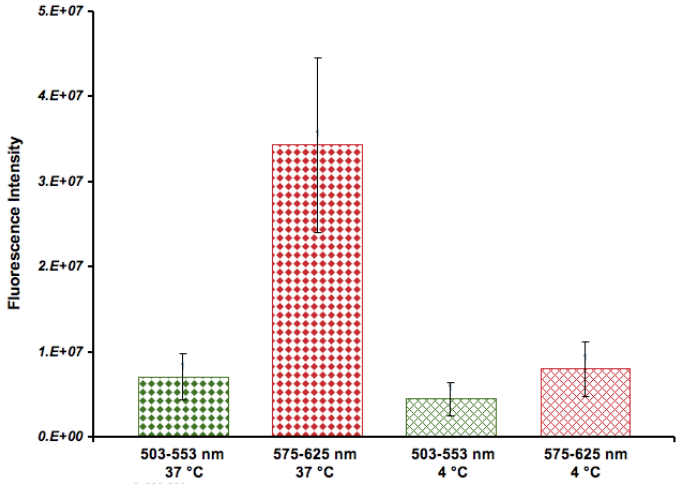

b

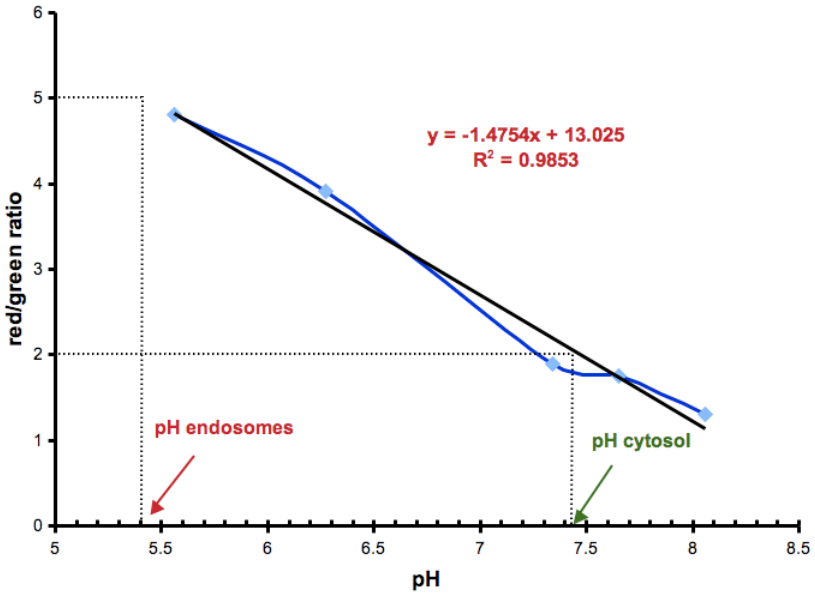

Figure 2.13. (a) Corrected relative intensities observed in the green and red channels for **BSA-16** imported into COS-7 cells at 37 and 4 °C; (b) *Ex-vivo* calibration curve of **BSA-16** with pH values corresponding to those observed within endosomes (red/green = 5.03; import at 37 °C) and the cytosol (red/green = 2.03; import at 4 °C). (c) *Ex-vivo* calibration curve of C.SNARF-1with pH values corresponding to that observed within the cytosol (red/green = 2.03; import at 4 °C). Emission spectra were obtained upon excitation at 530 nm.

c

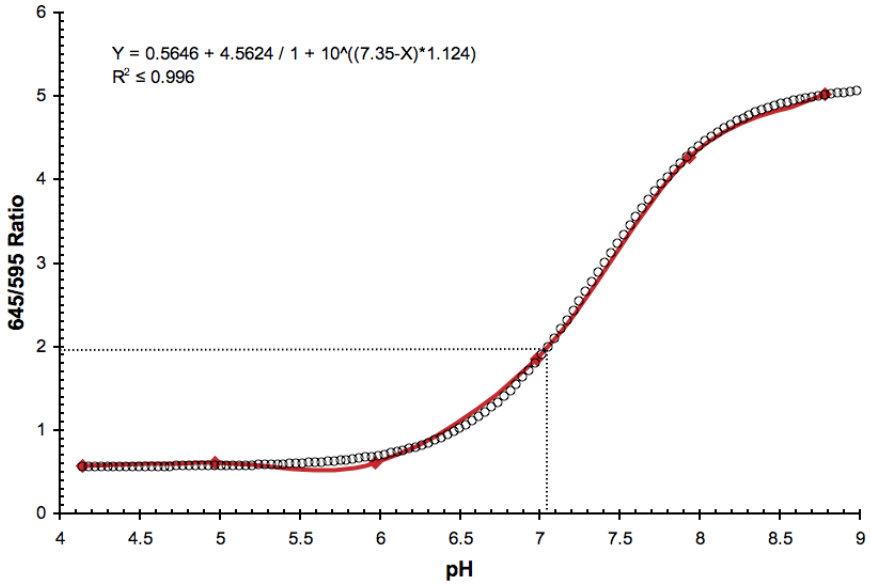

Figure 2.13. Continued.

3. Conclusions

Our interpretation of the C.SNARF-1 literature indicates that this probe is usually used as a non-conjugated form (*i.e.* not attached to proteins); presumably this is because it has a low quantum yield and cannot easily be visualized when present at low concentrations.[128] By contrast, the data presented in this study show that visualization of proteins conjugated to **16** is possible. This is highly significant because the new probe should facilitate observation of *processes* within the cell. Further, the energy transfer approach to pH probes for intracellular imaging has considerable potential for modifications with other pH sensitive donors to give a spectrum of probes with systematically varied pH response transitions. Design of probes of this type requires an understanding of the parameters underlying the fluorescence energy transfer processes. These parameters although not simple, have been elucidated in a parallel study that focuses on the redox behavior of the cassette components; this is to be reported in the following chapter in detail.

C. "STOP-GO" FLUORESCENT PROTON SENSORS BASED ON THROUGH-BOND ENERGY TRANSFER

Intracellular sensing of protons is a non-trivial task; it is often achieved via oblique methods that do not allow direct observation of sensors that fluoresce at different wavelengths according to pH. Such sensors would be preferred relative to ones that switch off completely at certain pH values, because probes of the latter type are not easy to locate inside cells in their "off-state". The former chapter that precedes this work described how a through-bond energy transfer cassette **16**, a derivative of compound **22** in this paper, could be used for intracellular imaging of pH. This probe *does* have a desirable pH-fluorescence profile and it is always in the "on-state". Described here are syntheses of three other cassettes; another one containing two xanthene donors **23**, and two more that each have two BODIPY-based donors, **24** and **25**. Remarkably, both the cassettes with xanthene-based donors, **22** and **23**, fluoresce red under slightly acidic conditions (pH < *ca* 6), and green when the medium is more basic (> *ca* 7), whereas the corresponding cassettes with BODIPY donors, **24** and **25**, give almost complete energy transfer regardless of pH. Further, the quantum yield of the xanthene donor parts in cassettes **22** and **23** were much less (< 0.1) than the unsubstituted reference compound F (0.7 – 0.9). Cassettes **24** and **25**, by contrast, show no significant fluorescence from the donor parts, but the overall quantum yields of the cassettes when excited at the donor (observation of acceptor fluorescence) are high (*ca* 0.6 and 0.9). Electrochemical measurements were performed to help explain the marked differences between the pH-fluorescence profiles of cassettes **22** and **23** relative to **24** and **25**. Relative energies of

the HOMO and LUMOs for the donor and acceptor parts were deduced from the oxidation and reduction potentials of reference compounds representing the donor and acceptor fragments in the BODIPY-donor cassette **24** and the xanthene donor cassette **22** in different protonation states. This led to a unifying hypothesis to explain the pH-fluorescence profiles of these cassettes (Figures 1.17 – 1.19). It is suggested that the concept of designing through-bond energy transfer cassettes wherein orbital levels can be perturbed by analytes, is a relatively new, and potentially useful, approach to sensors for biomedical applications.

1. Introduction

Fluorescent sensors are widely used for detection of protons and metals in several applications, especially intracellular imaging.[129] Types of indicators may be divided into three: (i) ones that are insignificantly fluorescent in the absence of analyte, but are much more emissive when it is present; (ii) the inverse, where fluorescence of the probe is quenched by the analyte; and, (iii) sensors which have observable spectroscopic differences when the analyte is present compared to when it is absent. The third type of sensor is "always on" and this is a significant advantage because it is clear that the probe is present even if the analyte is not (Figure 2.14).

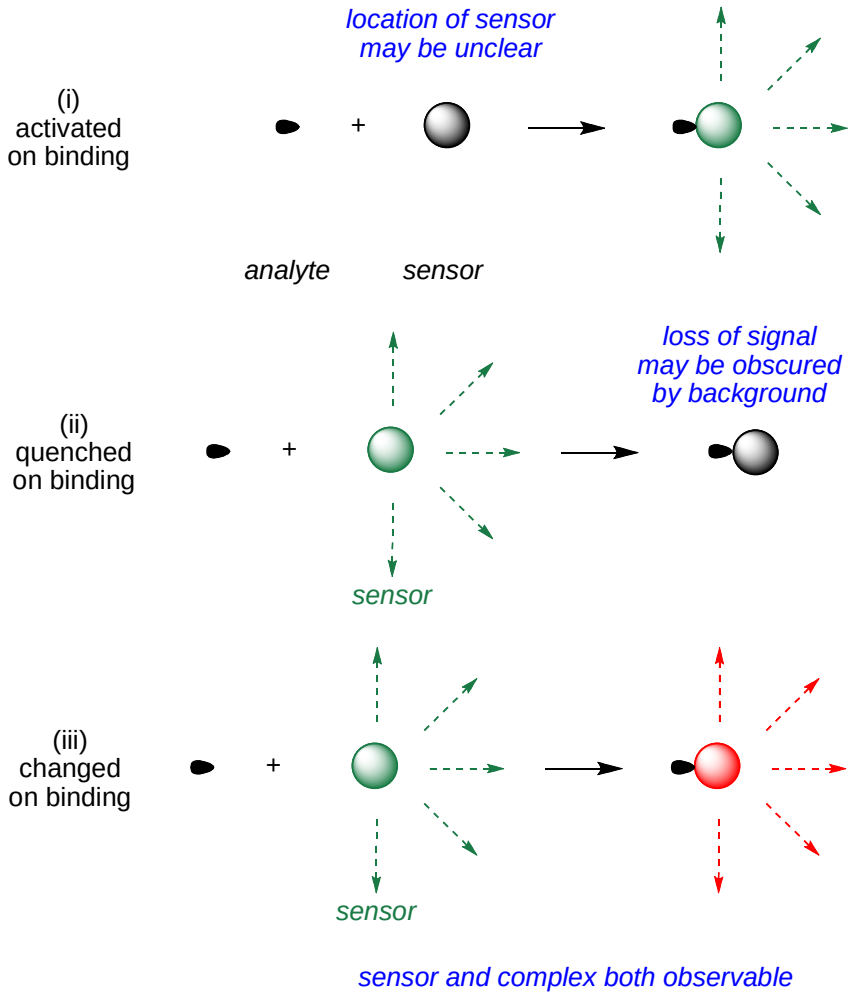

Figure 2.14. Fluorescent sensors may be activated (i) or quenched (ii) by analytes; ones that are "always on" (iii) but change wavelength of fluorescence emissions on binding.

When imaging inside cells, it is hard, and in some cases impossible, to gauge if a probe that is invisible in cells until it is activated [*ie* a type (i) probe as defined above] has permeated to the relevant place. Conversely, probes that are always fluorescent inside cells until they bind an analyte [type (ii)] are of little value because the absence of signal tends not to be observable over background. Probes of the third type outlined above tend to be more useful than the others if they fluoresce at different wavelengths in the presence and in the absence of analyte.[130] To detect protons, however, there are very

few probes of this kind.[115,131-136] Consequently, researchers are forced to rely on much less conspicuous changes in sensors that are "always on". Typical fluorescence based methods to detect intracellular proton concentrations (pH),[29,60,70,82,88,97,104,106,137] for instance, gauge emission intensities as a function of excitation wavelength that change as pH varies.[104] Fluorescein-based probes, for example, can be used in this way. [138-140]However, these sensors *do not change emission wavelength maxima* as the pH is varied; if they did, they would be far easier to use. A simple analogy is that traffic lights based on only a green or a red light would be less effective than ones that switch between the colors.

This paper focuses on how red-green, "stop-go" sensors can be produced using through-bond energy transfer (TBET) cassettes arranged to exploit photoinduced electron transfer (PeT). The background on "TBET cassettes" and "PeT" is as follows. Rapid and efficient through-bond energy transfer may be possible when a fluorescent donor fragment is joined to a fluorescent acceptor part in such a way that the two fragments would be electronically conjugated if they became planar, but they are sterically prevented from doing so.[98-100,141,142] The fact that they cannot easily achieve planarity means that the absorption spectra of the complete system, the "cassette", resembles that of the sum of the donor and acceptor parts. However, the donor part will not fluoresce when it is excited in an efficient TBET cassette; instead the energy will be rapidly transferred to the acceptor fragment that will then fluoresce (Figure 2.15a). Through space energy transfer may occur simultaneously, but the through-bonds routes tends to be faster.[143-145]

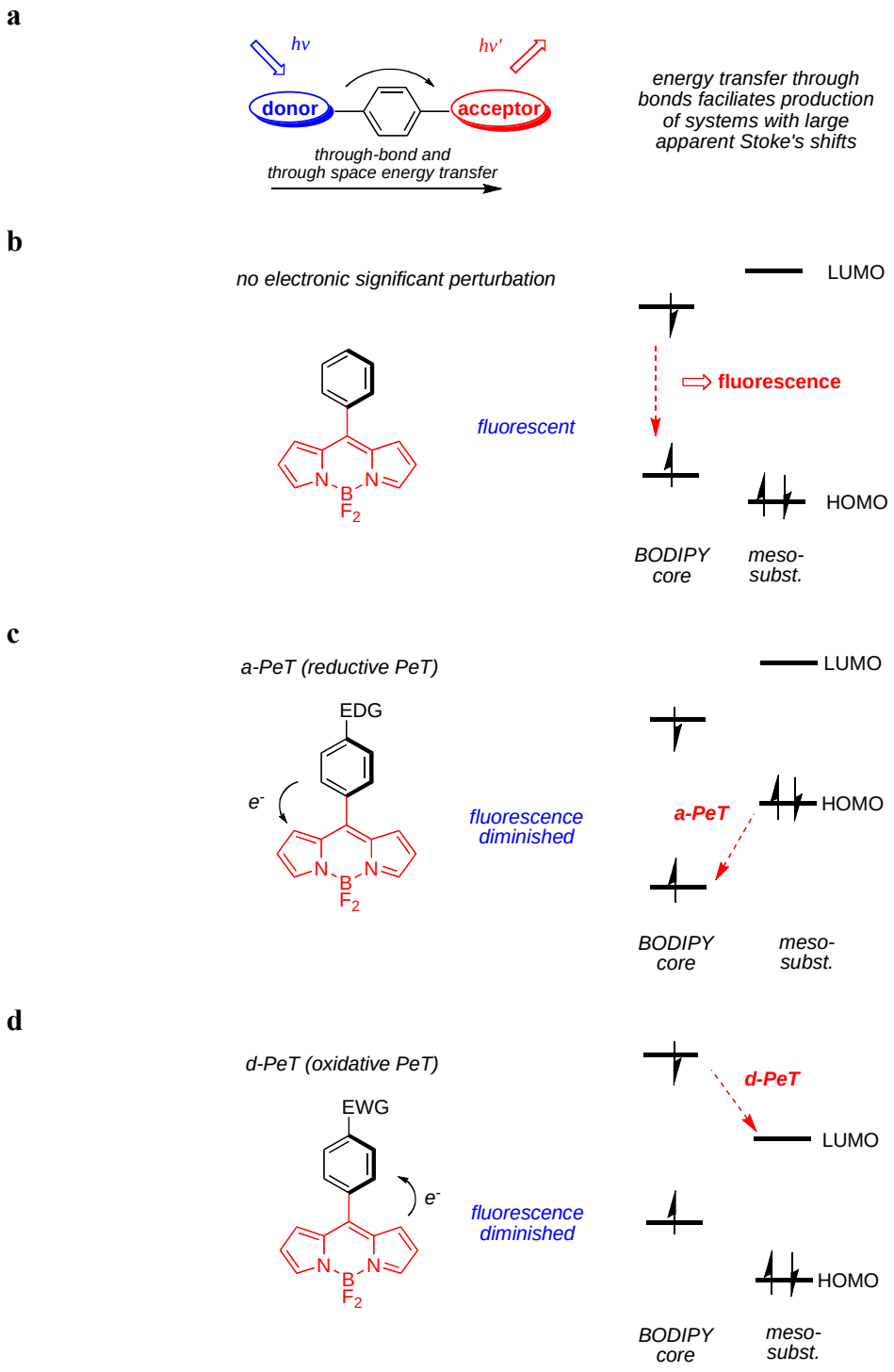

Figure 2.15. The concepts of: (a) through-bond energy transfer cassettes; (b) fluorescent probes not effected by PeT; (c) reductive PeT for a *meso*-substituted BODIPY; and, (d) oxidative PeT for a *meso*-substituted BODIPY.

Photoinduced electron transfer (PeT) generally quenches fluorescence via the two ways that are illustrated for the hypothetical fluorescent 8-aryl (or *meso*-aryl) BODIPY system in Figure 2.15b.[146] 8-Aryl substituents that raise the HOMO of this aromatic part facilitate reduction of the BODIPY core in the excited state; fluorescence of this fragment then becomes impossible (Figure 2.15c). Conversely, 8-aryl substituents that lower its LUMO facilitate oxidation of the BODIPY excited state, and fluorescence of this is also impossible (Figure 2.15d).

Nagano and co-workers recently described PeT in the context of both fluorescein-[147,148] and BODIPY-[149] based dyes. This led them to demonstrate some elegant ways in which PeT could be exploited. Some examples of the application of this strategy include development of probes to sense: singlet oxygen when it undergoes a cycloaddition to a fluorescein *meso*-substituent,[150] nitric oxide,[151,152] nitrite,[153] nitronium ions that nitrate BODIPY *meso*-aryl substituents,[154] and thiols when they add to a 2'-*N*-maleimide on an 8-aryl BODIPY.[155] More recently, Dan Yang and co-workers have devised a hypochlorous acid probe that responds by oxidizing a 8-(4'-methoxyphenol)BODIPY substituent to a quinone.[156] Most of this work features oxidation by analytes causing "on-off" responses in sensors of type (i) and (ii) as defined above. A possible exception is the thiol probe that probably functions by changing the electron donating properties of the substituents near a BODIPY core.

An application of probe **16** to monitoring intracellular pH has already been demonstrated in the last chapter. That work shows this to be a "stop-go" probe that

fluoresces red at pH values less than about 6.5, and green at pH values above about 7.0 and, significantly, it is always on.

Data shown in this paper features the four TBET cassettes **22** – **25**. The research described here includes: (i) syntheses of these four TBET cassettes; (ii) the observation that the change of the *meso*-substituent on the central BODIPY [acceptor] fragment represented by the difference between cassettes **22** and **23** and between **24** and **25** is largely inconsequential to their fluorescence *vs* pH profiles indicating that PeT between the acceptors and *meso*-substituents does not play a significant role in the photophysical properties of the cassettes; (iii) the observation that the change of donor fragment from xanthene to BODIPY represented by the structural differences between **22** or **23**, and **24** or **25** have *profound* differences on the fluorescence characteristics of these cassettes; and, (iv) electrochemical data that can be interpreted to comprehensively explain these differences. We feel this work is significant because it highlights the underlying electronic properties of TBET cassettes **22** and **23** that make them type (iii) stop-go, pH sensors. One may conclude that it is reasonable this same strategy could be used to prepare "always on", stop-go sensors for other analytes, and this would be particularly important in intracellular imaging.

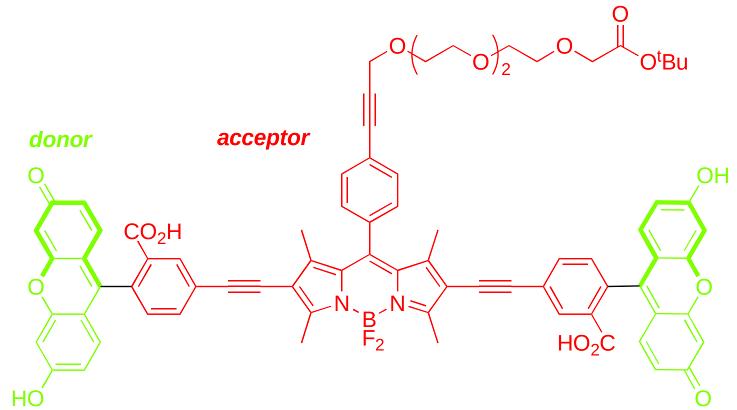

22

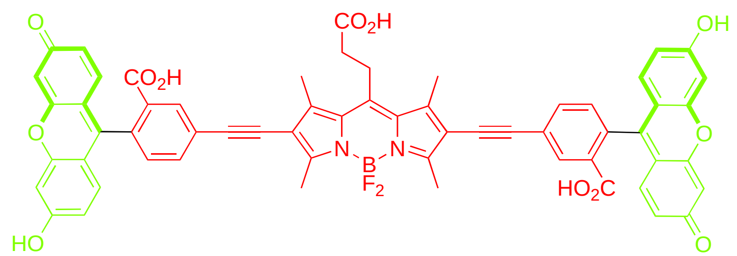

23

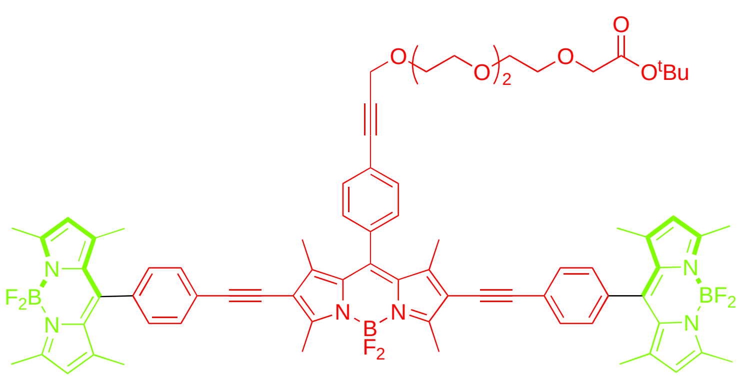

24

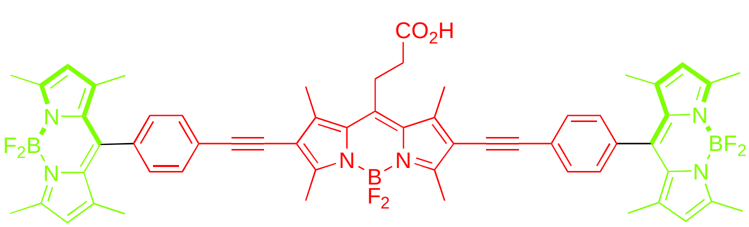

25

2. Syntheses of the Cassettes 22 - 25

Two key diiodinated BODIPY intermediates, **20** and **27**, were prepared to make the cassettes featured in this paper. Synthesis of the first compound **20** is shown in Scheme 2.6. The second, compound **25** (Scheme 2.7), was formed via a route that is analogous to one used for a homolog formed from glutaric anhydride.[157] Synthons **20** and **27** lead to cassettes with different *meso* substituents: aryl and alkyl functionalities. A minor objective of this study was to determine if these differences would have any significant effects on the electronic spectra of these cassettes as explained above; in fact, they did not (*see below*).

Scheme 2.7. Syntheses of pivotal diiodinated synthons BODIPY **27**.

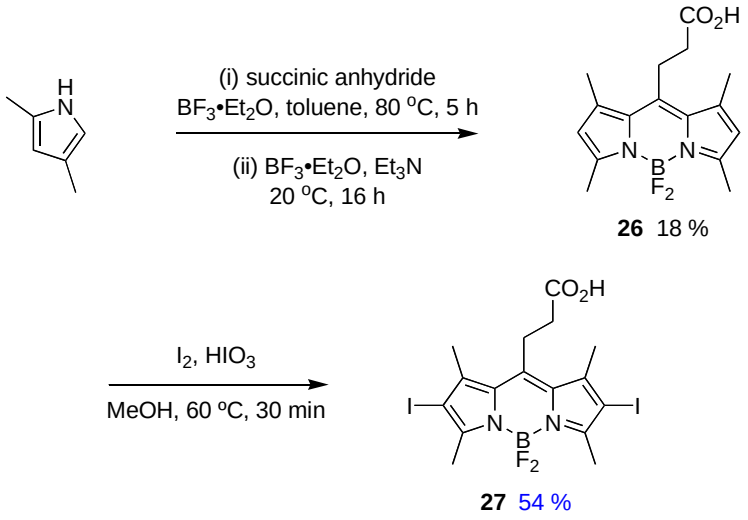

Sonogashira reactions[158,159] were used to assemble the cassettes from the acceptor components **20** and **27**, and the fluorescein-based and BODIPY-based donor components **C**[100,160,161] and **D**[56] (Scheme 2.8). The diacetate intermediate **21** is of some

importance because this compound has been shown to be cell permeable, and hydrolyzes in the cytosol to give green fluorescence. (Data are not shown here) The fluorescein-based cassettes **22** and **23** are soluble in lower alcohol solvents giving pink solutions.

Scheme 2.8. Syntheses of cassettes: **a**, **22**; and, **b, 24**.

a

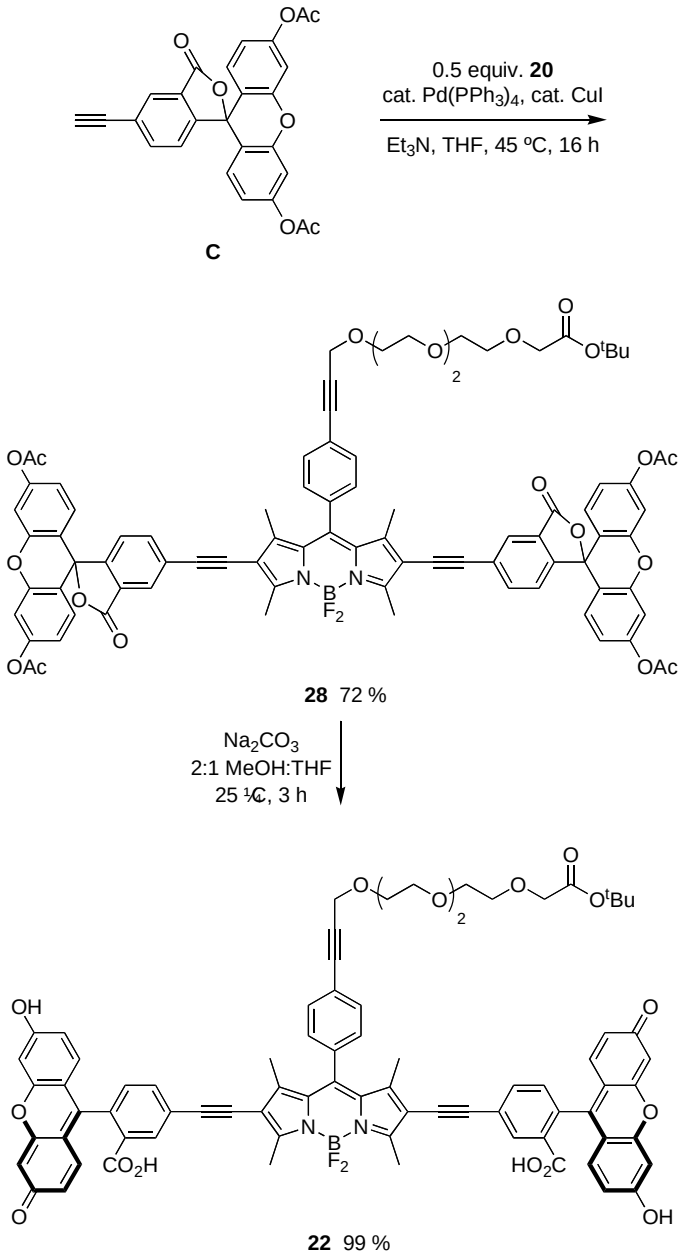

Scheme 2.8. Continued.

b

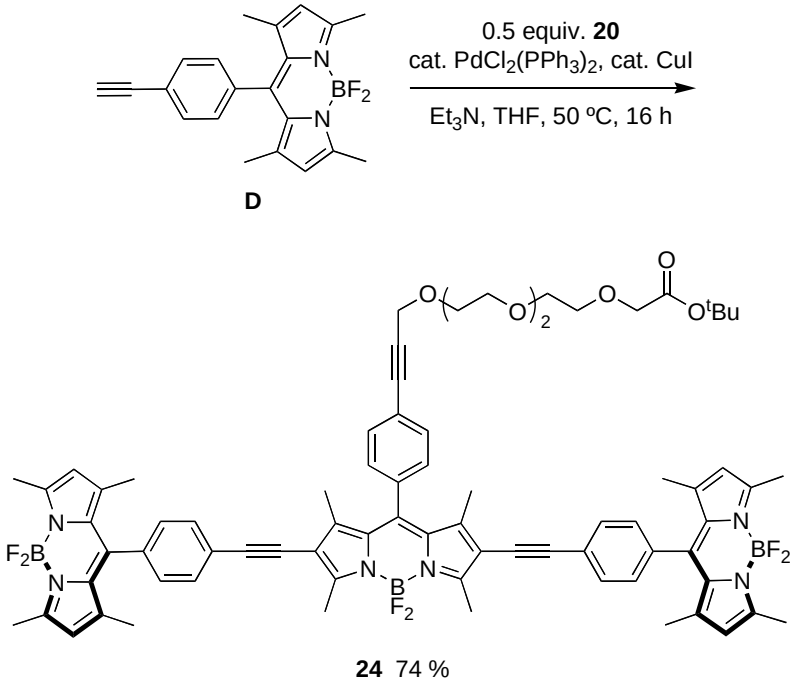

24 74 %

Cassette **23** (Scheme 2.9) was difficult to purify. Flash chromatography did not give pure material, but the compound was isolated via preparative reverse phase HPLC in 4 % yield. Both cassettes **24** and **25** are soluble in lipophilic solvents like CH_2Cl_2, and give strongly colored pink or red solutions.

Scheme 2.9. Syntheses of cassettes: **a**, **23**; and, **b, 25**.

a

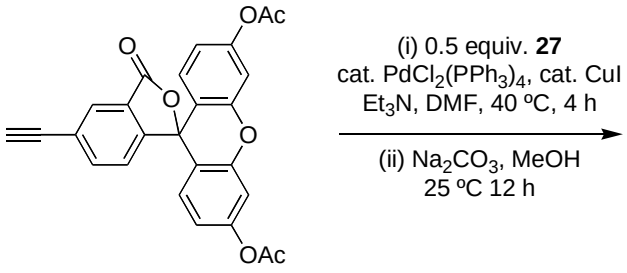

C

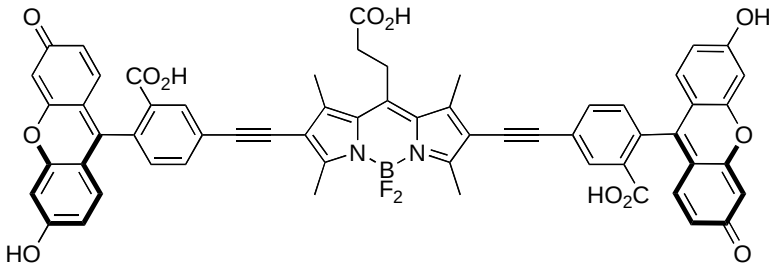

23 4 %

b

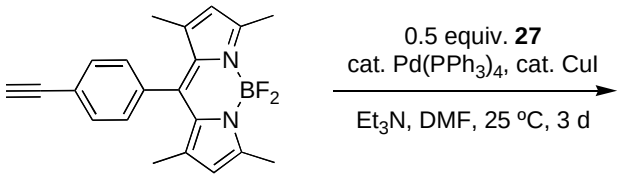

D

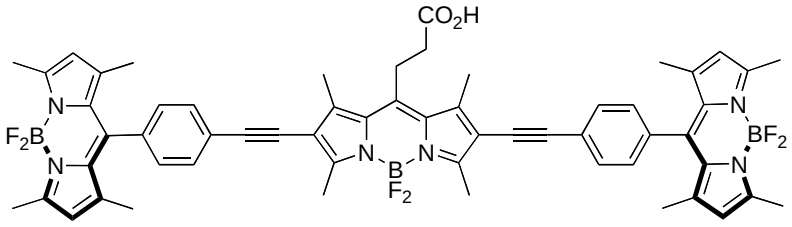

25 53 %

During the course of these studies the methyl ester of cassette **29** was also generated, and crystallized for single crystal X-ray diffraction studies. The solid state structure of this molecule (Figure 2.16) demonstrates how the BODIPY donor fragments

can rest in conformations that are perpendicular to the acceptor part. In part, it is this molecular twist that differentiates cassettes from planar dyes consisting of a single conjugated chromophore. Interestingly, the molecule appears to "sag" around the central BODIPY fragment; this is because the alkyne parts are not exactly in the same plane. In the solid state this degree of sagging can be quantitated from the angle formed between two lines that connect the two carbons of each alkyne. An ideally linear arrangement would give a 180° angle; in fact, the observed angle was 168.2 degrees. This parameter may have some relevance because if the angle were 180° and rigid then the transition dipoles of the BODIPY acceptor and the two donor fragments (which are aligned with their long axes)[144] would be exactly perpendicular in any conformation about the alkyne. In that orientation there can be no dipole-dipole coupling hence fluorescence resonance energy transfer (FRET) could not occur. The fact that the molecule is not perfectly linear means that FRET cannot be completely excluded because rotation about the alkyne bond could place the BODIPY donors in conformations in which weak dipole-dipole coupling could occur. However, the "sag-angle" is small, and conformations that allow dipole-dipole coupling also take the phenyl group out of conjugation with the rest of the acceptor; consequently, energy transfer via this mechanism[162] is unfavorable.

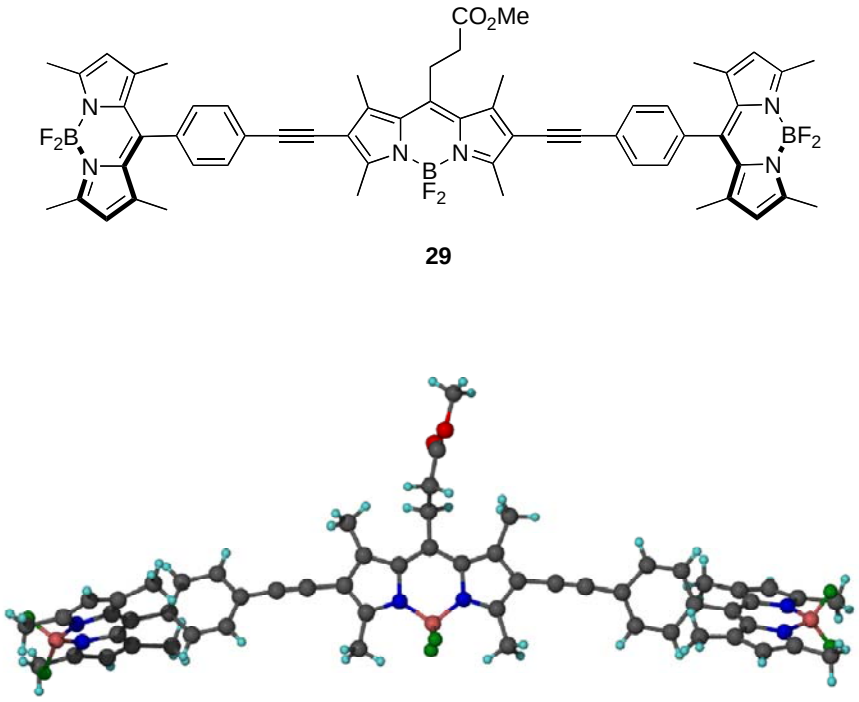

29

Figure 2.16. Single crystal X-ray structure of **29**.

An important set of new acceptor fragments **30 - 33** and known BODIPY **E** and xanthene **F** reference compounds were also generated for this study. Photophysical and electrochemical properties in cassettes tend to be accurately represented by the individual donor and acceptor fragments.[163] Consequently, electrochemical studies were performed on these constituents, thus avoiding the need for destructive experiments (electrochemistry) on the valuable cassette samples. All these acceptors **30 - 33** were synthesized by Sonogashira coupling reactions of **20** and **27** with the corresponding phenyl alkynes. Detailed syntheses of the new materials are outlined in the supporting material.

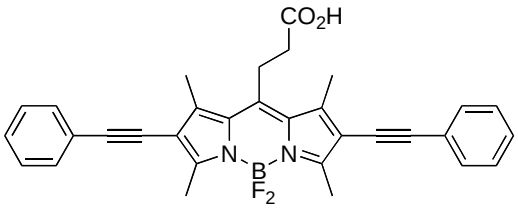

30
an acceptor mimic

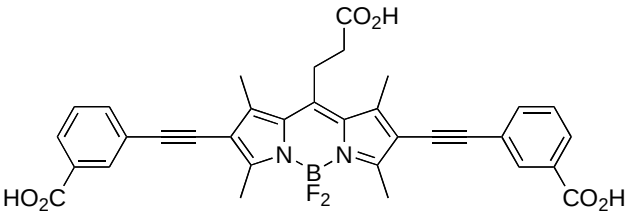

31
an acceptor mimic

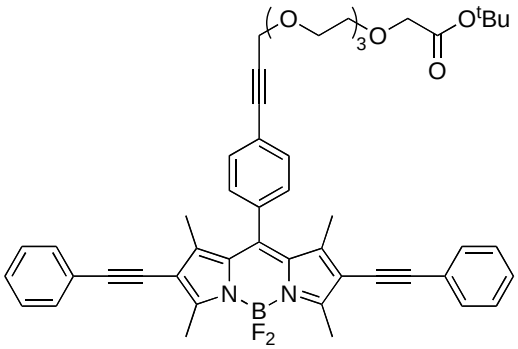

32
an acceptor mimic

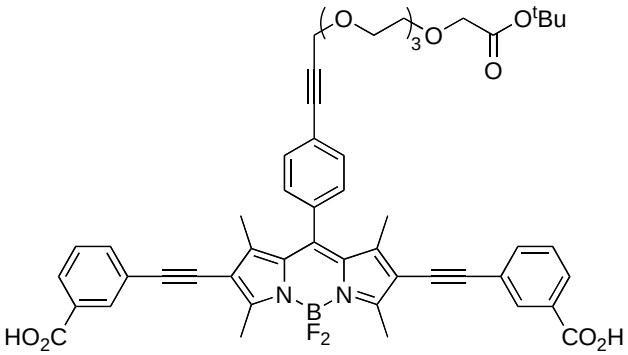

33
an acceptor mimic

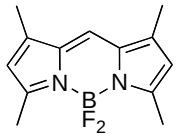

E

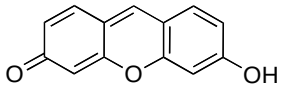

F

donor fragments

3. Results and Discussion

3.1. Photophysical Properties.

Salient photophysical properties of the cassettes are shown in Table 2.1. The key feature of these is that the acceptor fragment is formed by the 2,6-(alkyne-aryl) substituents because these impose a dramatic red-shift on the absorbance and fluorescence properties of that BODIPY core; Ziessel and co-workers have also observed this.[159] The fluorescein and BODIPY donor parts exhibit characteristically large extinction coefficients, and absorb/fluoresce at wavelengths that are characteristic of the free dye fragments (see Table 2.2 below).

Through-bond energy transfer cassettes are usually designed to absorb light at the donor excitation wavelength, relay it to the acceptor part, then emit fluorescence from there. The term "energy transfer efficiency" (ETE %) quantifies this, and we define it as follows:

$$\text{ETE \%} = \frac{\text{quantum yield of the acceptor fragment in the cassette excited at the donor}}{\text{quantum yield of the acceptor fragment in the cassette excited at the acceptor}} \times 100$$

ETE % is a measure of the quantum yield of the cassette when irradiated at the donor. It reflects the extent of energy transfer including the negative effects of non-radiative loss in the transfer process. The product of the extinction coefficient of the

donor in the cassette and the ETE give a measure of the brightness of the acceptor in the system.

Values of the ETE % for the cassettes **22** – **25** are shown in Table 2.1. Several important observations are clear. First, the fluorescein-based cassettes **22** and **23** have moderate ETE values in the absence of base, but not when Bu_4NOH is added. Second, the BODIPY-based cassettes **24** and **25** have excellent ETE values, and these are *not* influenced by added base. This contrast between the cassettes with fluorescein- and BODIPY-based donors is the key observation presented in this paper.

Table 2.1. Photophysical properties of **22** - **25** in 1:1 ethanol:CH_2Cl_2.

		absorption[b]		fluorescence[c]					
cmpd	base[a]	$\lambda_{max\ D}$(nm) / log ε	$\lambda_{max\ A}$(nm) / log ε	$\lambda_{max\ D}$ (nm)	$\lambda_{max\ A}$ (nm)	ϕ_A excited at A[d]	ϕ_A excited at D[e,j]	ETE (%)[f]	ϕ_{donor}[g]
22	-	505 / 4.73	575 / 4.55	521	600	0.30[i]	0.15	51	0.05
22	+	505 / 5.06	578 / 4.48	529	-	0.01[i]	-	< 5	0.09
23	-	506 / 4.57	560 / 4.29	528	579	0.24[j]	0.09	38	0.07
23	+	505 / 5.13	561 / 4.45	529	-	0.01[j]	-	< 5	0.08
24	-	502 / 5.14	566 / 4.82	513	606	0.62[i]	0.58	93	-[h]
24	+	502 / 5.13	566 / 4.82	516	604	0.66[i]	0.60	92	-[h]
25	-	502 / 5.03	561 / 4.67	521	588	0.84[j]	0.79	94	-[h]
25	+	502 / 5.06	560 / 4.72	515	588	0.93[j]	0.85	91	-[h]

[a] with $^nBu_4NOH$ at a concentration of 8 x 10^{-5} M. [b] At 1 x 10^{-5} M. A acceptor, D donor [c] At 1 x 10^{-6} M. [d] Quantum yield of acceptor when excited at the acceptor. [e] Quantum yield of acceptor while excited at the donor. [f] Energy transfer efficiency calculated with the quantum yield of the acceptor with excitation at donor divided by that with excitation at the acceptor. [g] Fluorescein (ϕ = 0.92 in 0.1 M NaOH)[164] was used as a standard. [h] Donors in these cassettes show no significant fluorescence emission. [i] Rhodamine 101 (ϕ = 1.00 in EtOH)[165] was used as a standard. [j] Rhodamine B (ϕ = 0.97 in EtOH)[164] was used as a standard.

Effects of base on the cassettes are probably best visualized by considering their absorbance and fluorescence spectra (Figures 1.17 and 1.18). Addition of $^{n}Bu_4NOH$ to cassettes **22** and **23** increases the absorption corresponding to the fluorescein component relative to that from the BODIPY acceptor part. This is logical because addition of base forces the fluorescein donor into its ring-opened phenolate carboxylate form. Absorbance spectra of cassettes **24** and **25** are almost completely insensitive to base, as would be predicted since the electronic spectra of BODIPY dyes are not significantly affected by pH.

a *cassette **22** (fluorescein donor)*

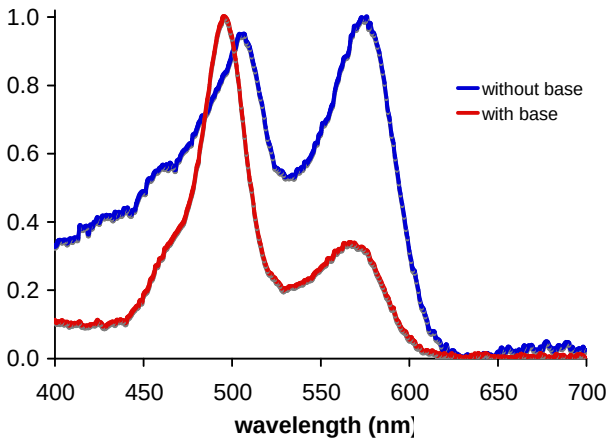

Figure 2.17. (a – d) Normalized absorption spectra of cassettes **22** - **25** (at 1 x 10^{-5} M conc in 1:1 ethanol/CH_2Cl_2); throughout, spectra recorded without added bases are shown in blue, and with $^{n}Bu_4NOH$ (concentration of 1 x 10^{-4} M) are shown in red.

b cassette **23** (fluorescein donor)

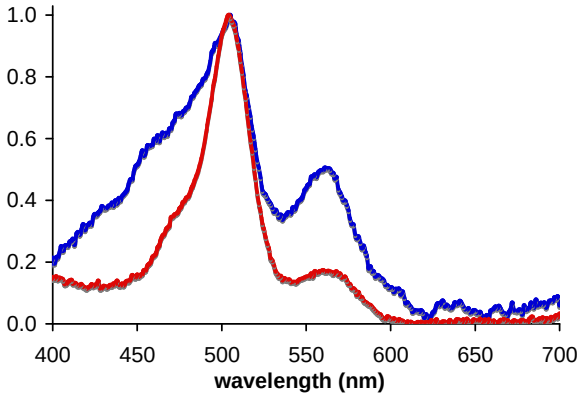

c cassette **24** (BODIPY donor)

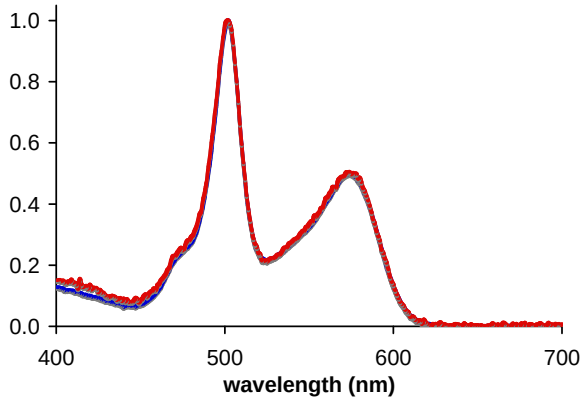

d cassette **25** (BODIPY donor)

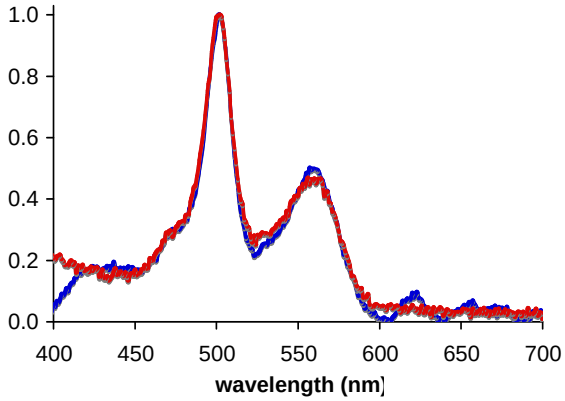

Figure 2.17. Continued.

In the absence of base, excitation of the fluorescein donor of cassettes **22** and **23** leads to significant fluorescence from the BODIPY acceptor. However, no significant fluorescence is observed from the BODIPY part when base is added to the same solutions (Figure 2.18a and b). Conversely, addition of base has no significant effect on the extent of energy transfer for the cassettes **24** and **25** that have BODIPY donors. The conclusion from these experiments is that in 1:1 ethanol/CH_2Cl_2 the fluorescein donor parts of cassettes **22** and **23** are, at least partially, protonated, and energy transfer to the BODIPY acceptor is possible in this form. This energy transfer is quenched when the fluorescein donors are completely deprotonated. Cassettes **24** and **25** have BODIPY, not fluorescein, donor parts, but they are otherwise identical to **22** and **23**. These systems are not affected by base indicating that the pH sensitivity at the fluorescein donor makes these cassettes sensitive to treatment with acids or bases.

a cassette **22** (fluorescein donor)

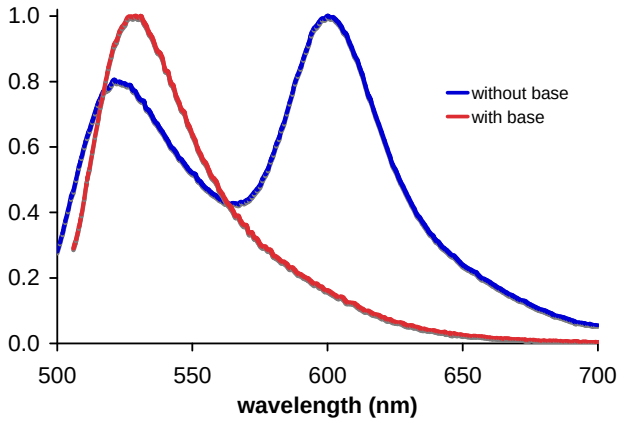

Figure 2.18. (a – d) Fluorescence spectra of cassettes **22** - **25** (1 x 10^{-6} M in 1:1 ethanol/CH_2Cl_2); throughout, spectra recorded without added base are shown in blue, and with $^{n}Bu_4NOH$ (concentration of 1 x 10^{-4} M) are shown in red.

b cassette **23** (fluorescein donor)

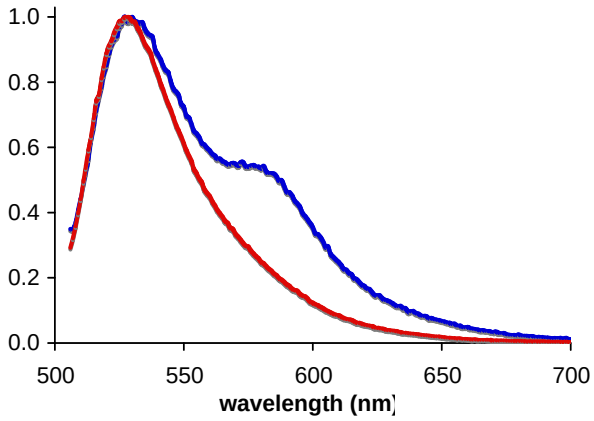

c cassette **24** (BODIPY donor)

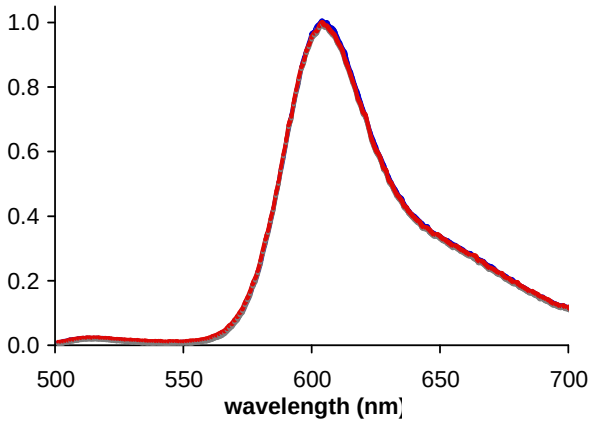

d cassette **25** (BODIPY donor)

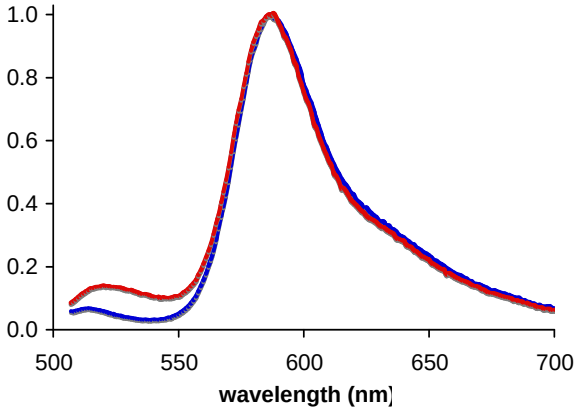

Figure 2.18. Continued.

Table 2.3 shows photophysical properties for the reference compounds **30** – **33**, **E** and **F**. A striking observation from this data is that *none of the building blocks that were assembled to give cassettes **22** – **25** have fluorescence characteristics that are significantly changed by added base.* The largest change in quantum yield is seen for the dicarboxylate **31** and xanthene **F**: for these compounds a 25 % increase in the presence of base. There are no appreciable shifts in λ_{abs}, λ_{em}, or even the peak width values when these fragments are compared without and with base.

Table 2.2. Photophysical properties of reference compounds in 1:1 ethanol/CH_2Cl_2. Absorption spectra taken at 1 x 10^{-5} M. Emission spectra taken at 1 x 10^{-6} M.

cmpd	base[b]	λ_{abs} (nm) / log ε	λ_{em} (nm)	fwhm (nm)	ϕ[a]
30	_	560 / 4.41	587	41	0.72
30	+	559 / 4.42	587	41	0.71
31	_	565 / 3.94	593	46	0.46
31	+	563 / 4.00	592	43	0.61
32	_	574 / 4.50	606	44	0.52
32	+	574 / 4.50	605	53	0.54
33	_	573 / 4.36	612	53	0.42
33	+	578 / 4.40	613	52	0.44
E	_	506 / 4.94	511	16	0.98
E	+	506 / 4.94	511	17	0.90
F	_	508 / 4.87	517	26	0.76
F	+	508 / 5.04	517	25	0.95

[a] Rhodamine 101 (ϕ = 1.0 in ethanol)[165] was the standard for **30** - **33** and fluorescein (ϕ = 0.92 in 0.1 M NaOH)[164] for **E** and **F**. [b] with Bu_4NOH at a concentration of 8 x 10^{-5} M.

None of the reference compounds can undergo changes like that shown in equilibrium 1, but this has been comprehensively studied for fluorescein in aqueous

media.[123] These data show that the quantum yield of fluorescein is highest in its dianion state. However, Table 2.2 shows that the quantum yield of the donor part in the fluorescein-based cassettes **22** and **23** are less than 0.1, with or without base. Without base there is significant energy transfer to the acceptor, so some quantum yield reduction is anticipated. With base, however, less of the energy transferred between the donor and acceptor is emitted as acceptor fluorescence. Further, the xanthene quantum yields in the cassettes are much less than for fluorescein in any of the accessible protonation states, or for the xanthene **F**. *Integration of the fluorescein donors in cassettes **22** and **23** reduces their quantum yields relative to the parent fragments.*

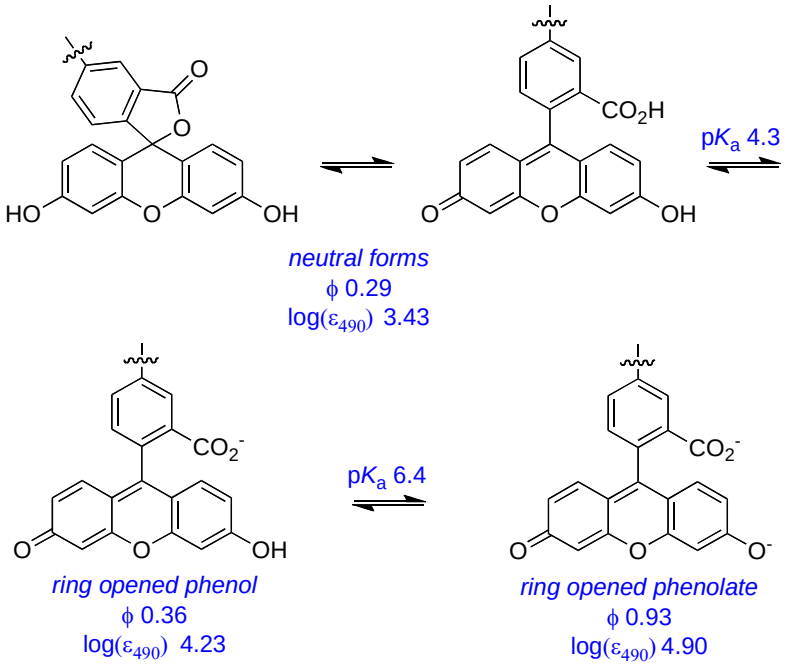

equilibrium 1

3.2. Electrochemical Studies

Oxidation and reduction potentials were measured for the reference fragments **E**, **F**, **32** – **33**, and for cassette **24** relative to the ferrocene/ferrocinium couple. BODIPY **32** shows a reversible reduction wave, while for **33** and **E** the wave is *quasi*-reversible for the first reduction events. For **F** and $\mathbf{F}_{Na}$ the first reduction wave is irreversible. The oxidation events for all compounds are irreversible. In a method similar to the one used by Reynolds *et al.*[166] the ferrocene/ferrocenium couple in Volts is estimated to an orbital level of 5.15 eV and 5.16 eV relative to vacuum in DMF and CH_2Cl_2, respectively.[167,168] Thus energy levels of HOMO and LUMOs can be pegged relative to this reference point. The same data was acquired for compounds **30** and **31** (see supporting information).

Table 2.3. Electrochemical data for reference compounds **E**, **F**, **32** – **33**, and cassette **24**. Cyclic voltammograms were recorded using a glassy carbon working electrode (A = 0.071 cm^2) referenced to Fc/Fc^+ and a Pt counter electrode at a scan rate of 200 mV/s. All potentials are reported vs. Fc/Fc+ and all HOMO and LUMO energies are derived from electrochemical results based on Fc/Fc^+ = 5.15 eV (DMF) and 5.16 eV (CH_2Cl_2) vs vacuum. All solvents were flushed with $Ar_{(g)}$ before use.

Cmpd	$E_{onset,ox}$ (V)	HOMO (eV)	$E_{onset,red}$ (V)	LUMO (eV)	E_g (eV)
E[a]	+1.22	6.38	-1.43	3.73	2.65
F[b]	+0.72	5.87	-1.25	3.90	1.97
$\mathbf{F}_{Na}$[b, d]	+0.25	5.40	-1.89	3.26	2.14
32[a]	+1.21	6.37	-1.12	4.04	2.33
33[b]	+0.79	5.94	-1.09	4.06	1.88
33[c]	+0.80	5.95	-1.12	4.03	1.92
24[a]	+1.27	6.43	-1.10	4.06	2.37
			-1.36	3.80	2.63

(a) In CH_2Cl_2. (b) In DMF. (c) In DMF and 0.1 M pyridine. (d) Xanthene was first reacted with NaOH to obtain the sodium salt.

Figure 2.19a plots HOMO and LUMO energy levels for the reference BODIPY **E** and the acceptor mimic **32** that represent cassette **24** (BODIPY donor and acceptor). The HOMO level of the acceptor part is marginally higher than that of the donor, and the energy transfer efficiency observed (ETE) is high (93 %). This could be due to two single electron transfer processes as shown in Figure 2.19b that are both favorable because they move electrons from higher to lower orbital levels. The net effect is that the compound fluoresces strongly from the acceptor, and the donor fluorescence is almost completely quenched.

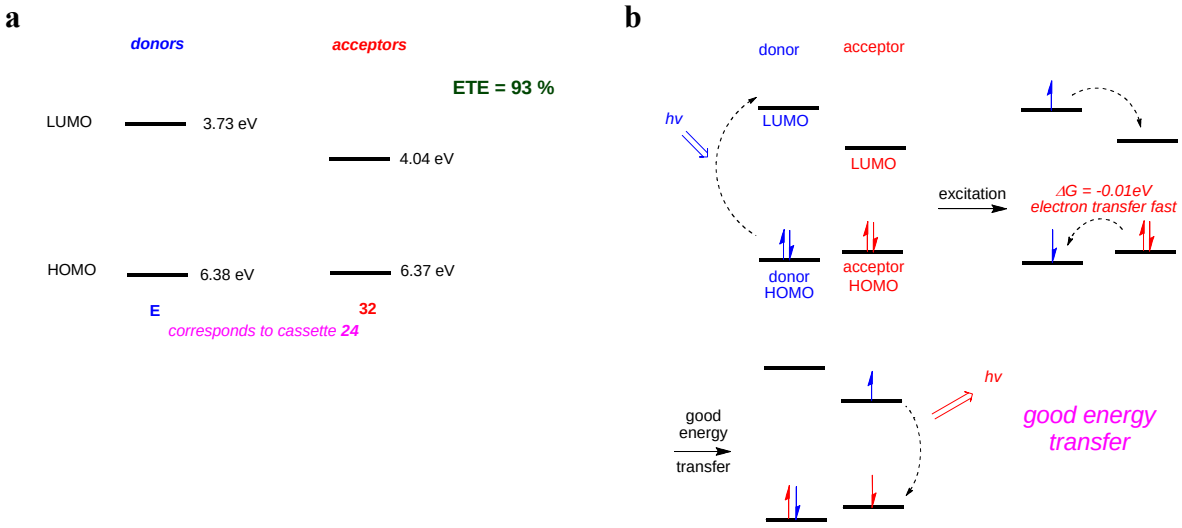

Figure 2.19. (a) HOMO and LUMO levels of the reference compounds representing cassette **24**; and, (b) rationale for the good energy transfer and strong fluorescence of the acceptor.

Fragments of cassette **22** under neutral conditions are represented by the reference compounds **F** (protonated on xanthene) and **33** (Figure 2.20). Here we suggest the situation is similar to that depicted in Figure 2.19, but with one key difference: the HOMO energy level for the acceptor is marginally below that of the donor. Electron transfer from the acceptor to the donor becomes slow while that in the reverse direction

is fast. This would explain the attenuated energy transfer efficiency (51 %) and the fact that the donor also fluoresces, but with a low efficiency because it is quenched by oxidative PeT.

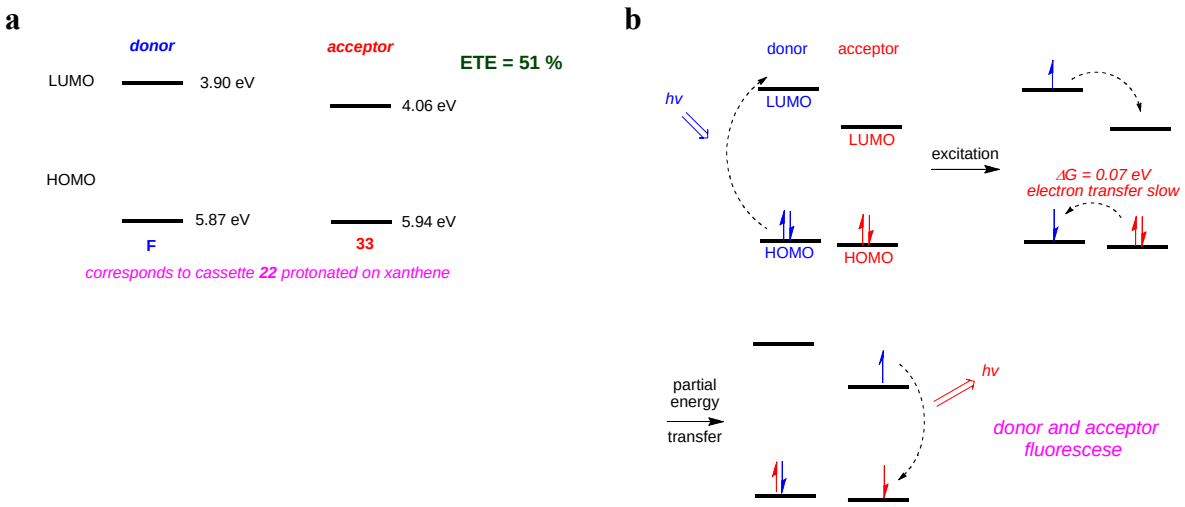

Figure 2.20. (a) HOMO and LUMO levels of the reference compounds representing cassette **22** under neutral conditions; and, (b) rationale for the partial energy transfer.

Figure 2.21 depicts the situation for cassette **22** under basic conditions. Deprotonation of the xanthene fragment (represented by **F-Na**) would be expected to elevate the HOMO/LUMO orbital levels for the donor, and, in actuality, this is supported by the electrochemical data. Electrons cannot be transferred from the highest filled (2*e*) orbital of the acceptor to the donor hence fluorescence emission is observed only from the donor part. The quantum yield of the donor is diminished (from 0.95 to 0.09) because of electron transfer from the donor excited state to the acceptor (Figure 2.21b).

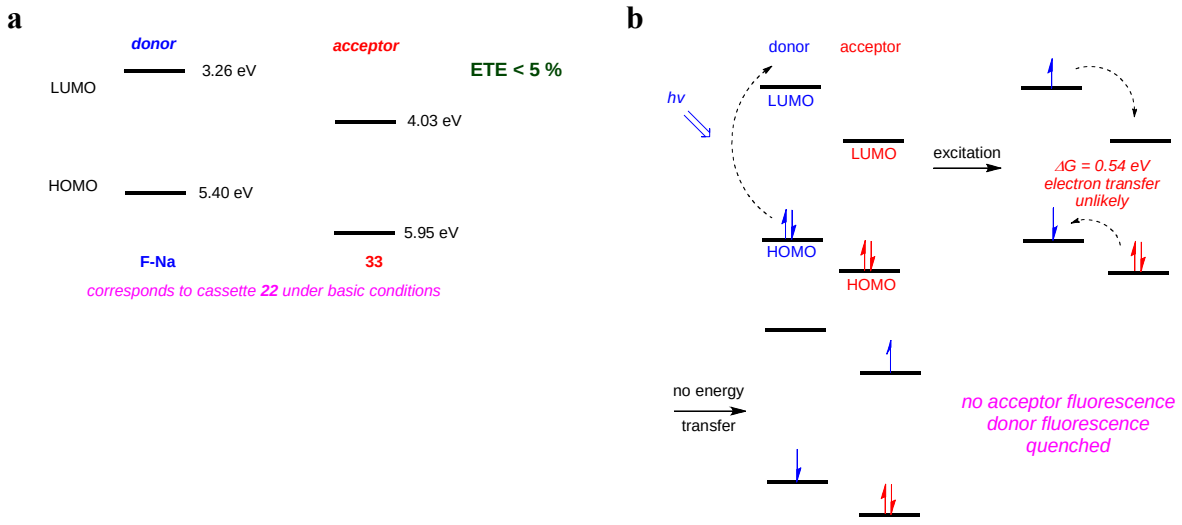

Figure 2.21. (a) HOMO and LUMO levels of the reference compounds representing cassette **22** under basic conditions; and, (b) rationale for the poor energy transfer.

4. Conclusions

Previous studies from these laboratories in collaboration with Topp, Hochstrauser and co-workers measured energy transfer rates between donor and acceptor fragments for TBETs based on BODIPY and fluorescein components.[144,145,169] The rates were faster than would be expected from a FRET mechanism, and for some systems the orientations of the transition dipoles are suboptimal for this mechanism anyway, just as outlined here. Dependence on HOMO and LUMO energy levels for the donors and acceptor parts is consistent with electron transfer.[163,170-172]

Probably the majority of fluorescent sensors tends to feature ligands that quench fluorescence in the absence of analyte, usually via electron transfer, but which are switched on when a metal or proton binds to prevent this. Ratiometric dyes that are "always on" can be formed by combining FRET coupled dyes in a single molecule.[173,174]

To the best of our knowledge, the data reported here, and in our communication on **16** in intracellular imaging, is the first that describes how TBET cassettes can be used as proton probes. The closest work in the literature is from Akkaya's group who have made two metal-sensing cassettes functionalized with coordinating groups that allow them to detect Ag(+1)[175] and Hg(+2)[176], *ie* compounds **G** and **H** respectively. In our cassettes **22** and **23** the analyte modulates the electronic properties of the donor part, but in **G** and **H** they effect the acceptor. In fact, in TBETs the donor, acceptor, and linker fragments[177] could all be modified to give sensors. The work described here may represent the beginning of a new paradigm in which electronically coupled dye pairs can be used to sense analytes in biomedical applications.

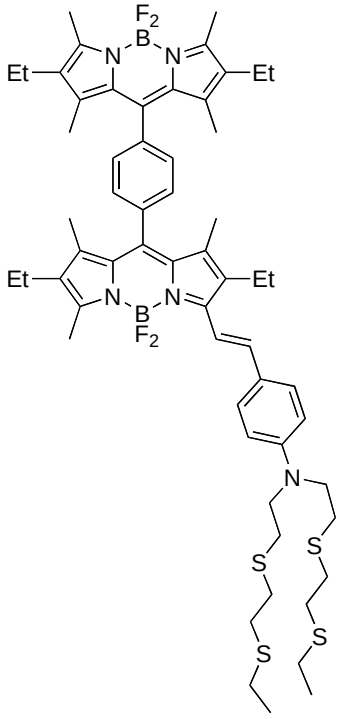

G

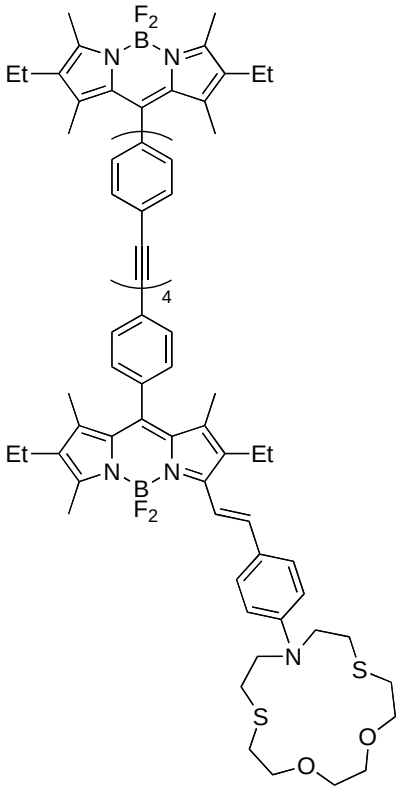

H

CHAPTER III

SYNTHESIS OF WATER SOLUBLE THROUGH-BOND ENERGY TRANSFER CASSETTES FOR PROTEIN LABELING

A. SYNTHESIS OF WATER-SOLUBLE FUNCTIONALIZED BODIPYS

1. Introduction

Behind fluorescein, rhodamine, and possibly cyanine derivatives, 4,4-difluoro-4-bora-3a,4a-diaza-*s*-indacene, or BODIPY®[51,146,178,179] (hereafter abbreviated to BODIPY) dyes are probably the most useful fluorescent probes in biotechnology. This is because they tend to absorb UV radiation efficiently, and emit relatively sharp fluorescence peaks at useful wavelengths (typically 520 – 650 nm) with high quantum yields.

The core of BODIPY dyes is hydrophobic, and does not contain any functionality to attach the probes to proteins. Both these obstacles can be surmounted via synthetic modifications. For instance, there are many BODIPY dyes with carboxylic acid functional groups[154,157,180,181] that can be activated then linked to amino groups on proteins or DNA-derivatives. Further, such carboxylic acids can be activated using sulfonated succinimide reagents;[182] this makes the hydrophobic dyes more water-soluble enabling them to be dissolved in aqueous media for coupling to various water-soluble biomolecules. Once hydrophobic BODIPY dyes are conjugated to biomolecules then they tend to embed into hydrophobic pockets, or even create micellular-like environments via aggregation effects. This is not always disadvantageous; indeed, variations of BODIPY fluorescence with the polarity of their immediate environment

can be useful.[183-188] However, in other cases it is definitely advantageous to have water-soluble BODIPY dyes that can be conjugated easily, and that will tend to exist in the aqueous environment that surrounds a biomolecule without perturbing it.

Despite the obvious practical value of water-soluble BODIPY dyes, very few have been reported in the open literature. This is even more surprising in view of the fact that BODIPY dyes were first reported in 1969,[189] and have been investigated with increasing vigor since then.[146,179] Indeed, the sum total of synthetic procedures to obtain BODIPY dyes includes only the four sulfonated derivatives **I** – **L**[190,191] and several closely related oligoethylene-glycol-containing systems, of which **M**[192] is illustrative (Figure 3.1a). The fact that water-soluble BODIPYs are relatively under-represented in the literature is unsurprising to anyone who has attempted to sulfonate these dyes. Sulfonation reagents tend to be highly reactive whereas the BODIPY core is relatively fragile. Further, many sulfonated products are not isolated via flash chromatography. Consequently, reaction conditions for sulfonation of BODIPY dyes must be controlled carefully, and some optimization is required to isolate pure materials from these transformations.

a

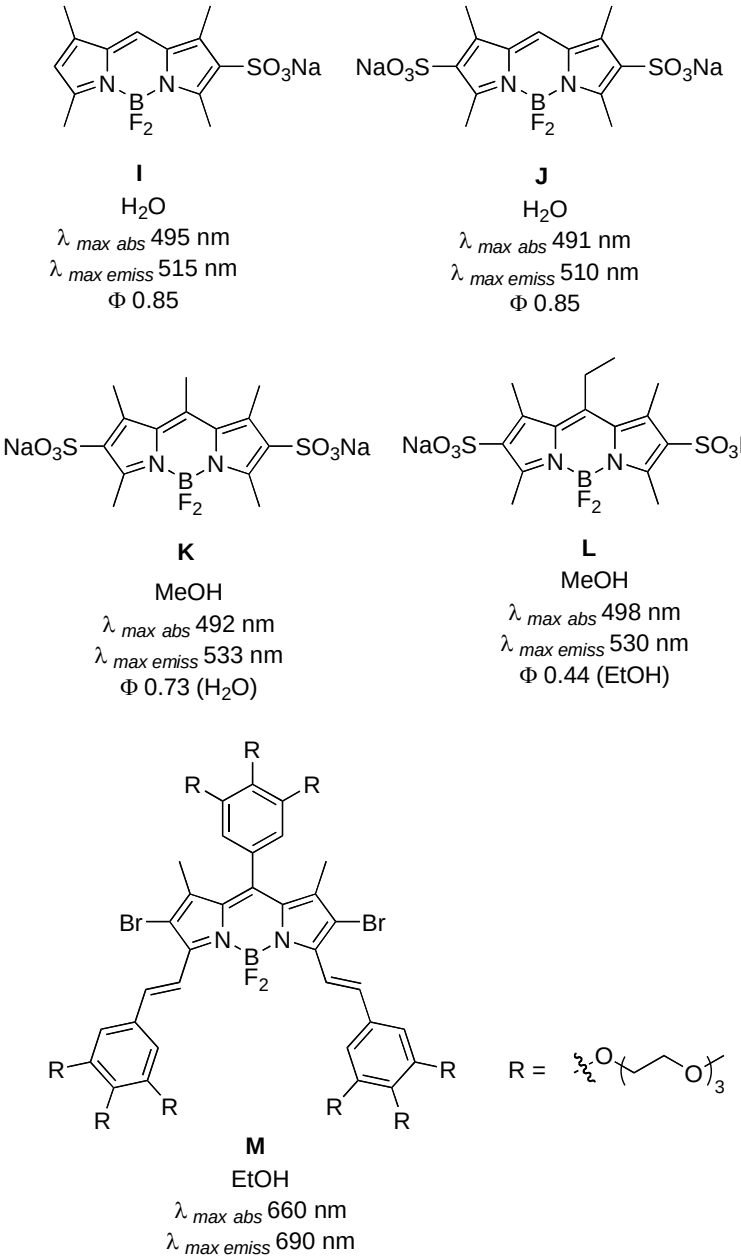

Figure 3.1 **(**a) Previously known water-soluble BODIPY systems; and, (b) compounds prepared in this work.

b

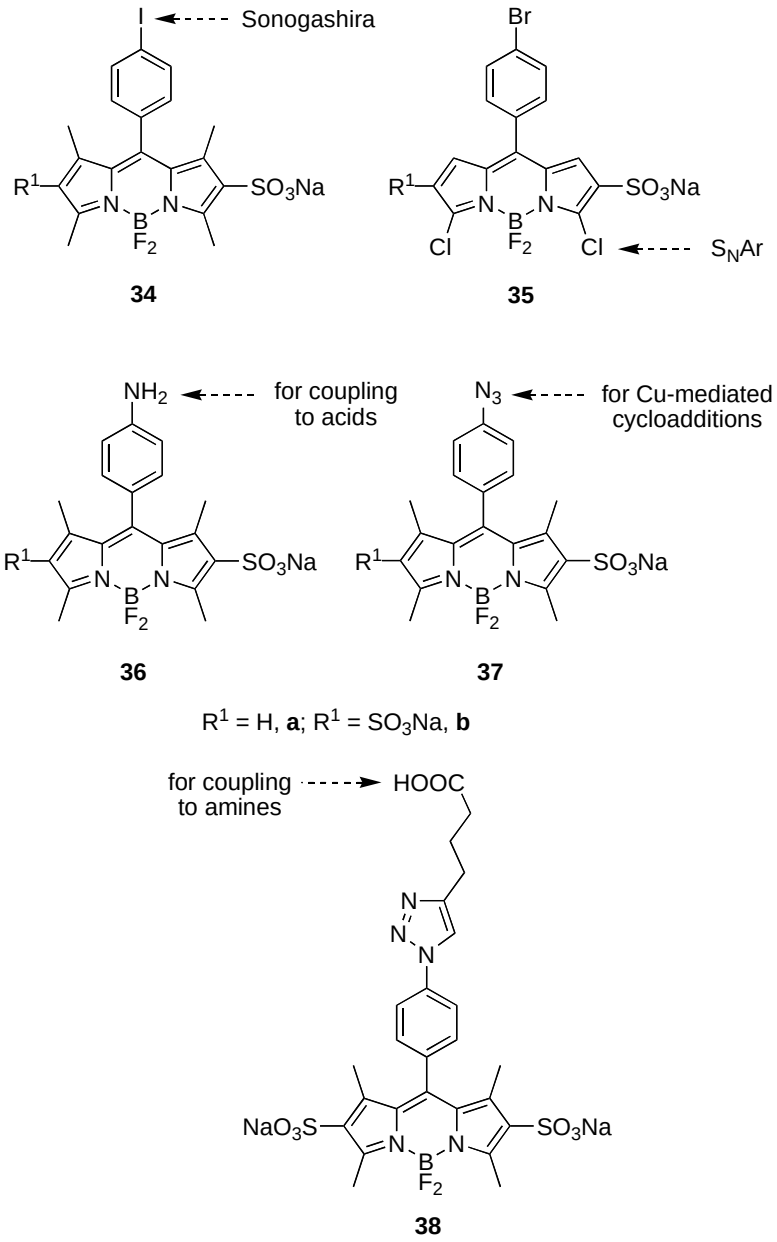

Figure 3.1 Continued.

This paper describes several procedures for the preparation of several sulfonated, water-soluble BODIPY systems (Figure 3.1b). Mono (a) and di-substituted (b)

tetramethyl-BODIPYs **34** have a 4-iodo-benzene substituent at the *meso*-position to enable further functionalization via organometallic cross coupling reactions. The bromo compounds **35** can be similarly derivatized, but they are also potentially reactive towards nucleophiles in S_NAr reactions.[193-195] Compounds **36** are valuable since they can be coupled to active carbonyl groups, the azides **37** are amenable to copper-mediated cycloadditions to alkynes,[196,197] and the disulfonate **38** can be activated and coupled to amino groups on biomolecules. Thus the end-products of this work have potential uses in many different scenarios for labeling biological molecules.

2. Results and Discussion

The following sections describe the preparation of the unusual BODIPY starting materials, the pivotal sulfonation reactions, and reactions of the sulfonated products to further transform them into useful probes. Finally, the spectral properties of the target molecules are discussed.

2.1. BODIPY Starting Materials

The lipophilic starting materials used in this project were generally known compounds,[143,153,198] with the exception of compounds **39** shown in Scheme 3.1. Condensation of 4-substituted benzaldehydes with pyrrole is a known reaction for formation of the dipyrromethane **N**;[199] this was repeated here, and an analogous procedure was used to prepare the bromoderivative **37**. Chlorination of compounds similar to **37** has been reported by Boens and co-workers.[200] Slight modifications of their procedures enabled us to obtain gram amounts of the dipyrromethenes **38** after a

"one-pot" chlorination oxidation sequence and a flash chromatographic separation. Incorporation of the difluoroboron groups was achieved via the standard procedure, though we found that the products **39** could be isolated via recrystallizations rather than column chromatography.

Scheme 3.1. Synthesis of **41**

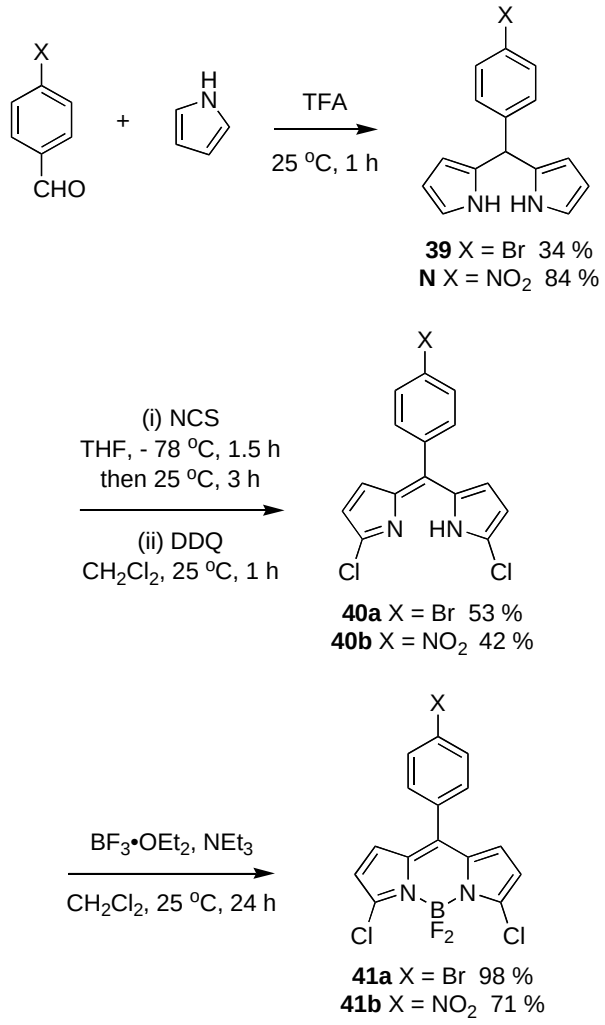

2.2. Sulfonation of Various BODIPY Derivatives

Scheme 3.2 shows the key sulfonation reactions featured in this paper. After considerable experimentation it was discovered that monosulfonations (Scheme 3.2a) of BODIPYs tend to proceed efficiently using 1.2 eq of fresh chlorosulfonic acid in CH_2Cl_2. The sulfonating agent in CH_2Cl_2 was added dropwise over a few minutes to a solution of the BODIPY starting material at – 40 °C. After the addition was complete, the cooling bath was removed and the reaction was allowed to warm to 25 °C and stirred for 20 min. For syntheses of compounds **34a**, **35a**, and **42a** the reactions were quenched with $NaHCO_{3(aq)}$, and (after an extraction procedure) the crude products were purified via flash chromatography on silica. A critical observation in this work was the need for the bicarbonate quench; it appears that the protic forms of these sulfonic acids tend to be unstable (though this is not always the case, see below).

Disulfonations of the same starting materials to give products **34b**, **35b**, and **42b** are shown in Scheme 3.1.2b. Two equivalents of the chlorosulfonic acid were used to achieve the second sulfonation. Separation in this case is relatively easy because the disulfonic acids precipitate from the dichloromethane solution after 20 min at room temperature. The products were collected by filtration, dissolved in a small amount of aqueous $NaHCO_3$, evaporated to dryness, then reprecipitated from brine to give essentially pure products. No chromatography is involved, so the procedure is convenient and amenable to scale up.

Scheme 3.2. Sulfonation Reactions

a

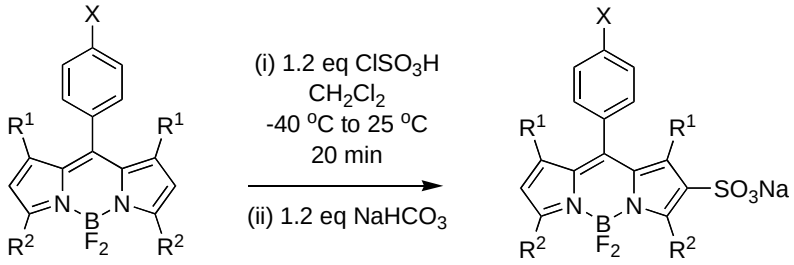

	X	R^1	R^2	%
34a	I	CH_3	CH_3	60
35a	Br	H	Cl	92
42a	NO_2	CH_3	CH_3	63

b

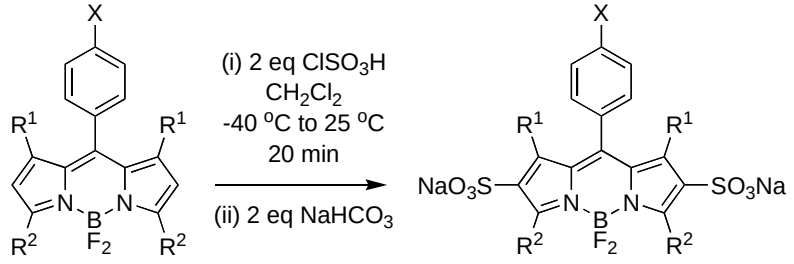

	X	R^1	R^2	%
34b	I	CH_3	CH_3	88
35b	Br	H	Cl	85
42b	NO_2	CH_3	CH_3	100

One exception to the preferred sulfonation conditions was for the alkyne-functionalized BODIPY;[143,160] as shown in reaction 1. Here the disulfonate **43** precipitated out of the CH_2Cl_2 solution in near pure form. This is very fortunate because compound **43** is unstable in aqueous media, undergoing relatively rapid hydrolysis at the

alkyne group. For that reason, this is not a particularly useful building block unless the sulfonic acid was neutralized with a base, e.g. Et_3N.

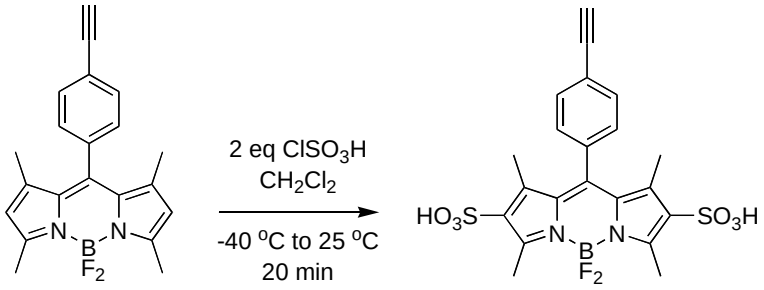

O **43** 60 %

reaction 1

Reaction 2 shows a sulfonation of the relatively electron-poor BODIPY system **41b** with varying equivalents of chlorosulfonic acid. A mixture of mono- **44a** and disulfonation **44b** products formed if less than 3.5 equivalents of the sulfonating agents were used, and neither of these materials precipitated from the solution; it was, however, possible to obtain the yields indicated via flash chromatography. Clean disulfonation was obtained when 3.5 equivalents of chlorosulfonic acid were used and, under those conditions, the product **44b** precipitated in a relatively pure form and the sample could be further purified by re-precipitation from brine as described for compounds **34b** and **35b**. The water-solubility of the monosulfonate **44a** was lower than the similar tetramethyl-BODIPY monosulfonates **34a**, **36a**, **37a**, and **42a**; for instance, it was impossible to obtain a clear ^{13}C NMR spectrum of **44a** in D_2O.

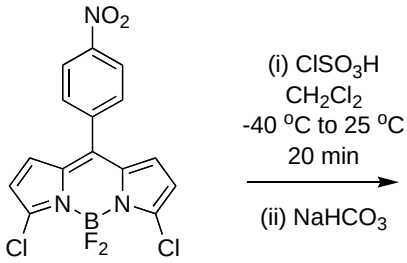

41b

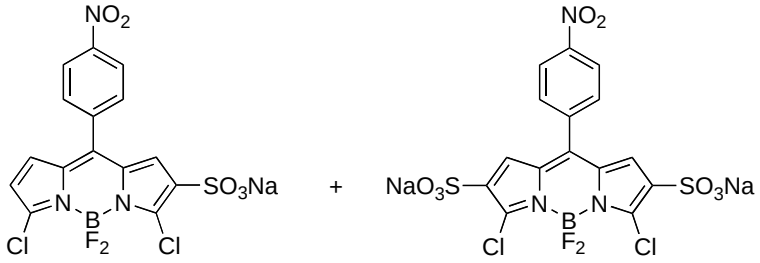

44a **44b**

amount of $ClSO_3H$ (eq)	yield of **44a** (%)	yield of **44b** (%)
1.2	90	0
2.0	68	21
3.0	22	74
3.5	0	97

reaction 2

2.3. Derivatization of Some BODIPY Sulfonates

Nitro functionalities on BODIPYs have few direct applications, but this group allows access to more useful derivatives that contain amine or azido "handles". Exploratory work to establish conditions for hydrogenation of the nitro-compounds **42** was not encouraging. Almost no reduction was observed under 1 atm of hydrogen in aqueous media. In ethanol, the rates were very slow, and the product amine was contaminated by N-ethyl impurities (this is a relatively common occurrence).[201]

Reactions featuring $SnCl_2$ in $HCl_{(aq)}$ tended to be complicated, probably by tin complexes that did not elute from silica. Ultimately, hydrazine and catalytic palladium on carbon proved to be effective (Scheme 3.3).[153] To decrease the risk of an explosion during this reaction, the hydrazine was added dropwise to the substrate and reagents in refluxing ethanol. This procedure has been repeated several times on up to 400 mg of the nitro compound without any mishaps; however, we advocate use of a blast shield and certainly do not recommend that this reaction be performed on a much larger scale. The amino derivatives **36** were isolated via flash chromatography.

Scheme 3.3. Synthesis of **36** and **37.**

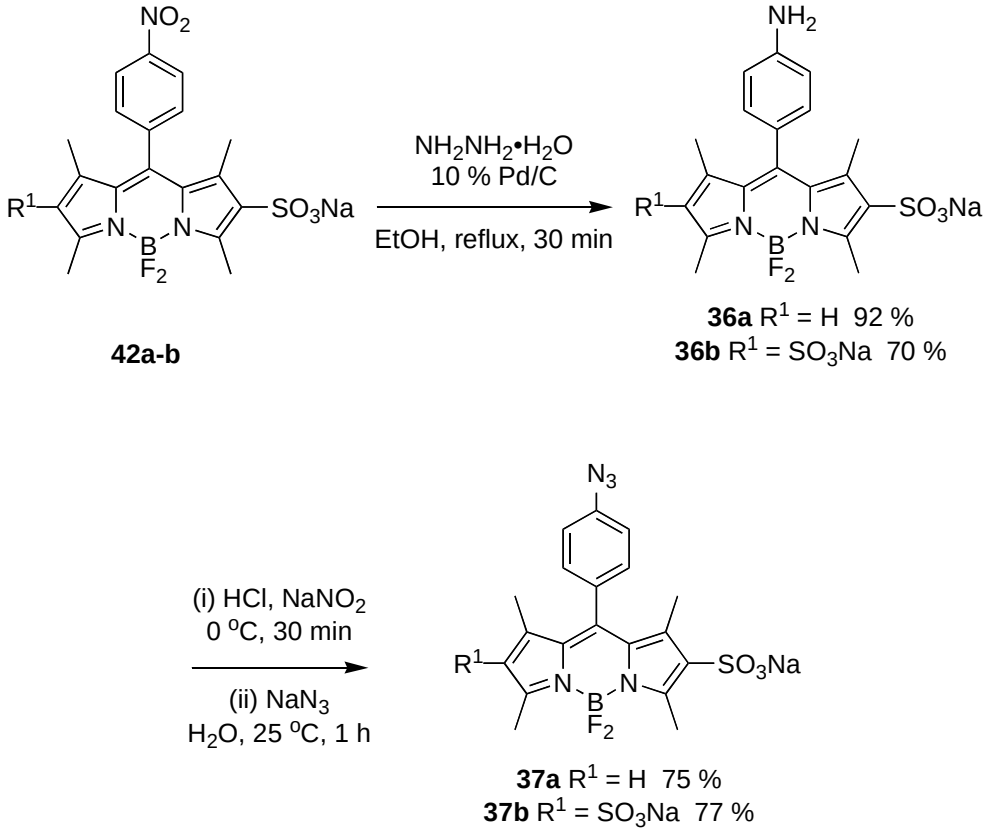

A diazotization/azide treatment reaction was used to convert the amines **36** into the corresponding azides **37**. Visually, this reaction is interesting. The amine starting materials are weakly green fluorescent, it becomes more fluorescent under acidic conditions, but this fluorescence disappears when sodium nitrite is added, corresponding to formation of the diazocompound. However, addition of azide gives a solution that is more fluorescent than the starting amine.

Reaction 3 shows how the disulfonate **37b** was functionalized via a copper-mediated azide-alkyne cycloaddition reaction. Attempts to perform this reaction in the absence of *tris*-(benzyltriazolylmethyl)amine **(**TBTA)[202] gave very little product, but addition of this ligand made the reaction viable. The disulfonate **38** is freely water-soluble and contains an easily accessible carboxylic acid for activation and conjugation to biomolecules.

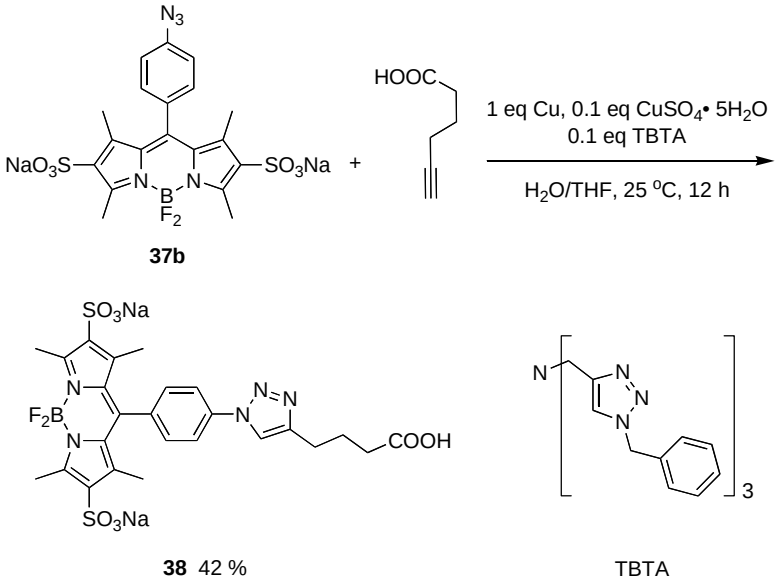

reaction 3

2.4. Spectroscopic Properties of BODIPY Derivatives

Table 2.1 summarizes the spectroscopic data collected for the target materials **34 - 38** and some interesting intermediates **42** and **44**. In general, all these compounds are sufficiently water-soluble to allow their UV and fluorescence properties to be recorded in aqueous media. All of the disulfonates are freely soluble whereas the monosulfonates will not form relatively concentrated solutions.

All the compounds shown in Table 2.1 have absorption maxima in the range 492 – 518 nm, and their molar absorption coefficients are high (5.60 – 14.9 x 10^4 $M^{-1}cm^{-1}$), as is characteristic of BODIPY dyes in general;[146] they fluoresce in the 507 – 540 nm range. Throughout, there are small differences between the emission maxima of the mono- and disulfonated forms; in fact, the maxima shift bathochromically between 2 and 4 nm when going from the mono- to disulfonated compound, except for the nitro derivatives where the opposite trend is observed. Longest wavelength fluorescence emission maxima in the series are associated with the dichlorinated compounds **35** and **44**; all the other probes emit between 507 and 513 nm. Sharp emissions, as seen in small fwhm (full width at half maximum height) values (904 – 1752 cm^{-1}); for comparison it is informative to consider the series of water-soluble Nile Red derivatives recently reported;[203] these have fwhm values for their fluorescence emission of between 1410 – 1680 cm^{-1}. Figure 3.2 shows the spectra obtained.

Quantum yields for the target compounds **34**, **35**, **37**, and **38** were all reasonably high for fluorescent probes (0.15 – 0.49). Some BODIPY dyes have quantum yields that are greater than 0.5; the slightly diminished values for **34**, **35**, **37**, and **38** can be

attributed to non-radiative decay mechanisms associated with free rotation of the meso-substituent.[204] Compounds **36** have a 4-aminobenzene meso-substituent; this electron rich aromatic ring probably quenches the fluorescence of the BODIPY core via photoinduced electron transfer (PeT) in which the excited state of the BODIPY fluorophore is reduced by electron transfer from the relatively high-lying HOMO of the electron-rich meso-substituent quencher (i.e., reductive electron transfer). Such effects have been elegantly described as a-PeT by Nagano et al.[148,149,162,205,206] The "a" denotes that the fluorescent chromophore acts as an acceptor. The low quantum yield observed for compounds **36** is not a concern if the amine group is transformed into an amide in the bioconjugation process, because that will adjust the oxidation potential of the meso-substituent, bringing down its HOMO level, and restoring the fluorescence.

Table 3.1. Spectroscopic properties of the BODIPY Derivatives.

dye	$\lambda_{max\ abs}$ [a] (nm)	$\log(\varepsilon_{max})$ [a,b]	$\lambda_{max\ emiss}$ [a] (nm)	Fwhm [a] (cm^{-1})	Φ [a]
34a [c]	494	5.18 ± 0.01	507	1021	0.47 ± 0.02 [d]
34b [c]	498	5.00 ± 0.01	509	994	0.34 ± 0.02 [d]
35a [c]	509	4.86 ± 0.01	523	997	0.27 ± 0.01 [e]
35b [c]	512	4.89 ± 0.01	524	904	0.41 ± 0.01 [e]
36a [f]	492	4.93 ± 0.01	507	1050	0.001 [d]
36b [f]	496	5.06 ± 0.01	511	945	0.001 [d]
37a [f]	494	4.84 ± 0.01	507	1062	0.34 ± 0.01 [d]
37b [f]	498	4.89 ± 0.01	509	1053	0.15 ± 0.001 [d]
38 [g]	498	4.90 ± 0.01	511	1027	0.49 ± 0.01 [d]
42a [c]	497	4.76 ± 0.01	513	1752	0.001 [d]
42b [c]	501	4.96 ± 0.01	511	1409	0.002 [d]
44a [h]	514	4.82 ± 0.01	540	1440	0.002 [e]
44b [h]	518	4.76 ± 0.01	538	1177	0.008 [e]

[a] In H_2O. [b] ε_{max} were estimated by linear fit of absorbance A vs dye concentration c at four dye concentrations (one dye concentration was at zero). [c] Scheme 3.1.2. [d] Fluorescein was used as a standard (Φ = 0.92 in 0.1 M $NaOH_{(aq)}$).[207] [e] Rhodamine 6G was used as a standard (Φ = 0.95 in EtOH)[208]. [f] Scheme 3.1.3. [g] Reaction 2.1.3. [h] Reaction 2.1.2

Compounds **42** and **44** are intermediates rather than target materials. They both have relatively low quantum yields, and these can be rationalized via PeT effects. For these materials, the LUMO of the *meso*-substituent is relatively low-lying due to the influence of the 4-nitro group. This means that the excited state of the BODIPY chromophore can act as an electron donor to the electron-poor *meso*-substituent quencher (i.e., oxidative electron transfer).

a

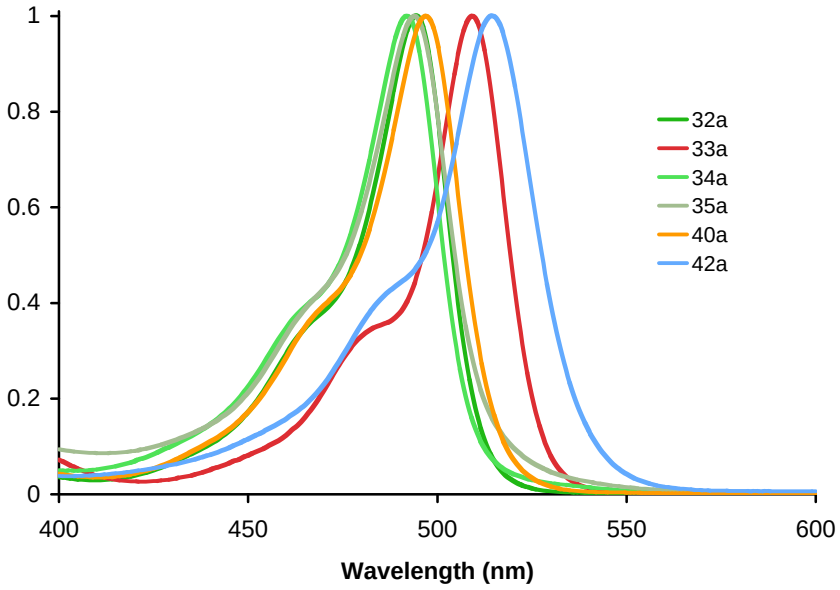

Figure 3.2. (a) UV absorption, and (b) fluorescence: spectra for the mono-sulfonated BODIPYs. (c) UV absorption, and (d) fluorescence: spectra for the bis-sulfonated BODIPYs. All these spectra were recorded in deionized water at concentrations of approximately 10^{-6} M for the UV spectra and 10^{-7} to 10^{-6} M for the fluorescence, then normalized.

b

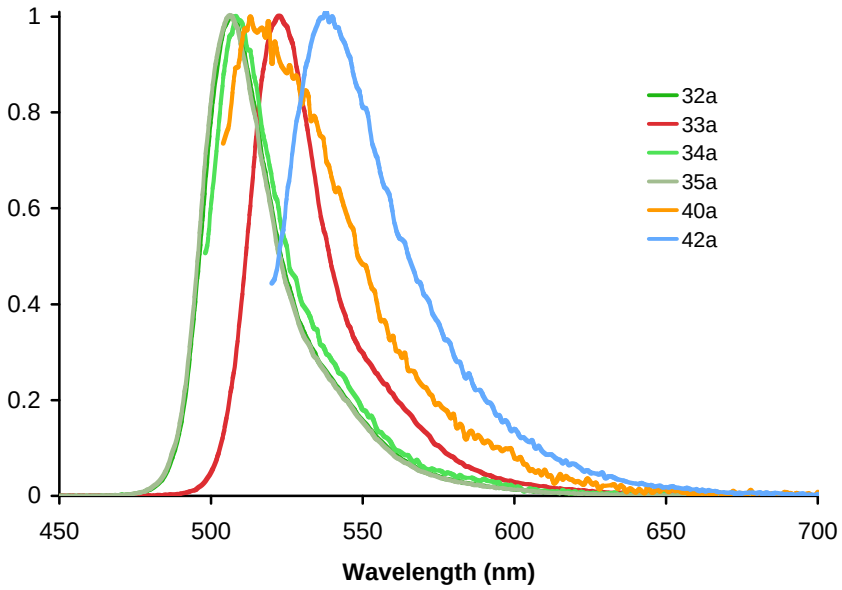

c

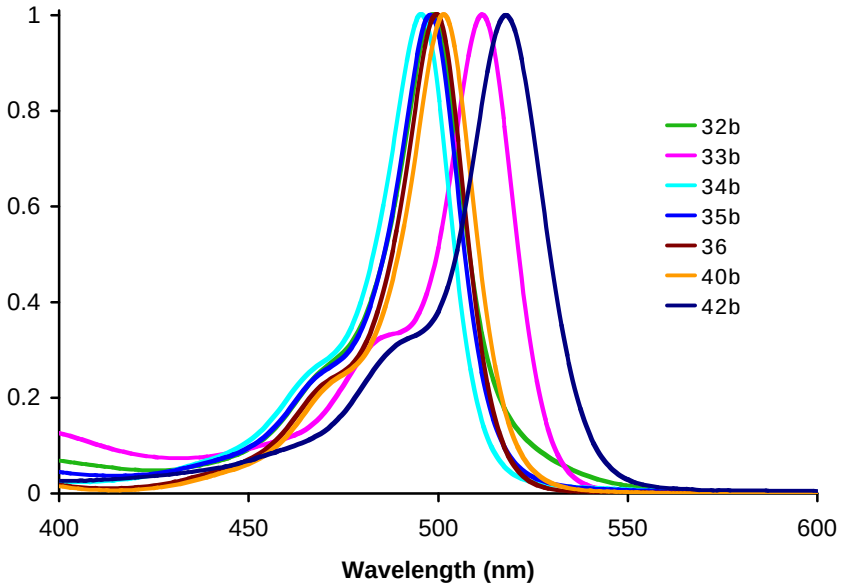

Figure 3.2. Continued.

d

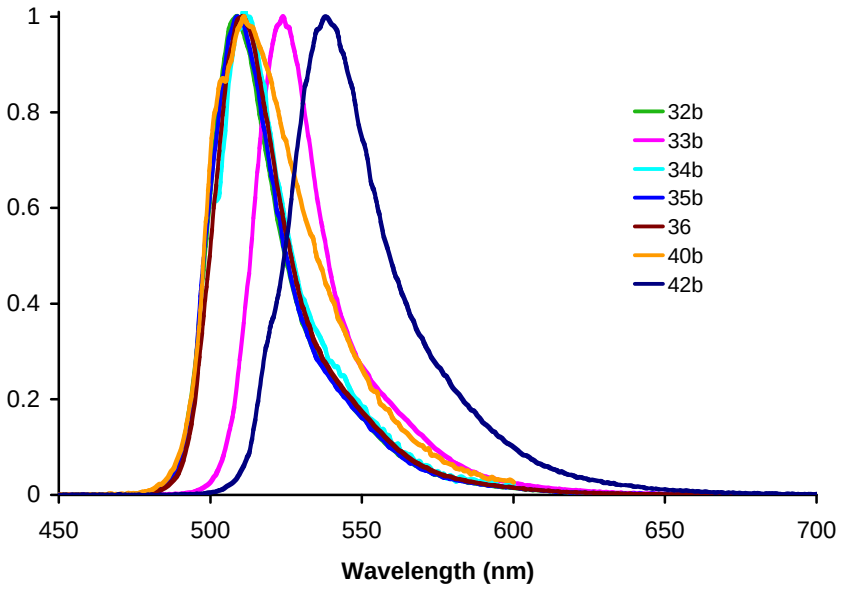

Figure 3.2. Continued.

3. Conclusions

Sulfonation reactions of BODIPY derivatives are hard to develop into useful synthetic procedures for two reasons: (i) inappropriate conditions give mixtures of products; and (ii) sulfonic acid derivatives of BODIPYs can be hard to purify. The sulfonation reactions shown in Scheme 3.2 tend to give predominantly one product, and reactions 1 and 2 give essentially binary mixtures that are easily separated by flash chromatography. Conjugation of the target materials to biomolecules could be achieved via amide bond formation to amines or acids, or "click" chemistry. Further, some of the dyes presented here can be derivatized via organometallic couplings to the organic halide functionalities, and, in the case of the chlorinated derivatives **35** and **44**, via S_NAr reaction.

B. 3- and 5-FUNCTIONALIZED BODIPYs VIA THE LIEBESKIND-SROGL REACTION

1. Introduction

Organometallic cross coupling reactions are useful for extending the conjugation of 4,4-difluoro-4-bora-3a,4a-diaza-*s*-indacene, or BODIPY® (here abbreviated BODIPY) dyes to give probes that fluoresce at longer wavelengths. Usually this is achieved via inherently basic processes (Suzuki[209] and Sonogashira[210]) that tend to cause partial decomposition of BODIPY dyes. Furthermore, chemoselective reactions involving different halides in the same molecule are sometimes desirable, but hard to achieve via these transformations. For instance, the *C*-*Cl* sites of systems like **41a**[211] are reactive for Sonogashira and Suzuki reactions, but competitive reactions of the aryl bromide site would be expected. This paper describes how Liebeskind-Srogl reactions can be used to achieve chemoselective couplings to BODIPY dyes under neutral conditions; further, this transformation was used to give a water-soluble two dye cassette system.

Scheme 3.4. Synthesis of 3-,5- functionalized BODIPY via Liebeskind-Srogl reaction.

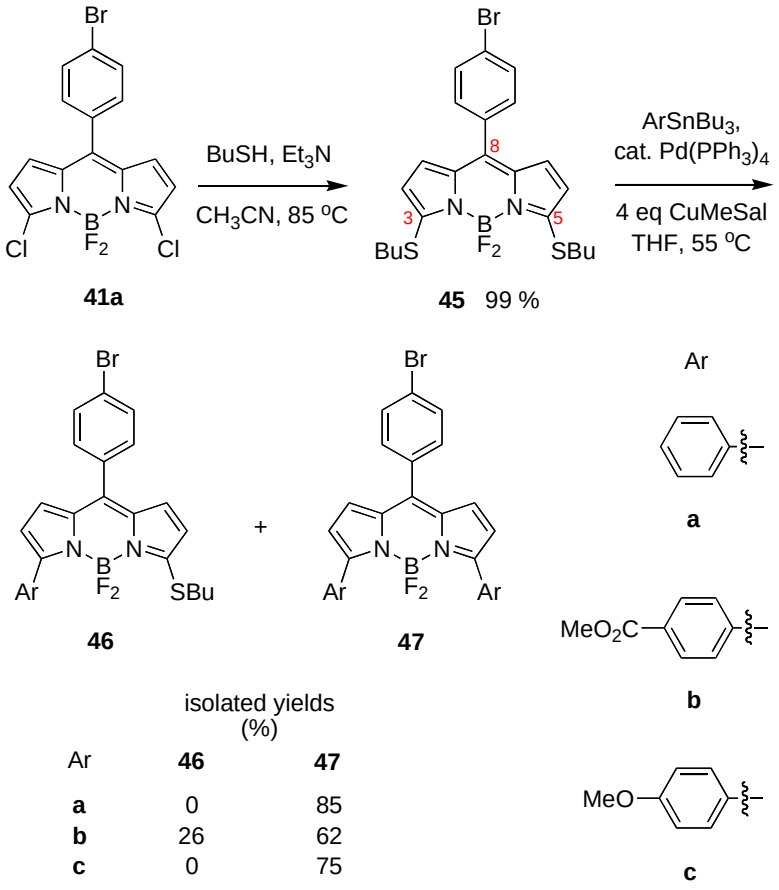

Ar	isolated yields (%) 46	47
a	0	85
b	26	62
c	0	75

CuMeSal = copper (I) 3-methylsalicylate

2. Results and Discussion

It has been demonstrated that Liebeskind-Srögl couplings can be used to substitute thioalkyl groups at the *C*[8] position of the BODIPY core.[212] Chemoselective Liebeskind-Srögl couplings at thioalkyl groups over aryl bromides have also been demonstrated.[213] Consequently we felt that selective substitution at the 3,5-positions as in compound **45** would be possible. In actuality, phenyltin (**a**) and electron-rich aryl-tin (**c**) reagents cleanly gave the disubsituted products **47**, some monosubstituted

intermediate was isolated for the electron-deficient aryl group tested (**b**), but in no case was the aryl-bromide affected. The synthesis of electron-deficient tin compound **49**, methyl 4-(tributylstannyl)benzoate, is outtined in the supporting information.

a

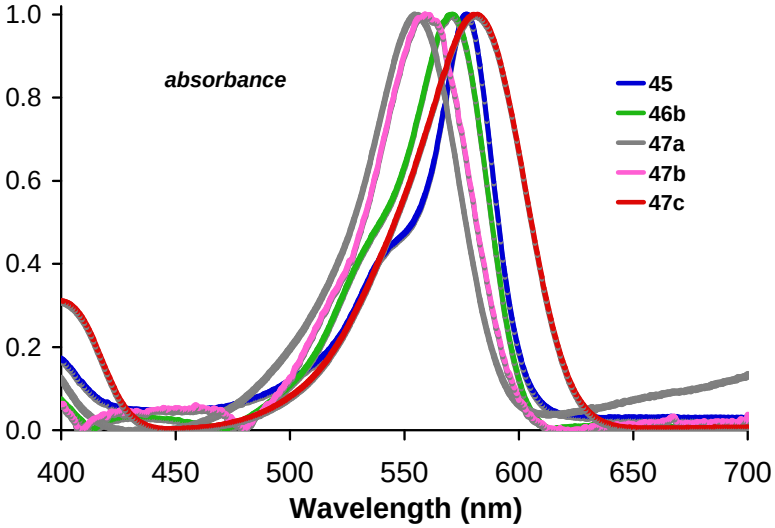

b

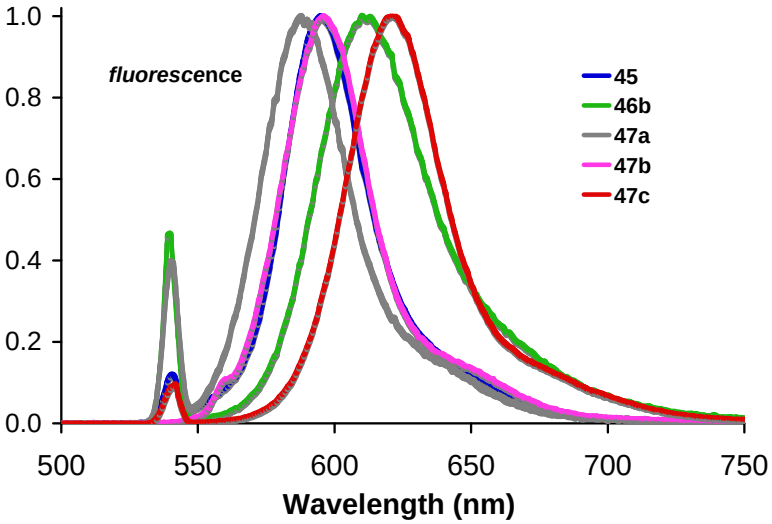

Figure 3.3. (a) Normalized absorbance spectra of compounds **45 - 47** (1 x 10^{-6} M) in EtOAc; and, (b) normalized fluorescence spectra of compounds **45 - 47** (1 x 10^{-7} M) in EtOAc with excitation at 540 nm.

Figure 3.3 shows normalized absorbance (a) and fluorescence (b) spectra for compounds **45 - 47**. The newly installed aryl groups shift both maxima to the red, as previously described for 3,5-diaryl-BODIPY dyes.[214] More extensive spectroscopic data for these products is shown in Table 2.2. Both *para*-electron withdrawing (CO_2Me) and donating (OMe) groups shifted the maximum fluorescence wavelength to red (8 nm and 33 nm respectively, compare **47a**, **47b** and **47c**).

Table 2.2. Photophysical properties of compounds **45 - 47** in EtOAc.

compd	$\lambda_{abs\ max}$ (nm)	ε_{max} ($L \cdot mol^{-1} \cdot cm^{-1}$)	$\lambda_{fl\ max}$ (nm)	fwhm (nm) [a]	Φ_f [b]
45	577	46700	595	47	0.40 ± 0.04
46b	571	50600	597	59	0.58 ± 0.01
47a	555	52400	588	49	0.14 ± 0.01
47b	559	44000	596	48	0.36 ± 0.03
47c	581	51900	621	41	0.38± 0.01

[a] Full width at half maximum height of fluorescence (fwhm). [b] Rhodamine 101 (Φ = 1.0 in ethanol) as standard

C. SYNTHESIS OF WATER-SOLUBLE CASSETTE FOR PROTEIN LABELING

1. Synthesis of Two-dye Cassette 55

Meso-(4-bromoaryl)BODIPY substituents like those in compounds **46** and **47** can be further elaborated via Sonogashira reactions. However, recent unpublished data from our laboratories have shown that there are advantages to using copper-mediated alkyne-azide coupling reactions[196,197] to join two BODIPY fragments together to form two-dye cassette systems. Azido-functionalized dyes are required to achieve this. Thus the sequence outlined in Scheme 3.4a was performed to generate the azidodicarboxylic acid system **53**. Coupling of the dithioether **48**, which is synthesized from **41b**,[211] to the appropriate 4 eq stannane gave 17 % of the corresponding monosubstituted material **50a**, and 66 % the desired disubstituted product **50b** (data not shown here). However, using 4eq 4-methoxycarbonylphenylboronic acid afforded **50b** in quantitative yield. We think the boronic acid is much more stable than the tin compound under the reaction condition. A mild ester hydrolysis[215] of this material, and reduction of the nitro group gave the amine **53** which was then converted to the azide **53**.

The sulfonated BODIPY alkyne **54** was formed from the known starting material **Q**[160] via sulfonation conditions recently reported by us (Scheme 3.4b).[211] Finally, the appropriately functionalized BODIPYs, azide **53** and alkyne **54**, were joined via the click reaction shown in Scheme 3.4c. The final product **55** is highly water soluble. It was isolated via preparative reverse phase HPLC.

Scheme 3.5. Synthesis of energy transfer cassette **55**.

a

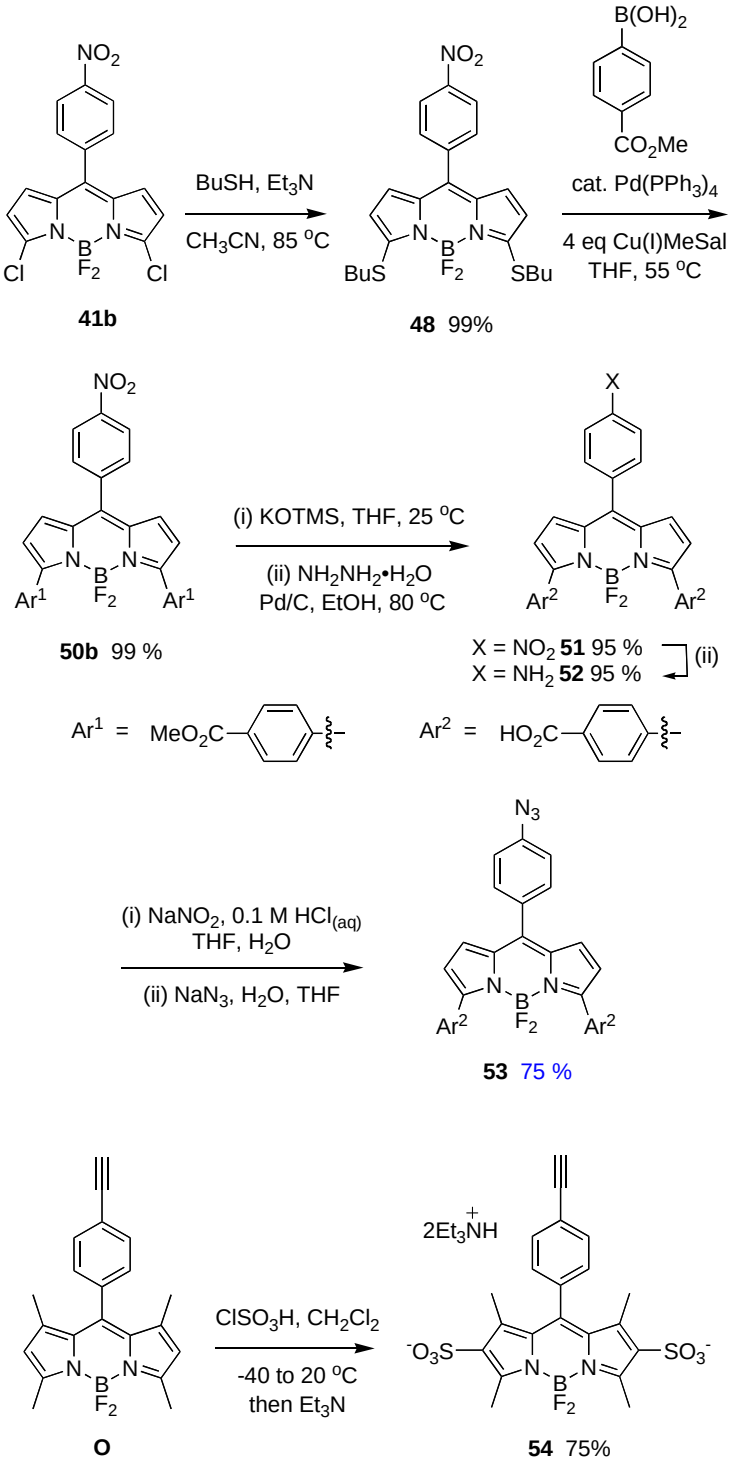

b

Scheme 3.5. Continued.

c

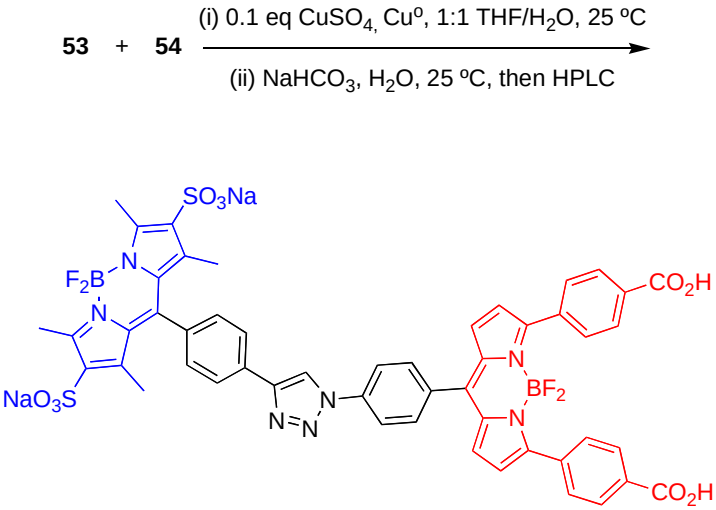

55 30 %

2. Spectral Properties of 55 and BSA-55

Cassette **55** is designed to function as a "through-bond energy transfer" (TBET) system. These feature two dye components that are prevented from becoming completely planar because of steric issues. Thus the UV-visible absorption spectrum of **55** and **BSA-55** has two maxima corresponding to the donor fragment and the acceptor part (Figure 3.4a).

Motivation for making TBET cassettes is derived from the fact that they can be excited at a much shorter wavelength (donor absorbance) than their fluorescence emission (from acceptor part). This leads to enhanced spectral resolution of emission peaks if several dyes are used together. However, three major obstacles have emerged from our research efforts: (i) making the cassettes in water soluble form; (ii) obtaining good energy transfer from the donor to the acceptor in an aqueous medium (cassettes

that work well in less polar solvents can be poor in water); and, (iii) maintaining good energy transfer when the cassette is conjugated to a protein. Cassette **55** is quite water soluble, so that parameter is satisfied. To quantitate the function of the cassettes we measure their overall quantum yields for the acceptor fluorescence emission when excited at the donor.

The overall quantum yield of **55**, and its ETE % for **55** in pH 7.4 phosphate buffer were determined as 0.23 and 85%. Qualitatively, the undesirable "leakage" of fluorescence from the donor is seen at about 520 nm in Figure 3.4b.

Cassette **55** was activated by forming an ester of *N*-hydroxysuccinimide (see supporting information) and conjugated to bovine serum albumin (BSA). This caused the absorbance maxima to be red-shifted by about 8 mm, but had little impact on the fluorescence maxima (Figure 3.4). The overall quantum yield of the **BSA-55** conjugate, and its ETE % for pH 7.4 phosphate buffer were determined as 0.10 and 75 %. Again these data are comparable to the best TBET-conjugates prepared so far.

In summary, the work described here indicates that Liebeskind-Srogl couplings provide another dimension for chemoselectivity in construction of BODIPY dye derivatives.

a

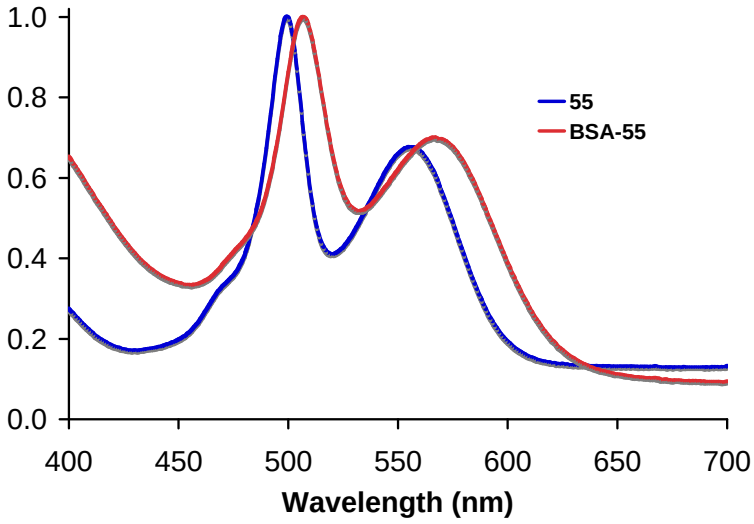

b

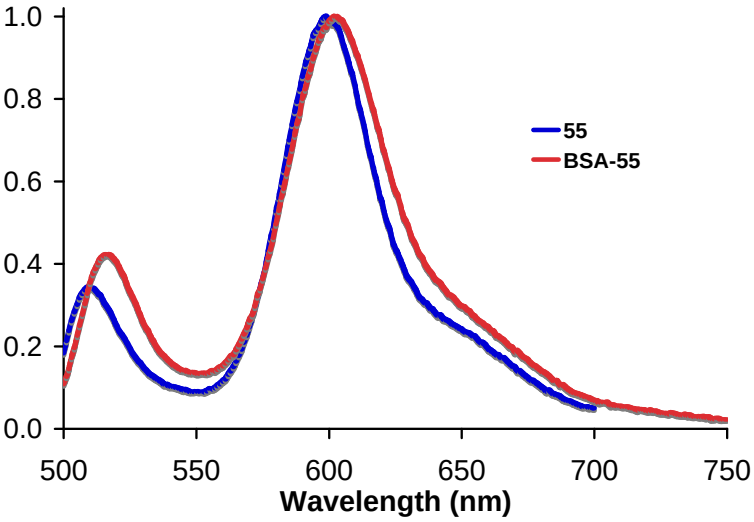

Figure 3.4. (a) Normalized absorption of **55** and **BSA-55** in pH = 7.4 PBS buffer; and, (b) Normalized fluorescence spectra of **55** and **BSA-55** in pH = 7.4 PBS buffer.

CHAPTER IV

CHEMILUMINESCENT ENERGY TRANSFER CASSETTES BASED ON FLUORESCEIN AND NILE-RED

A. Introduction

The two most common ways to induce chemiluminescence in purely organic, non-biological, systems are to treat either oxalate esters or luminol derivatives with basic hydrogen peroxide.[216,217] Both these types of mixtures give light of relatively short wavelengths that are not ideal for applications in biotechnology. Luminol, for instance, emits in the range 420 - 450 nm, depending on the solvent media.[218] Intimate mixtures of oxalate esters or luminol,[219] an oxidant, and an acceptor dye give longer wavelength emissions via intermolecular energy transfer. This results in the mesmerizing, long-lived emissions seen in "light stick toys". However, the options for forming discrete probes for biotechnology that emit at longer, and generally more useful, wavelengths are limited.[124,220-224]

An ongoing project in our group features twisted, but otherwise conjugated, donor and acceptor cassettes for labelling biomolecules.[98,99,124] The motivation for this is that energy transfer can occur through-bonds as well as through space, hence it can be relatively fast and efficient. All our published research to date features cassettes based on UV-absorbing donors, like compound **P**. We thought it would be intriguing to make cassettes where the donor might be activated chemically instead. Oxalate esters are not useful donors for through-bond energy transfer cassettes because it is impossible to

conjugate an acceptor to the oxalate fragment. Consequently, luminol-based systems were selected. Described here are the syntheses and spectroscopic properties of the fluorescein- and Nile Red-based, chemically activated, cassettes **56** and **57**.

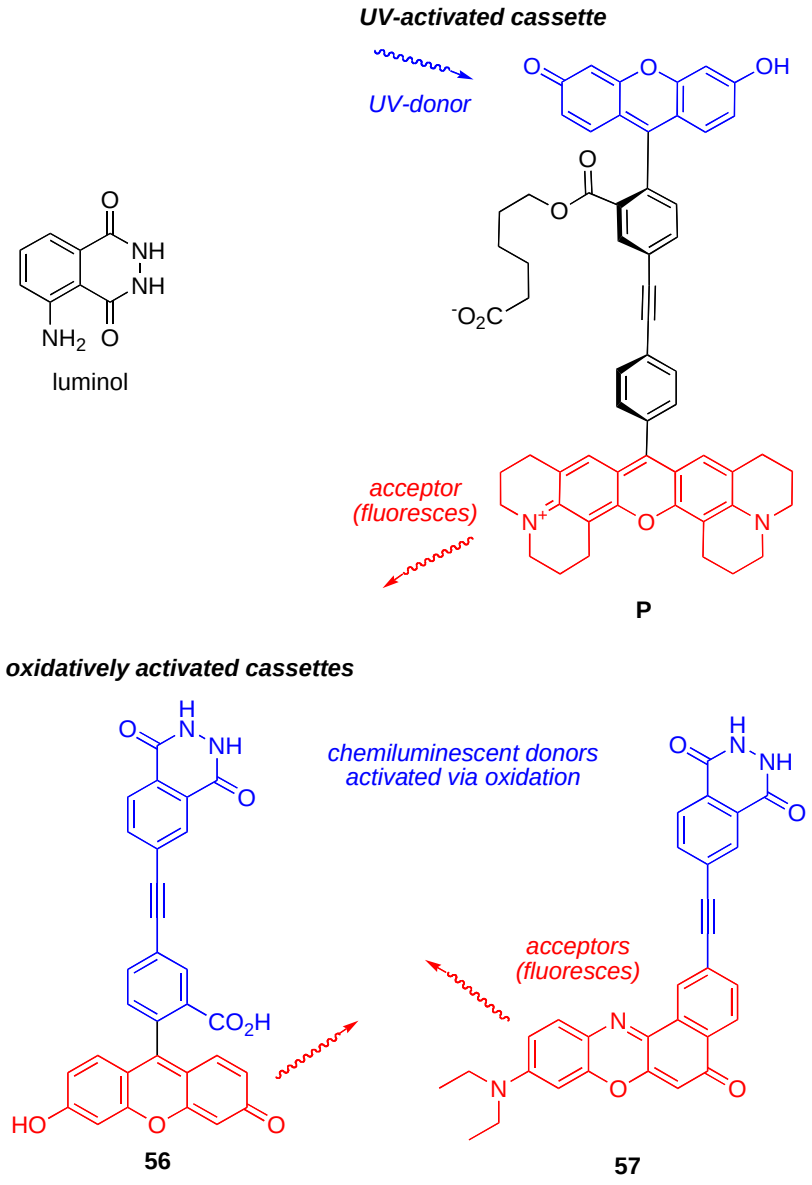

B. Synthesis of Cassettes 56, 57, 63 and 64

Nearly all luminol derivatives are almost insoluble in most organic media, and this makes them extremely difficult to manipulate. After considerable experimentation, one solution to this problem emerged: bis(*N*-protection) of compounds like **58** with 4-methoxybenzyl (PMB) groups. This approach gave organic-soluble, easily chromatographed, intermediates, and the PMB group is removed in the closing stages of the synthesis via treatment with TFA. Thus, Scheme 4.1 shows the syntheses that evolved for compounds **56** and **57**. In both routes, the cyclic hydrazide **58** was bis-*N*-protected, then elaborated via Sonogashira reactions.[210] These featured derivatives of 5-bromofluorescein[35] and 2-hydroxy Nile Red.[225] The route to the cassette**s** would have been more convergent if an alkyne derivative of luminol could have been coupled with halogenated/triflated acceptors, but that approach was ineffective. The approach to the control fluorescein and Nile Red compounds **66** and **68** are similar to luminol cassettes **56** and **57**. Sonogashira coupling reaction of fluorescein alkyne **C** and 2-hydroxy Nile Red alkyne **S** with dimethyl 4-bromophthalate, followed by hydrolysis afforded the water soluble dyes **66** and **68**.

Scheme 4 .1. Preparation of: (a) the fluorescein cassette **56**; (b) the Nile Red based cassette **57**; (c) the fluorescein control **66**; and, (d) the Nile Red control **68**.

a

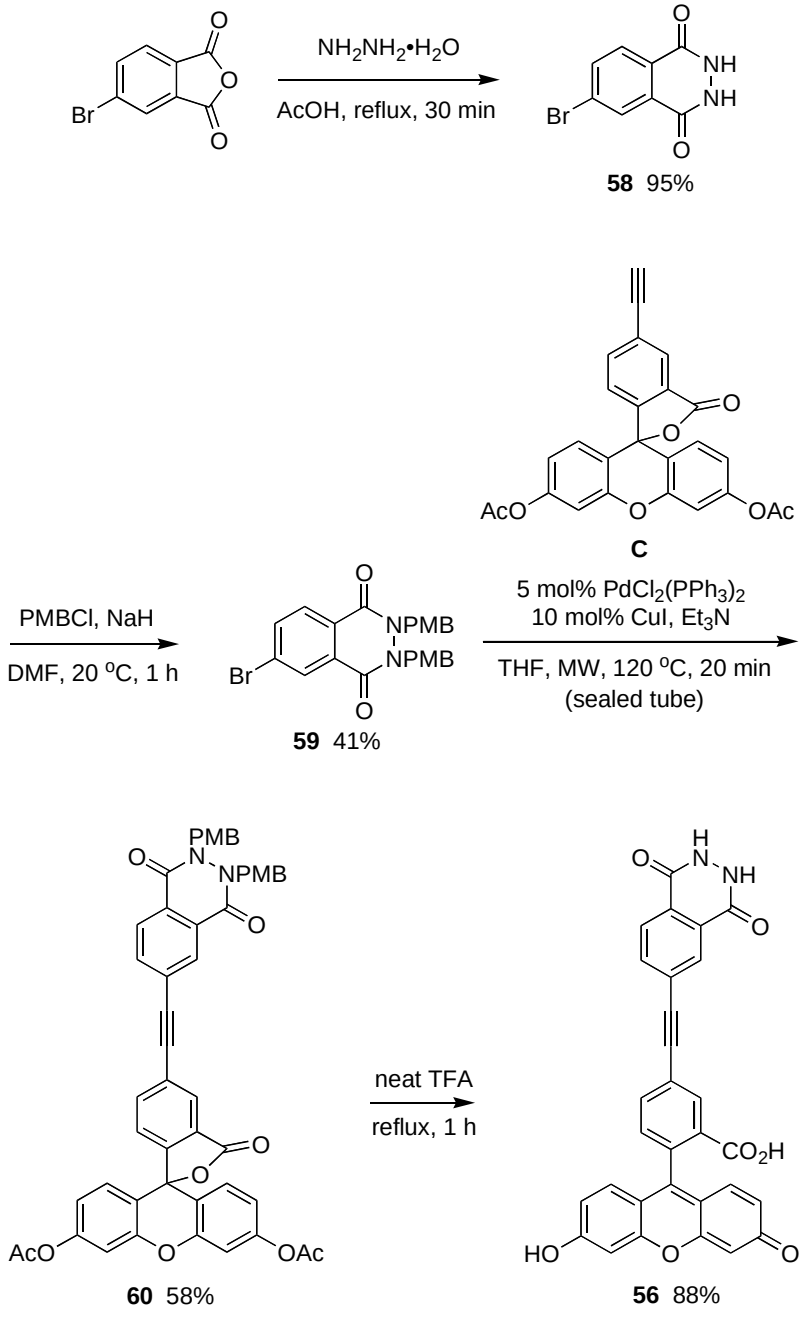

Scheme 4.1. Continued.

b

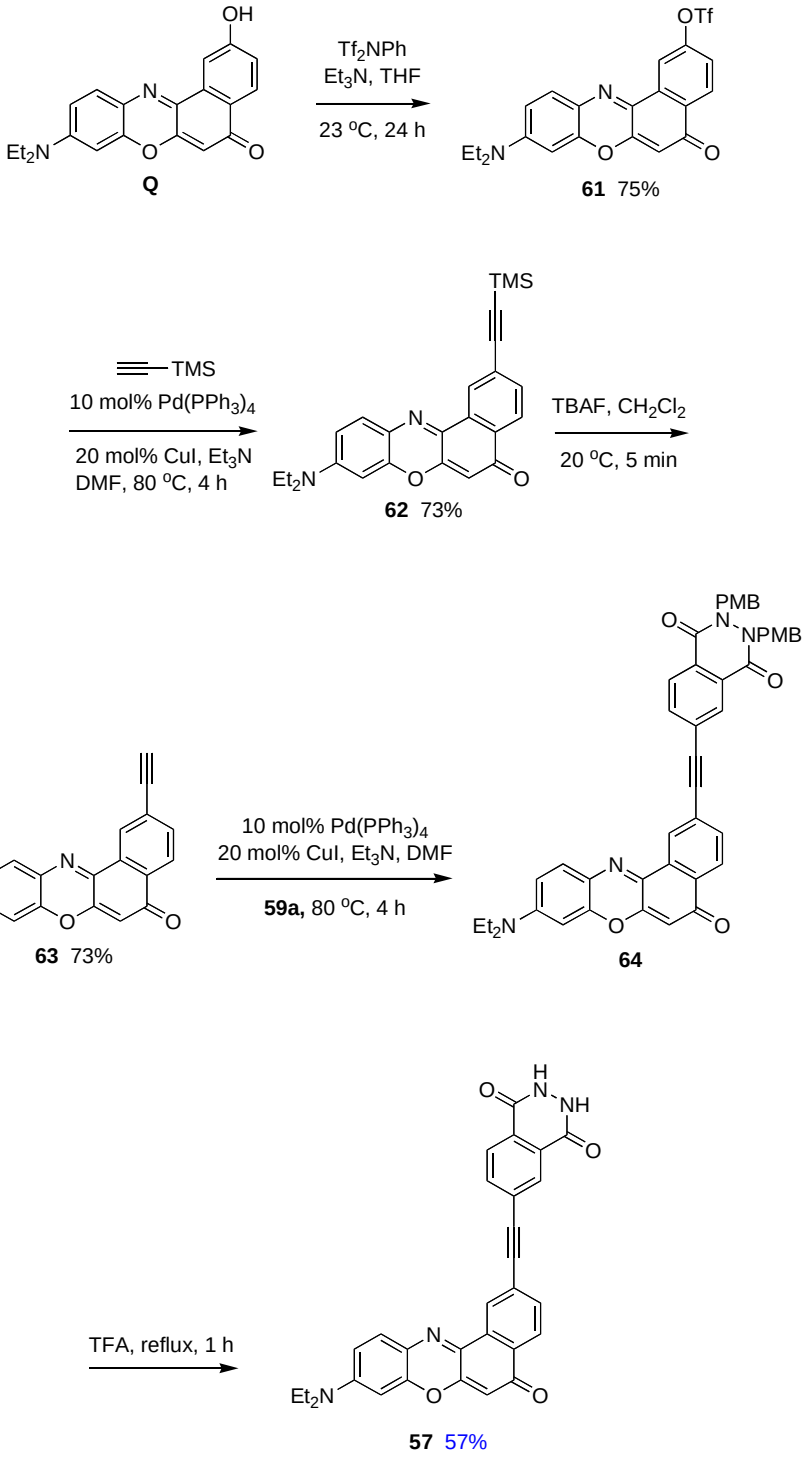

Scheme 4.1. Continued.

c

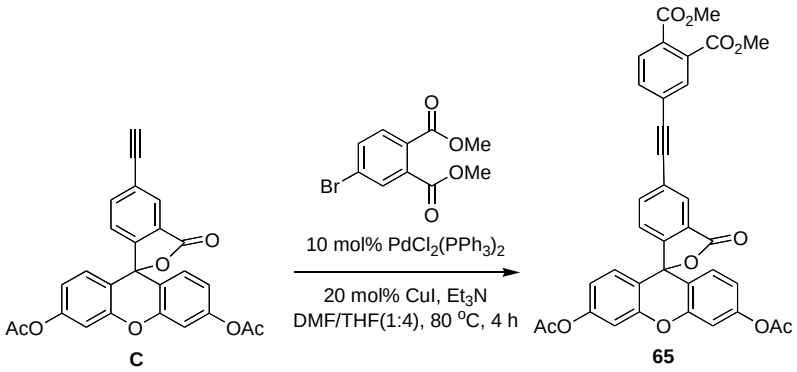

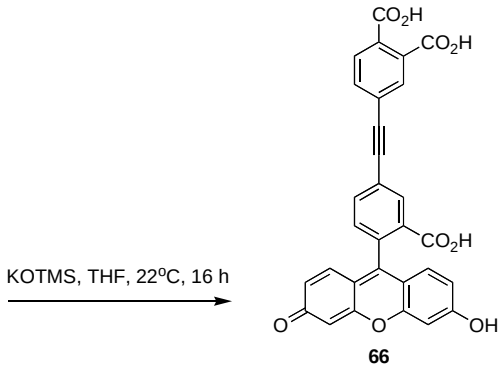

d

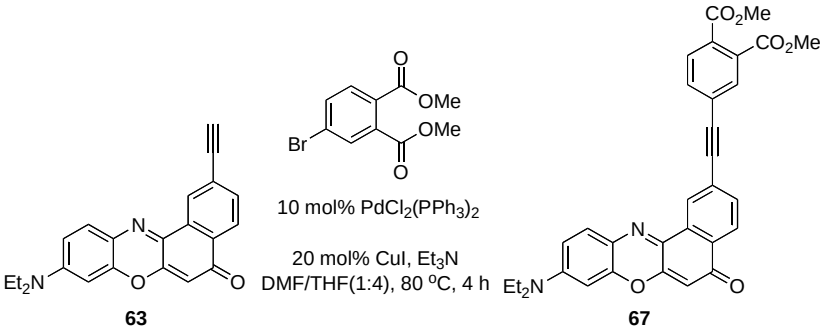

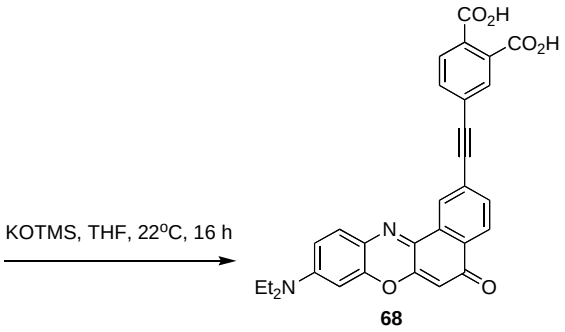

68

C. Results and Discussion

It is hard to describe the spectacular chemiluminescence of these compounds without moving pictures of the experiments to support the words (Figure 4.1). For cassette **56**, a 100 μl aliquots of the compound (10^{-5} M, in pH = 10 aqueous $Na_2CO_3/NaHCO_3$ buffer) was added to a sample cell containing $CuSO_4$ (1.5 x 10^{-3} M) and H_2O_2 (2.0 x 10^{-3} M) with stirring. Cassette **57** is not very soluble in aqueous media and, in any case, the quantum yield for Nile Red emission is less than 0.1 in water. Consequently, for **57**, potassium *tert*-butoxide in THF (10^{-2} M) was added to the compound dissolved in dry DMF (10^{-5} M). This experiment is done open to the air and oxygen is presumed to be the oxidant. Luminol under the conditions used for cassette **56** gives a bright blue emission. If efficient energy transfer occurred for compounds **56** and **57** then we were expecting them to emit yellow/green and red chemiluminescence instead, characteristic of fluorescein and Nile Red, respectively. This is exactly what we saw. Cassette **56** gave a bright yellow/green emission, while **57** glowed with a less intense red colour. No trace of blue in the emission was seen in either case.

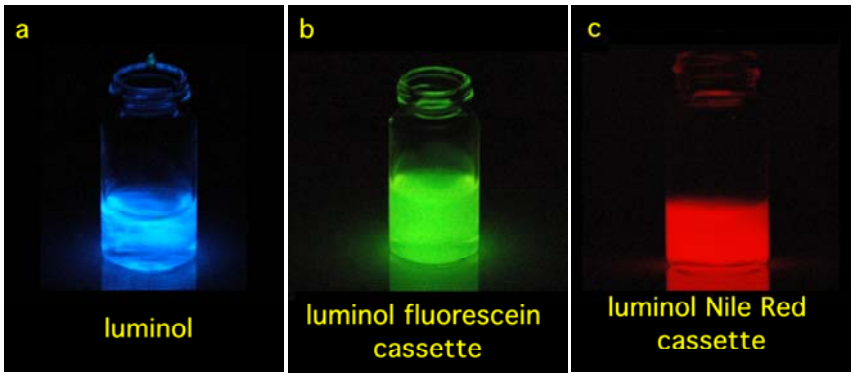

Figure 4.1. Pictures of (a) luminol, (b) cassette **56**, and (c) cassette **57** when activated with an oxidant.

Compounds **63** and **64** were prepared as controls (see Scheme 4.1c) since it is thought that the excited species from luminol derivatives involves the corresponding phthalate dianions. Indeed, ESI-MS analysis of cassettes **56** and **57** after the oxidative activation revealed the presence of **63** and **64**, respectively. This was confirmed via HPLC analyses in the case of **56**.

Figure 4.2a shows normalized UV absorption and fluorescence spectra for **66**, and **68**. The extent of overlap between the chemiluminescence output of the phthalate derived from luminol and the UV absorption of the acceptor part of cassettes **66** and **68** is shown in Figure 4.2b. Normalized chemiluminescence emissions for **56** and **57** are shown in Figure 4.2c. The emissions of **56** and **57** are sharp and characteristic of the acceptors only; no chemiluminescence from the donor was detected.

a

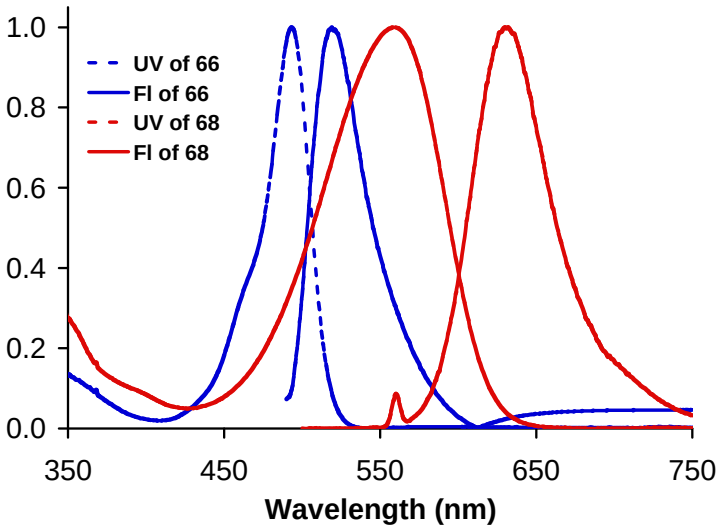

Figure 4.2. Normalized: (a) UV/visible and fluorescence spectra of **66** in pH = 10 aqueous sodium carbonate/bicarbonate buffer solution, and of **68** in dry DMF; (b) chemiluminescence spectrum of luminol (blue), UV/vis absorption bands of compound **66** (green) and compound **68** (red); (c) chemiluminescence spectra of luminol (blue), cassette **56** (green), and cassette **57** (red).

b

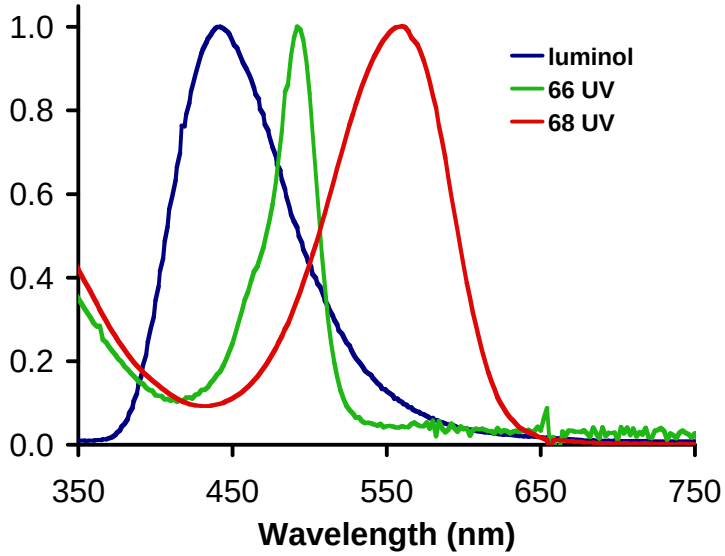

c

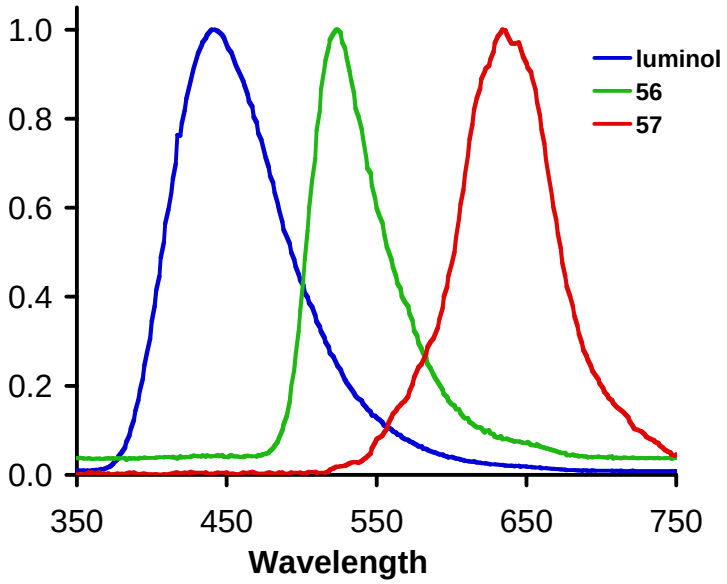

Figure 4.2. Continued.

Sometimes, the eyes can play tricks on the brain, and that is partially true in this case. The chemiluminescence from cassette **57** appears to be weaker than that for **56**, but the quantitative data collected in Table 4.1 indicates this is not the case. Chemiluminescent quantum yields measured relative to luminol indicate **57** actually emits more strongly. Probably, chemiluminescence from **57** appears to be weaker than that from **56** because the human eye is about five times more sensitive to light near the emission maximum of fluorescein than it is to light emitted from the Nile Red acceptors.[226]

Table 4.1. Selected spectroscopic properties of luminol, **56**, **66, 57, 68** and **R**.

Compds	UV	Fluorescence	Chemiluminesence	
	$\lambda_{abs\ max}$ (nm)	$\lambda_{fluor\ max}$ (nm)[b]	$\lambda_{chemi\ max}$ (nm)[b]	Relative Φ_{chemi}
luminol[a]	-	-	442	100[a]
56[a]	494	518	524	61[b]
66[a]	493	519	-	-
57[b]	558	628	634	>100[b]
68[b]	558	628	-	-
R	-	-	412	0.02[d]

a In carbonate/bicarbonate buffer. b In dry DMF. c From ref. 221.

The relative quantum yields for chemiluminescence that are presented in Table 4.1 use luminol as a standard. However, the donor fragments of cassettes **56** and **57** do not have the amino substituent of luminol. Small changes to the luminol structure tend to reduce its chemiluminescence dramatically.[218] If the emissions from cassettes **56** and **57** were compared with the hydrazide **R** (which has a much lower absolute quantum yield for chemiluminescence) then the data for cassettes **56** and **57** would appear to be even more impressive.

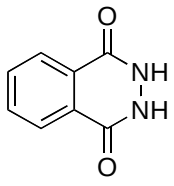

R

Experimentally, it is extremely challenging to determine the extent of energy transfer through-bonds and through space in twisted but otherwise conjugated cassettes. For the UV-activated system **P** we asserted that through-bond energy transfer must be fast and efficient by considering rates of energy transfer.[144] However, direct observation of rates is hard in chemically activated systems where excitation of the donor occurs continuously. Further, we have so far been unable to prepare the logical control compounds for comparison: those in which the alkyne linker of cassettes **56** or **57** are replaced by an ethylene fragment. In any case, *through-space* energy transfer for those controls might differ considerably from that occurring in **56** or **57** because the orientation of the donor and acceptor fragments would be dynamic in the reduced compounds. However, the *through-space* energy transfer cassette **S**, based on luminol, was prepared approximately four decades ago and does provide an interesting comparison.[227-229] The reported relative chemiluminescence quantum yield for this compound (luminol standard) is significantly less than that measured here for cassettes **56** and **57**. It may be that, just as in our UV-activated cassettes like **P**, rapid and efficient energy transfer can occur for the systems that facilitate the possibility of through-bond energy transfer.

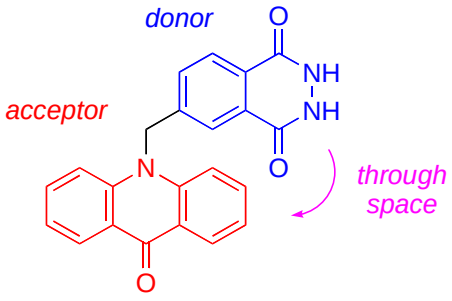

S
relative Φ_{chemi} = 8
(luminol = 100)

Calculations of Förster energy transfer for systems that have donor and acceptor fragments arranged within a few Ångstroms are not correct because the theory implies a point dipole approximation which fails when the distance becomes less than the special size of the donor and acceptor charge distributions. Nevertheless, these calculations were performed; the dipole-dipole energy transfer efficiency was smaller (39 and 42% for **56** and **57**, respectively) than actually observed.

Chemiluminescence provides detection methods that approach the sensitivity of ones based on radioactivity.[230] In the context of intracellular imaging, it has the advantage that no excitation irradiation is required. Simple *in vitro* experiments show that cassettes **56** and **57** can be activated via treatment with peroxidase under physiological conditions, and they emit in longer wavelength regions that are more transparent to cellular tissues than the 420 - 450 nm range where luminol chemiluminesces. Consequently, there is a possibility that probes based on chemically-activated energy transfer can be applied in biotechnology.

CHAPTER V

NON-COVALENT DELIVERY OF PROTEINS INTO MAMMALIAN CELLS

A. Introduction

Import of proteins into cells is an important problem that is frequently encountered in many aspects of biological chemistry. One of the best-studied approaches is to *covalently* attach a peptide carrier, either chemically or genetically, to the protein of interest. Perhaps the most commonly used carriers of this type are the short peptide segments derived from HIV-1 Tat and *Drosophila* Antennapedia homeodomain proteins.[231,232] Use of the HIV-1 Tat carrier, in particular, has motivated researchers to look for simpler peptides for more efficient intracellular[233] cellular uptake. In living cells, both R8 and R16 have been reported to facilitate significant cellular uptake, while R_4 gave relatively little internalization.[234,235] A major drawback to the use of these peptide delivery agents, however, is that cargo proteins imported into the cells tend to be concentrated in vesicular structures.[236,237] These vesicles are widely assumed to correspond to endosomes, hence the cargo proteins are *not* released in the cytoplasm. This has inspired many groups to investigate the mechanism of import, and to look for ways of liberating the cargo proteins from the endosomes. For instance, Wender and co-workers have suggested that the oligo-guanidine moieties can form an ideal hydrogen bonding networks with the cell surface phosphates, and this facilitates the import on a molecular level.[233,238,239] Meanwhile, an elegant series of experiments by Dowdy indicates the macromolecular mechanism of import involves macropinocytosis,[240] and

liberation of protein cargo-Tat conjugates from endosomes could be achieved by adding the *N*-terminal 20 amino acids of the influenza virus hemagglutinin protein, HA-2,[241] to the carrier sequence.[236]

Genetic or chemical methods for covalently attaching carrier peptide sequences to cargo proteins are experimentally inconvenient, time consuming, and restrictive with respect to the scope of the experiments that can be performed. Conversely, carrier vehicles that can import proteins *without being covalently attached* have the potential to circumvent all these disadvantages. "Non-covalent carriers" include "Pep-1" (also known as Chariot®),[127] the cationic pyridinium amphiphile and a helper lipid, SAINT-PhD,[242] BPQ24 BioPORTER® QuikEase™ (a protein delivery kit of unspecified composition),[243] and a few used systems like the peptide K16SP[244] and the somewhat cytotoxic polymer, polyethyleneimine (PEI) (Figure 5.1).[245,246] However, the issue of whether or not the imported cargo proteins are trapped in endosomes blurs the true utility of these systems. It is clear from some reports in the literature that fluorescently labeled proteins imported using these systems become concentrated in cytoplasmic vesicles; this was our experience in previous studies.[99,247] However, some papers claim imported fluorescently labeled proteins appear to be free in the cytoplasm, and there have been papers wherein import of proteins using these systems is thought to give a predictable functional response.[248]

a

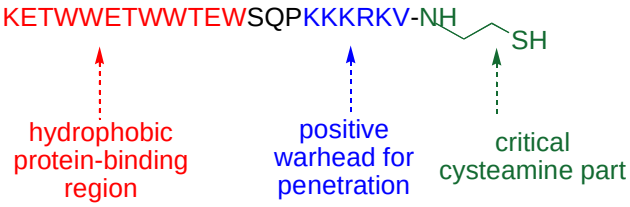

pep-1

b

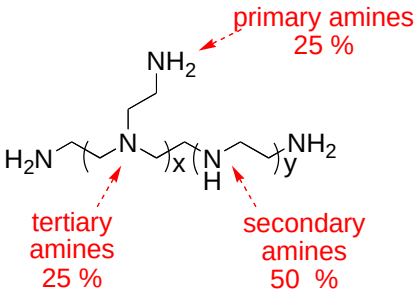

PEI
(MM ~ 25,000 from Aldrich)

c

KKKK KKKK KKKK KKKK AAVA LLPA VLLA LLAP

K16SP

Figure 5.1. Structures of the "Non-covalent Carriers" (a) Pep-1 (also known as Chariot™), (b) polyethyleneimine (PEI) and (c) K16SP.

There were no reports of simple Arg-oligomers being useful for *non-covalent* import until recent work by Lee *et al*.[249,250] They described experiments in which high concentrations (600 mM) of R_9 mediated import of various fluorescent proteins (*eg* GFP) and b-galactosidase into plant (onion root tip) and animal (MCF7) cells. It was claimed that this produced diffuse fluorescence in the cytosol and in the nucleus, however, only low resolution images were shown, and in these cells, the fluorescence appears as small green aggregates. Furthermore, the b-galactosidase was imaged after fixing the cells, and this is known to give different results relative to live cells.[249,250]

Data presented in this paper deal with import of four proteins labeled with Alexa Fluor® 488 (F*):[51] specifically, avidin, bovine serum albumin (BSA), b-galactosidase (b-gal), and a recombinant streptavidin. These cargoes were chosen to represent proteins with different pI values and sizes (Table 5.1). The potential carriers examined were Pep-1, R_8, and a novel system that was synthesized "in house", azo-R_8, all of which were *not* covalently attached to the protein. The key observations are that: (i) at 37°C, avidin was imported by all three carriers (Pep-1, R_8, and azo-R_8) but in each case the labeled protein primarily accumulated in vesicles that co-localized with the endosomal marker FM 4-64; however, (ii) at 4°C weak, diffuse fluorescence was observed within the cytoplasm with little evidence of punctate vesicle formation for all four proteins. These observations indicate a temperature dependence of carrier-mediated protein delivery that was similar for three chemically different carriers.

Table 5.1. Proteins Studied For the $(Arg)_8$ Mediated Cellular Uptake

Protein	Molecular Weight (kDa)	Size (a.a.)	pI (unlabeled protein)
Avidin	66-68	512	10 – 10.5
BSA	66	583	4.7
Streptavidin, rec.	52	560	7.4 – 7.7
β-Galactosidase	540	1171	4.8

B. Results and Discussion

1. R_8 and Azo-R_8: Design and Synthesis

At the onset of this project, we had hypothesized that mimics of Pep-1 could be made by fusing well-known "promiscuous binders" (molecules that seem to bind many proteins in high throughput screens for drug leads)[251,252] to a cell-penetrating warhead. The idea was that the promiscuous binder parts of several pep-1 analogs might non-covalently attach to the protein, coating it with entities that promote cell penetration. Thus, an azo-compound was chosen for the promiscuous binder part, and R_8 for the cell-penetrating unit; these were synthetically joined to give azo-R_8. However, azo-R_8 was found to behave in much the same way as R_8, but with some minor differences as indicated below.

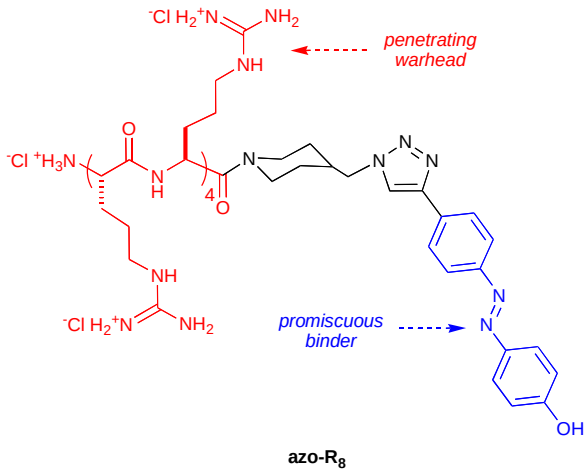

Figure 5.2. Structure of azo-R_8.

Starting from commercially available bis-N protected amino acid, R_8 was synthesized in 10 steps according to the literature procedure.[253] The coupling reagent

EDC was used to replace isobutyoxycarbonyl chloride because the reaction is clean, and the working up and purification procedure for the reaction are easy. The coupling products can be easily isolated in > 95% pure using extraction by simply washing away the byproduct from organic phase with aqueous acid and base solutions.

Scheme 5.1. Synthesis of azo-R_8

a

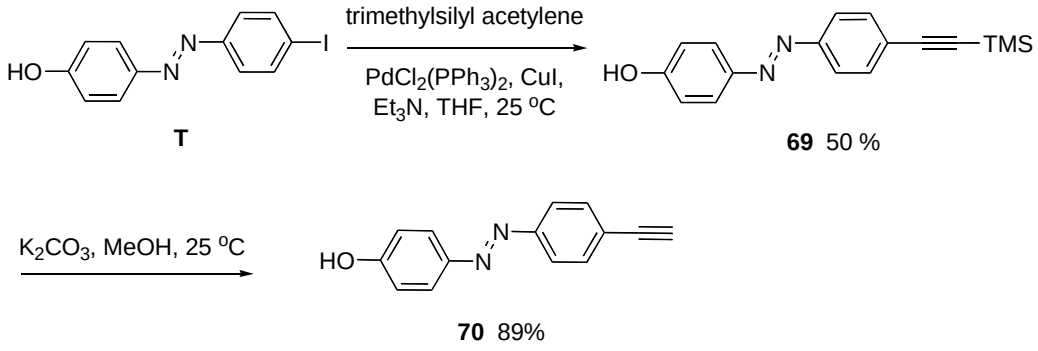

b

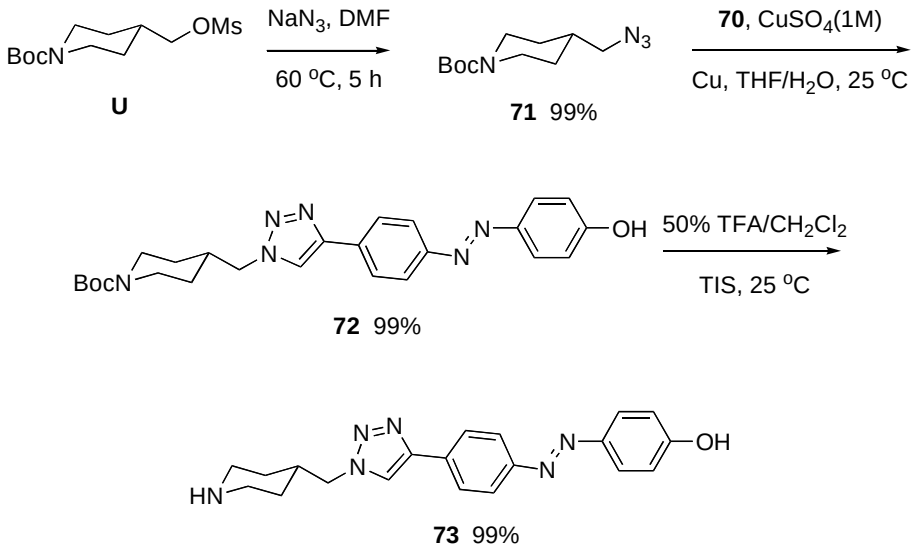

Scheme 5.1. Continued.

c

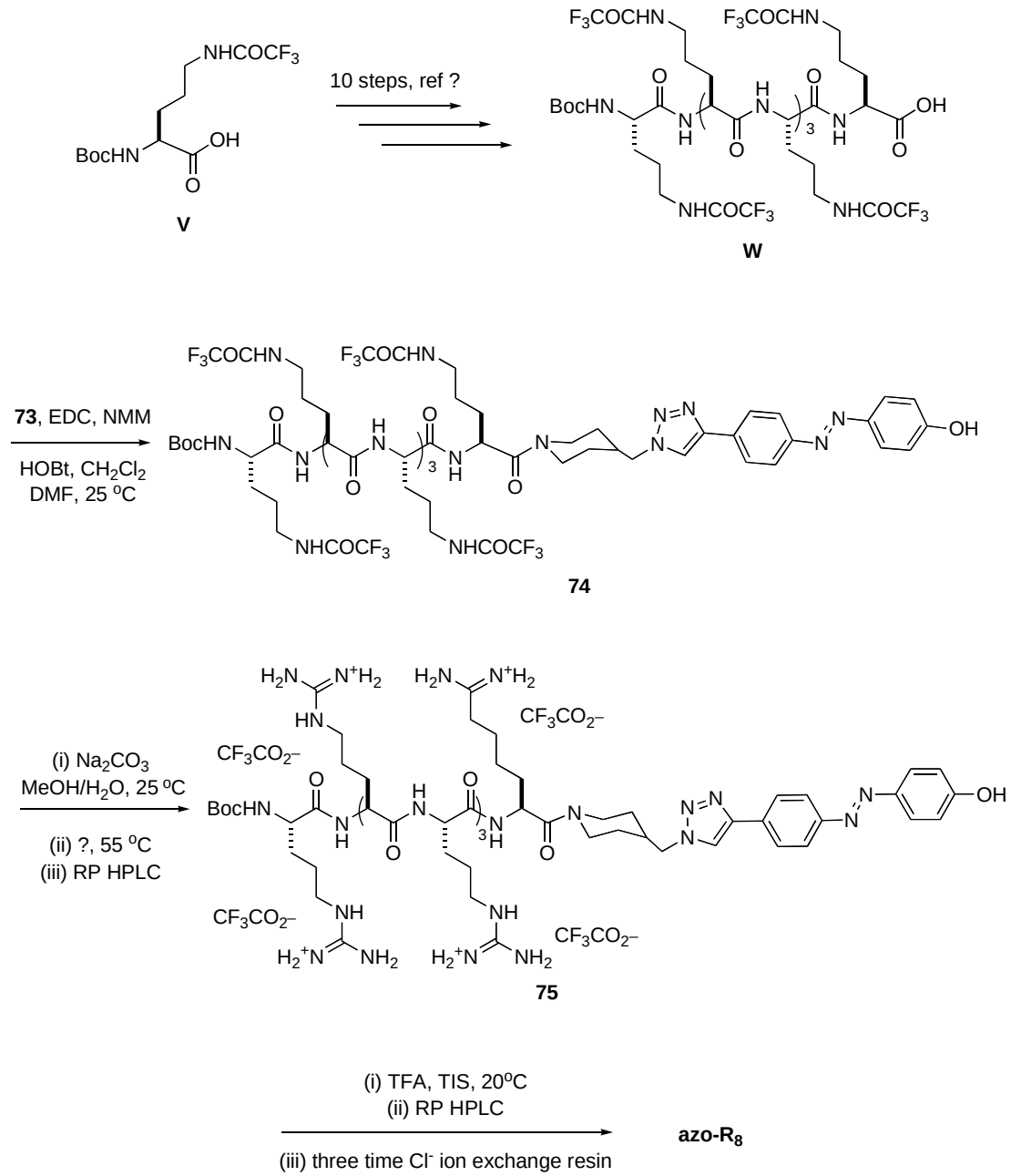

The **azo-R_8** synthesis starts from a known nasty compound azo-phenol **T**, which is synthesized from the coupling reaction of phenol and 4-iodophenyldiazonium salts. The submission of the azo-phenol to Sonogashira coupling reaction with trimethylsilyl acetylene afforded trimethylsilyl alkyne **72** in moderate yield, which might result from decomposition of the s.m. under the reaction conditions. Terminal alkyne **73** was achieved by deprotection of the TMS group with K_2CO_3 in methanol. The key promiscuous binder intermidiate triazole **73** was synthesized by copper I catalyzed cyclo addition of terminal alkyne **70** and azide **71**, followed by deprotection of Boc group of **72**. Azide **71** was synthesized from **U** by simple SN_2 reaction as shown in Scheme 5.1b. The standard EDC mediated coupling of the known acid **W** with **73** produced the key intermediate **74** in 80% yield in 95% purity after washing away the by products from CH_2Cl_2 phase with 5% $NaHSO_4$ and 5% $NaHCO_3$ aqueous solution. Removal of the trifluoroacetyl protection group, followed perguanidilation afforded the desired products **75** as a light yellow solid after prep HPLC. The final **azo-R_8** was transformed from **75** by Boc deprotection, followed by RP HPLC purification and counter anion exchange with Cl^- resin. The **azo-R_8** was 95% pure as indicated by analytical HPLC; also it has the correct MS peak.

2. Formation of Carrier: Cargo Complexes

Pep-1 and azo-R_8 are amphipathic peptides, while R_8 is cationic. Pep-1 is known to associate with protein cargoes through non-covalent electrostatic or hydrophobic interactions and form stable complexes**.** [127,254-256] The formation of the carrier:cargo

complex for azo-R_8 was easily monitored by fluorescence spectroscopy. The azo compound can act as quencher of the label on the protein, proving that the two are in close contact. Figure 5.3 shows the intense fluorescecne of BSA-F* (2 μM in DMEM) was greatly quenced when azo-R_8 was added (1.0:10 mol ratio protein:carrier). In a control experiment, a solution of fluorescein (0.1 μM) was mixed with 1 μM azo-R_8 under almost identical conditions and no quenching was observed.

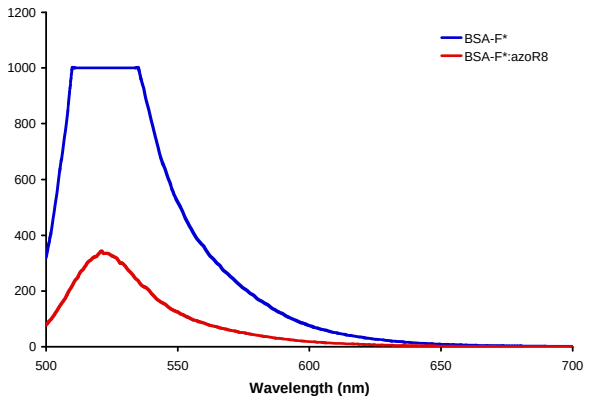

Figure 5.3. Azo-R_8 forms a non-covalent complex with BSA-F*. The fluorescence of BSA-F* upon excitation at 488 nm is compared to the one of a 1:10 molar ratio protein:carrier mixture.

3. Delivery at 37ºC: Uptake into Punctuate Vesicular Structures

Cellular uptake of avidin-F* into COS-7 at 37°C was studied in the first phase of this work. All three carriers, pep-1, R_8, and azo-R_8, were used at 10:1 carrier:cargo mol:mol ratio, and similar results were observed in all cases. Figure 5.4 for avidin uptake is illustrative. After 1 h of incubation, followed by a 15 min incubation period with FM 4-64, the Alexa Fluor 488-labeled protein accumulated as green, punctate cytoplasmic vesicles. These green vesicles were localized in endosomes as suggested by co-loading with the endosomal marker FM 4-64 (Figure 5.4C). [257] When the cells were

co-incubated with avidin-F* and FM 4-64 for 1h at 37 °C, little to no co-localization was observed with the endosomes, as the mitochondria were labeled under those conditions and not the endosomes (see supplementary). The perinuclear distribution of these vesicles suggests potential sorting and transport to Golgi and lysosomes. This was confirmed by co-loading the cells with the Golgi marker BODIPY TR ceramide complexed to BSA (Figure 5.4D). [51] After extended incubation times (up to 24 h) the vesicles persisted, and no significant dispersed fluorescence was observed in the cytosol. These observations are consistent with the imported protein being trapped in endosomes, even after long periods of time.

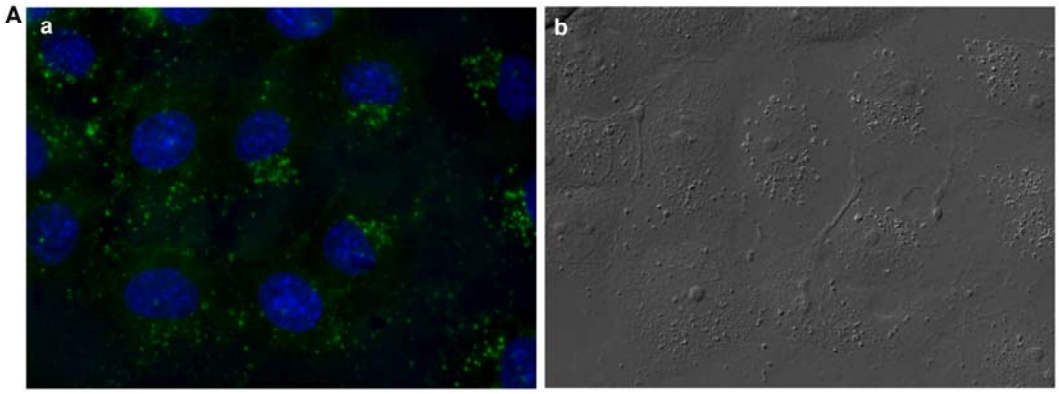

Figure 5.4. Delivery of avidin-F* in COS-7 cells at 37 ºC. (A) Non-covalent protein delivery mediated by R_8; (B) Non-covalent protein delivery mediated by azo-R_8; (C) Endosomal colocalization of avidin-F* and FM 4-64 (fluorescent general endosomal marker); (D) Golgi colocalization of avidin-F* and BODIPY TR ceramide complexed to BSA (fluorescent marker for Golgi); (E) Cell autofluorescence; (F) Non-mediated protein delivery. Throughout the carrier (5.0 μM), avidin-F* (0.5 μM) and the COS-7 cells were incubated at 37 ºC for 1 h; the cells were then washed with PBS and analyzed by fluorescence microscopy. For endosomal colocalization, the cells were incubated with FM 4-64 at 37 ºC for 15 min, then washed with PBS before imaging. For Golgi colocalization, the cells were incubated for 30 min at 4 ºC in DMEM containing 5 μM BODIPY TR ceramide complexed to BSA, washed several times with ice-cold medium and incubated in fresh medium for 30 min at 37 ºC. (a) Overlaid images of the avidin-F* (green) and the nuclei (blue, Hoechst 33342 marker). (b) Differential interference contrast (DIC) images.

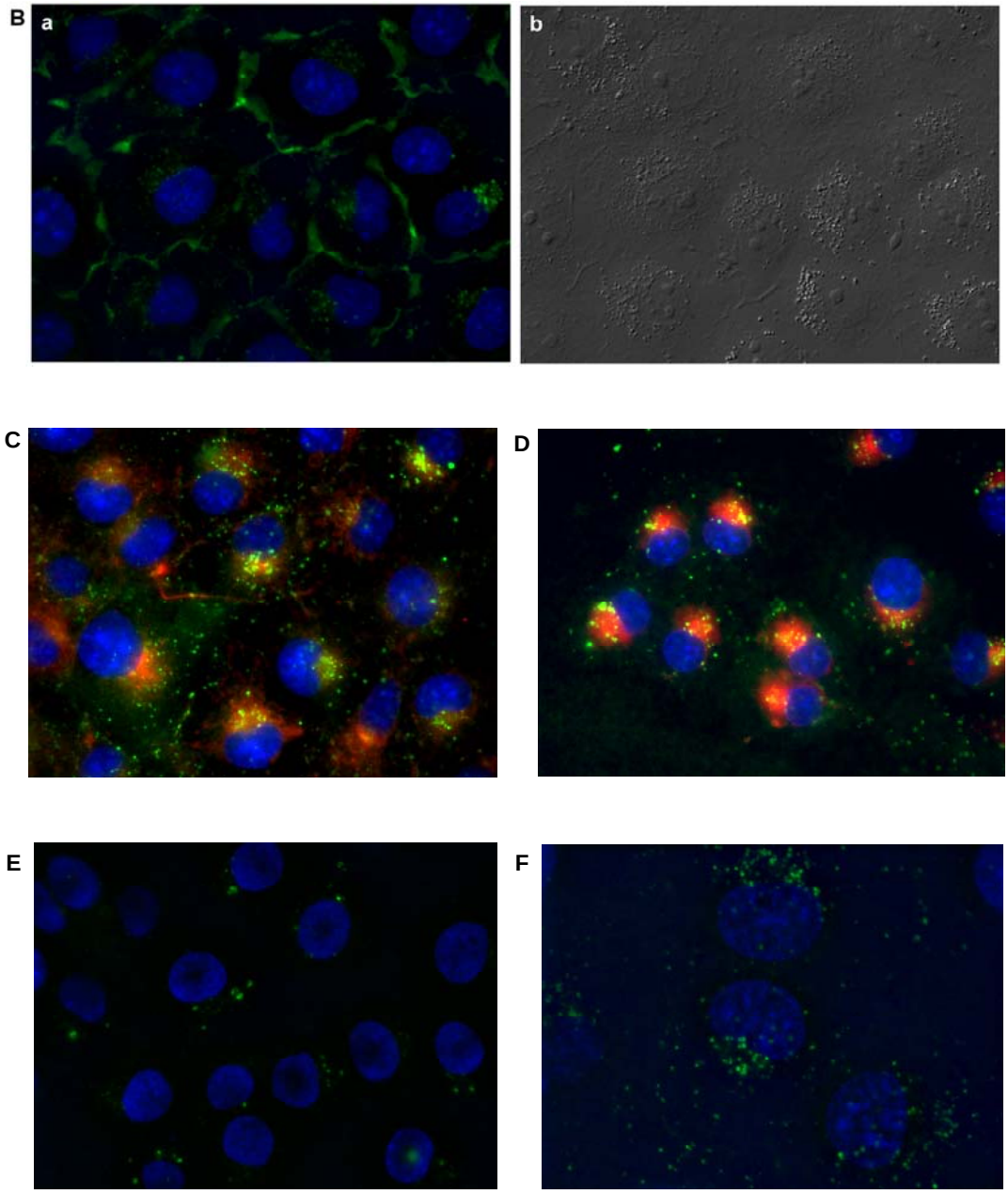

Figure 5.4. Continued.

Consideration of the images from import mediated by **azo-R_8** shows this consistently directs more of the labeled protein into the cellular membrane compared with R_8 and pep-1. This observation implies some protein/azo-R_8 complex may be

trapped in the membrane in these experiments. It was also observed that when confluent cell cultures were used, more membrane staining was observed for *all* three carriers, but more so for azo-R_8.

4. Delivery at 4ºC: Diffuse Cytosolic Fluorescence

Punctate vesicle formation was largely suppressed when the experiments described in the previous section were repeated at 4°C. As an added precaution against surface binding,[240] the cells were treated with heparin (3 x 5 min, 1 mg/mL of PBS) after the PBS washes. Nevertheless, a weak, diffuse fluorescence signal was observed (see supplementary). Further, fluorescence deconvolution imaging of the cells showed the same diffuse fluorescence pattern. These observations indicate that at 4°C, the protein is indeed being imported inside the cytoplasm by all the carriers.

Experiments were performed to increase the fluorescence signal in the cytosol by increasing the concentration of the protein from 2 mM and to 5 mM (carrier:protein = 10:1 mol:mol, as before). At 2 μM, the fluorescence intensity in the cytosol was increased but some additional binding to the cell membrane was observed. At 5 mM, the intensity of membrane labeling was considerably brighter, however, the cytoplasmic signal was retained (Figure 5.5).

Similar experiments on BSA-F*, β-gal-F*, and recombinant Streptavidin-F* also gave diffuse cytoplasmic fluorescence (see supplementary). Uptake of β-gal-F* was significantly lower than for the avidin and BSA dye-conjugates, even when a higher

ratio of carrier:protein (20:1) ratio was used. This difference was confirmed in the flow cytometry experiments described in the next section.

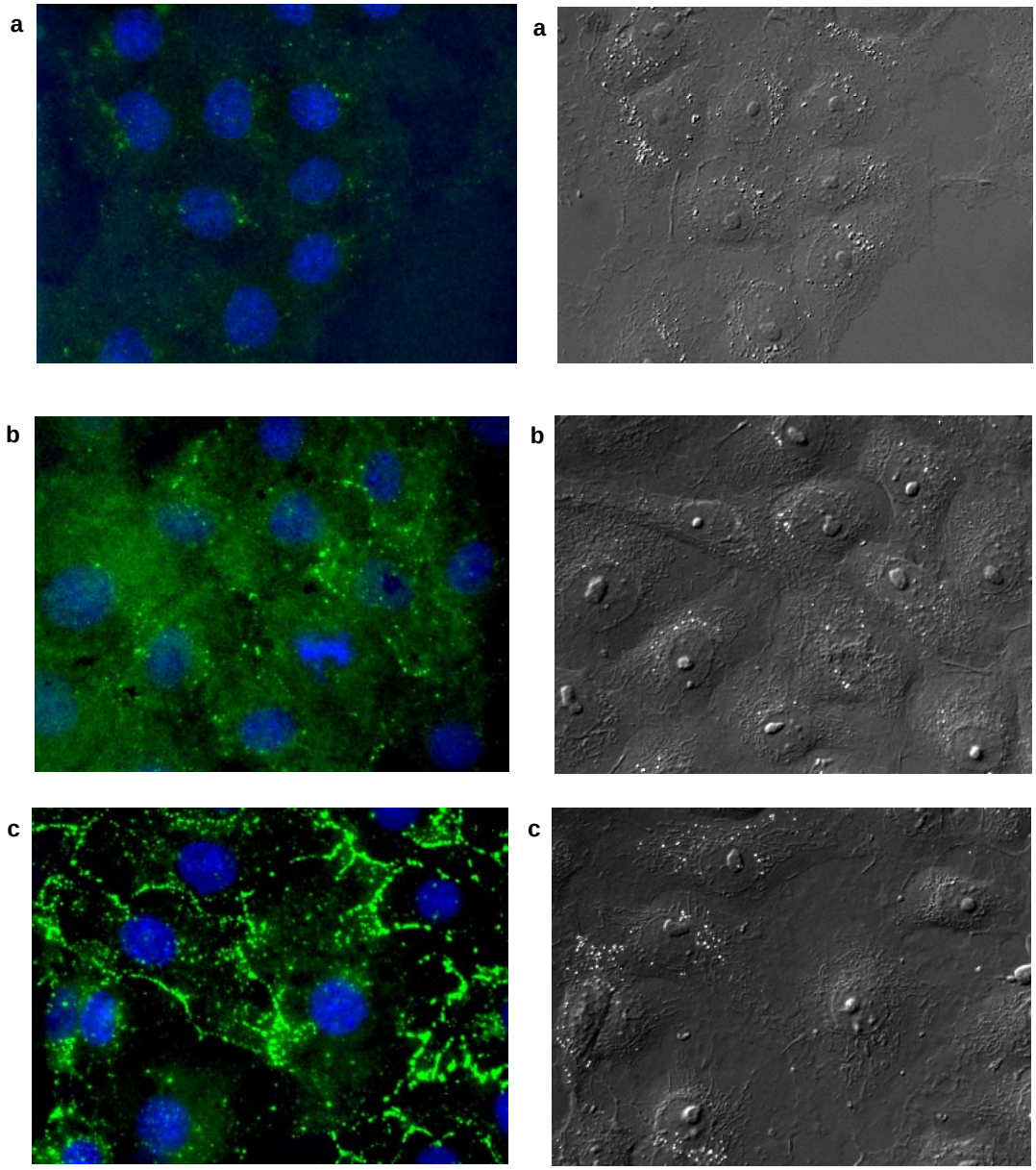

Figure 5.5. Delivery of avidin-F* in COS-7 cells at 4 ºC mediated by R_8. (a) 0.5 μM of avidin–F*. (b) 2 μM avidin–F*. (c) 5 μM avidin–F*. (d) No carrier used Throughout COS-7 cells were incubated for 1 h at 4°C with R_8 and avidin-F* (10:1.0 mol:mol), then washed 4x with PBS buffer. Images shown are after deconvolution; *left* images are fluorescence images of avidin-F* and Hoechst 33342, *right* images are DIC.

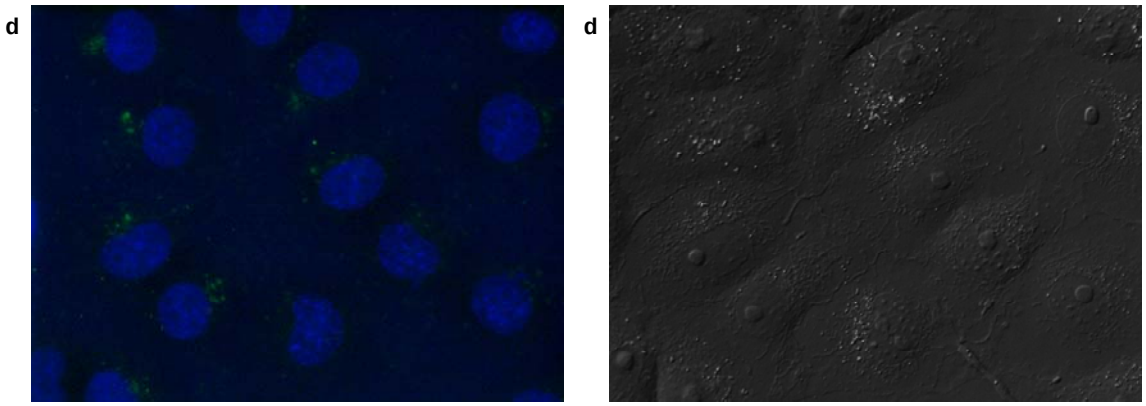

Figure 5.5. Continued.

5. Comparison of Uptake Levels For Different Carriers via Flow Cytometry

Flow cytometry was used to analyze and compare the non-covalent protein transduction (Figure 5.6). Before the analyses, the cells were washed with PBS, treated with trypsin, then washed with heparin (3 x 5 min, 0.5 mg/mL PBS) to minimize the possibilities for surface binding. In each case, the uptake measured by flow cytometry was greater when the carrier molecule was included (0.5 mM protein; carrier:protein 10:1.0 for avidin-F* and BSA-F*, and 20:1.0 for b-gal-F*). Import of avidin-F* was significant, with pep-1 and R_8 being more effective than azo-R_8 at 4 ^{o}C (Figure 5.6A). However, for BSA-F* the reverse was true: azo-R_8 was far more effective than the other two carriers. The largest protein-dye conjugate, b-gal-F*, was the least well imported of the three proteins that were tested, with pep-1 and azo-R_8 being the most effective carriers.

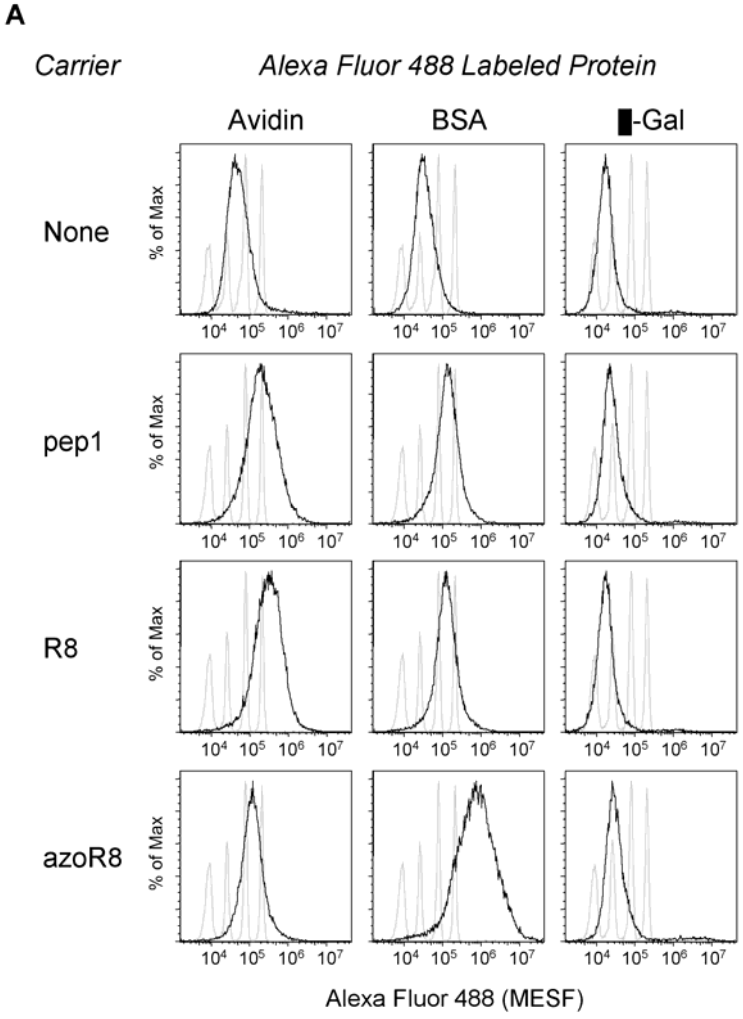

Figure 5.6. (a) Flow cytometric analysis of the uptake of the Alexa Fluor 488 labeled proteins, avidin-F*, BSA-F* and b-gal-F* at 4°C relative to FITC Quantum Bead standards (shaded histograms). Each histogram for avidin-F* and BSA-F* represents 20,000 to 24,000 cells and 20,000 beads. For b-gal-F*,each histogram represents 10,000 cells and 20,000 beads. The FITC Quantum Beads peaks represent 8534, 25857, 79264, and 214887 MESF units each. The scale for the X-axis is MESF units. (b) Summary of the flow cytometric data for each protein with the carriers tested. Results are presented as the median MESF units for each protein-carrier combination.

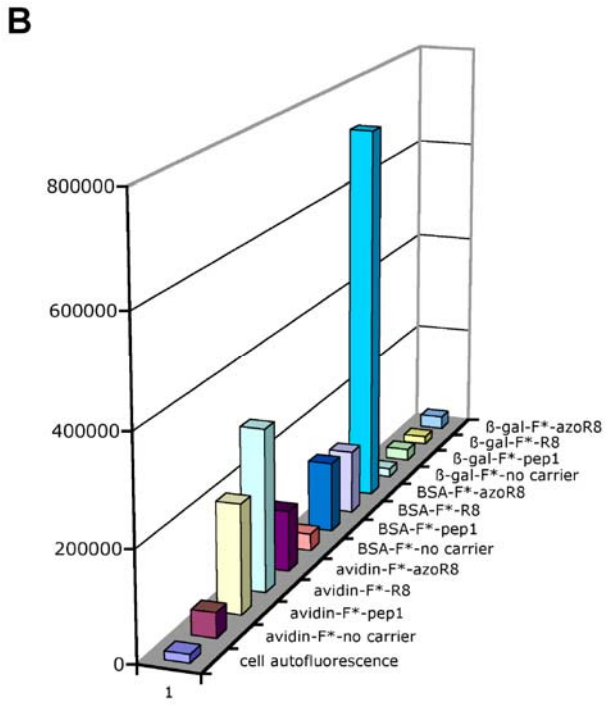

Figure 5.6. Continued.

6. Evaluation of the Cytotoxicity of the Carriers

Cell viability during the non-covalent protein internalization mediated by R_8 and azo-R_8 was accessed using ethidium homodimer. Thus COS 7 cells were treated with a l.0:10 mol ratio protein:carrier (2 μM protein) for 1 h at 4°C, washed with PBS and treated with ethidium homodimer (2 μg/mL). Figure 7A illustrates that cells treated with R_8 and azo-R_8 peptides for 1 h at 4°C did not result in any cytotoxicity. Incubation at 37°C for another 16 h gave no cytotoxicity (the fluorescence was now mostly concentrated into vesicles, probably lysosomes, Figure 5.7B). After a further incubation period of 24 h at 37°C however, all the cells were dead (Figure 5.7C).

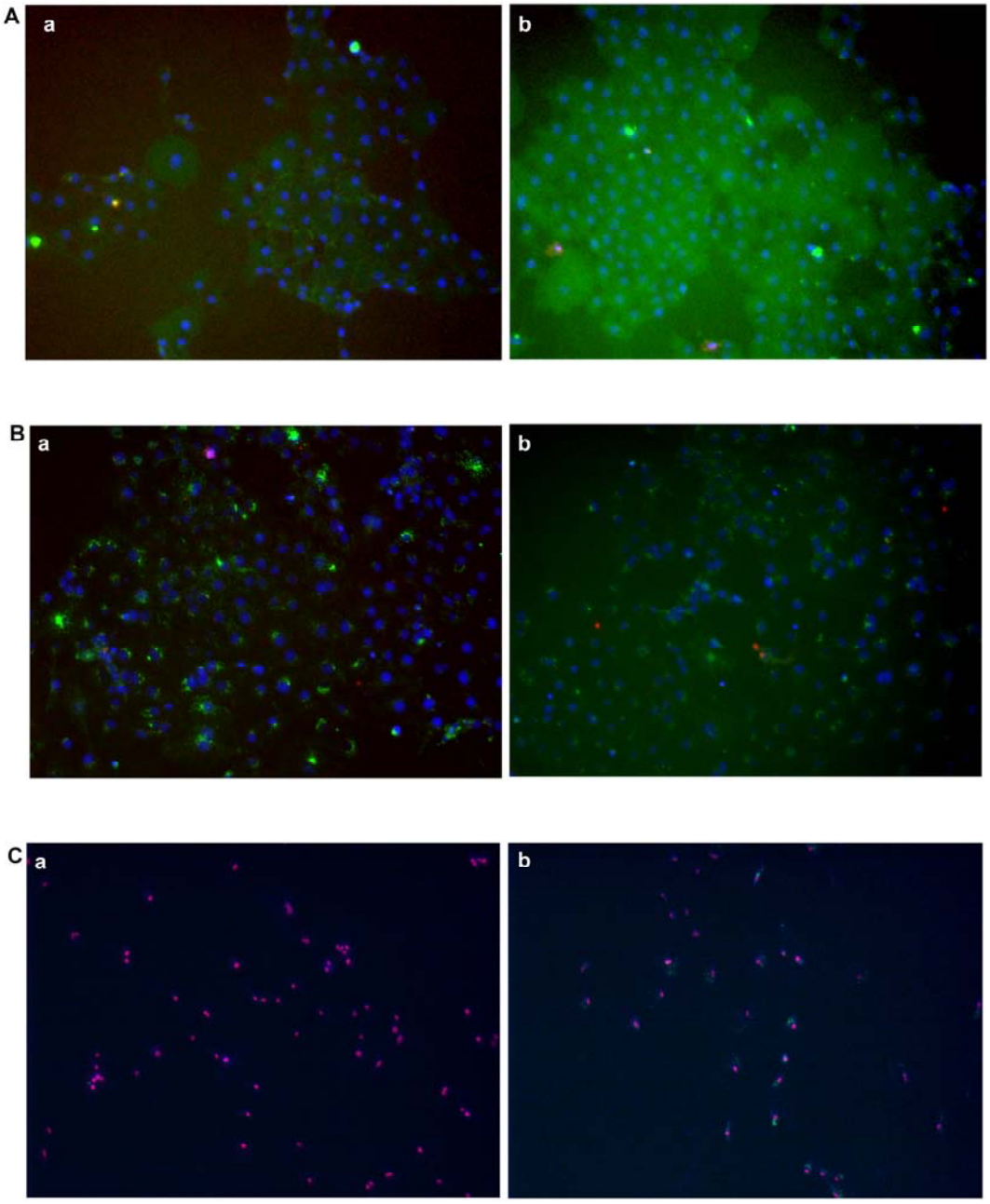

Figure 5.7. Viability Assay**.** Delivery of avidin-F* (2 μM) in COS-7 cells at 4 ºC mediated by (a) R_8 and (b) azo-R_8. (A) COS-7 cells were incubated for 1 h at 4°C with R_8 or azo-R_8 and avidin-F^* (10:1.0 mol:mol), then washed 4x with PBS buffer and treated with ethidium homodimer for 30 min. (B) The same cells were incubated at 37°C for 16 h. (C) The medium was removed, fresh PBS was added and the same cells were incubated at 37°C for another 24 h. Before imaging, 2 μL of ethidium homodimer were added.

C. Conclusions

Import into cells at 37°C could be regulated via energy-dependent or independent pathways, but at 4°C it is generally accepted that only energy independent pathways are operative. The data accumulated here indicate that at 37°C import into endosomes is prevalent and significant diffuse fluorescence in the cytosol was not observed. However, the relative brightness of the vesicular staining may obscure low level cytoplasmic fluorescence. Thus, at least two different pathways appear to be operative for three different carrier molecules, and the desired one, diffuse import into the cytosol, prevails at 4°C. This observation is parallel and consistent with work reported by Futaki *et al*.[237] They studied the mechanism of translocation of R_8-Texas Red at 37 and 4°C, *without* cargo proteins and observed vesicular staining at 37°C and diffuse fluorescence in the cytosol at 4°C. The simplest explanation for the reduced efficiency for import of b-gal-F* relative to the other proteins is that it is approximately eight times larger. Similarly, the simplest explanation for the observation that three chemically different carriers facilitate import of three different proteins at 4°C via an energy independent pathway is that they form pores in the cells membrane that allow leakage into the cells, even at 4°C. This would explain the fact that the levels of diffuse fluorescence observed are weak, and that the larger protein was the one least effectively imported. At 37°C, other mechanisms, perhaps involving macropinocytosis (an energy dependant process), become dominant.

CHAPTER VI

SUMMARY AND CONCLUSIONS

In summary that we have demonstrated that TBET cassettes with specific characteristics are useful in three different biological areas. TBET cassettes have desired spectral properties for studying proteins' interactions. The well-resolved muitiple fluorescence emission spectra for multiplexing could be obtained. I have synthesized a water-soluble cassette **55** based on bissulfonated BODIPYs, it has been demonstrated to be a good protein labeling dye. A series of this kind of cassettes will be ideal for studying multi-protein interactions in vivo. A ratiometric fluorescent pH_i indicator **16** based on energy transfer has been shown to image protein-dye conjugates in living cells. It has better quantum yields than a widely used pH probe C.SNARF-1. The pH sensitive range of this cassette is also complementary to the C.SNARF-1. Also we have demonstrated that the descrete long-wavelength chemiluminescence probe could be obtained via TBET cassettes. Described in chapter IV are the syntheses and spectroscopic properties of the fluorescein- and Nile Red-based, chemically activated, cassettes, **56** and **57.** The chemiluminescence spectra and figure indicate that the energy transfer efficiency is very efficient (>90%). These two cassettes could be activated by H_2O_2 at physiological pH, therefore it might be a potential indicator for reactive oxegen species in living cells.

Importing proteins into cytosol is a challenged problem in biology. The data accumulated in chapter V indicate that at 4 °C import into cytosol is prevalent and

significant accumulation of fluorescence in the endosome was not observed. This observation is parallel and consistent with work reported by Futaki *et al*.[237] The simplest explanation for the observation that three chemically different carriers facilitate import of three different proteins at 4°C via an energy independent pathway is that they form pores in the cells membrane that allow leakage into the cells, even at 4°C. This would explain the fact that the levels of diffuse fluorescence observed are weak, and that the larger protein was the one least effectively imported.

REFERENCES

(1) Perez-Sala, D.; Collado-Escobar, D.; Mollinedo, F. *J. Biol. Chem.* **1995**, *270*, 6235-6242.

(2) Ishaque, A.; Al-Rubeai, M. *J. Immunol. Meth.* **1998**, *221*, 43-57.

(3) Gottlieb, R. A.; Nordberg, J.; Skowronski, E.; Babior, B. M. *Proc. Natl. Acad. Sci.* **1996**, *93*, 654-658.

(4) Simon, S.; Roy, D.; Schindler, M. *Proc. Natl. Acad. Sci.* **1994**, *91*, 1128-1132.

(5) Varadi, A.; Rutter, G. A. *Endocrinology* **2004**, *145*, 4540-4549.

(6) Liang, E.; Liu, P.; Dinh, S. *Int. J. Pharm.* **2007**, *338*, 104-109.

(7) Bullock, A. J.; Duquette, R. A.; Buttell, N.; Wray, S. *Pfluegers Arch.* **1998**, *435*, 575-577.

(8) Chin, E. R.; Allen, D. G. *J. Physiol.* **1998**, *512*, 831-840.

(9) Chesler, M. *Phys. Rev.* **2003**, *83*, 1183-1221.

(10) Deitmer, J. W.; Rose, C. R. *Prog. Neurobiology* **1996**, *48*, 73-103.

(11) Izumi, H.; Torigoe, T.; Ishiguchi, H.; Uramoto, H.; Yoshida, Y.; Tanabe, M.; Ise, T.; Murakami, T.; Yoshida, T.; Nomoto, M.; Kohno, K. *Cancer Treatment Rev.* **2003**, *29*, 541-549.

(12) Davies, T. A.; Fine, R. E.; Johnson, R. J.; Levesque, C. A.; Rathbun, W. H.; Seetoo, K. F.; Smith, S. J.; Strohmeier, G.; Volicer, L.; et al. *Biochem. Biophys. Res. Commun.* **1993**, *194*, 537-543.

(13) Schindler, M.; Grabski, S.; Hoff, E.; Simon, S. *Biochem.* **1996**, *35*, 2811-2817.

(14) Mathieu, Y.; Guern, J.; Kurkdjian, A.; Manigault, P.; Manigault, J.; Zielinska, T.; Gillet, B.; Beloeil, J.-C.; Lallemand, J.-Y. *Plant Physiol.* **1988**, *89*, 19-26.

(15) Ohkuma, S.; Poole, B. *Proc. Natl. Acad. Sci.* **1978**, *75*, 3327-3331.

(16) Abiko, A.; Masamune, S. *Tetrahedron Lett* **1996**, *37*, 1081-1084.

(17) Thiebaut, F.; Currier, S. J.; Whitaker, J.; Haugland, R. P.; Gottesman, M. M.; Pastan, I.; Willingham, M. C. *J. Histochem. Cytochem.* **1990**, *38*, 685-690.

(18) McNeil, P. L.; Murphy, R. F.; Lanni, F.; Taylor, D. L. *J. Cell Biol.* **1984**, *98*, 1556-1564.

(19) Green, F. A. *Inflammation,* **1988**, *12*, 133-140.

(20) Han, J.; Loudet, A.; Barhoumi, R.; Burghardt, R. C.; Burgess, K. *J. Am. Chem. Soc.* **2009**, *131*, 1642-1643.

(21) Bundgaard, H.; Moerk, N.; Hoelgaard, A. *Int. J. Pharm.* **1989**, *55*, 91-97.

(22) Neuenschwander, M.; Iseli, R. *Helv. Chim. Acta.* **1977**, *60*, 1061-1072.

(23) Tsien, R. Y. *Nature* **1981**, *290*, 527-528.

(24) Whitaker, J. E.; Haugland, R. P.; Prendergast, F. G. *Anal. Biochem.* **1991**, *194*, 330-344.

(25) Rink, T. J.; Tsien, R. Y.; Pozzan, T. *J. Cell Biol.* **1982**, *95*, 189-196.

(26) Bright, G. R.; Whitaker, J. E.; Haugland, R. P.; Taylor, D. L. *J. Cell Physiol.* **1989**, *141*, 410-419.

(27) Seksek, O.; Henry-Toulme, N.; Sureau, F.; Bolard, J. *Anal. Biochem.* **1991**, *193*, 49-54.

(28) Opitz, N.; Merten, E.; Acker, H. *Pfluegers Arch.* **1994**, *427*, 332-342.

(29) Thomas, J. A.; Buchsbaum, R. N.; Zimniak, A.; Racker, E. *Biochem.* **1979**, *18*, 2210-2218.

(30) Kotyk, A.; Slavik, J. *Intracellular pH and Its Measurement*; CRC Press: Boca Raton, Florida, 1989.

(31) Weiner, I. D.; Hamm, L. L. *Am. J. Physiol.* **1989**, *256*, F957-F964.

(32) Kim, J. H.; Johannes, L.; Goud, B.; Antony, C.; Lingwood, C. A.; Daneman, R.; Grinstein, S. *Proc. Natl. Acad. Sci.* **1998**, *95*, 2997-3002.

(33) Martinez, G. M.; Gollahon, L. S.; Shafer, K.; Oomman, S. K.; Busch, C.; Martinez-Zaguilan, R. *Proc. SPIE - Int. Soc. Opt. Eng.* **2001**, *4259*, 144-156.

(34) Graber, M. L.; DiLillo, D. C.; Friedman, B. L.; Pastoriza-Munoz, E. *Anal. Biochem.* **1986**, *156*, 202-212.

(35) Jiao, G.-S.; Han, J. W.; Burgess, K. *J. Org. Chem.* **2003**, *68*, 8264-8267.

(36) Orndorff, W. R.; Hemmer, A. J. *J. Am. Chem. Soc.* **1927**, *49*, 1272-1280.

(37) Ioffe, I. S.; Devyatova, N. I. *Zhurnal Obshchei Khimii* **1962**, *32*, 2111-2115.

(38) Banan, A.; Fields, J. Z.; Talmage, D. A.; Zhang, Y.; Keshavarzian, A. *Am. J. Physiol.* **2001**, *281*, G833-G847.

(39) Ueno, Y.; Jiao, G.-S.; Burgess, K. *Synthesis* **2004**, *15*, 2591-2593.

(40) Rossi, F. M.; Kao, J. P. *Bioconjugate Chem.* **1997**, *8*, 495-497.

(41) Grabowski, J.; Ke-Cheng, H.; Baker, P. R.; Bornman, C. H. *Environ. Pollut.* **1997**, *98*, 1-5.

(42) Lanz, E.; Gregor, M.; Slavik, J.; Kotyk, A. *J. Fluoresc.* **1997**, *7*, 317-319.

(43) Breeuwer, P.; Drocourt, J.-L.; Rombouts, F. M.; Abee, T. *Appl. Environ. Microb.* **1996**, *62*, 178-183.

(44) Zanker, V.; Peter, W. *Chem. Berichte.* **1958**, *91*, 572 - 580.

(45) Invitrogen, Chapter 20, pH Indicators, **2007**, http://www.probes.invitrogen.com.

(46) Lee, L. G.; Berry, G. M.; Chen, C.-H. *Cytometry* **1989**, *10*, 151-164.

(47) Song, A.; Parus, S.; Kopelman, R. *Anal. Chem.* **1997**, *69*, 863-867.

(48) Sun, W.-C.; Gee, K. R.; Klaubert, D. H.; Haugland, R. P. *J. Org. Chem.* **1997**, *62*, 6469-6475.

(49) Lin, H.-J.; Szmacinski, H.; Lakowicz, J. R. *Anal. Biochem.* **1999**, *269*, 162-167.

(50) Nedergaard, M.; Desai, S.; Pulsinelli, W. *Anal. Biochem.* **1990**, *187*, 109-114.

(51) Invitrogen, Molecular Probes, **2006**, http://www.probes.invitrogen.com

(52) Piechowski, A. P.; Bird, G. R. *Opt. Commun.* **1984**, *50*, 386-392.

(53) Li, J.; Yao, S. Q. *Org. Lett.* **2009**, *11*, 405-408.

(54) Whitaker, J. E.; Haugland, R. P.; Ryan, D.; Hewitt, P. C.; Haugland, R. P.; Prendergast, F. G. *Anal. Biochem.* **1992**, *207*, 267-279.

(55) Brinkmann, K.; Linnertz, H.; Amler, E.; Lanz, E.; Herman, P.; Schoner, W. *Eur. J. Biochem.* **1997**, *249*, 301-308.

(56) Yang, Y.; Lowry, M.; Xu, X.; Escobedo, J. O.; Sibrian-Vazquez, M.; Wong, L.; Schowalter, C. M.; Jensen, T. J.; Fronczek, F. R.; Warner, I. M.; Strongin, R. M. *Proc. Natl. Acad. Sci.* **2008**, *105*, 8829-8834.

(57) Fabian, W. M. F.; Schuppler, S.; Wolfbeis, O. S. *J. Chem. Soc., Perkin Trans. 2* **1996**, 853-856.

(58) Yang, Y.; Lowry, M.; Schowalter, C. M.; Fakayode, S. O.; Escobedo, J. O.; Xu, X.; Zhang, H.; Jensen, T. J.; Fronczek, F. R.; Warner, I. M.; Strongin, R. M. *J. Am. Chem. Soc.* **2007**, *129*, 1008.

(59) Liu, J.; Diwu, Z.; Leung, W.-Y. *Bioorg. Med. Chem. Lett.* **2001**, *11*, 2903-2905.

(60) Balut, C.; vande Ven, M.; Despa, S.; Lambrichts, I.; Ameloot, M.; Steels, P.; Smets, I. *Kidney Int.* **2008**, *73*, 226-232.

(61) Wieder, E. D.; Hang, H.; Fox, M. H. *Cytometry* **1993**, *14*, 916-921.

(62) Haugland, R. P.; Whitaker, J.; (Molecular Probes, Inc., USA). Application: *US*1990/004592364, **1990**, 17.

(63) Masuda, A.; Oyamada, M.; Nagaoka, T.; Tateishi, N.; Takamatsu, T. *Brain Res.* **1998**, *807*, 70-77.

(64) Martinez-Zaguilan, R.; Martinez, G. M.; Lattanzio, F.; Gillies, R. J. *Am. J. Physiol.* **1991**, *260*, C297-C307.

(65) Minta, A.; Tsien, R. Y. *J. Biol. Chem.* **1989**, *264*, 19449-19457.

(66) Marcotte, N.; Brouwer, A. M. *J. Phys. Chem. B* **2005**, *109*, 11819-11828.

(67) Cheng, Y. M.; Kelly, T.; Church, J. *Neurosci.* **2008**, *151*, 1084-1098.

(68) Zhou, Y.; Marcus, E. M.; Haugland, R. P.; Opas, M. *J. Cell. Physiol.* **1995**, *164*, 9-16.

(69) Parker, D. *Chem. Soc. Rev.* **2004**, *33*, 156-165.

(70) Pal, R.; Parker, D. *Chem. Commun.* **2007**, *5*, 474-476.

(71) Yao, S.; Schafer-Hales, K. J.; Belfield, K. D. *Org. Lett.* **2007**, *9*, 5645-5648.

(72) O'Brien, J.; Wilson, I.; Orton, T.; Pognan, F. *Eur. J. Biochem.* **2000**, *267*, 5421-5426.

(73) Valet, G.; Raffael, A.; Moroder, L.; Wunsch, E.; Ruhenstroth-Bauer, G. *Naturwissenschaften* **1981**, *68*, 265-266.

(74) Kurtz, I.; Balaban, R. S. *Biophys. J.* **1985**, *48*, 499-508.

(75) Cook, J. A.; Fox, M. H. *Cytometry* **1988**, *9*, 441-447.

(76) Musgrove, E.; Rugg, C.; Hedley, D. *Cytometry* **1986**, *7*, 347-355.

(77) Zhang, Z.; Seitz, W. R. *Anal. Chim. Acta* **1984**, *160*, 47-55.

(78) Wolfbeis, O. S.; Fuerlinger, E.; Kroneis, H.; Marsoner, H. *Freseius' Zeitschrift fuer Analytische Chemie* **1983**, *314*, 119-124.

(79) Giuliano, K. A.; Gillies, R. J. *Anal. Biochem.* **1987**, *167*, 362-371.

(80) Overly, C. C.; Lee, K.-D.; Berthiaume, E.; Hollenbeck, P. J. *Proc. Natl. Acad. Sci.* **1995**, *92*, 3156-3160.

(81) Pena, A.; Ramirez, J.; Rosas, G.; Calahorra, M. *J. Bacteriol.* **1995**, *177*, 1017-1022.

(82) Briggs, M. S.; Burns, D. D.; Cooper, M. E.; Gregory, S. J. *Chem. Commun.* **2000**, 2323-2324.

(83) Tang, B.; Yu, F.; Li, P.; Tong, L.; Duan, X.; Xie, T.; Wang, X. *J. Am. Chem. Soc.* **2009**, *131*, 3016-3023.

(84) Kiwu, Z. *Chem. Biol.* **1999**, *6*, 411-418.

(85) de Silva, A. P.; Rupasinghe, R. A. D. D. *J. Chem. Soc., Chem. Commun.* **1985**, *23*, 1669-1670.

(86) Bissell, R. A.; Bryan, A. J.; Prasanna de Silva, A.; McCoy, C. P. *J. Chem. Soc., Chem. Commun.* **1994**, *4*, 405-407.

(87) Lin, H.-J.; Herman, P.; Kang, J. S.; Lakowicz, J. R. *Anal. Biochem.* **2001**, *294*, 118-125.

(88) Galindo, F.; Burguete, M. I.; Vigara, L.; Luis, S. V.; Kabir, N.; Gavrilovic, J.; Russell, D. A. *Angew. Chem., Int. Ed.* **2005**, *44*, 6504-6508.

(89) Cools, A. A.; Janssen, L. H. M. *Experientia* **1986**, *42*, 954-956.

(90) Palmgren, M. G. *Anal. Biochem.* **1991**, *192*, 316-321.

(91) Millot, C.; Millot, J.-M.; Morjani, H.; Desplaces, A.; Manfait, M. *J. Histochem. Cytochem.* **1997**, *45*, 1255-1264.

(92) Palmgren, M. G. *Plant Physiol.* **1990**, *94*, 882-886.

(93) Marty, A.; Bourdeaux, M.; Dell'Amico, M.; Viallet, P. *Eur. Biophy. J.* **1986**, *13*, 251-257.

(94) Casadio, R. *Eur. Biophy. J.* **1991**, *19*, 189-201.

(95) Dufour, J. P.; Goffeau, A.; Tsong, T. Y. *J. Biol. Chem.* **1982**, *257*, 9365-9371.

(96) Yogo, T.; Urano, Y.; Mizushima, A.; Sunahara, H.; Inoue, T.; Hirose, K.; Lino, M.; Kikuchi, K.; Nagano, T. *Proc. Natl. Acad. Sci.* **2008**, *105*, 28-32.

(97) Tang, B.; Liu, X.; Xu, K.; Huang, H.; Yang, G.; An, L. *Chem. Commun.* **2007**, *36*, 3726-3728.

(98) Jiao, G.-S.; Thoresen, L. H.; Burgess, K. *J. Am. Chem. Soc.* **2003**, *125*, 14668-14669.

(99) Bandichhor, R.; Petrescu, A. D.; Vespa, A.; Kier, A. B.; Schroeder, F.; Burgess, K. *J. Am. Chem. Soc.* **2006**, *128*, 10688-10689.

(100) Han, J.; Jose, J.; Mei, E.; Burgess, K. *Angew. Chem., Int. Ed.* **2007**, *46*, 1684-1687.

(101) Han, J.; Gonzalez, O.; Aguilar-Aguilar, A.; Pena-Cabrera, E.; Burgess, K. *Org. Biomol. Chem.* **2009**, *7*, 34-36.

(102) Zanker, V.; Peter, W. *Chem. Ber.* **1958**, *91*, 572-580.

(103) Loudet, A.; Han, J.; Barhoumi, R.; Pellois, J.-P.; Burghardt, R. C.; Burgess, K. *Org. Biomol. Chem.* **2008**, *6*, 4516-4522.

(104) Bradley, M.; Alexander, L.; Duncan, K.; Chennaoui, M.; Jones, A. C.; Sanchez-Martin, R. M. *Bioorg. Med. Chem. Lett.* **2008**, *18*, 313-317.

(105) Hilderbrand, S. A.; Kelly, K. A.; Niedre, M.; Weissleder, R. *Bioconjugate Chem.* **2008**, *19*, 1635-1639.

(106) Liu, Y.-S.; Sun, Y.; Vernier, P. T.; Liang, C.-H.; Chong, S. Y. C.; Gundersen, M. A. *J. Phys. Chem. C* **2007**, *111*, 2872-2878.

(107) Burns, A.; Ow, H.; Wiesner, U. *Chem. Soc. Rev.* **2006**, *35*, 1028-1042.

(108) Burns, A.; Sengupta, P.; Zedayko, T.; Baird, B.; Wiesner, U. *Small* **2006**, *2*, 723-726.

(109) McNamara, K. P.; Nguyen, T.; Dumitrascu, G.; Ji, J.; Rosenzweig, N.; Rosenzweig, Z. *Anal. Chem.* **2001**, *73*, 3240-3246.

(110) Chalfie, M.; Tu, Y.; Euskirchen, G.; Ward, W. W.; Prasher, D. C. *Science* **1994**, *263*, 802-805.

(111) Tsien, R. Y. *Annu. Rev. Biochem.* **1998**, *67*, 509-544.

(112) Wu, L.; Burgess, K. *J. Am. Chem. Soc.* **2008**, *130*, 4089-4096.

(113) Heim, R.; Prasher, D. C.; Tsien, R. Y. *Proc. Natl. Acad. Sci.* **1994**, *91*, 12501-12504.

(114) Wachter, R. M.; King, B. A.; Heim, R.; Kallio, K.; Tsien, R. Y.; Boxer, S. G.; Remington, S. J. *Biochemistry* **1997**, *36*, 9759-9765.

(115) McAnaney, T. B.; Park, E. S.; Hanson, G. T.; Remington, S. J.; Boxer, S. G. *Biochemistry* **2002**, *41*, 15489-15494.

(116) Elsliger, M.-A.; Wachter, R. M.; Hanson, G. T.; Kallio, K.; Remington, S. J. *Biochemistry* **1999**, *38*, 5296-5301.

(117) Robey, R. B.; Ruiz, O.; Santos, A. V.; Ma, J.; Kear, F.; Wang, L. J.; Li, C. J.; Bernardo, A. A.; Arruda, J. A. *Biochemistry* **1998**, *37*, 9894-901.

(118) Kneen, M.; Farinas, J.; Li, Y.; Verkman, A. S. *Biophys. J.* **1998**, *74*, 1591-1599.

(119) Llopis, J.; McCaffery, J. M.; Miyawaki, A.; Farquhar, M. G.; Tsien, R. Y. *Proc. Natl. Acad. Sci.* **1998**, *95*, 6803-6808.

(120) Patterson, G. H.; Knobel, S. M.; Sharif, W. D.; Kain, S. R.; Piston, D. W. *Biophysi. J.* **1997**, *73*, 2782-2790.

(121) Mellman, I.; Fuchs, R.; Helenius, A. *Annu. Rev. Biochem.* **1986**, *55*, 663-700.

(122) Gerweck, L. E.; Seetharaman, K. *Cancer Res.* **1996**, *56*, 1194-1198.

(123) Klonis, N.; Sawyer, W. H. *J. Fluoresc.* **1996**, *6*, 147-157.

(124) Burghart, A.; Thoresen, L. H.; Chen, J.; Burgess, K.; Bergström, F.; Johansson, L. B.-A. *Chem. Commun.* **2000**, 2203-2204.

(125) Lu, G.; Lam, S.; Burgess, K. *Chem. Commun.* **2006**, 1652-1654.

(126) Geisow, M. J.; Evans, W. H. *Exp. Cell. Res.* **1984**, *150*, 36-46.

(127) Morris, M. C.; Depollier, J.; Mery, J.; Heitz, F.; Divita, G. *Nature Biotech.* **2001**, *19*, 1173-1176.

(128) Brasselet, S.; Moerner, W. E. *Single Mol.* **2000**, *1*, 17-23.

(129) Que, E. L.; Domaille, D. W.; Chang, C. J. *Chem. Rev.* **2008**, *108*, 1517-1549.

(130) Coskun, A.; Yilmaz, M. D.; Akkaya, E. U. *Org. Lett.* **2007**, *9*, 607-609.

(131) McAnaney, T. B.; Shi, X.; Abbyad, P.; Jung, H.; Remington, S. J.; Boxer, S. G. *Biochemimstry* **2005**, *44*, 8701-8711.

(132) Snee, P. T.; Somers, R. C.; Nair, G.; Zimmer, J. P.; Bawendi, M. G.; Nocera, D. G. *J. Am. Chem. Soc.* **2006**, *128*, 13320-13321.

(133) Kim, S.; Pudavar, H. E.; Prasad, P. N. *Chem. Commun.* **2006**, 2071-2073.

(134) Sun, H.; Scharff-Poulsen, A. M.; Gu, H.; Almdal, K. *Chem. Mater.* **2006**, *18*, 3381-3384.

(135) Gao, F.; Tang, L.; Dai, L.; Wang, L. *Spectrochim. Acta Part A* **2007**, *67*, 517-521.

(136) Charier, S.; Ruel, O.; Baudin, J.-B.; Alcor, D.; Allemand, J.-F.; Meglio, A.; Jullien, L. *Angew. Chem., Int. Ed.* **2004**, *43*, 4785-4788.

(137) Bizzarri, R.; Arcangeli, C.; Arosio, D.; Ricci, F.; Faraci, P.; Cardarelli, F.; Beltram, F. *Biophysi. J.* **2006**, *90*, 330-314.

(138) Diehl, H.; Horchak-Morris, N. *Talanta* **1987**, *34*, 739-741.

(139) Klonis, N.; Sawyer, W. H. *J. Fluoresc.* **1996**, *6*, 147-157.

(140) Koo, M. K.; Oh, C. H.; Holme, A. L.; Pervaiz, S. *Cytometry, Part A* **2007**, *71A*, 87-93.

(141) Tamblyn, B.; Burgess, K. *US Patent* 6472533 United States, 2002.

(142) Burgess, K. *US Patent No. US2005/*0032120 *A1*; (The Texas A&M University System, USA). US, 2005; Vol. U.S. Application Serial No. 10/876,919, p 7.

(143) Wan, C.-W.; Burghart, A.; Chen, J.; Bergstroem, F.; Johansson, L. B. A.; Wolford, M. F.; Kim, T. G.; Topp, M. R.; Hochstrasser, R. M.; Burgess, K. *Chem. Eur. J.* **2003**, *9*, 4430-4441.

(144) Kim, T. G.; Castro, J. C.; Loudet, A.; Jiao, J. G. S.; Hochstrasser, R. M.; Burgess, K.; Topp, M. R. *J. Phys. Chem. A* **2006**, *110*, 20-27.

(145) Jiao, G.-S.; Thoresen, L. H.; Kim, T. G.; Haaland, W. C.; Gao, F.; Topp, M. R.; Hochstrasser, R. M.; Metzker, M. L.; Burgess, K. *Chem. Eur. J.* **2006**, *12*, 7816-7826.

(146) Loudet, A.; Burgess, K. *Chem. Rev.* **2007**, *107*, 4891-4932.

(147) Miura, T.; Urano, Y.; Tanaka, K.; Nagano, T.; Ohkubo, K.; Fukuzumi, S. *J. Am. Chem. Soc.* **2003**, *125*, 8666-8671.

(148) Ueno, T.; Urano, Y.; Setsukinai, K.; Takakusa, H.; Kojima, H.; Kikuchi, K.; Ohkubo, K.; Fukuzumi, S.; Nagano, T. *J. Am. Chem. Soc.* **2004**, *126*, 14079-14085.

(149) Sunahara, H.; Urano, Y.; Kojima, H.; Nagano, T. *J. Am. Chem. Soc.* **2007**, *129*, 5597-5604.

(150) Tanaka, K.; Fu, G. C. *J. Am. Chem. Soc.* **2001**, *123*, 11492-11493.

(151) Sasaki, E.; Kojima, H.; Nishimatsu, H.; Urano, Y.; Kikuchi, K.; Hirata, Y.; Nagano, T. *J. Am. Chem. Soc.* **2005**, *127*, 3684-3685.

(152) Zhang, X.; Wang, H.; Li, J.-S.; Zhang, H.-S. *Anal. Chim. Acta* **2003**, *481*, 101-108.

(153) Li, M.; Wang, H.; Zhang, X.; Zhang, H.-s. *Spectrochim. Acta, Part A* **2004**, *60A*, 987-993.

(154) Ueno, T.; Urano, Y.; Kojima, H.; Nagano, T. *J. Am. Chem. Soc.* **2006**, *128*, 10640-10641.

(155) Matsumoto, T.; Urano, Y.; Shoda, T.; Kojima, H.; Nagano, T. *Org. Lett.* **2007**, *9*, 3375-3377.

(156) Sun, Z.-N.; Liu, F.-Q.; Chen, Y.; Tam, P. K. H.; Yang, D. *Org. Lett.* **2008**, *10*, 2171-2174.

(157) Li, Z.; Mintzer, E.; Bittman, R. *J. Org. Chem.* **2006**, *71*, 1718-1721.

(158) Sonogashira, K.; Tohda, Y.; Hagihara, N. *Tetrahedron Lett.* **1975**, 4467-4470.

(159) Bonardi, L.; Ulrich, G.; Ziessel, R. *Org. Lett.* **2008**, *10*, 2183-2186.

(160) Burghart, A.; Thoresen, L. H.; Chen, J.; Burgess, K.; Bergstrom, F.; Johansson, L. *Chem. Commun.* **2000**, 2203-2204.

(161) Thoresen, L. H.; Jiao, G.-S.; Haaland, W. C.; Metzker, M. L.; Burgess, K. *Chem. Eur. J.* **2003**, *9*, 4603-4610.

(162) Lakowicz, J. R. *Principles of Fluorescence Spectroscopy*; 3rd ed.; Springer: New York, 2006.

(163) Holten, D.; Bocian, D.; Lindsey, J. S. *Acc. Chem. Res.* **2002**, *35*, 57-69.

(164) Weber, G.; Teale, F. W. J. *Trans. Faraday Soc.* **1957**, *53*, 646-655.

(165) Karstens, T.; Kobs, K. *J. Phys. Chem.* **1980**, *84*, 1871-1872.

(166) Thompson, B. C.; Kim, Y.-G.; McCarley, T. D.; Reynolds, J. R. *J. Am. Chem. Soc.* **2006**, *128*, 12714-12725.

(167) Connelly, N. G.; Geiger, W. E. *Chem. Rev.* **1996**, *96*, 877-910.

(168) Hansen, W. N.; Hansen, G. J. *Phys. Rev. A: At., Mol., Opt. Phys.* **1987**, *36*, 1396-1402.

(169) Wan, C.-W.; Burghart, A.; Chen, J.; Bergstroem, F.; Johansson, L.; Wolford, M. F.; Kim, T. G.; Topp, M. R.; Hochstrasser, R. M.; Burgess, K. *Chem. Eur. J.* **2003**, *9*, 4430-4441.

(170) Ghiggino, K. P.; Yeow, E. K. L.; Haines, D. J.; Scholes, G. D.; Smith, T. A. *J. Photochem. Photobiol., A* **1996**, *102*, 81-86.

(171) Vollmer, M. S.; Würthner, F.; Effenberger, F.; Emele, P.; Meyer, D. U.; Stümpfig, T.; Port, H.; Wolf, H. C. *Chem. Eur. J.* **1998**, *4*, 260-269.

(172) Dexter, D. L. *J. Chem. Phys.* **1953**, *21*, 836-850.

(173) Ouyang, X.; Chen, Z.; Liu, L.; Dominguez, C.; Kiselyov, A. S. *Tetrahedron* **2000**, *56*, 2369-2377.

(174) Kikuchi, K.; Takakusa, H.; Nagano, T. *TrAC, Trends Anal. Chem.* **2004**, *23*, 407-415.

(175) Coskun, A.; Akkaya, E. U. *J. Am. Chem. Soc.* **2005**, *127*, 10464-10465.

(176) Coskun, A.; Akkaya, E. U. *J. Am. Chem. Soc.* **2006**, *128*, 14474-14475.

(177) Coskun, A.; Baytekin, B. T.; Akkaya, E. U. *Tetrahedron Lett.* **2003**, *44*, 5649-5651.

(178) Haugland, R. P. *Handbook of Fluorescent Probes and Research Chemicals*; 6th ed.; Molecular Probes: Eugene, OR, **1996**.

(179) Ziessel, R.; Ulrich, G.; Harriman, A. *New J. Chem.* **2007**, *31*, 496-501.

(180) Li, J.-S.; Wang, H.; Cao, L.-W.; Zhang, H.-S. *Talanta* **2006**, *69*, 1190-1199.

(181) Matsui, M.; Funabiki, K.; Nakaya, K.-i. *Bull. Chem. Soc. Jpn.* **2005**, *78*, 464-467.

(182) Gee, K. R.; Archer, E. A.; Kang, H. C. *Tetrahedron Lett.* **1999**, *40*, 1471-1474.

(183) Karolin, J.; Johansson, L. B.-A.; Strandberg, L.; Ny, T. *J. Am. Chem. Soc.* **1994**, *116*, 7801-7806.

(184) Bergstrom, F.; Hagglof, P.; Karolin, J.; Ny, T.; Johansson, L. B. A. *Proc. Natl. Acad. Sci.* **1999**, *96*, 12477-12481.

(185) Bergstroem, F.; Mikhalyov, I.; Haeggloef, P.; Wortmann, R.; Ny, T.; Johansson, L. B. A. *J. Am. Chem. Soc.* **2002**, *124*, 196-204.

(186) Mikhalyov, I.; Gretskaya, N.; Bergstroem, F.; Johansson, L. *Phys. Chem.* **2002**, *4*, 5663-5670.

(187) Marushchak, D.; Kalinin, S.; Mikhalyov, I.; Gretskaya, N.; Johansson, L. B. A. *Spectrochim. Acta, Part A* **2006**, *65A*, 113-122.

(188) Baruah, M.; Qin, W.; Flors, C.; Hofkens, J.; Vallee, R. A. L.; Beljonne, D.; Van der Auweraer, M.; De Borggraeve, W. M.; Boens, N. *J. Phys. Chem. A* **2006**, *110*, 5998-6009.

(189) Treibs, A.; Kreuzer, F.-H. *Liebigs Ann. Chem.* **1968**, *718*, 208-223.

(190) Shah, M.; Thangaraj, K.; Soong, M.-L.; Wolford, L. T.; Boyer, J. H.; Politzer, I. R.; Pavlopoulos, T. G. *Heteroat. Chem.* **1990**, *1*, 389-399.

(191) Wories, H. J.; Koek, J. H.; Lodder, G.; Lugtenburg, J.; Fokkens, R.; Driessen, O.; Mohn, G. R. *Recl. Trav. Chim. Pays-Bas* **1985**, *104*, 288-291.

(192) Atilgan, S.; Ekmekci, Z.; Dogan, A. L.; Guc, D.; Akkaya Engin, U. *Chem. Commun.* **2006**, 4398-4400.

(193) Rohand, T.; Baruah, M.; Qin, W.; Boens, N.; Dehaen, W. *Chem. Commun.* **2006**, 266-268.

(194) Rohand, T.; Qin, W.; Boens, N.; Dehaen, W. *Eur. J. Org. Chem.* **2006**, 4658-4663.

(195) Baruah, M.; Qin, W.; Vallee, R. A. L.; Beljonne, D.; Rohand, T.; Dehaen, W.; Boens, N. *Org. Lett.* **2005**, *7*, 4377-4380.

(196) Tornoe, C. W.; Christensen, C.; Meldal, M. *J. Org. Chem.* **2002**, *67*, 3057-3064.

(197) Rostovtsev, V. V.; Green, L. G.; Fokin, V. V.; Sharpless, K. B. *Angew. Chem., Int. Ed.* **2002**, *41*, 2596-2599.

(198) Chen, J.; Burghart, A.; Derecskei-Kovacs, A.; Burgess, K. *J. Org. Chem.* **2000**, *65*, 2900-2906.

(199) Littler, B. J.; Miller, M. A.; Hung, C.-H.; Wagner, R. W.; O'Shea, D. F.; Boyle, P. D.; Lindsey, J. S. *J. Org. Chem.* **1999**, *64*, 1391-1396.

(200) Baruah, M.; Qin, W.; Basaric, N.; De Borggraeve, W. M.; Boens, N. *J. Org. Chem.* **2005**, *70*, 4152-4157.

(201) Filira, F.; Biondi, L.; Gobbo, M.; Rocchi, R. *Tetrahedron Lett.* **1991**, *32*, 7463-7464.

(202) Chan, T. R.; Hilgraf, R.; Sharpless, K. B.; Fokin, V. V. *Org. Lett.* **2004**, *6*, 2853-2855.

(203) Jose, J.; Burgess, K. *Tetrahedron* **2006**, *62*, 11021-11037.

(204) Yamada, K.; Toyota, T.; Takakura, K.; Ishimaru, M.; Sugawara, T. *New J. Chem.* **2001**, *25*, 667-669.

(205) Tanaka, K.; Miura, T.; Umezawa, N.; Urano, Y.; Kikuchi, K.; Higuchi, T.; Nagano, T. *J.Am. Chem. Soc.* **2001**, *123*, 2530-2536.

(206) Gabe, Y.; Urano, Y.; Kikuchi, K.; Kojima, H.; Nagano, T. *J. Am. Chem. Soc.* **2004**, *126*, 3357-3367.

(207) Weber, G.; Teale, F. W. J. *Trans. Faraday Soc.* **1958**, *54*, 640-648.

(208) Kubin, R. F.; Fletcher, A. N. *J. Lumin.* **1983**, *27*, 455-462.

(209) Miyaura, N.; Suzuki, A. *Chem. Rev.* **1995**, *95*, 2457-2483.

(210) Sonogashira, K.; Tohda, Y.; Hagihara, N. *Tetrahedron Lett.* **1975**, *16*, 4467-4470.

(211) Li, L.; Han, J.; Nguyen, B.; Burgess, K. *J. Org. Chem.* **2008**, *73*, 1963-1970.

(212) Pena-Cabrera, E.; Aguilar-Aguilar, A.; Gonzalez-Dominguez; Lager, E.; Zamudio-Vazquez, R.; Godoy-Vargas, J.; Villanueva-Garcia, F. *Org. Lett.* **2007**, *9*, 3985-3988.

(213) Kusturin, C.; Liebeskind, L. S.; Rahman, H.; Sample, K.; Schweitzer, B.; Srogl, J.; Neumann, W. L. *Org. Lett.* **2003**, *5*, 4349-4352.

(214) Thoresen, L. H.; Kim, H.; Welch, M. B.; Burghart, A.; Burgess, K. *Synlett* **1998**, 1276-1278.

(215) Cox, R. J.; Durston, J.; Roper, D. I. *J. Chem. Soc., Perkin Trans. 1,* **2002**, 1029-1035.

(216) Haas Jr., J. W. *J. Chem. Ed.* **1967**, *44*, 396-402.

(217) Gundermann, K.-D. *Angew. Chem., Int. Ed.* **1965**, *4*, 565-572.

(218) White, E. H.; Roswell, D. F. *Acc. Chem. Res.* **1970**, *3*, 54-62.

(219) Diaz, A. N.; Garcia, J. A. G.; Lovillo, J. *J. Biolumin. Chemilumin.* **1997**, *12*, 199-205.

(220) White, E. H.; Bursey, M. M. *J. Org. Chem.* **1966**, *31*, 1912-1917.

(221) Spruit-Van Der Burg, A. *Recl. Trav. Chim. Pays-Bas* **1950**, *69*, 1536-1544.

(222) Wei, C. C.; White, E. H. *Tetrahedron Lett.* **1971**, 3559-3562.

(223) Gadek, T. R.; Burdick, D. J.; McDowell, R. S.; Stanley, M. S.; Marsters, J. C.; Paris, K. J.; Oare, D. A.; Reynolds, M. E.; Ladner, C.; Zioncheck, K. A.; Lee, W. P.; Gribling, P.; Dennis, M. S.; Skelton, N. J.; Tumas, D. B.; Clark, K. R.; Keating, S. M.; Beresini, M. H.; Tilley, J. W.; Presta, L. G.; Bodary, S. C. *Science* **2002**, *295*, 1086-1089.

(224) Campbell, A. K. *Chemiluminescence. Principles and Applications in Biology and Medicine*; VCH: Weinheim, Germany,**1988**.

(225) Briggs, M. S. J.; Bruce, I.; Miller, J. N.; Moody, C. J.; Simmonds, A. C.; Swann, E. *J. Chem. Soc., Perkin Trans. 1* **1997**, *7*, 1051-1058.

(226) *Documenta Geigy, Scientific Tables*; 6th ed.; Diem, K., Ed.; Geigy Pharmaceuticals: Ardsley, NY, 1962.

(227) White, E. H.; Roswell, D. F. *J. Am. Chem. Soc.* **1967**, *89*, 3944-3945.

(228) Roberts, D. R.; White, E. H. *J. Am. Chem. Soc.* **1970**, *92*, 4861-4867.

(229) Roswell, D. F.; Paul, V.; White, E. H. *J. Am. Chem. Soc.* **1970**, *92*, 4855-4860.

(230) Wampler, J. E. Instrumnettation: Seeing the Light and Measuring It, In *Chemi- and Bioluminescence*; Burr, J. G., Ed.; Marcel Dekker: New York, 1985; pp 1-44.

(231) Brooks, H.; Lebleu, B.; Vives, E. *Adv. Drug Delivery Rev.* **2005**, *57*, 559-577.

(232) Magzoub, M.; Graeslund, A. *Q. Rev. of Biophys.* **2004**, *37*, 147-195.

(233) Rothbard, J. B.; Jessop, T. C.; Wender, P. A. *Adv. Drug Delivery Rev.* **2005**, *57*, 495-504.

(234) Futaki, S. *Adv. Drug Delivery Rev.* **2005**, *57*, 547-558.

(235) Kosuge, M.; Takeuchi, T.; Nakase, I.; Jones, A. T.; Futaki, S. *Bioconjugate Chem.* **2008**, *19*, 656-664.

(236) Wadia, J. S.; Stan, R. V.; Dowdy, S. F. *Nat. Med.* **2004**, *10*, 310-315.

(237) Nakase, I.; Niwa, M.; Takeuchi, T.; Sonomura, K.; Kawabata, N.; Koike, Y.; Takehashi, M.; Tanaka, S.; Ueda, K.; Simpson, J. C.; Jones, A. T.; Sugiura, Y.; Futaki, S. *Mol. Ther.* **2004**, *10*, 1011-1022.

(238) Rothbard, J. B.; Jessop, T. C.; Lewis, R. S.; Murray, B. A.; Wender, P. A. *J. Am. Chem. Soc.* **2004**, *126*, 9506-9507.

(239) Goun, E. A.; Pillow, T. H.; Jones, L. R.; Rothbard, J. B.; Wender, P. A. *ChemBioChem* **2006**, *7*, 1497-1515.

(240) Kaplan, I. M.; Wadia, J. S.; Dowdy, S. F. *J. Contro. Release* **2005**, *102*, 247-253.

(241) Wagner, E.; Plank, C.; Zatloukal, K.; Cotten, M.; Birnstiel, M. L. *Proc. Natl. Acad. Sci.* **1992**, *89*, 7934-7938.

(242) Synvoluxproducts, SAINT-PhD, **2009**, http://www.synvoluxproducts.com.

(243) Sigmaaldrich, BPQ24 BioPORTER® QuikEase™, **2009**, http://www.sigmaaldrich.com.

(244) Mahlum, E.; Mandal, D.; Halder, C.; Maran, A.; Yaszemski, M. J.; Jenkins, R. B.; Bolander, M. E.; Sarkar, G. *Anal. Biochem.* **2007**, *365*, 215-221.

(245) Vinogradov, S. V.; Batrakova, E. V.; Li, S.; Kabanov, A. V. *J. Drug Targeting* **2004**, *12*, 517-526.

(246) Didenko, V. V.; Ngo, H.; Baskin, D. S. *Anal. Biochem.* **2005**, *344*, 168-173.

(247) Bandichhor, R.; Petrescu, A. D.; Vespa, A.; Kier Ann, B.; Schroeder, F.; Burgess, K. *Bioconjugate Chem.* **2006**, *17*, 1219-1225.

(248) Gros, E.; Deshayes, S.; Morris, M. C.; Aldrian-Herrada, G.; Depollier, J.; Heitz, F.; Divita, G. *Biochim. Biophys. Acta, Biomembr.* **2006**, *1758*, 384-393.

(249) Wang, Y.-H.; Chen, C.-P.; Chan, M.-H.; Chang, M.; Hou, Y.-W.; Chen, H.-H.; Hsu, H.-R.; Liu, K.; Lee, H.-J. *Biochem. Biophys. Res. Commun.* **2006**, *346*, 758-767.

(250) Chang, M.; Chou, J.-C.; Chen, C.-P.; Liu, B. R.; Lee, H.-J. *New Phytologist* **2007**, *174*, 46-56.

(251) McGovern, S. L.; Shoichet, B. K. *J. Med. Chem.* **2003**, *46*, 1478-1483.

(252) McGovern, S. L.; Caselli, E.; Grigorieff, N.; Shoichet, B. K. *J. Med. Chem.* **2002**, *45*, 1712-1722.

(253) Wender, P. A.; Jessop, T. C.; Pattabiraman, K.; Pelkey, E. T.; VanDeusen, C. L. *Org. Lett.* **2001**, *3*, 3229-3232.

(254) Deshayes, S.; Morris, M.; Heitz, F.; Divita, G. *Adv. Drug Delivery Rev.* **2008**, *60*, 537-547.

(255) Morris, M. C.; Vidal, P.; Chaloin, L.; Heitz, F.; Divita, G. *Nuc. Acid. Res.* **1997**, *25*, 2730-2736.

(256) Morris, M. C.; Chaloin, L.; Mery, J.; Heitz, F.; Divita, G. *Nuc. Acid. Res.* **1999**, *27*, 3510-3517.

(257) Vida, T. A.; Emr, S. D. *J. Cell Biol.* **1995**, *128*, 779-792.

APPENDIX A
EXPERIMENTAL DATA FOR CHAPTER II

General Experimental Procedure

Bovine serum albumin (BSA) was purchased from Calbiochem. Sephadex™ G-25 (PD-10) was bought from GE healthcare. Pep-1 (Chariot) was purchased from Active Motif. Et_3N were distilled from CaH_2. Unless otherwise mentioned, other solvents and reagents were used as received. NMR spectra were recorded on a VXP-300 MHz and Inova-500 MHz spectrometers (^1H at 300 MHz or 500 MHz, ^{13}C at 75 or 125 MHz) at room temperature unless otherwise mentioned. Chemical shifts of ^1H NMR spectra were recorded and reported in ppm from the solvent resonance ($CDCl_3$ 7.26 ppm, CD_3OD 3.30 ppm). Data are reported as follows: chemical shift, multiplicity (s = singlet, bs = broad singlet. d = doublet, t = triplet, q = quartet, br = broad, m = multiplet), coupling constants, and number of protons. Proton decoupled ^{13}C NMR spectra were also recorded in ppm from solvents resonance ($CDCl_3$ 77.0, CD_3OD 49.1ppm). Analytical thin layer chromatography (TLC) was performed on EM Reagents 0.25 mm silica-gel 60-F plates, and visualized with UV light. Flash chromatography was performed using silica gel (230–600 mesh). UV/Visible and fluorescence spectra were taken in pH 7.4 PBS buffer unless otherwise mentioned. MS were measured under ESI or MALDI conditions.

Determination of Quantum Yields and Extinction Coefficients

UV/Vis absorbance spectra were recorded on a Cary 100 Bio spectrophotometer. Steady-state fluorescence spectroscopic studies were performed on a Cary Eclipse

fluorometer. The slit width was 5 nm for both excitation and emission. The excitation wavelength for the test sample and the standard is the same. Fluorescence spectra were corrected for detector sensitivity. The relative quantum yields of the samples were obtained by comparing the area under the corrected emission spectrum of the test sample with that of a solution of standard. The quantum efficiencies of fluorescence were average of two measurements with the following equation:

$$\Phi_x = \Phi_{st} (I_x/I_{st}) (A_{st}/A_x) (\eta_x^2/\eta_{st}^2)$$

Where Φ_{st} is the reported quantum yield of the standard, I is the area under the emission spectra, A is the absorbance at the excitation wavelength and η is the refractive index of the solvent used, measured on a pocket refractometer from ATAGO. X subscript denotes unknown, and st means standard.

Fluorescein (ϕ = 0.92 in 0.1M NaOH)[1] and Rhodamine 6G (ϕ = 0.95 in EtOH)[2] were used as the standards for measurements of quantum yields of **BSA-18** in pH 4.1 and 8.8 buffers respectively, and the excitation wavelength was 488 nm.

Cell Culture

COS-7 cells (American Type Culture Collection) were cultured as subconfluent monolayers on 75 cm^2 culture flask with vent caps in DMEM supplemented with 10 % fetal bovine serum (FBS) in a humidified incubator at 37 ºC with 5 % CO_2. Cells grown to subconfluence were enzymatically dissociated from the surface with trypsin and plated 2-3 days prior to the experiments in Lab-Tek two well chambered coverglass slides (Nunc).

Fluorescence Microscopy

Cells were washed several times with PBS buffer and then put on the stage of the Bio-Rad 2000MP system (Bio-Rad Laboratories, Hercules, CA) equipped with a Nikon T300 inverted microscope with a 60x (NA1.2) water immersion objective lens and an Argon laser tuned to 488 nm wavelength. Through-bond Energy Transfer data in COS-7 cells loaded with 5-bromo-fluorescein diacetate (D, control donor) alone (2 min at 37 ºC), BODIPY derivative (A, control acceptor) (30 min at 37 ºC) alone or with BSA-1 (1:20 mol ratio of BSA-1:pep-1 for 1h at 37 ºC; the complex BSA-1:pep-1 was preformed by mixing both reagents and incubating them at room temperature for 30 min) were collected using 488 nm excitation wavelength. Both **SA** and **SB** were excited at 488 nm and emission of **SA** (FITC channel; donor signal) was collected using a 560 DCLP XR dichroic mirror and a HQ 528/50 –nm emission filter whereas emission of **SB** (FRET channel; acceptor signal) was collected using a HQ 600/50-nm filter. Donor bleed through signal to the FRET channel was calculated by measuring the FRET channel signal resulting from COS cells loaded only with the donor. Acceptor bleed through to the FRET channel was calculated by measuring the FRET channel signal resulting from COS cells loaded with **SB** alone. Accumulated images (N=6, F=1) at a 1024 x 1024 resolution were captured.

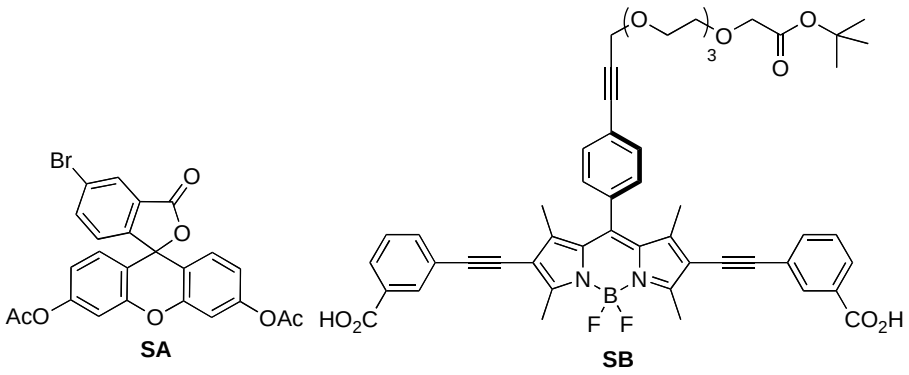

For the experiment done at 4 °C, the cells were pre-incubated at 4 °C for 30 min, before the addition of the complex. After addition of the complex, the cells were incubated for another hour at 4 °C.

Measurement of pH_i Using BSA-18

COS-7 cells (American Type Culture Collection) were cultured as subconfluent monolayers on 75 cm^2 culture flask with vent caps in DMEM supplemented with 10 % fetal bovine serum (FBS) in a humidified incubator at 37 ºC with 5 % CO_2. Cells grown to subconfluence were enzymatically dissociated from the surface with trypsin and plated 2-3 d prior to the experiments in Lab-Tek two well chambered coverglass slides (Nunc) in 1 mL DMEM. To measure pH_i with BSA-18, cells were incubated with the pre-formed BSA-18:pep-1 complex (1 μM BSA-18:20 μM pep-1) for 60 min at 37 or 4 °C. When the experiment was performed at 4 °C, the cells were pre-incubated at 4 °C for 30 min before the addition of the complex. After incubation, the cells were washed and analyzed on a Bio-Rad 2000MP system (Bio-Rad Laboratories, Hercules, CA) equipped with a Nikon T300 inverted microscope with a 60x (NA1.2) water immersion

objective lens and an Argon laser tuned to 488 nm wavelength (as described in the section *Fluorescence Microscopy* above).

Ex vivo calibration curve was obtained as follows. Briefly, after incubation with **BSA-16**, the cells were washed in ACAS medium of varying pH values (pH was adjusted by adding small amounts of 0.2 N solution of NaOH or 0.1 N solution of HCl). 1 μg/mL of nigericin (Aldrich) was added to the medium to allow a rapid exchange of K^+ for H^+ which resulted in a rapid equilibration of external and internal pH. The cells were then analyzed by fluorescence microscopy as described above.

The pH_i calibration was fit to a linear regression curve using Excel. The fitted parameters were used to generate an equation that converted ratio channel (red/green) number to pH_i.

Measurement of pH_i Using C.SNARF-1

COS-7 cells (American Type Culture Collection) were cultured as subconfluent monolayers on 75 cm^2 culture flask with vent caps in DMEM supplemented with 10 % fetal bovine serum (FBS) in a humidified incubator at 37 ºC with 5 % CO_2. Cells grown to subconfluence were enzymatically dissociated from the surface with trypsin and plated 2-3 d prior to the experiments in a 12 wells tissues culture plate (Falcon) in 1 mL DMEM. To measure pH_i with C.SNARF-1, cells were placed in 1 mL ACAS medium and 10 μM (2 μL) SNARF-1/AM (Invitrogen) was added from a 5 mM stock solution in DMSO and the sample was incubated for 60 min at 37 °C or 30 min at 4 °C. When the experiment was performed at 4 °C, the cells were pre-incubated at 4 °C for 30 min

before the addition of C.SNARF-1/AM. After incubation, the cells were washed and analyzed on a BioTek Synergy 4 plate reader. Emission spectra were obtained upon excitation at 530 nm.

A calibration curve was generated by staining the cells in high K^+ buffers of varying pH values, and adding 5 μg/mL nigericin (Aldrich) to equilibrate the intracellular/extracellular pH. High K^+ buffers contained 125 mM KCl, 20 mM NaCl, 0.5 mM $CaCl_2$, 0.5 mM $MgCl_2$, and 25 mM of one of the buffers, including acetate (4.14, 4.97), Mes (5.97), Mops (6.98) and HEPES (7.93).

The pH_i calibration was fit to a sigmoid. The fitted parameters were used to generate an equation that converted ratio channel ($\lambda_{645}/\lambda_{595}$) number to pH_i.

Electrochemistry

Cyclic voltammograms and differential pulse voltammograms were recorded on a BAS-100A electrochemical analyzer using a three-electrode cell. The working electrode was a glassy carbon disk (0.071 cm^2) and a coiled platinum wire was used as the counter electrode. The experimental reference electrode used was a Ag/AgCl prepared by electroplating method. Solutions were deaerated by an argon purge for 5-10 min and a blanket of argon was maintained over the solution while performing the measurements. Experiments were performed in CH_2Cl_2 or DMF solutions containing 0.1 M *n*-Bu_4NPF_6 at room temperature. All potentials are reported relative to Ag/AgCl electrode using Cp_2Fe/Cp_2Fe^+ as an internal reference ($E_{1/2}$ = 0.00 V vs Ag/AgCl in CH_2Cl_2 or DMF).

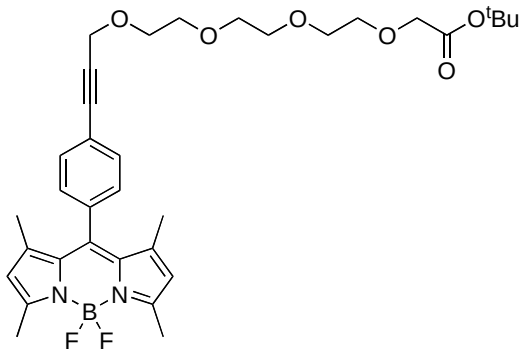

19

Iodophenyl BODIPY (142 mg, 0.316 mmol), **A** (100 mg, 0.331 mmol), $PdCl_2(PPh_3)_2$ (24 mg, 0.032 mmol, 10 mol %), CuI (12 mg, 0.064 mmol, 20 mol %), Et_3N (0.44 ml, 3.16 mmol) and 5 ml THF were added into a 50 mL round bottom flask. The solvent was degassed three times to remove oxygen, and then the reaction was kept at 55 ^oC for 5 h. The reaction solvent was removed under reduced pressure. The crude product was purified by flash column chromatography eluting with 30 % hexane/ethyl acetate to give the desired product as an orange solid (151 mg, 77 %). ^1H NMR (300 MHz, $CDCl_3$), δ7.53 (d, J = 8.1, 2H), 7.20 (d, J = 8.1 Hz, 2H), 5.95 (s, 2H), 4.42 (s, 2H), 3.98 (s, 2H), 3.72-3.78(m, 2H), 3.63-3.69(m, 10H), 2.51(s, 6H), 1.45(s, 9H), 1.36(s, 6 H) ^{13}C NMR (125 MHz, $CDCl_3$), δ169.5, 155.6, 142.8, 140.6, 135.0, 132.3, 131.0, 128.0, 123.4, 121.2, 86.5, 85.4, 81.4, 70.6, 70.5, 70.4, 70.3, 69.2, 68.9,59.0, 27.9, 14.4. MS (ESI) calcd for $C_{34}H_{43}BF_2N_2O_6$ $(M+H)^+$, 624.32, found 624.13. TLC (1:1 EtOAc/Hexane), R_f = 0.42.

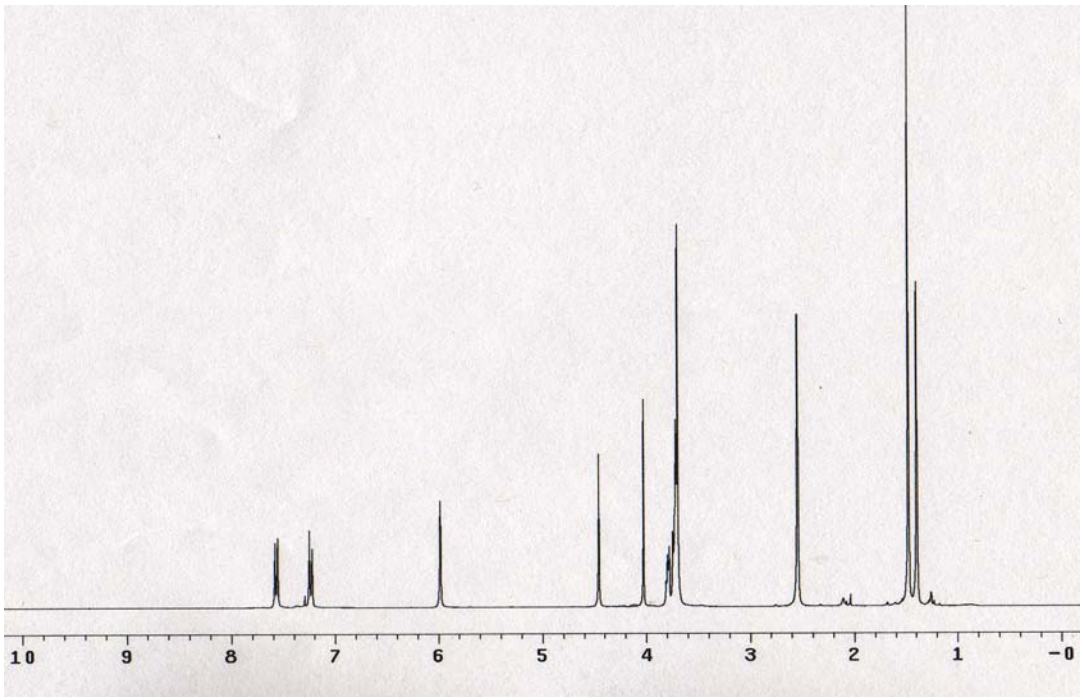

^{1}H NMR ($CDCl_3$)

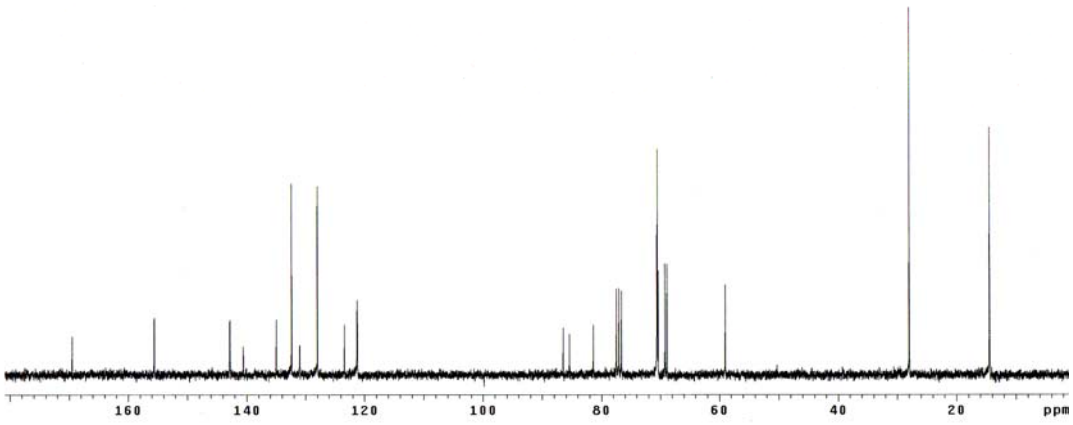

^{13}C NMR ($CDCl_3$)

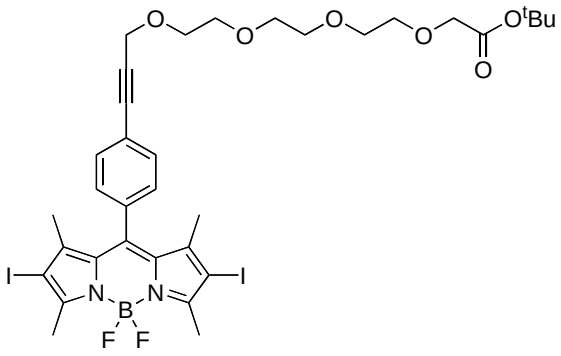

20

A mixture of **19** (104 mg, 0.165 mmol), I_2 (100 mg, 0.412 mmol), HIO_3 (58 mg, 0.33 mol) and 10 mL EtOH in a 50 mL flask were warmed up to 60 ^oC for 20 min, and then it was cooled to room temperature. The reaction was quenched by addition of Na_2SO_3 (2 mL 1M). Water (20 mL) was added to the reaction mixture, and the product was extracted from water with CH_2Cl_2 (25 mL x 3). The combined organics were concentrated under reduced pressure, and the resulting crude product was purified by flash chromatography eluting with hexane and ethyl acetate (1:1) to give **20** (145 mg, 99%) as a red solid that is very soluble in CH_2Cl_2. ^1H NMR (300 MHz, $CDCl_3$), δ 7.60 (d, J = 8.4 Hz, 2H), 7.21 (d, J = 8.4 Hz, 2H), 4.47 (s, 2H), 4.02 (s, 2H), 3.78-3.81 (m, 2H), 3.70-3.75 (m, 10H), 2.64 (s, 6H), 1.47 (s, 9H), 1.40 (s, 6 H). ^{13}C NMR (125 MHz, $CDCl_3$), δ 169.9, 157.3, 145.4, 140.6, 135.0, 133.0, 131.3, 128.2, 124.4, 87.3, 86.1, 85.5, 81.8, 71.0, 70.9, 70.9, 70.8, 70.7, 69.7, 69.3, 59.4, 28.4, 17.4, 14.4. MS (MALDI) calcd for $C_{34}H_{41}BF_2N_2NaO_6^+$ $(M+Na)^+$, 899.10, found 898.91. TLC (1:1 EtOAc/Hexane), R_f = 0.45.

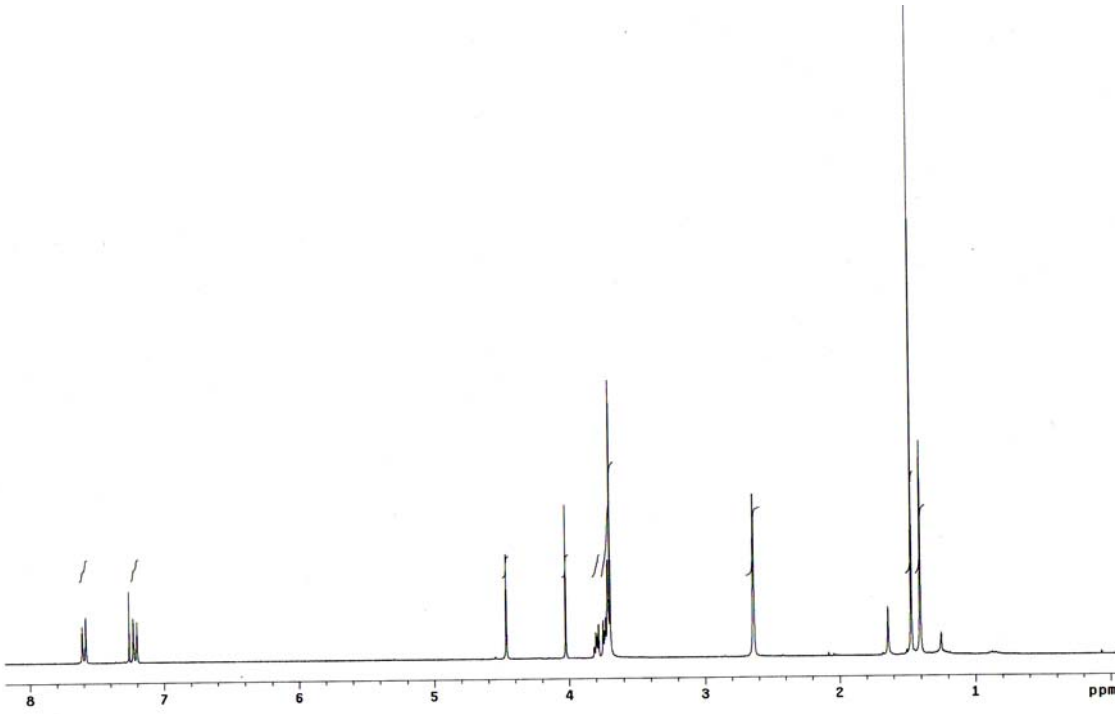

^{1}H NMR ($CDCl_3$)

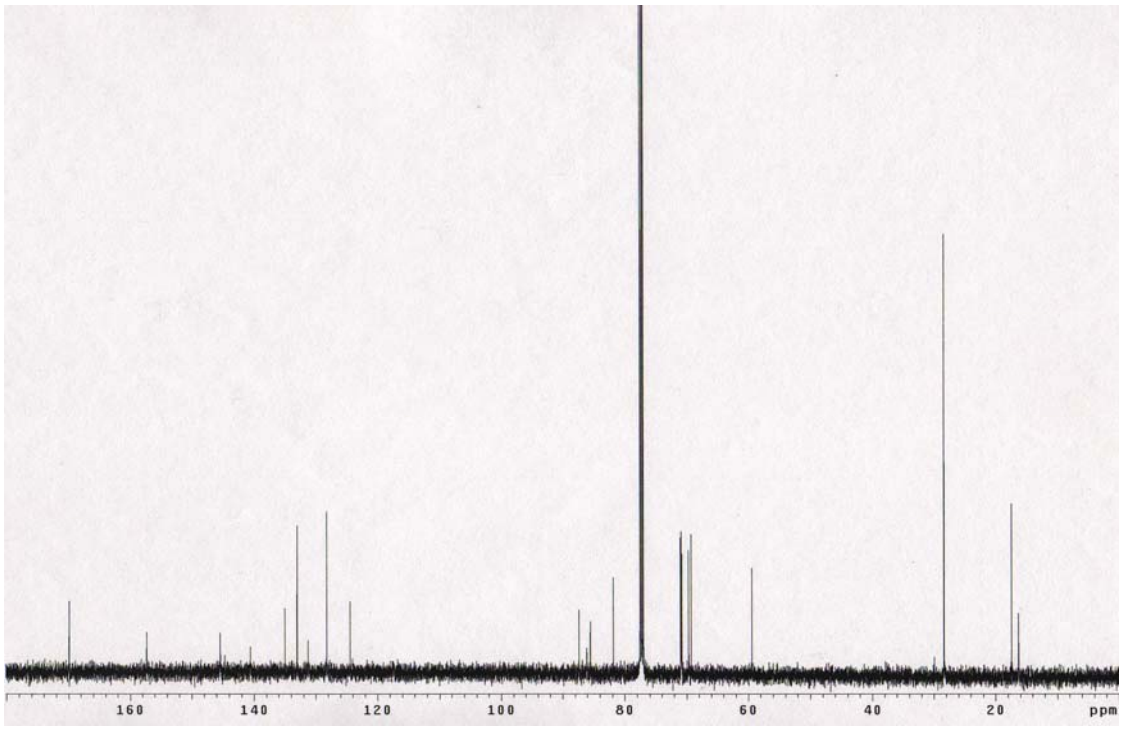

^{13}C NMR ($CDCl_3$)

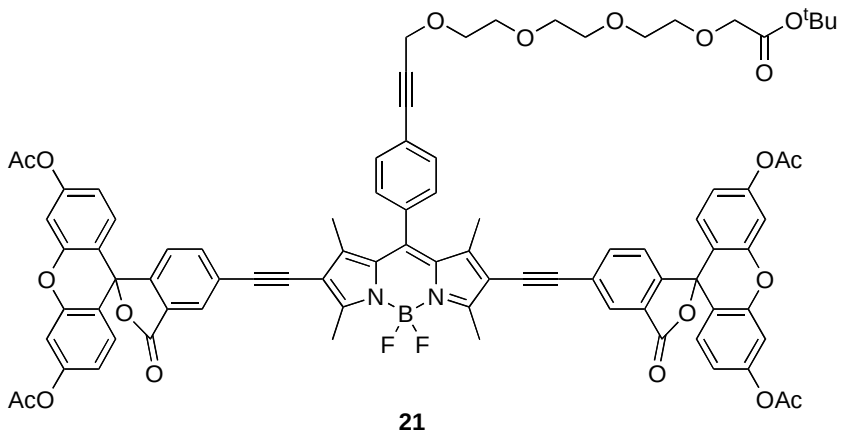

21

A mixture of **20** (65 mg, 0.074 mmol), diacetylfluoresceinalkyne **C,** (82 mg, 0.186mmol), Et_3N (0.11 mL, 0.74 mmol), $Pd(PPh_3)_4$ (8 mg, 0.007 mmol), CuI (3 mg, 0.014 mmol) were dissolved in THF (2 mL). After the solution was degassed three times via the freeze-thawed method, the mixture was heated up to 45 ^oC for 16 h. The reaction solvent was removed under reduced pressure and the crude product was purified by flash column eluting with 50% hexane:ethyl acetate to give the desired product as a light yellow solid (80 mg, 72%). ^1H NMR (500 MHz, $CDCl_3$), δ 8.08 (m, 2H), 7.73 (dd, J =8.0, 1.5 Hz, 2H), 7.65(d, *J* = 8.0 Hz, 2H), 7.29 (d, *J* = 8.5 Hz, 2H), 7.15 (d, J = 8.2 Hz, 2H), 7.10 (d, *J* = 2.0 Hz, 4H), 6.83 (bs, 4H), 6.83 (d, *J* = 2.0 Hz, 4H), 4.48 (s, 2H), 4.02 (s, 2H), 3.80-3.82 (m, 2H), 3.70-3.75 (m, 10H), 2.75 (s, 6H), 2.32 (s, 12H), 1.58 (s, 6H), 1.47(s, 9H). ^{13}C NMR (125 MHz, $CDCl_3$), δ 169.6, 168.8, 168.2, 159.1, 152.1, 151.8, 151.5, 144.6, 142.1, 137.9, 134.1, 132.8, 131.1, 128.9, 127.9, 127.7, 126.6, 125.8, 124.3, 124.2, 117.8, 116.0, 115.6, 110.5, 94.7, 87.2, 85.3, 84.1, 81.8, 81.5, 70.7, 70.6, 70.6, 70.5, 69.5, 69.0, 59.2, 28.1, 21.1, 13.8, 13.7 MALDI MS calcd for $C_{86}H_{71}BF_2N_2NaO_{20}^+$ $(M+Na)^+$ 1523.46, found 1523.26. TLC (1:1 EtOAc/Hexane), R_f = 0.20.

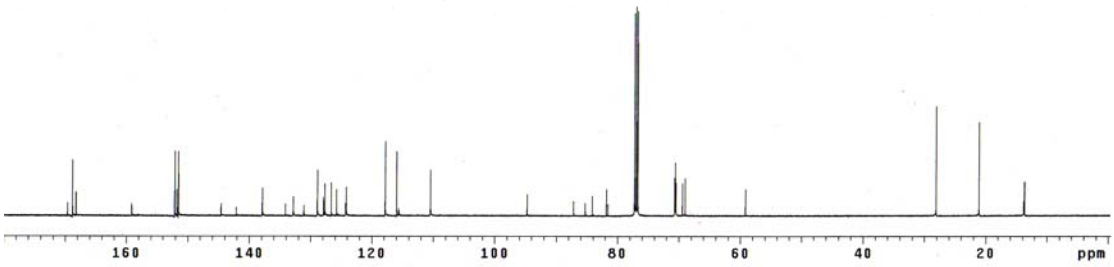

^{13}C NMR ($CDCl_3$)

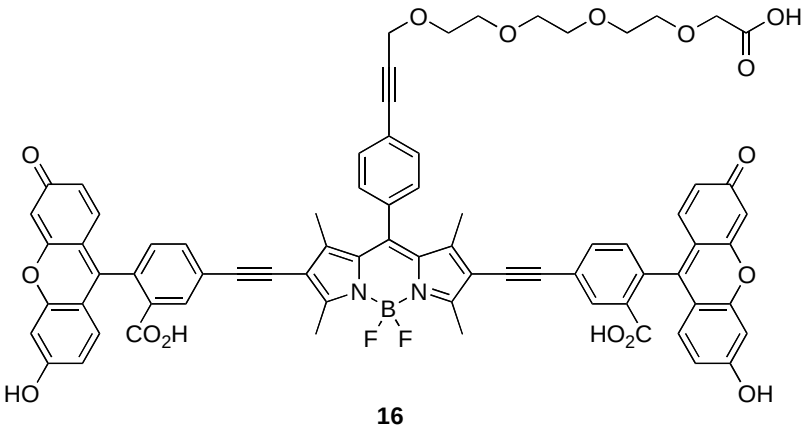

16

Compound **21** (6.1 mg, 0.004 mmol) in 5 mL ground bottom flask was heat up to 200 ^{o}C in a sand bath for 15 h. Then the crude product was dissolved in 1 mL MeOH, followed by addition of K_2CO_3 (3 mg, 0.022 mmol). The mixture was stirred at room temperature for overnight. Then 10 mL water was added to the mixture and the non-water-soluble impurity was extracted out of the aqueous solution with CH_2Cl_2 (5 mL x 2). The aqueous solution was carefully neutralized with 0.1M HCl and the product was extracted out of the water with 75% $CHCl_3$/iPrOH (10 mL x 3) to afford a dark red solid **16** (5 mg, 95 %). ^{1}H NMR (500 MHz, 75% $CD_3OD/CDCl_3$), δ 8.06 (s, 2H), 7.78 (dd, *J* = 8.5 Hz, 1.3 Hz, 2H), 7.68 (d, *J* = 8.5Hz, 2H), 7.36 (d, *J* = 8.5 Hz, 2H), 7.19 (d, *J* = 8.5 Hz, 2H), 6.74 (s, 4H), 6.67 (d, *J* = 7.5 Hz, 4H), 6.58 (d, *J* = 7.5 Hz, 4H), 4.49 (s, 2H), 4.13 (s, 2H), 3.81-3.83(m, 2H), 3.69-3.75 (m, 10H), 2.74 (s, 6H), 1.61 (s, 6H). ^{13}C NMR (125MHz,75%$CD_3OD/CDCl_3$),δ 180.8, 173.4, 169.8, 159.6, 154.1, 154.0, 153.9, 145.3, 143.0, 138.1, 134.8, 133.4, 131.8, 129.9, 128.7, 128.5, 128.4, 126.1, 125.5, 124.8, 116.4, 113.8, 111.0, 103.3, 95.6, 87.4, 86.0, 84.3, 71.2, 71.1, 71.0, 70.9, 70.8, 69.8, 68.8, 59.5, 30.2, 14.0. ^{19}F NMR (300 MHz, CD_3OD), 30.6 (q, *J* = 36.0 Hz). MS (MALDI) calcd for $C_{76}H_{55}BF_2N_2O_{16}^-$ $(M-H)^-$ 1275.35, found 1275.31.

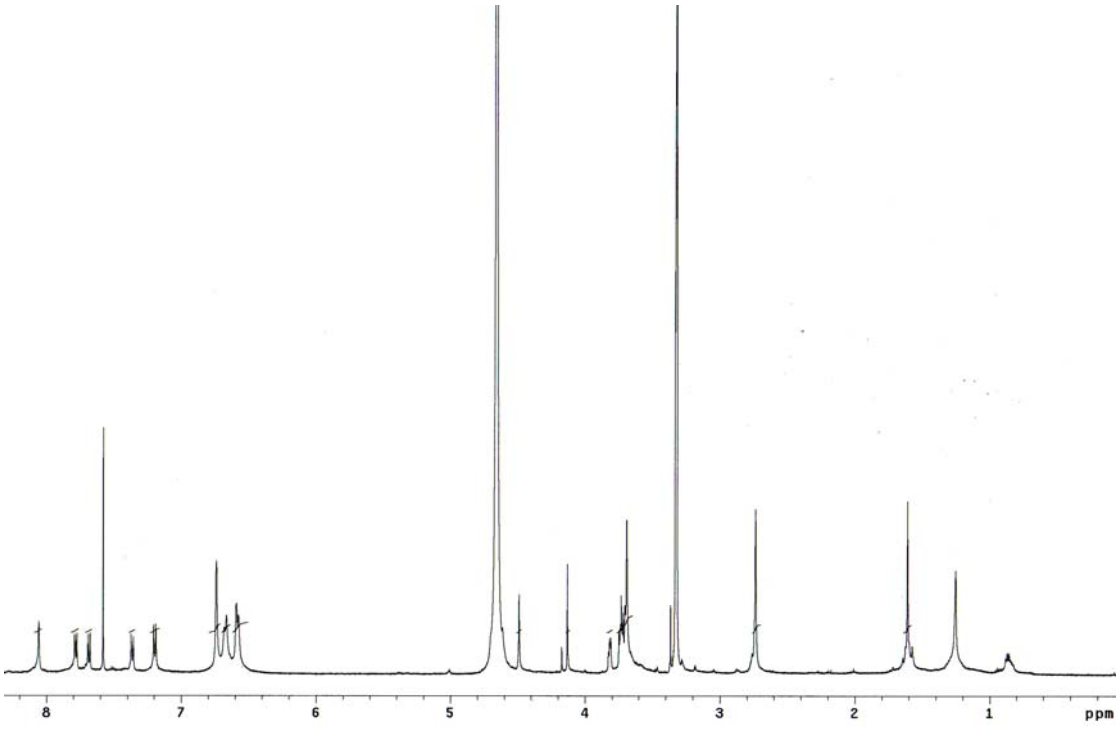

^{1}H NMR (75% CD_3OD:$CDCl_3$)

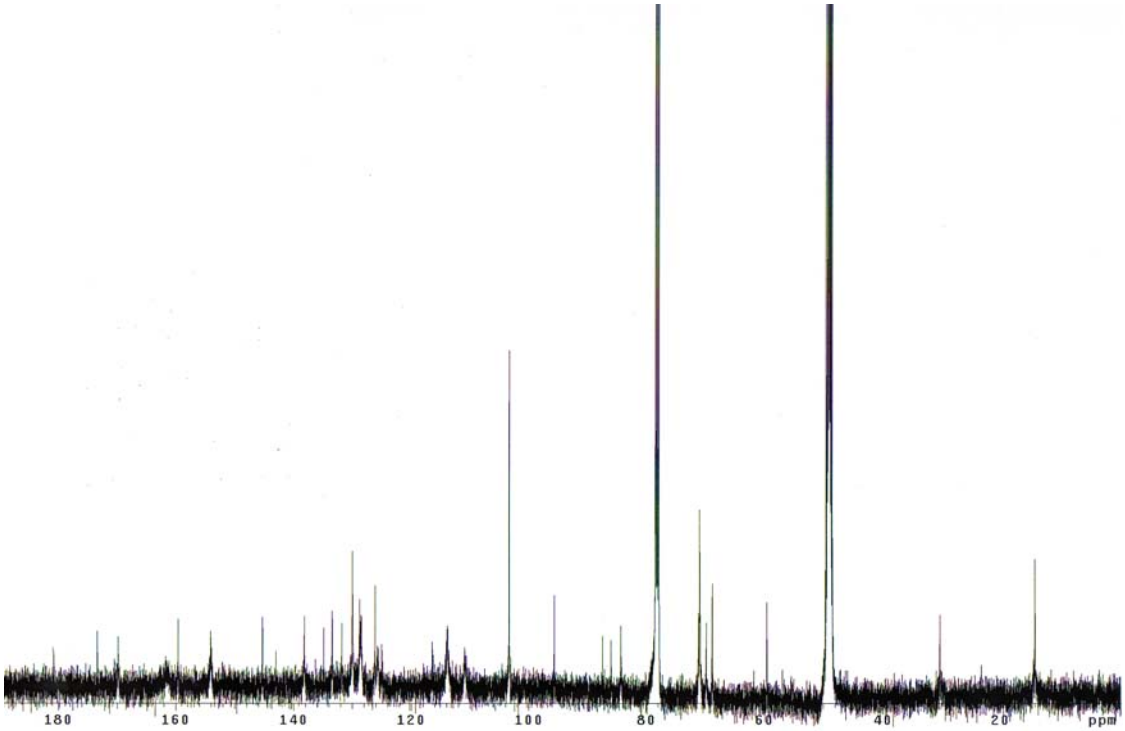

^{13}C NMR (75% CD_3OD:$CDCl_3$)

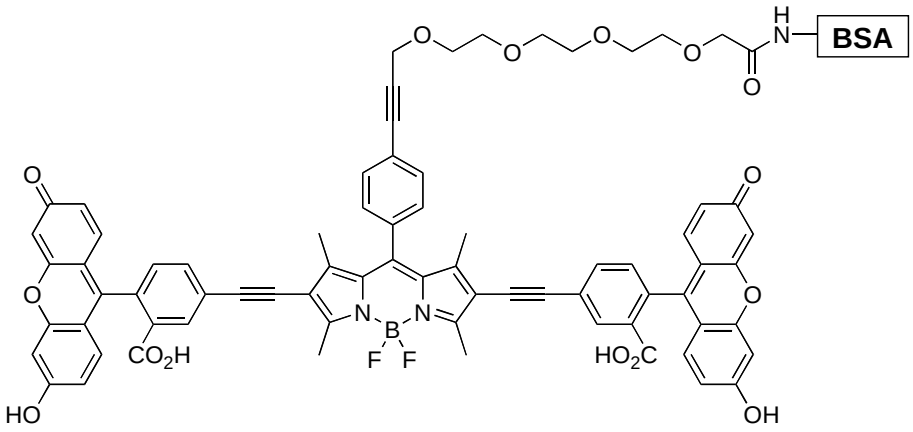

BSA-16

BSA-16. Cassette **16** (1.5 mg) was dissolved in dry DMF (0.15 mL) and *N*-hydroxysuccinimide (0.4 mg), diisopropyl carbodiimide (DIC, 0.7 μL) were added. The reaction mixture was stirred at room temperature for 24 h. The activated cassette **16** solution (100 μL, 6 eq.) was added to the solution of bovine serum albumin (13 mg, 1 eq.) in 1.5 mL freshly prepared sodium bicarbonate (0.1 M, pH 8.3). The solution was stirred at room temperature in the dark for 1 h. The desired product was purified by SephadexTM G-25 (PD-10) desalting column eluting with DI-water. The UV-vis spectra show the absorbance peak of avidin at 280 nm and the two maximum absorbance peaks of the cassettes **16** at 490 nm and 570 nm (Figure S1.1).

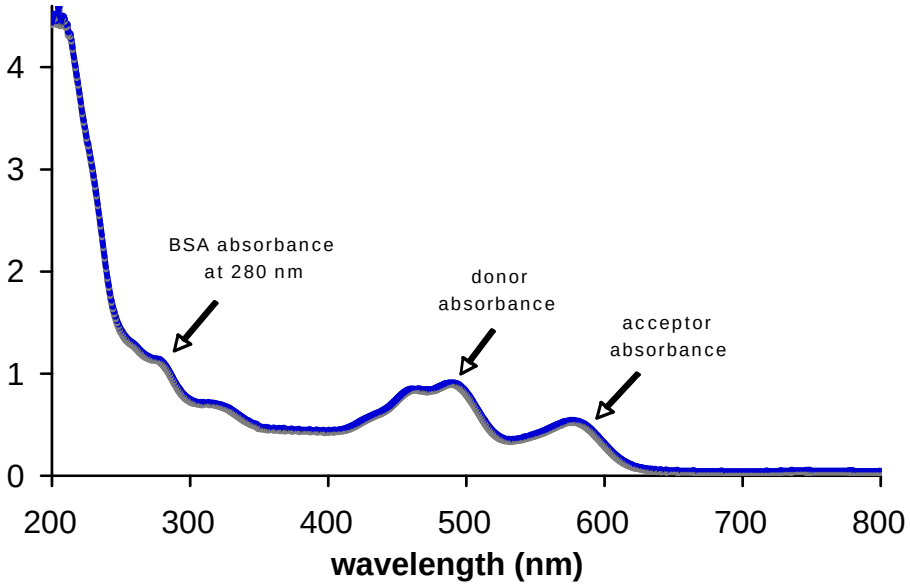

Figure S1.1 UV absorbance spectra of **BSA-16** conjugate in DI water.

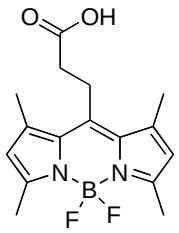

26

A solution of 2,4-dimethylpyrrole (1.0 mL, 10 mmol), succinic anhydride (400 mg, 4.0 mmol), and BF_3• Et_2O (0.50 mL, 4.0 mmol) in 30 mL toluene was heated to 80 °C under N_2 for 5 h. The mixture was cooled to 25 ºC and BF_3•Et_2O (5.0 mL, 40 mmol) and Et_3N (10 mL, 80 mmol) were then added. After stirring for 16 h at 25 ºC under N_2 the reaction was quenched with 60 mL of 0.1 M HCl aqueous solution. Extraction was performed and the organic fractions were combined and dried over magnesium sulfate. The organic solvent was removed under reduced pressure and the product was purified via flash silica column with 85 % ethyl acetate:hexane to afford the desired product as an orange solid (203 mg, 18 %). ^{1}H NMR (300 MHz, $CDCl_3$) δ (ppm) 6.07 (s, 2H), 3.29-3.35 (m, 2H), 2.62-2.68(m, 2H), 2.52 (s, 6H), 2.44 (s, 6H), ^{13}C NMR (75 MHz, $CDCl_3$), δ (ppm), 176.6 154.8, 142.8, 140.3, 131.2, 122.0, 35.1, 23.4, 16.4, 14.5. MS (ESI) calcd for $C_{16}H_{18}BF_2N_2O_2$ $[M-H]^-$ 319.15, found 319.15. TLC (50 % EtOAc:Hexane) R_f = 0.50.

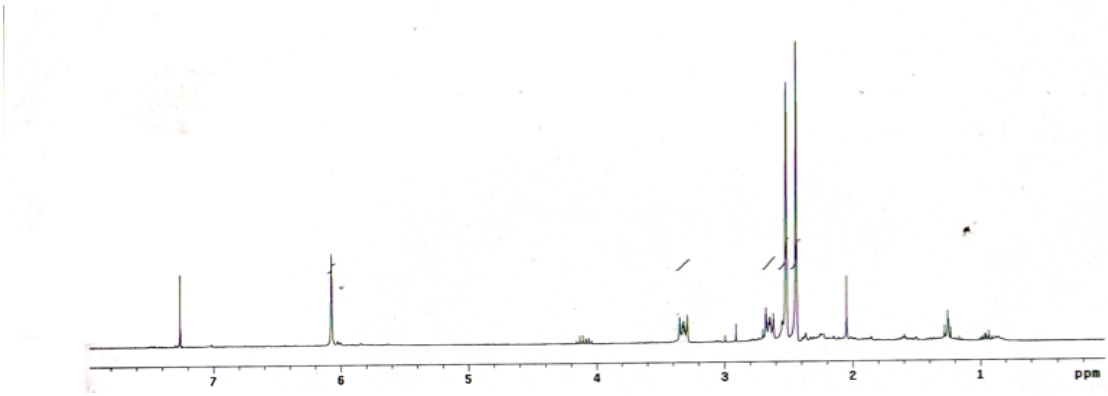

^{1}H NMR ($CDCl_3$)

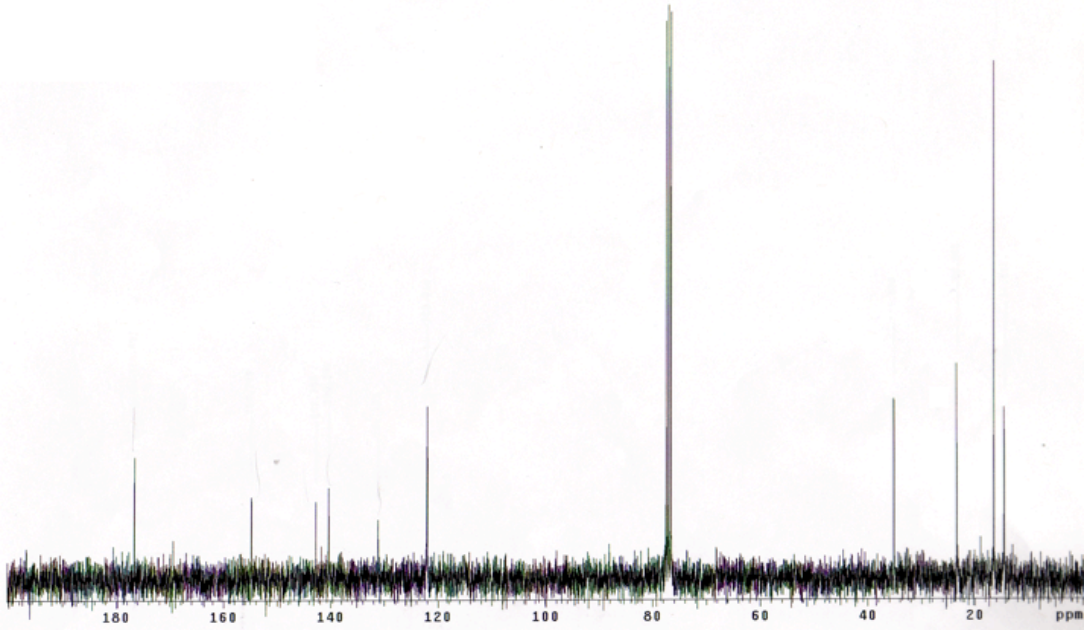

^{13}C NMR ($CDCl_3$)

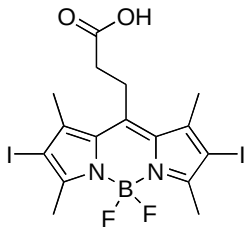

27

Tetramethyl-BODIPY acid **26** (600 mg, 1.87 mmol) was suspended in 200 mL of MeOH. I_2 (1.24 g, 4.87 mmol) was added followed by iodic acid (660 mg, 3.75 mmol) in ~3 mL water was added over 5 min. The mixture was stirred for 30 min at 25 ºC. The MeOH was then removed under reduced pressure and the crude product was purified via flash silica column with 50 % ethyl acetate:hexane to afford the desired product as a red solid (574 mg, 54 %). ^{1}H NMR (300 MHz, $CDCl_3$) δ (ppm) 3.28-3.32 (m, 2H), 2.45-2.52 (m, 2H), 2.50 (s, 6H), 2.43 (s, 6H), ^{13}C NMR (75 MHz, $CDCl_3$), δ (ppm), 175.1 156.3, 142.5, 142.3, 131.1, 87.0, 34.9, 24.2, 19.3, 16.5. MS (ESI) calcd for $C_{16}H_{17}BF_2I_2KN_2O_2[M + K]^+$ 610.9, found 611.6. TLC (50 % EtOAc:Hexane) R_f = 0.55.

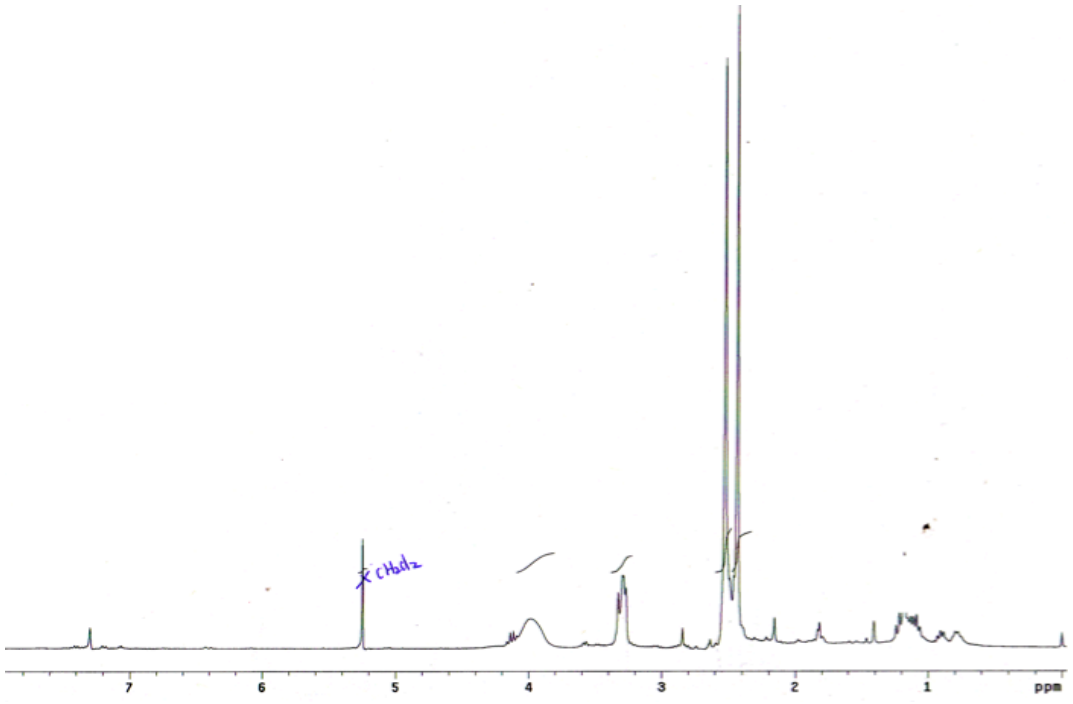

^{1}H NMR ($CDCl_3$)

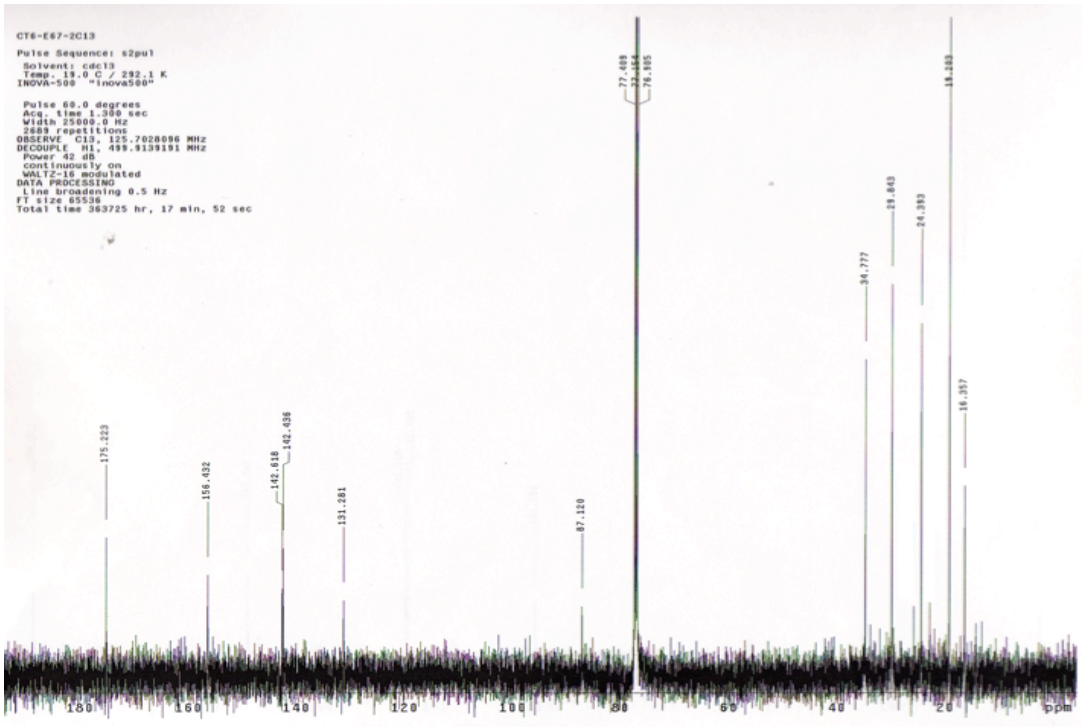

^{13}C NMR ($CDCl_3$)

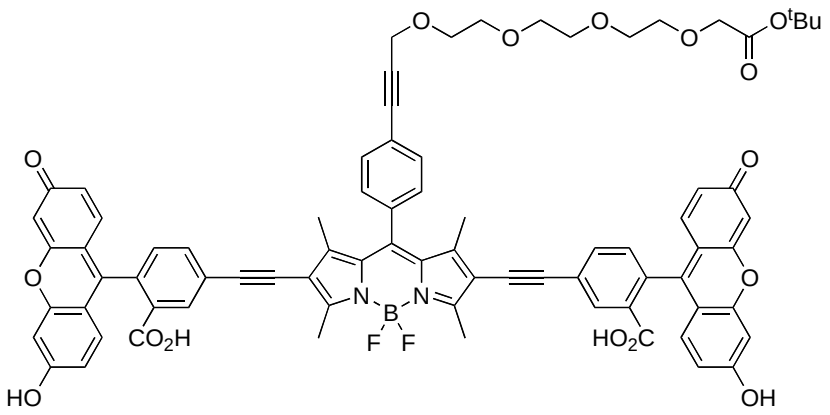

22

To **21** (12 mg, 0.01 mmol) in 5 mL 2:1 methanol/THF in was added Na_2CO_3 (3.5 mg, 0.03 mmol). The mixture was stirred for 3 h at 25 ºC under N_2. The reaction was quenched by adding aqueous HCl (0.1M, 10 mL) and the product was extracted out of the solution with 75% CH_2Cl_2:^{i}PrOH (5 mL x 3). The organic layers were washed with brine solution (10 mL) and dried with magnesium sulfate. The desired product was isolated as a purple solid (10 mg, 99 %). ^{1}H NMR (500 MHz, 75% CD_3OD:$CDCl_3$), δ 8.00 (s, 2H), 7.74 (dd, *J* = 8.0 Hz, 1.5 Hz, 2H), 7.65 (d, *J* = 7.5Hz, 2H), 7.33 (d, *J* = 8.5 Hz, 2H), 7.15 (d, *J* = 8.0 Hz, 2H), 6.67 (d, *J* = 2.5 Hz 4H), 6.59 (d, *J* = 8.0 Hz, 4H), 6.51 (dd, *J* = 9.0 Hz, 2.5 Hz, 4H), 4.47 (s, 2H), 4.00 (s, 2H), 3.79-3.81(m, 2H), 3.71-3.73(m, 2H), 3.66-3.69 (m, 8H), 2.71 (s, 6H), 1.58 (s, 6H), 1.44(s, 9H), ^{13}C NMR (125 MHz, 75% CD_3OD:CDCl3), δ 170.9, 170.1, 169.8, 159.5, 153.5, 145.2, 142.9, 138.3, 134.8, 133.4, 131.7, 131.2, 129.6, 128.7, 128.5, 128.0, 126.1, 125.9, 124.9, 116.3, 110.3, 108.2, 103.3, 95.6, 87.4, 86.0, 84.1, 82.7, 71.0, 70.9 (2 C), 70.8 (2 C), 69.7, 69.3, 59.5, 30.2, 28.3, 14.0. MS (MALDI) calcd for $C_{78}H_{63}BF2N_2O_{16}^+$ $(M+H)^+$ 1333.42, found 1333.44.

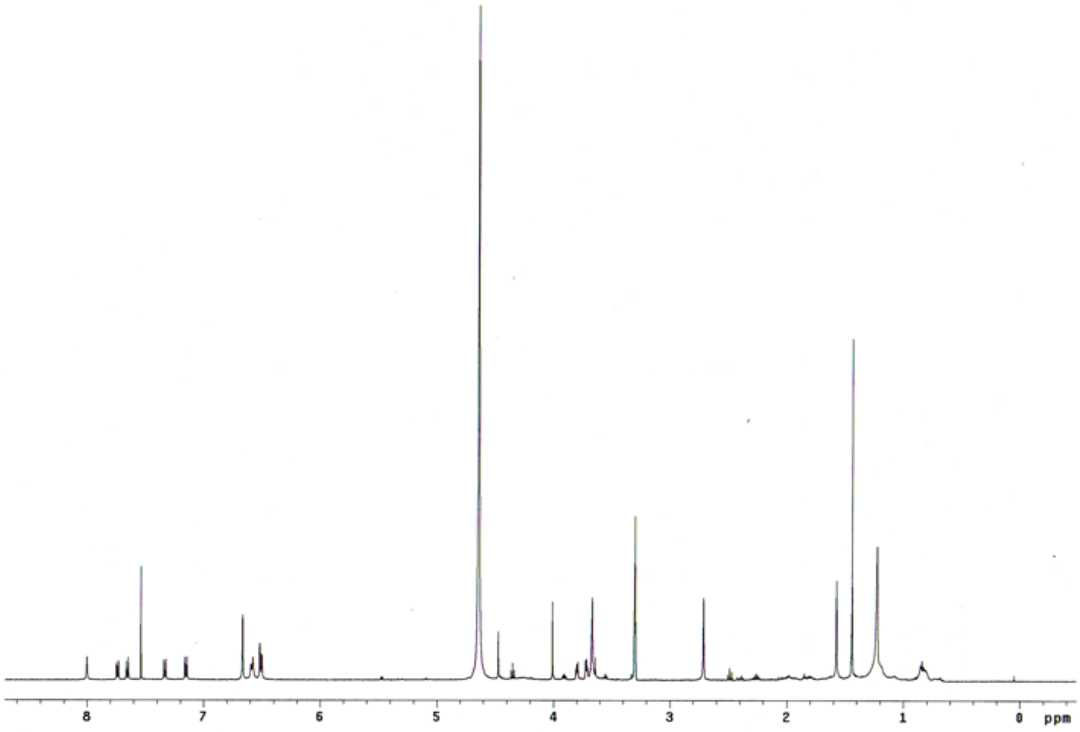

^{1}H NMR (1:2 $CDCl_3/CD_3OD$)

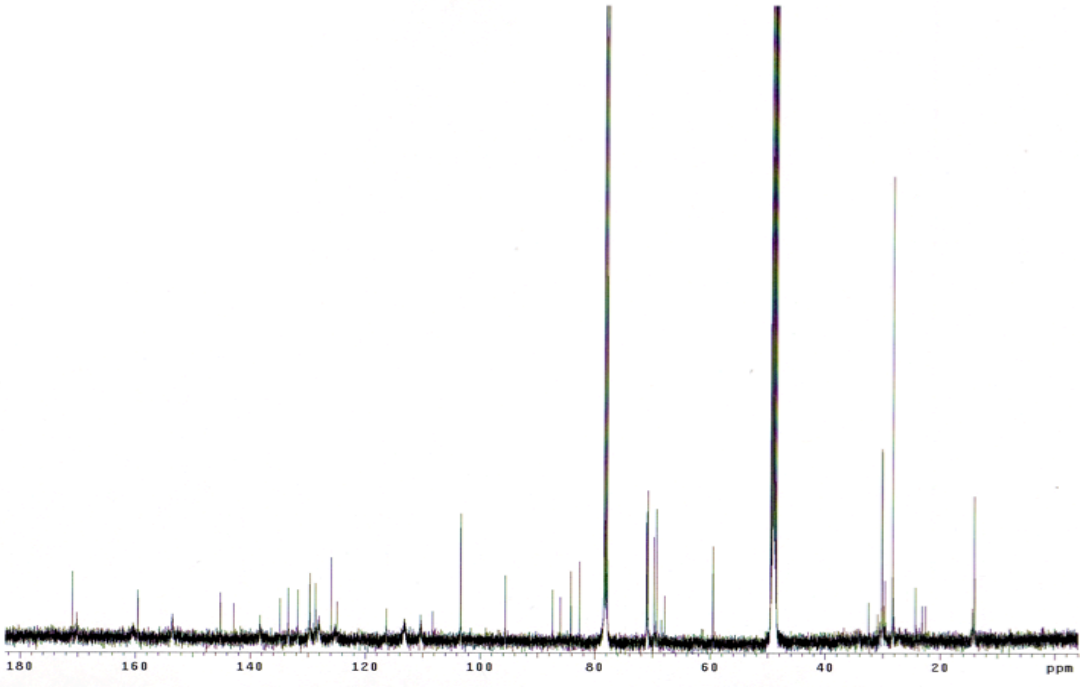

^{13}C NMR (1:2 $CDCl_3/CD_3OD$)

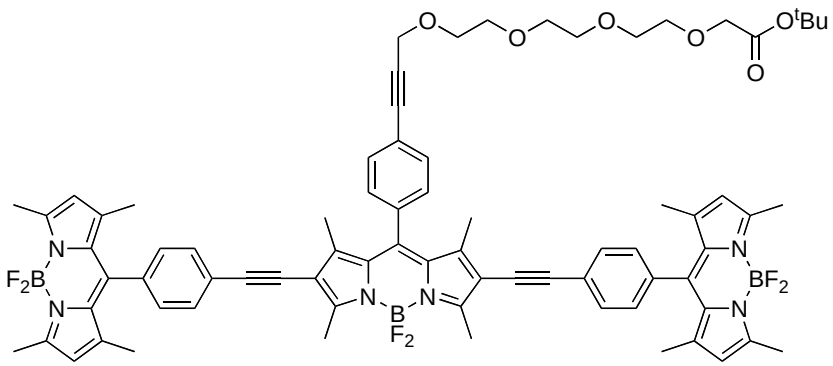

24

A mixture of **20** (80 mg, 0.09 mmol), **D** (69 mg, 0.20 mmol), Et_3N (0.13 mL, 0.91 mmol), $PdCl_2(PPh_3)_2$ (6 mg, 0.01 mmol), CuI (4 mg, 0.01 mmol) were dissolved in 3.0 mL THF. The solution was degassed three times via the freeze-thaw method and the mixture was heated to 50 $^{\circ}$C for 16 h under N_2. The reaction solvent was removed under reduced pressure and the crude product was purified via flash silica column eluting with 67% hexane:ethyl acetate to give the desired product as a purple solid (89 mg, 74 %). ^{1}H NMR (500 MHz, $CDCl_3$), δ 7.64 (d, *J* = 8.0 Hz, 2H), 7.59 (d, J =8.0 Hz, 4H), 7.29 (d, *J* = 8.5 Hz, 2H), 7.27 (d, *J* = 8.0 Hz, 4H), 5.99 (s, 4H), 4.48 (s, 2H), 4.02 (s, 2H), 3.80-3.82 (m, 2H), 3.70-3.75 (m, 10H), 2.76 (s, 6H), 2.55 (s, 12H), 1.58 (s, 6H), 1.47(s, 9H), 1.43 (s, 12H), ^{13}C NMR (125 MHz, $CDCl_3$), δ 169.6, 158.9, 155.7, 144.1, 143.0, 141.7, 140.7, 134.8, 134.3, 132.8, 131.9, 131.2, 128.2 (2 C), 128.0, 124.1 (2 C), 121.3, 116.0, 96.0, 87.1, 85.3, 82.9, 81.6, 70.7, 70.6 (3 C), 70.5, 69.5, 69.0, 59.2, 28.1, 14.6 (2 C), 14.6, 13.7. MALDI MS calcd for $C_{76}H_{77}B_3F_6N_6NaO_6^+$ $(M+Na)^+$ 1339.61, found 1339.68.

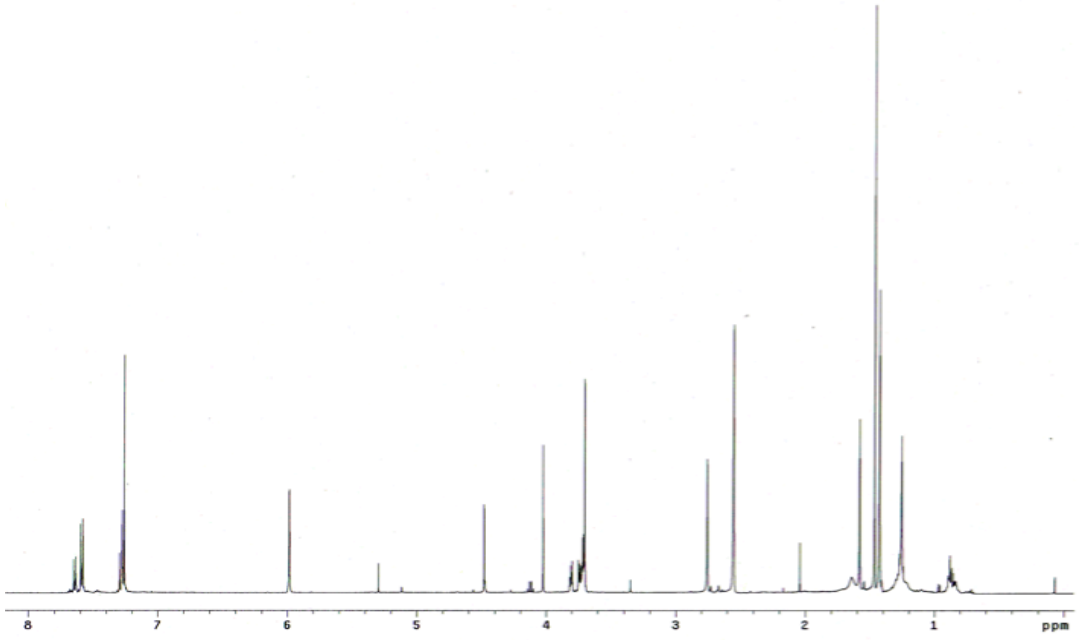

^{1}H NMR ($CDCl_3$)

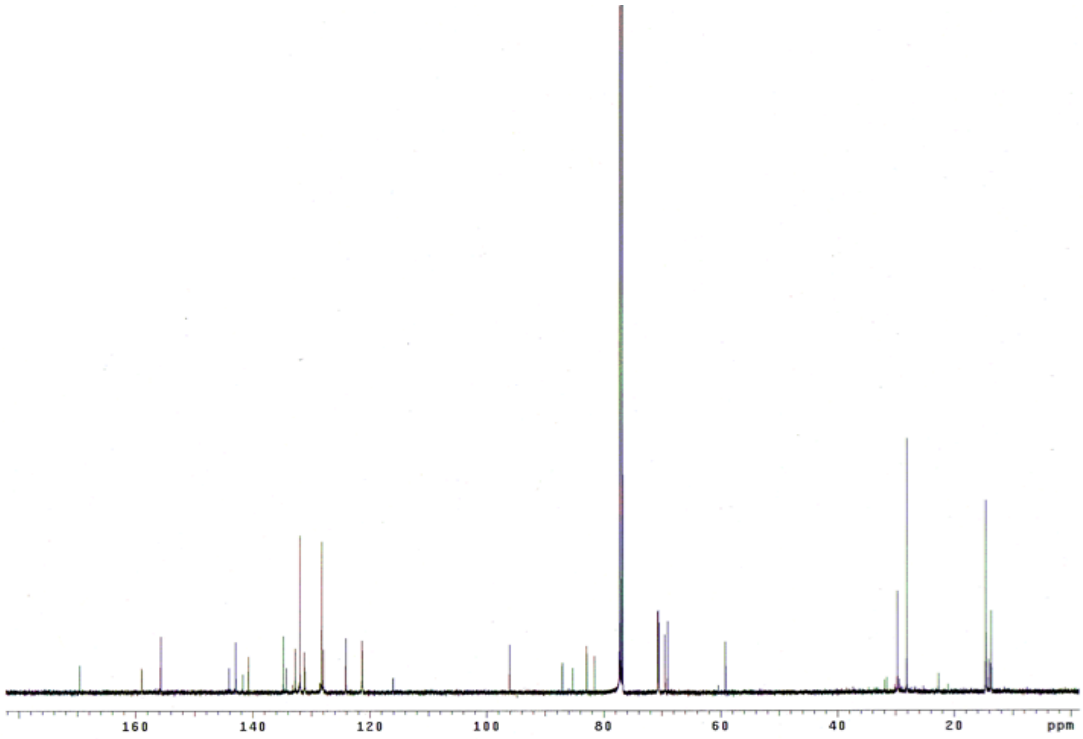

^{13}C NMR ($CDCl_3$)

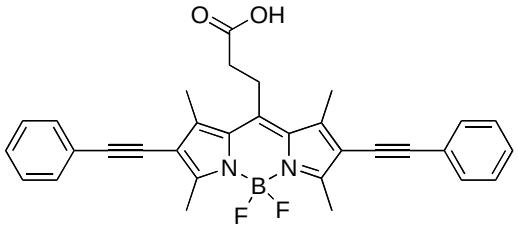

30

A mixture of **26** (34 mg, 0.11 mmol), phenylacetylene (47 μL, 0.43mmol), Et_3N (0.15 mL, 1.1 mmol), $PdCl_2(PPh_3)_2$ (8 mg, 0.01 mmol), and CuI (4 mg, 0.02 mmol) were dissolved in 2 mL THF under N_2. The solution was degassed three times via the freeze-thaw method and then heated to 50 °C for 16 h under N_2. The solvent was removed under reduced pressure and the crude product was purified via flash silica column eluting with 20% methanol:CH_2Cl_2 to give the desired product as a red solid (17 mg, 55%). ^{1}H NMR (500 MHz, $CDCl_3$), δ 7.44-7.46 (m, 4H), 7.27-7.31 (m, 6H), 3.32-3.36 (m, 2H), 2.62 (s, 6H), 2.56 (s, 6H), 2.53-2.57 (m, 2H), ^{13}C NMR (125 MHz, 3:1 $CDCl_3$:CD3OD), δ 174.0, 157.5, 144.9, 141.4, 131.4, 131.2, 128.4, 128.3, 123.2, 116.7, 96.7, 81.4, 24.2, 15.1, 15.1, 13.6. MALDI MS calcd for $C_{32}H_{27}BF_2N_2O_2$ $(M-H)^-$ 519.21, found 519.21. TLC (50 % EtOAc:Hexane) R_f = 0.20.

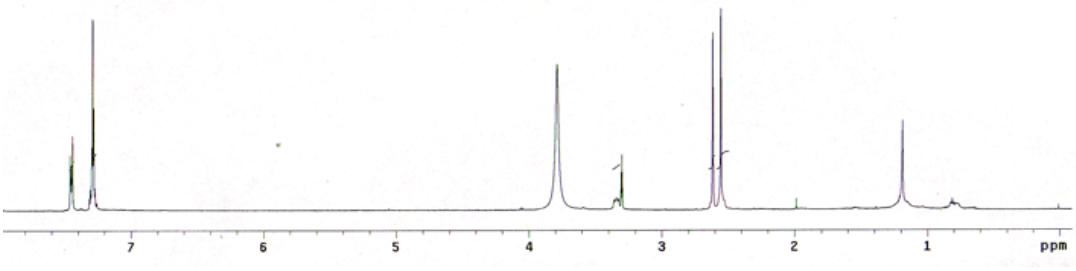

^{1}H NMR (1:2 $CDCl_3/CD_3OD$)

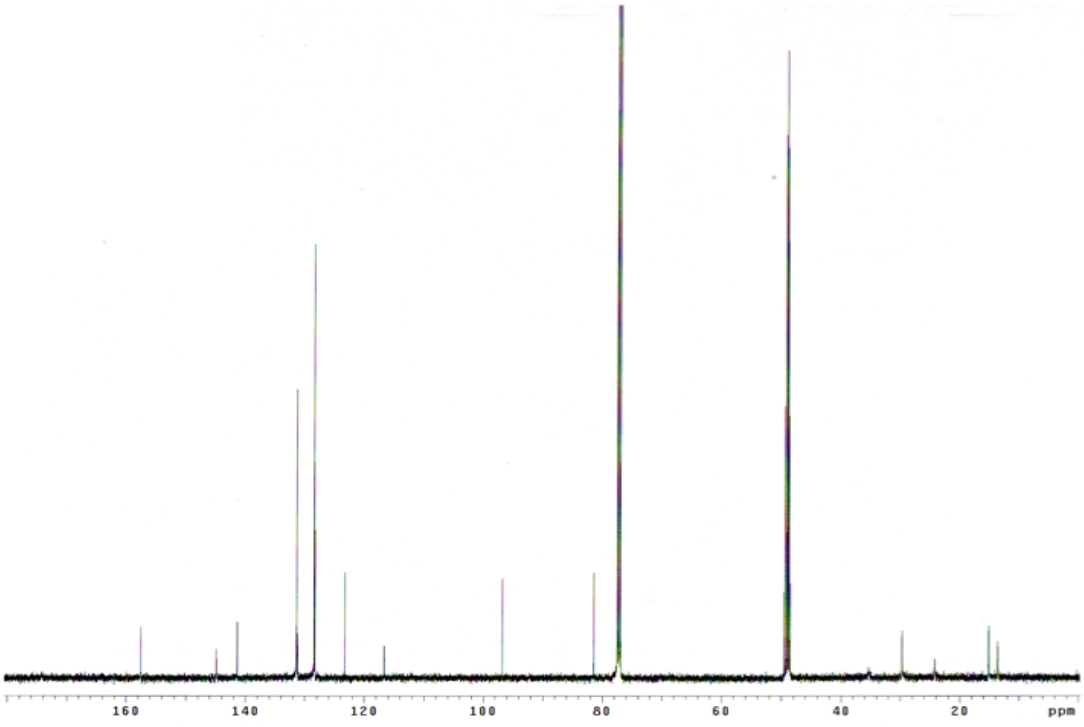

^{13}C NMR (1:2 $CDCl_3/CD_3OD$)

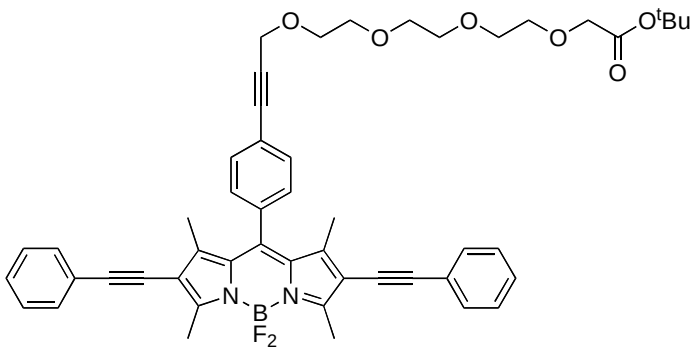

32

A mixture of **20** (66 mg, 0.08 mmol), phenylacetylene (42 μL, 0.38 mmol), Et_3N (0.10 mL, 0.75 mmol), $PdCl_2(PPh_3)_2$ (6 mg, 0.01 mmol), and CuI (3 mg, 0.01 mmol) were dissolved in 5.0 mL THF. The solution was degassed three times via the freeze-thaw method and then heated to 45 ^oC for 16 h under N_2. The reaction solvent was removed under reduced pressure and the crude product was purified via flash silica column eluting with 50% hexane:ethyl acetate to give the desired product as a purple solid (52 mg, 79%). ^1H NMR (500 MHz, $CDCl_3$), δ 7.62 (d, J = 8.0 Hz, 2H), 7.45-7.47 (m, 4H), 7.31-7.34 (m, 6H), 7.27 (d, J = 8.5 Hz, 2H), 4.47 (s, 2H), 4.02 (s, 2H), 3.80-3.81 (m, 2H), 3.69-3.75 (m, 10H), 2.72 (s, 6H), 1.54 (s, 6H), 1.47(s, 9H), ^{13}C NMR (125 MHz, $CDCl_3$), δ 169.6, 158.7, 143.7, 141.4, 134.5, 132.7, 131.3, 130.9, 128.3, 128.1, 128.0, 124.0, 123.2, 116.3, 96.6, 86.9, 85.4, 81.5, 81.4, 70.7, 70.6 (2 C), 70.5, 69.4, 69.0, 59.1, 28.1, 13.7, 13.6. MALDI MS calcd for $C_{50}H_{51}BF_2N_2NaO_6^+$ $(M+Na)^+$ 847.37, found 847.12.

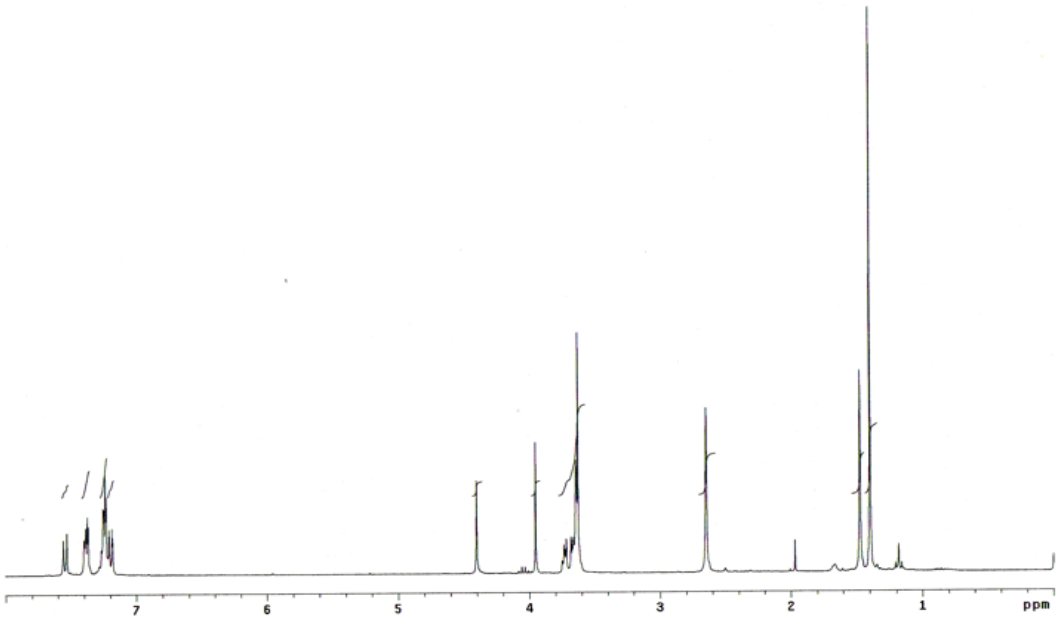

^{1}H NMR ($CDCl_3$)

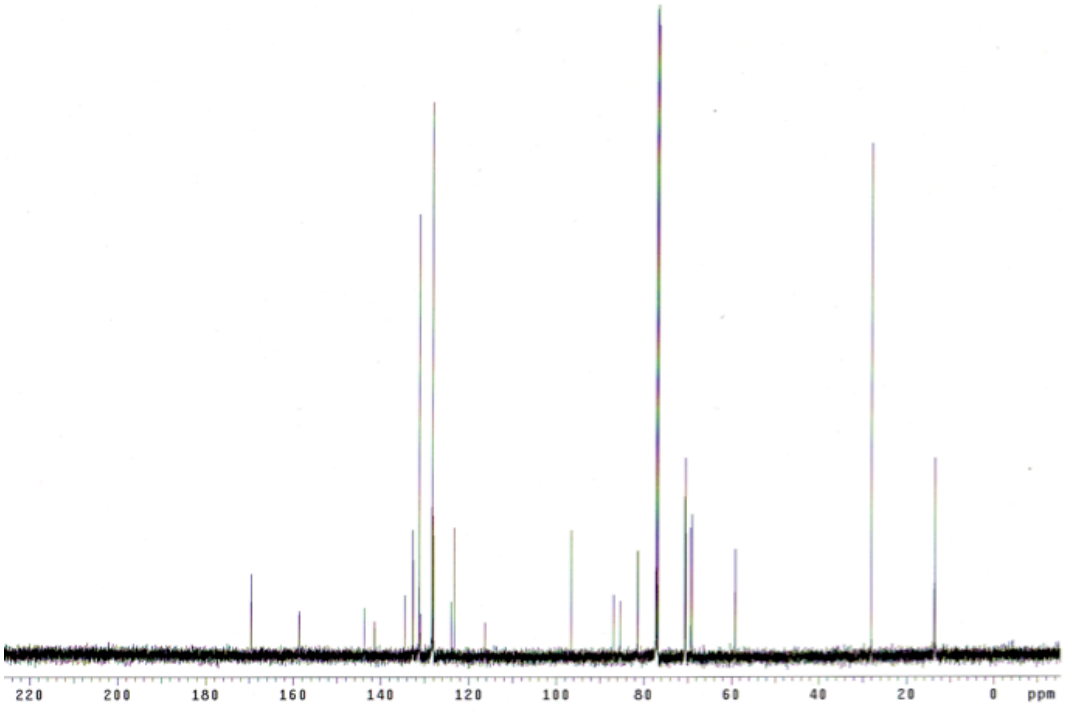

^{13}C NMR ($CDCl_3$)

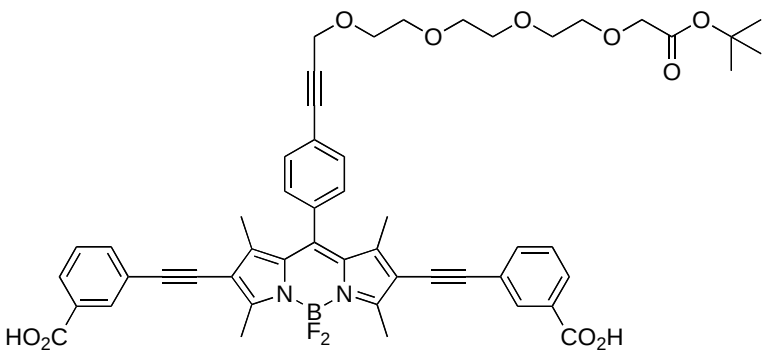

33

A mixture of **20** (58 mg, 0.066 mmol), 3-ethynylbenzoic acid (30 mg, 0.20 mmol), Et_3N (0.10 mL, 0.75 mmol), $PdCl_2(PPh_3)_2$ (5 mg, 0.003 mmol), and CuI (3 mg, 0.01 mmol) were dissolved in 5.0 mL THF. The solution was degassed three times via the freeze-thaw method and heated to 45 ^oC for 16 h under N_2. The reaction solvent was removed under reduced pressure and the crude product was purified by flash silica column eluting with 80% CH_2Cl_2:MeOH to give the desired product as a purple solid (35 mg, 58%). ^1H NMR (500 MHz, CD_3OD), δ 8.12 (s, 2H), 8.01 (d, J = 8.0 Hz, 2H), 7.75-7.78 (m, 4H), 7.53-7.58 (m, 6H), 4.49 (s, 2H), 4.00 (s, 2H), 3.76-3.77 (m, 2H), 3.66-3.69 (m, 4H), 3.61-3.64 (m, 6H), 2.71 (s, 6H), 1.60 (s, 6H), 1.44 (s, 9H), ^{13}C NMR (125 MHz, CD_3OD), δ 166.9, 159.2, 144.9, 141.4, 136.0, 135.0, 133.5, 132.8, 132.0, 131.8, 130.2, 129.7, 129.3, 125.1, 124.4, 116.5, 108.8, 96.6, 88.5, 85.6, 82.8, 81.2, 71.2, 71.1, 70.0, 69.3, 59.2, 32.6, 30.5, 28.2, 23.3, 14.3, 13.8. MALDI MS calcd for $C_{52}H_{51}BF_2N_2NaO_{10}^+$ $(M+Na)^+$ 935.35, found 935.37.

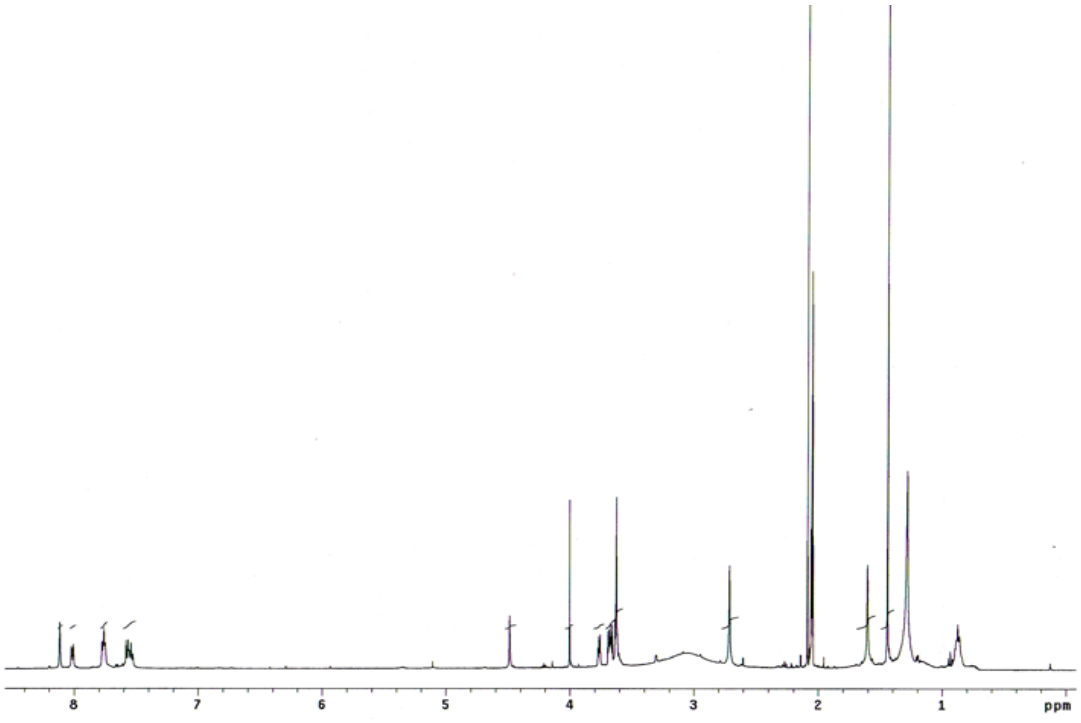

^{1}H NMR (CD_3OD)

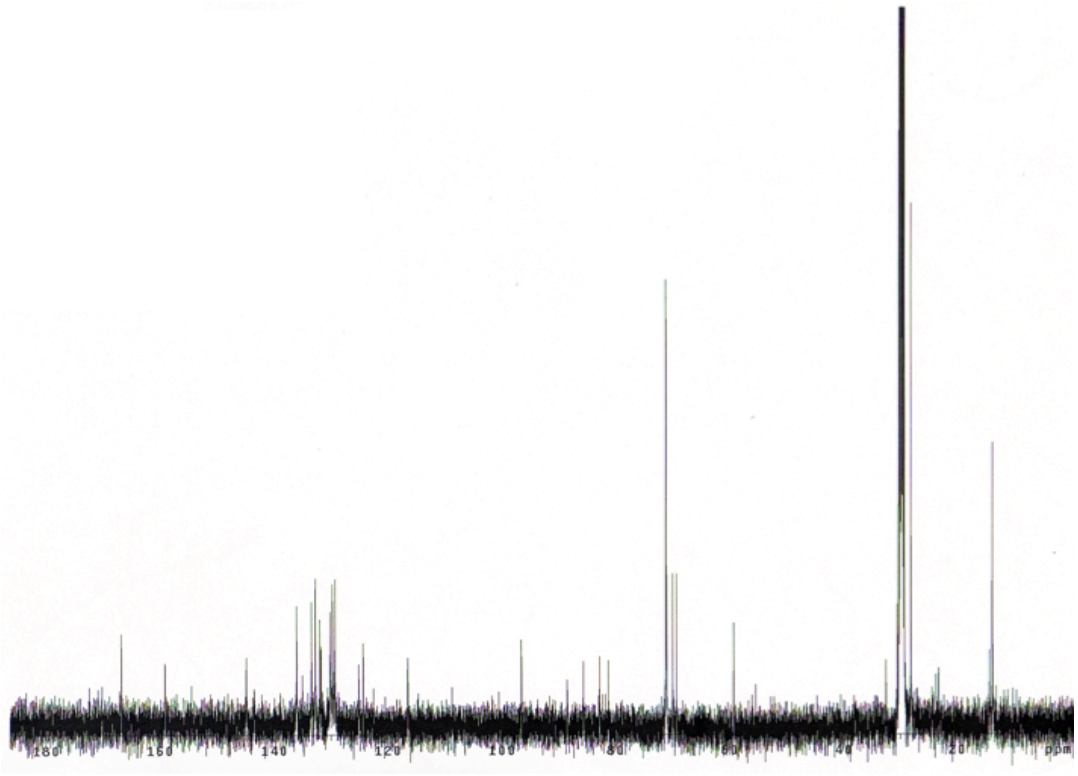

^{13}C NMR (CD_3OD)

4. Complete Electrochemical Data

cmpd	Cyclic Voltammetry (CV)					DPV[e]				
	$E_{onset,ox}$ (V)	HOMO (eV)	$E_{onset,red}$ (V)	LUMO (eV)	E_g (eV)	$E_{onset,ox}$ (V)	HOMO (eV)	$E_{onset,red}$ (V)	LUMO (eV)	E_g (eV)
E[a]	+1.22	6.38	-1.43	3.73	2.65	+1.15	6.31	-1.20	3.96	2.35
F[b]	+0.72	5.87	-1.25	3.90	1.97	+0.51	5.66	-1.08	4.07	1.59
$\mathbf{F}_{Na}$[b, d]	+0.25	5.40	-1.89	3.26	2.14	+0.11	5.26	-1.80	3.35	1.91
30[a]	+1.20	6.36	-1.22	3.94	2.42	-	-	-	-	-
31[b]	+0.80	5.95	-1.14	4.01	1.94	+0.67	5.82	-1.04	4.11	1.71
32[a]	+1.21	6.37	-1.12	4.07	2.33	+1.14	6.30	-0.94	4.22	2.08
33[b]	+0.79	5.94	-1.09	4.06	1.88	+0.66	5.81	-1.02	4.13	1.68
33[c]	+0.80	5.95	-1.12	4.03	1.92	-	-	-	-	-

Table S1.1 Electrochemical data for **30 - 33**, **E**, and **F**. All experiments were recorded using a glassy carbon working electrode (A = 0.071 cm^2) referenced to Fc/Fc^+ and a Pt counter electrode at a scan rate of 200 mV/s. All potentials are reported vs. Fc/Fc^+ and all HOMO and LUMO energies are derived form electrochemical results based on Fc/Fc^+ = 5.1 eV vs vacuum. All solvents were dearated using $Ar_{(g)}$. a. CH_2Cl_2 solution b. DMF solution. c. DMF solution (0.1 M pyridine). d. xanthene was first reacted with NaOH to obtain the sodium salt. e. DPV:Differential Pulse Voltammetry. Compounds **30** and **33** (base) decomposed during DPV scan.

Electrochemistry Spectra

Electrochemistry of **24**

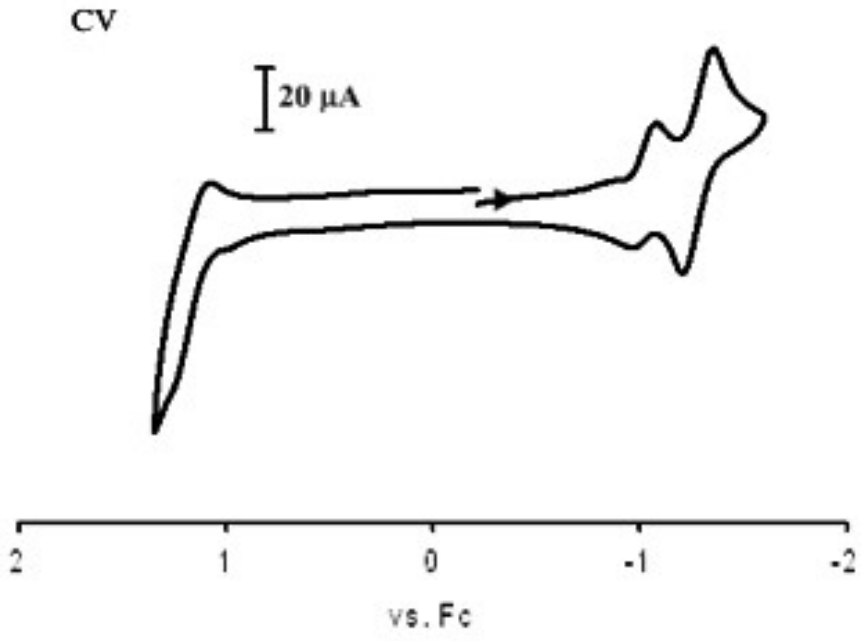

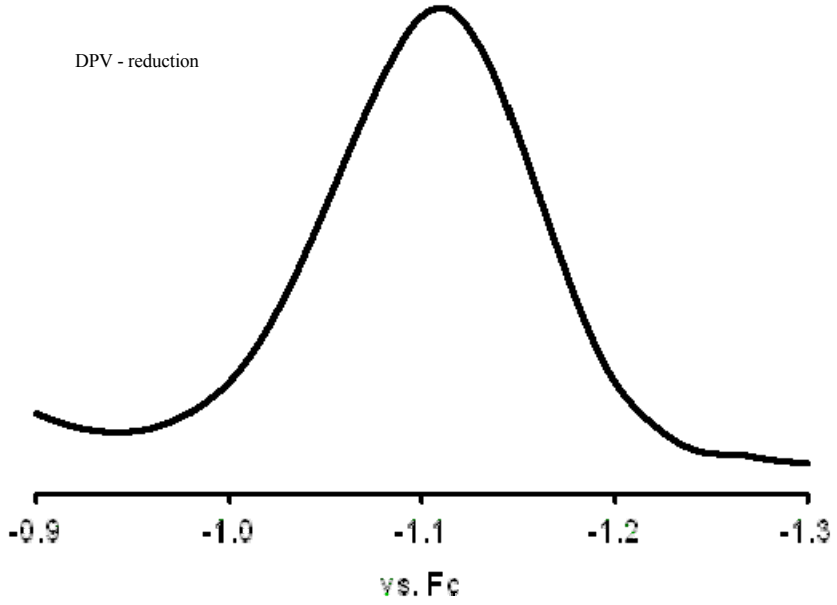
DPV - reduction
-0.9
-1.0
-1.1
-1.2
-1.3
vs. Fc

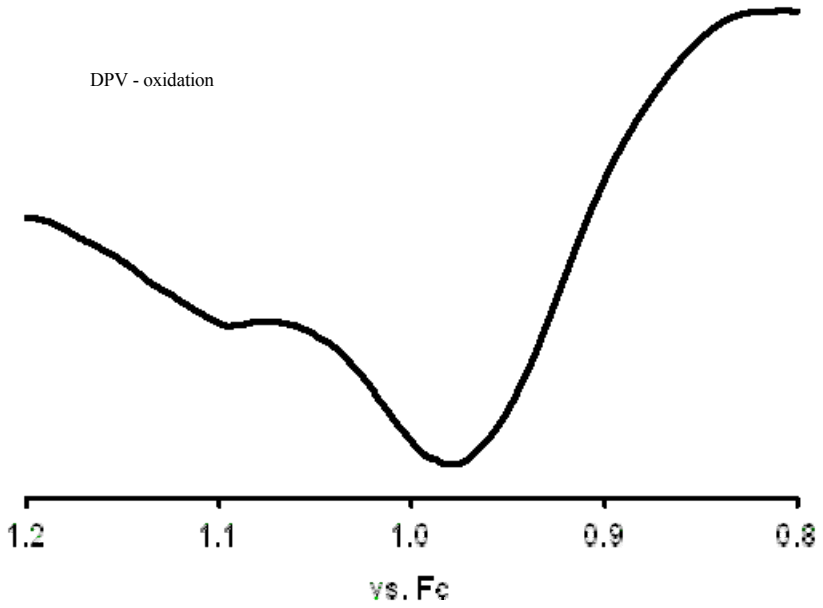
DPV - oxidation
1.2
1.1
1.0
0.9
0.8
vs. Fc

Electrochemistry of **30**

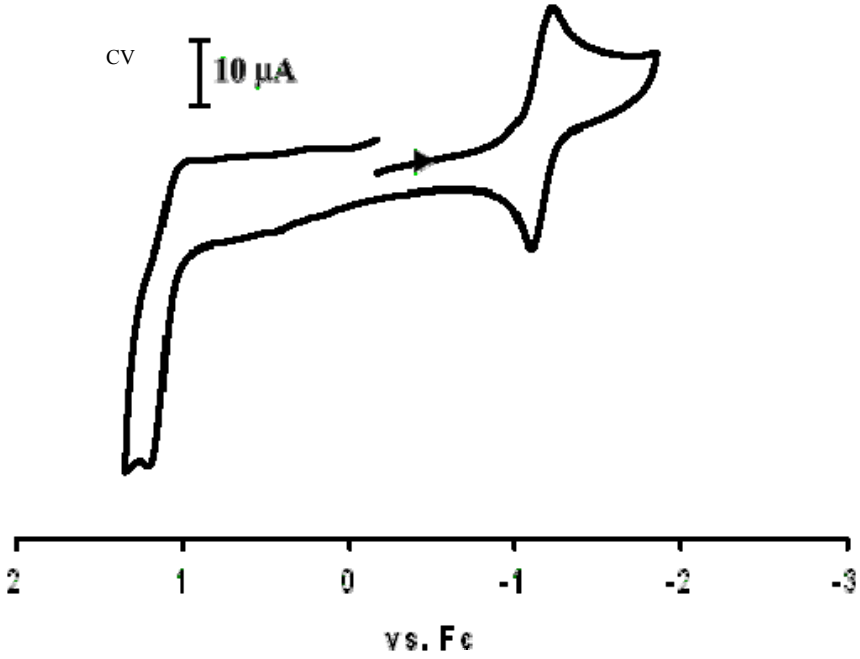

Electrochemistry of **31**

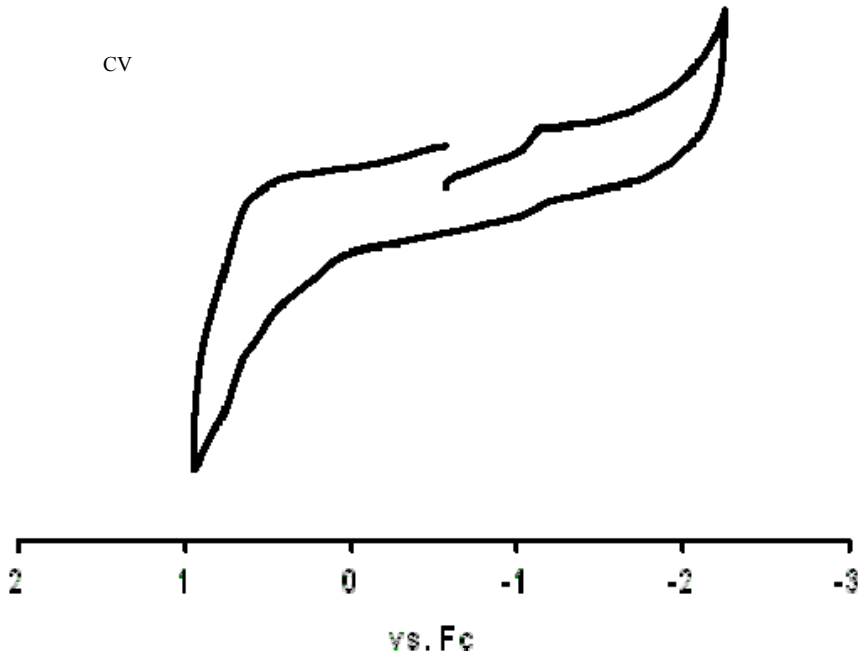

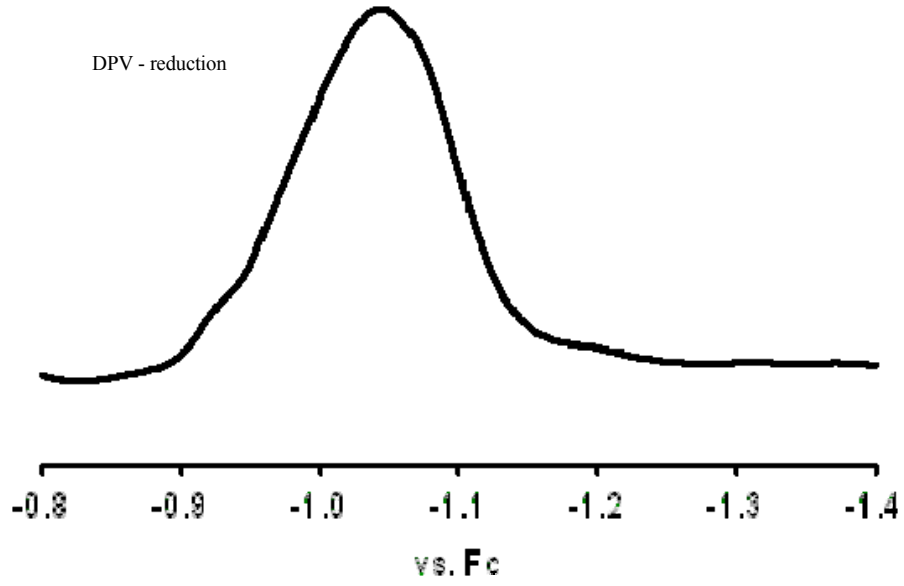
DPV - reduction
-0.8
-0.9
-1.0
-1.1
-1.2
-1.3
-1.4
vs. Fc

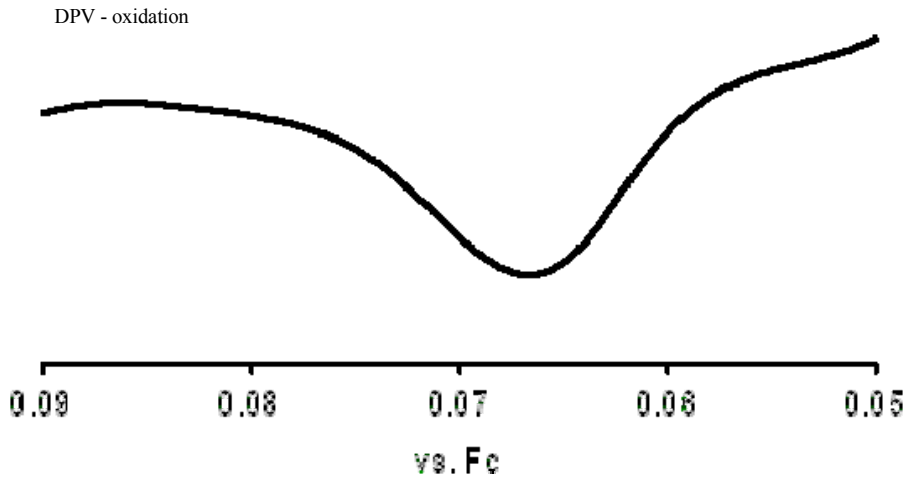
DPV - oxidation
0.09
0.08
0.07
0.06
0.05
vs. Fc

Electrochemistry of **32**

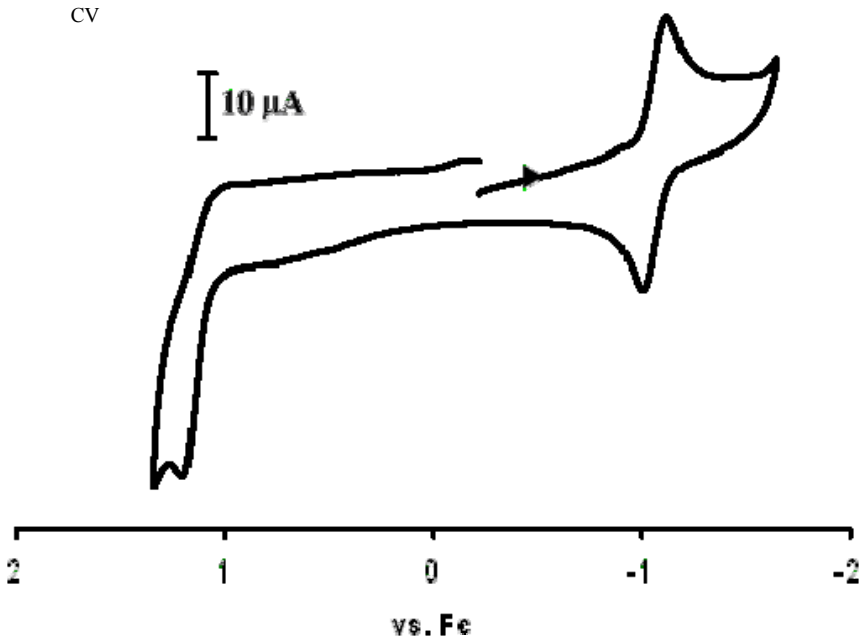

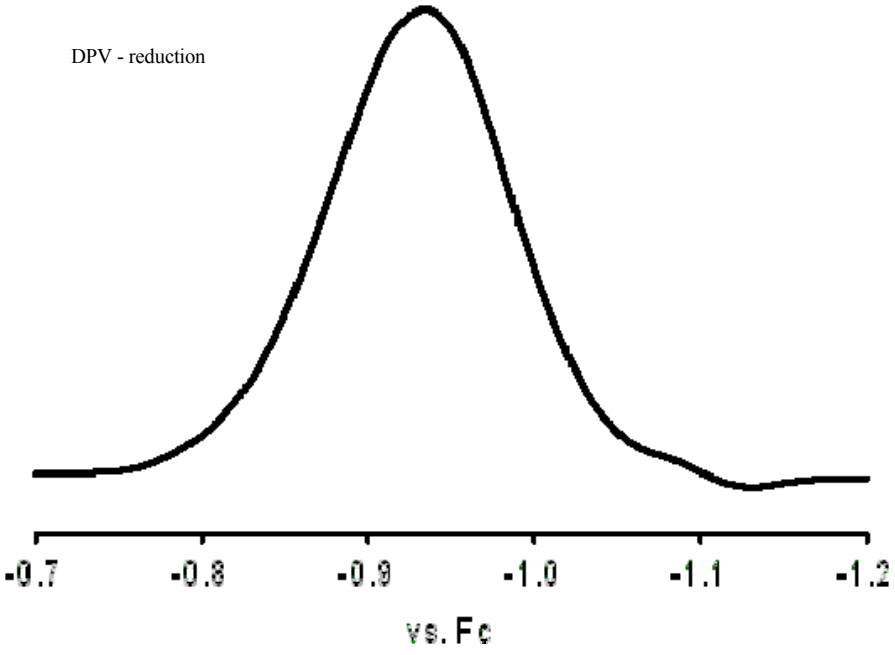
DPV - reduction
-0.7
-0.8
-0.9
-1.0
-1.1
-1.2
vs. Fc

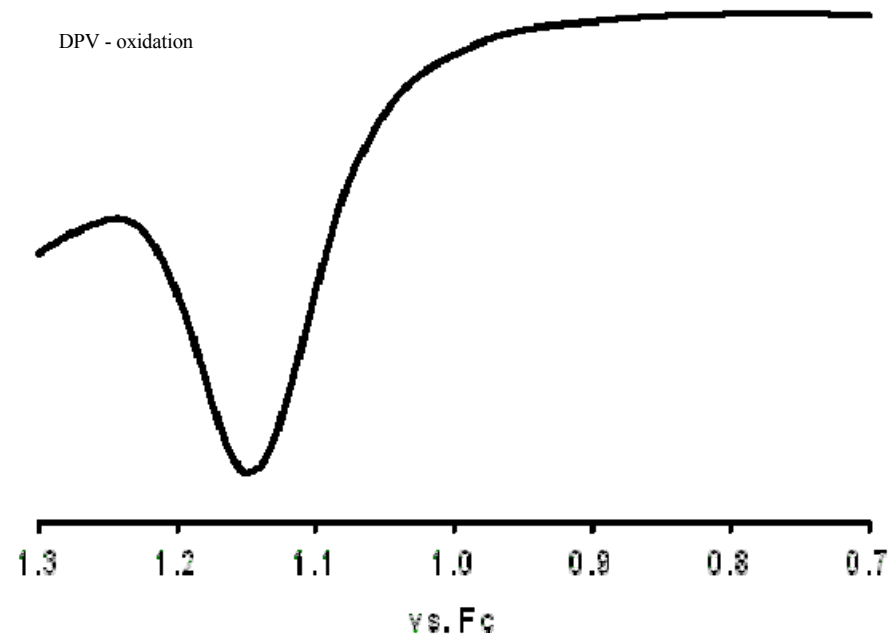
DPV - oxidation
1.3
1.2
1.1
1.0
0.9
0.8
0.7
vs. Fc

Electrochemistry of **33**

CV

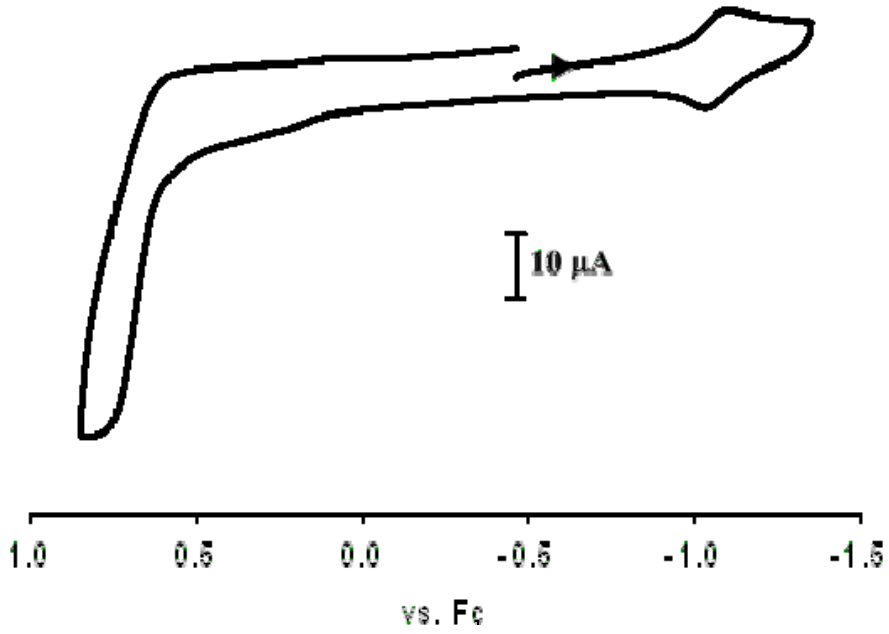

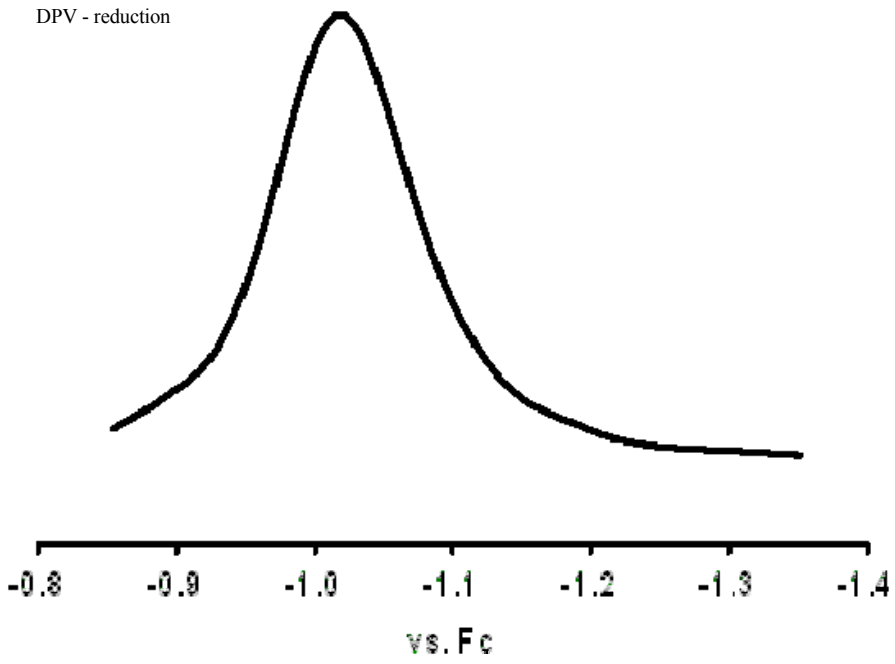
DPV - reduction
-0.8
-0.9
-1.0
-1.1
-1.2
-1.3
-1.4
vs. Fc

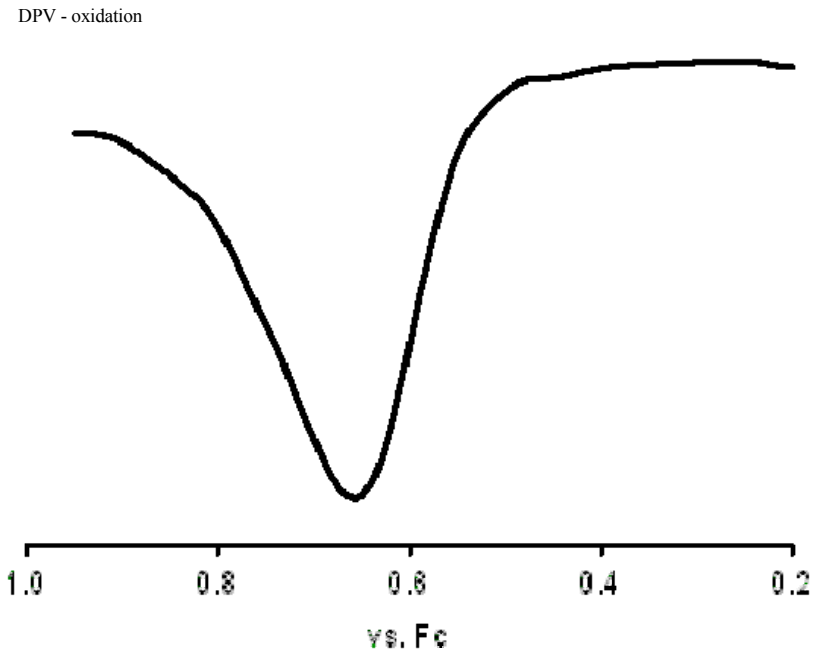
DPV - oxidation
1.0
0.8
0.6
0.4
0.2
vs. Fc

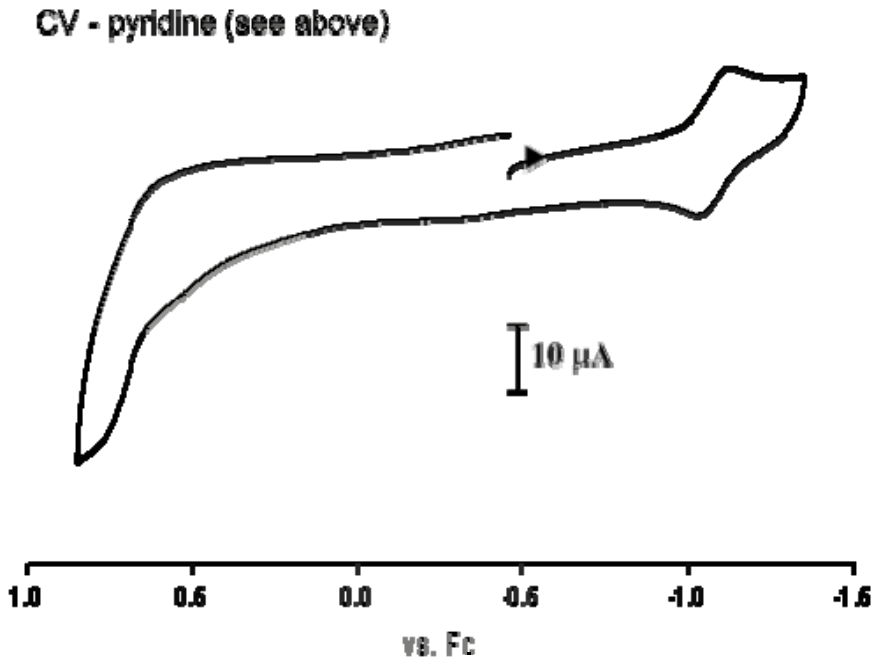
CV - pyridine (see above)
10 µA
1.0
0.5
0.0
-0.5
-1.0
-1.5
vs. Fc

Electrochemistry of **E**

CV

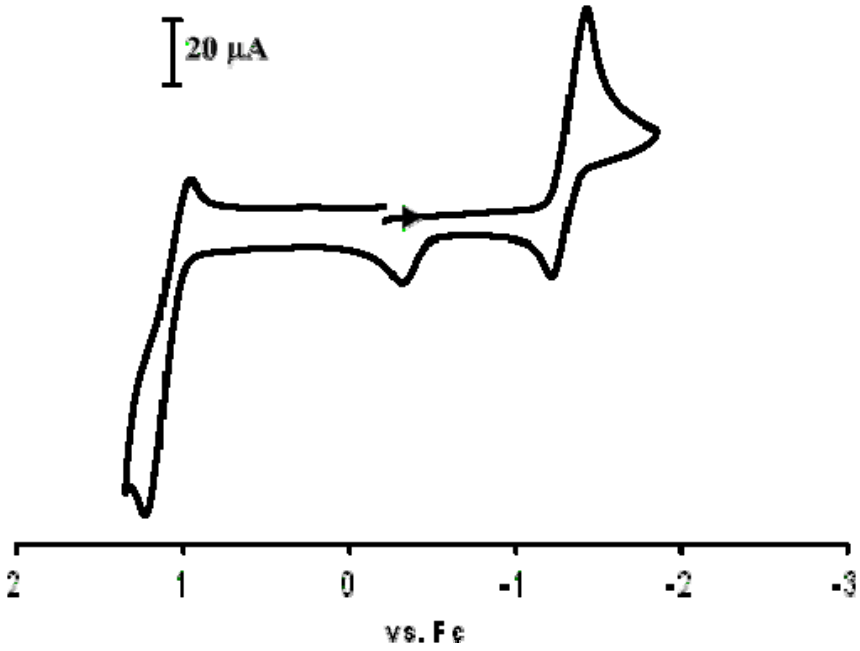

DPV - reduction

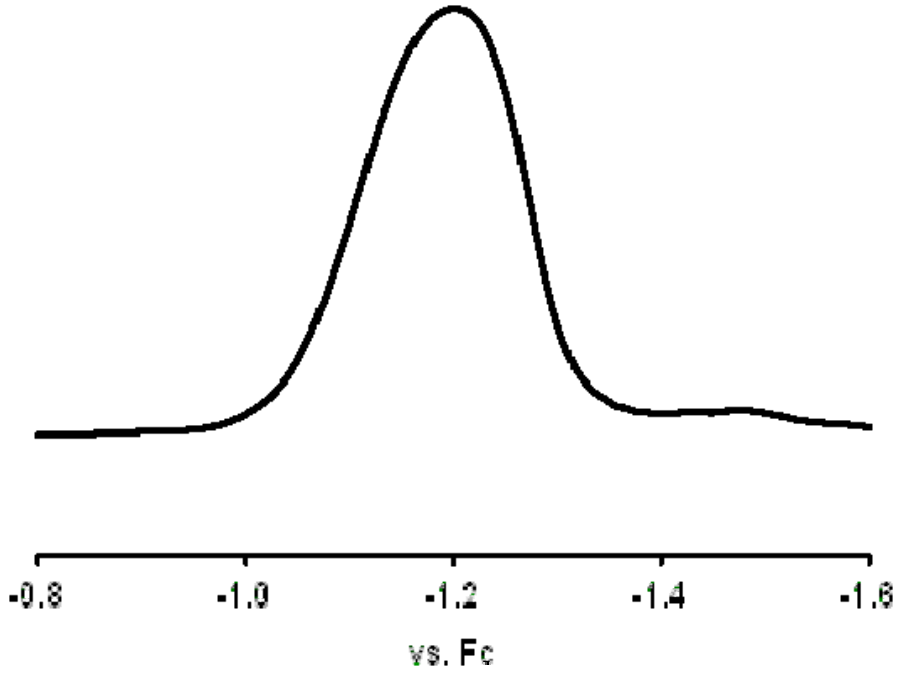

DPV - oxidation

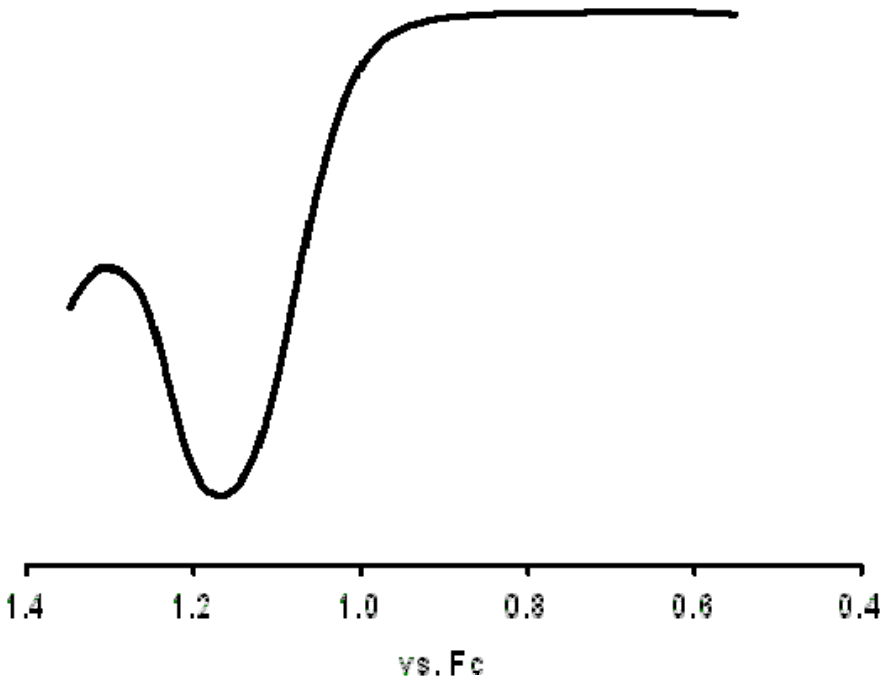

Electrochemistry of **F**

CV

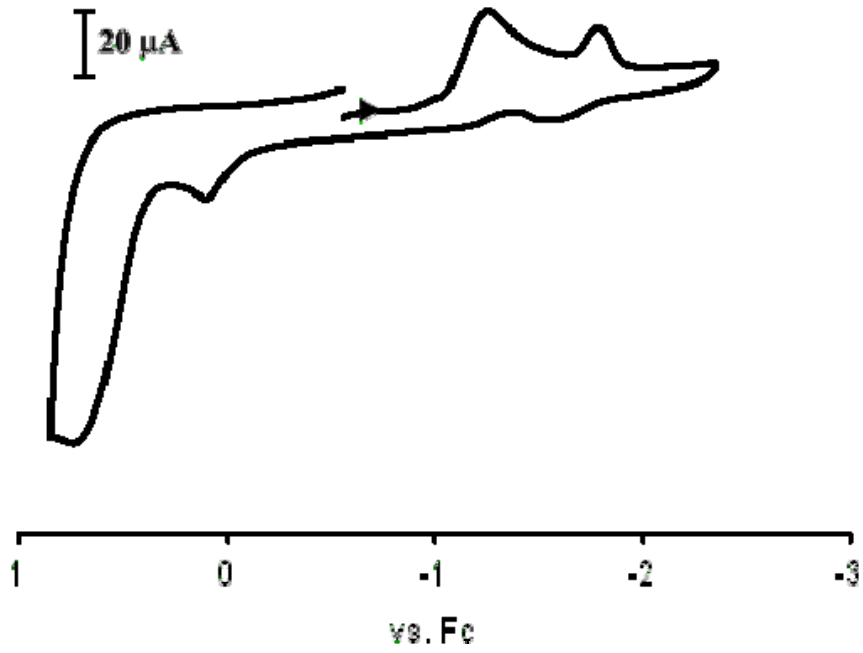

DPV - reduction

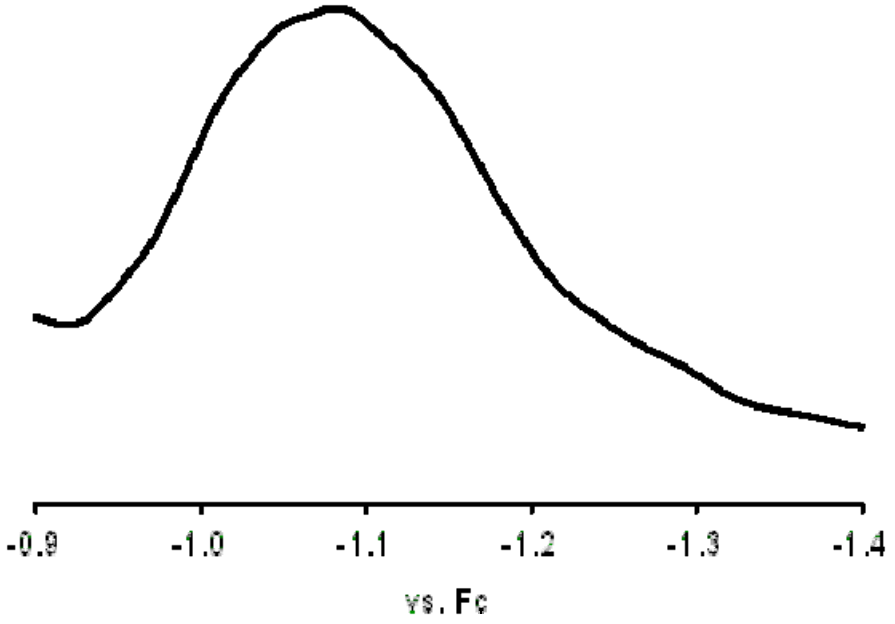

DPV - oxidation

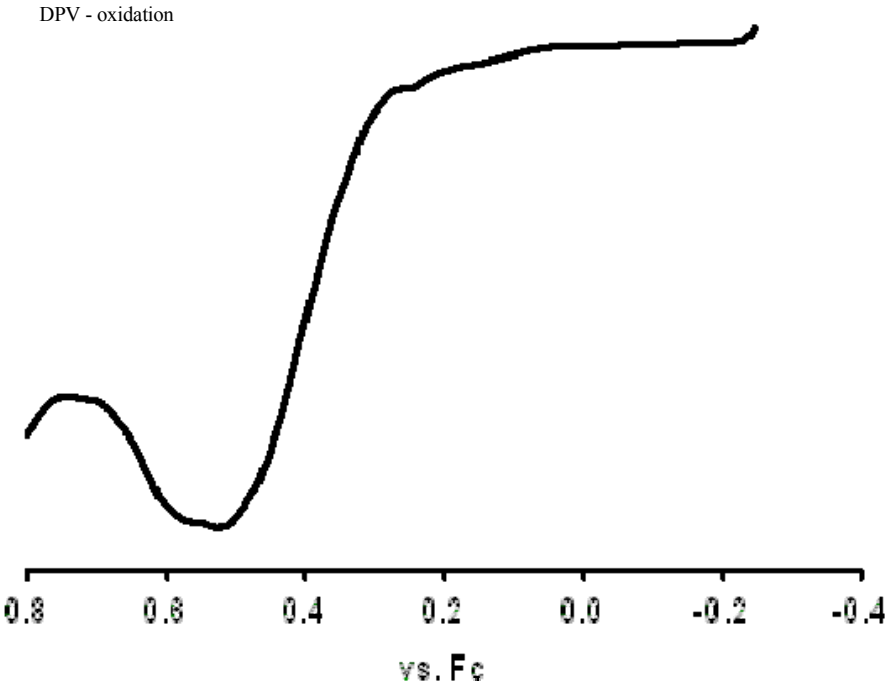

Electrochemistry of **F-Na**

CV

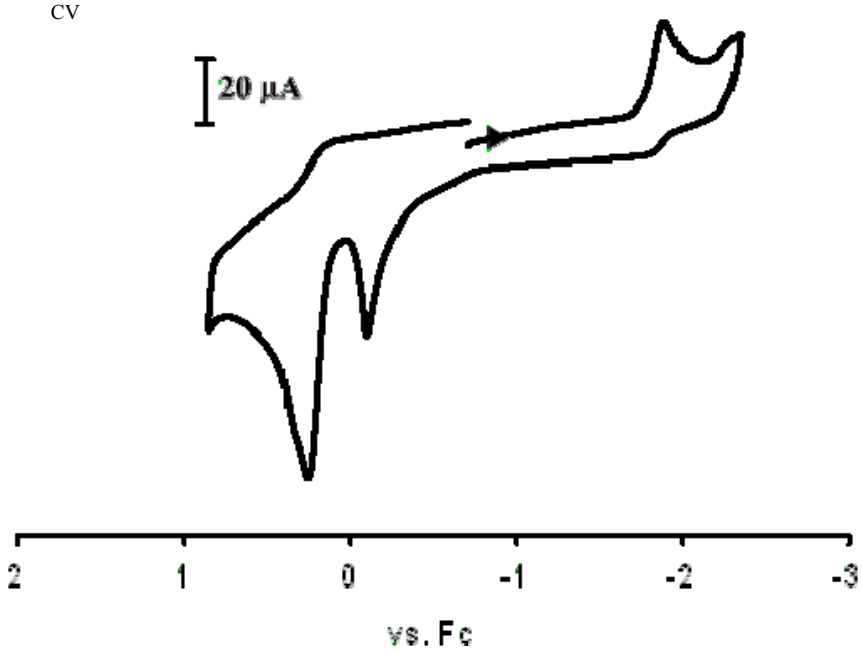

DPV - reduction

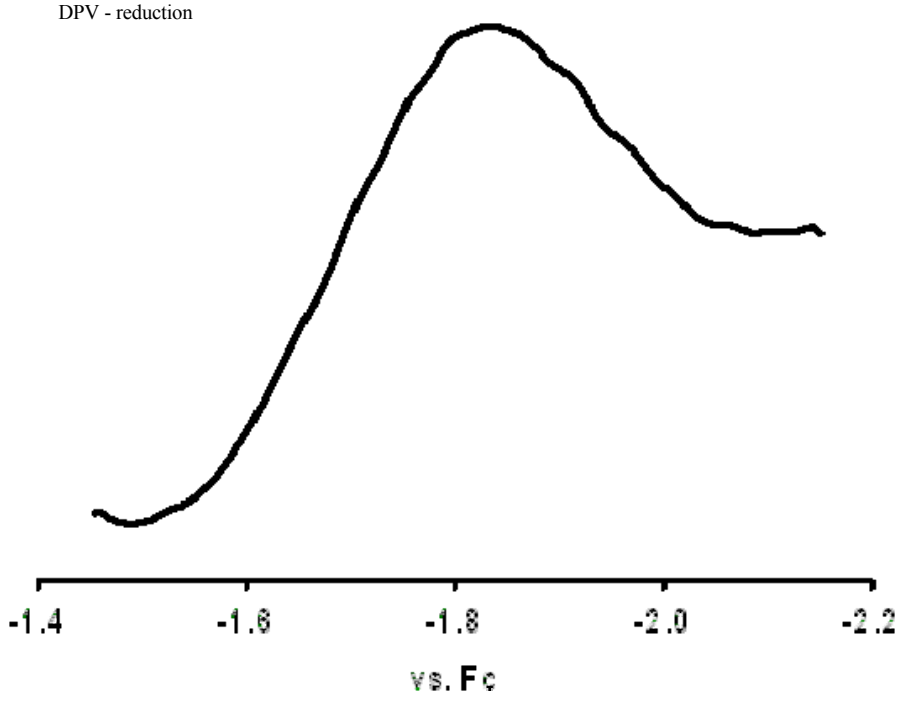

DPV - oxidation

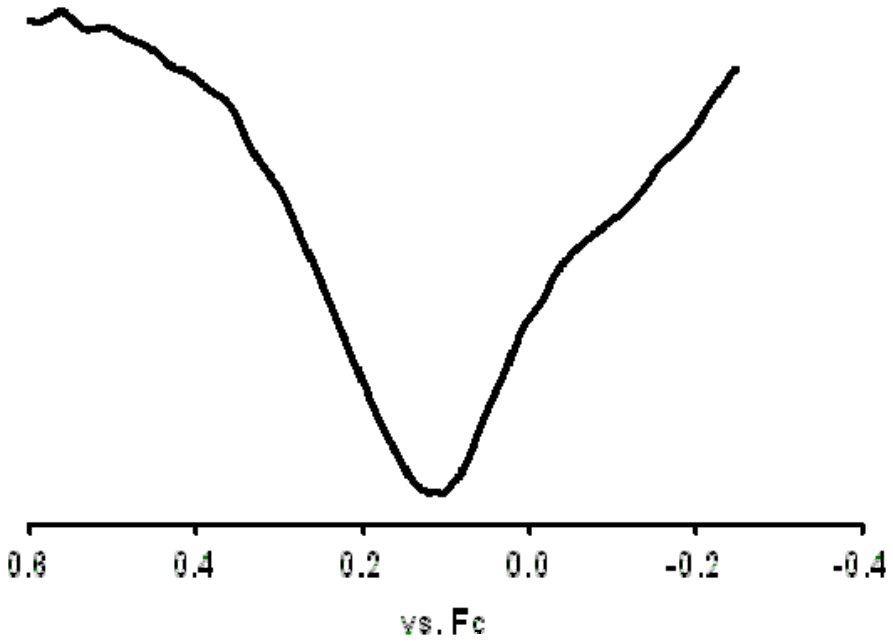

APPENDIX B

EXPERIMENTAL DATA FOR CHAPTER III

General Experimental Procedures

All chemicals were obtained from commercial suppliers and used without further purification. Chlorosulfonic acid was purchased from Aldrich and can be used within two to three months before it decomposed in to sulfuric acid. Dichloromethane was dried with MBRAUN MB-SPS solvent purification system. All organic tin compounds were received from commercially available sources unless otherwise mentioned. Chromatography on silica gel was performed using a forced flow of the indicated solvent on EM reagents silica gel 60 (230-400 mesh). ^{1}H NMR spectra were recorded at room temperature and chemical shifts are reports in ppm from the solvent resonance ($CDCl_3$ 7.24 ppm, DMSO-d_6 2.50 ppm, CD_3OD 3.31 ppm, D_2O 4.79 ppm). Data are reported as follows: chemical shift, multiplicity (s = singlet, d = doublet, t = triplet, q = quartet, br = broad, m = multiplet), number of protons, and coupling of constants. Proton decoupled ^{13}C NMR spectra were also reported at room temperature. Chemical shifts are reported in ppm from tetramethylsiliane resonance ($CDCl_3$ 77.2 ppm, DMSO-d_6 39.5 ppm, CD_3OD 49.1 ppm). Mass spectra were measured under ESI condition. Proton decoupled ^{19}F NMR spectra were also recorded in ppm comparing the standard BF_3•Et_2O resonance (CD_3COCD_3, 0.00 ppm). Some compounds were purified using preparative HPLC (Beckman Coulter, X Terra Prep-MS-C18 Column, 5mm, 19 x 160 mm) eluting with solvents A (H_2O with 0.1 % TFA) and B (CH_3CN with 0.1 % TFA).

Determination of Quantum Yields and Extinction Coefficients.

UV/Vis absorbance spectra were recorded on a Cary 100 Bio spectrophotometer. Steady-state fluorescence spectroscopic studies were performed on a Cary Eclipse fluorometer. The slit width was 5 nm for both excitation and emission. Fluorescence spectra were corrected for detector sensitivity. The quantum efficiencies of fluorescence were obtained from the average of three measurements with the following equation:

$$\mathbf{F_x = F_{st}\,(I_x/I_{st})\,(A_{st}/A_x)\,(\eta_x^2/\eta_{st}^2)}$$

Where $\mathbf{F_{st}}$ is the reported quantum yield of the standard, **I** is the area under the emission spectra, **A** is the absorbance at the excitation wavelength and η is the refractive index of the used solvent, measured on a pocket refractometer from ATAGO. **X** subscript denotes unknown, and **st** denotes standard. Extinction coefficients (ε) where measured from Beer's Law plots.

General Procedure for the Preparation of Disulfonated BODIPYs

A solution of chlorosulfonic acid (2 eq) in dry CH_2Cl_2 was added dropwise to a solution of BODIPY in dry CH_2Cl_2 over 10 min under N_2 at -40 ^oC. An orange precipitate was formed as the solution mixture warmed slowly to room temperature within 20 mins. The disulfonic acid was isolated by vacuum filtration and treated with water. The aqueous solution was neutralized with $NaHCO_3$ (2 eq), concentrated to 5-10 ml and treated with brine. The desired product was reprecipitated afterwards to afford an orange solid (85-100% yield).

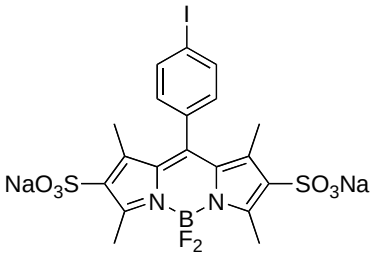

34b

Disodium 2,6-disulfonate-1,3,5,7-tetramethyl-8-(4'-iodophenyl)-4,4-difluoro-4-bora-3a, 4a-diaza-s-indacence (34b) 1,3,5,7-Tetramethyl-8-(4'-iodophenyl)-4,4-difluoro-4-bora-3a, 4a-diaza-s-indacence{Chen, 2000 #11402} (53 mg, 0.118 mmol) and chlorosulfonic acid (16 μl, 0.236 mmol) were reacted according to the general procedure giving an orange powder (68 mg, 88%). ^{1}H NMR (500 MHz, D_2O) ḍ7.84 (d, 2H, *J* = 8.0 Hz), 6.97 (d, 2H, *J* = 8.0 Hz), 2.57 (s, 6H), 1.49 (s, 6H); ^{13}C NMR (75 MHz, D_2O) ḍ155.5, 145.7, 144.0, 139.2, 133.1, 132.7, 130.6, 129.7, 95.7, 13.7, 13.0; MS (ESI) calcd for $C_{19}H_{17}BF_2IN_2O_6S_2^-$ $(M-2Na+H)^-$ 608.96 found 608.98.

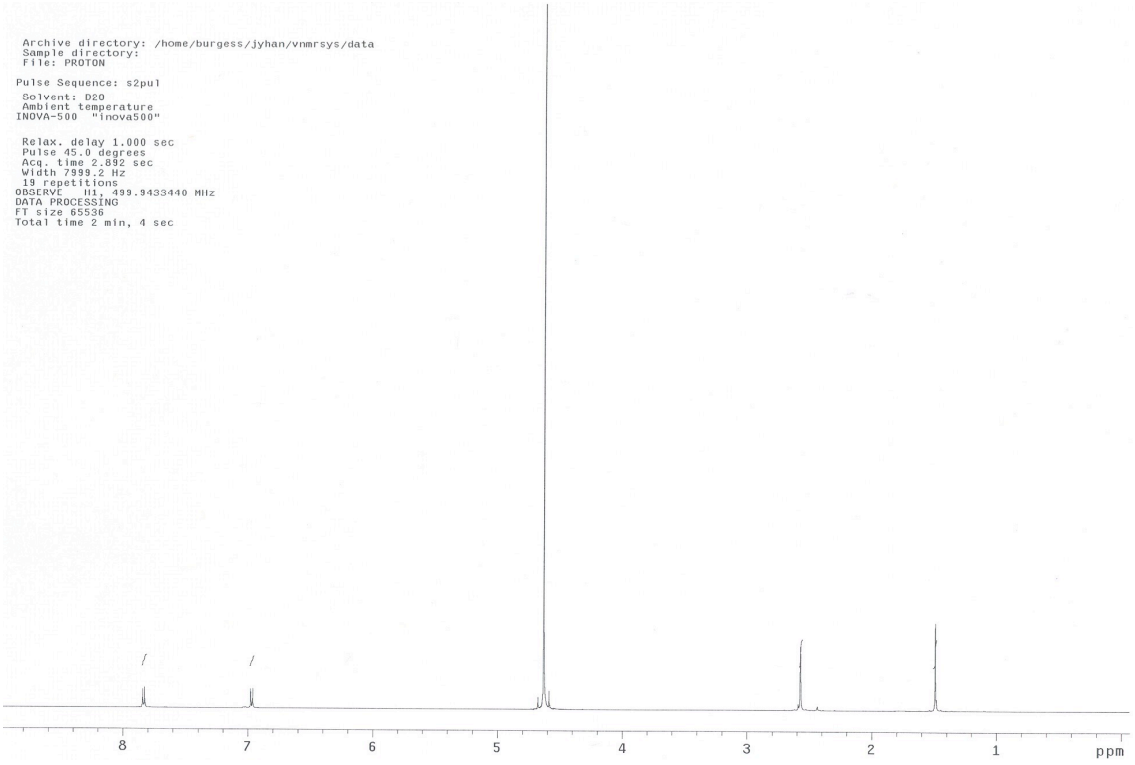

^{1}H NMR (D_2O)

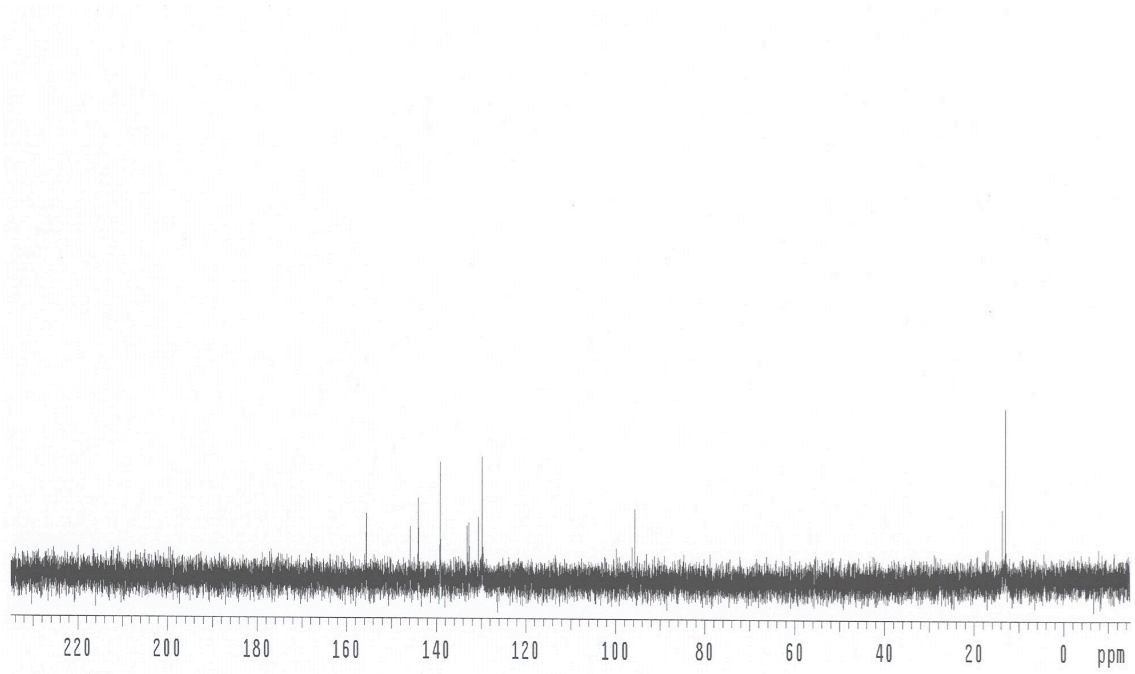

^{13}C NMR (D_2O)

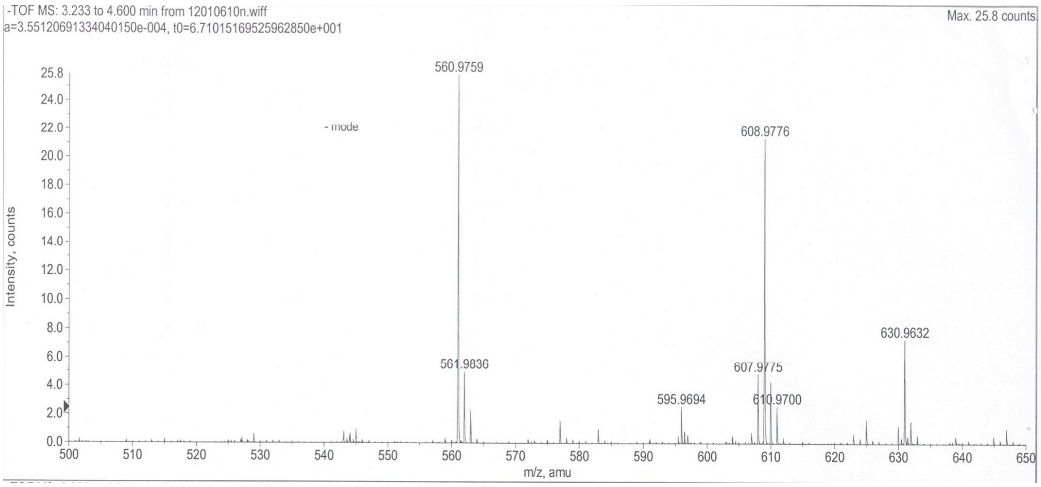
-TOF MS: 3.233 to 4.600 min from 12010610n.wiff
a=3.55120691334040150e-004, t0=6.71015169525962850e+001
Max. 25.8 counts
- mode
560.9759
608.9776
630.9632
561.9836
607.9775
595.9694
610.9700
Intensity, counts
m/z, amu

MS ESI

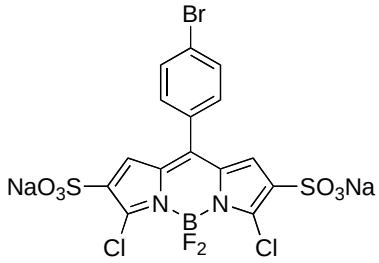

35b

Disodium 2,6-disulfonate-3,5-dichloro-8-(4'-bromophenyl)-4,4-difluoro-4-bora-3a,4a-diaza-s-indacence (35b) Compound **41b** (500 mg, 0.12 mmol) and chlorosulfonic acid (160 μl, 0.24 mmol) were reacted by the general procedure giving an orange powder (624 mg, 85%). ^{1}H NMR (500 MHz, D_2O) ḍ7.73 (d, 2H, *J* = 8.4 Hz), 7.45 (d, 2H, *J* = 8.4 Hz), 7.27 (s, 2H); ^{13}C NMR (75 MHz, D_2O) ḍ147.6, 141.9, 133.7, 132.6, 132.3, 131.8, 131.5, 130.0, 126.7; MS (ESI) calcd for $C_{15}H_6BBrCl_2F_2N_2O_6S_2^{2-}$ $(M-2Na)^{2-}$ 285.91 found 285.84; IR (thin film) 2968, 1572, 1382, 1206, 1033, 650 cm^{-1}.

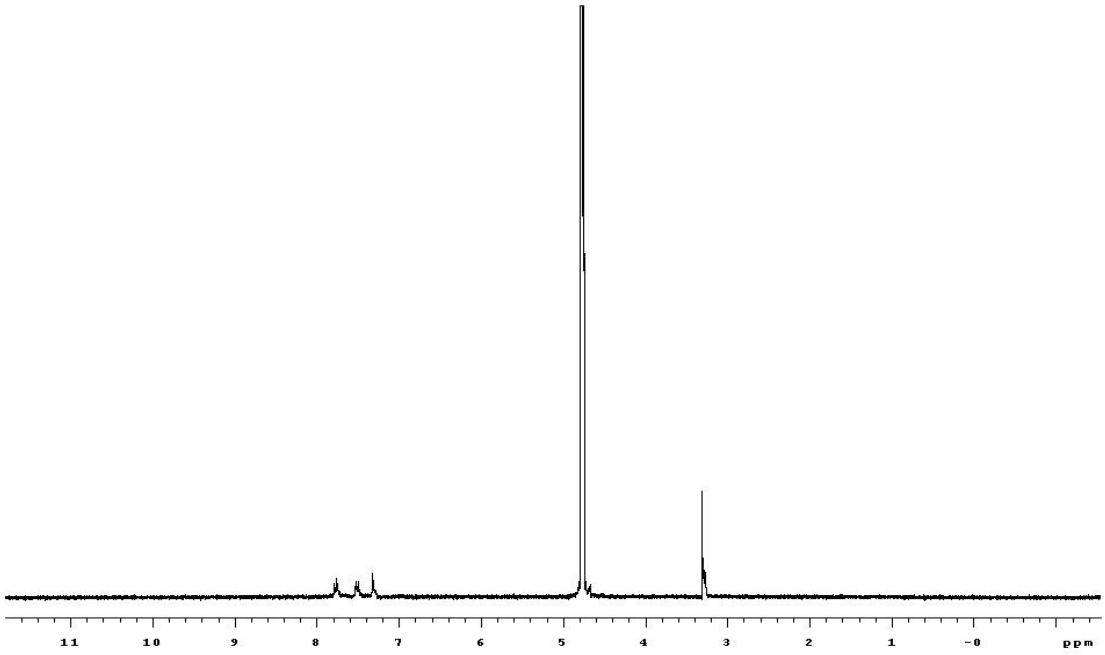

^{1}H NMR (D_2O)

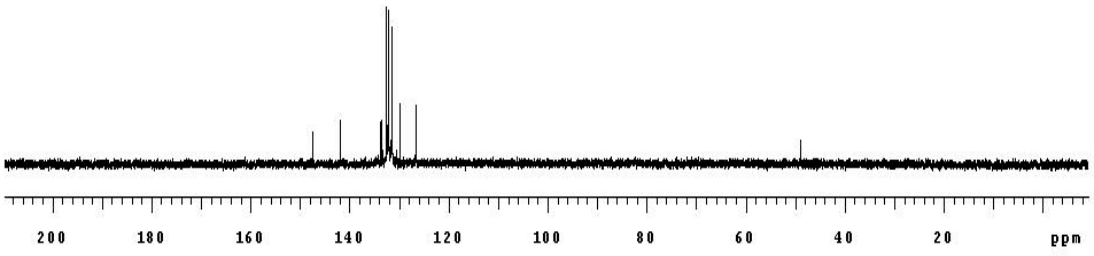

^{13}C NMR (D_2O)

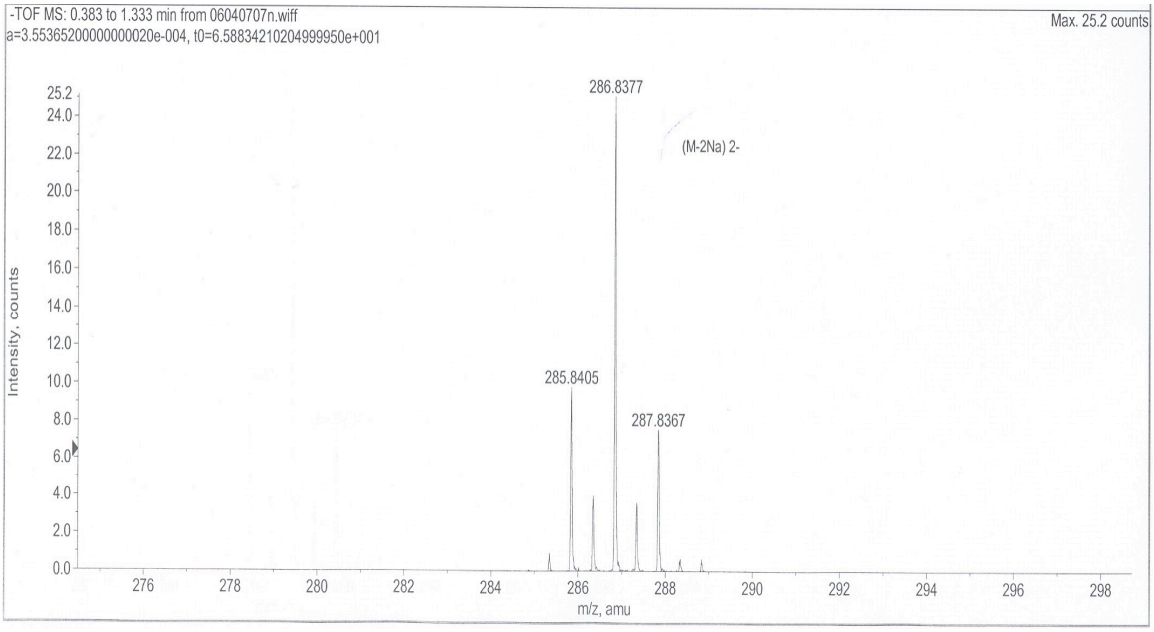
-TOF MS: 0.383 to 1.333 min from 06040707n.wiff
a=3.553652000000000020e-004, t0=6.588342102049999950e+001
Max. 25.2 counts
286.8377
(M-2Na) 2-
285.8405
287.8367
Intensity, counts
m/z, amu

MS ESI

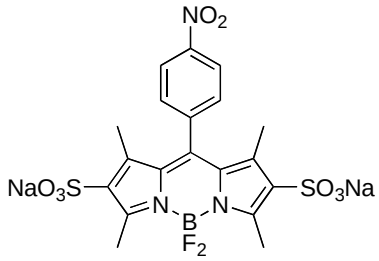

42b

Disodium 2,6-disulfonate-1,3,5,7-tetramethyl-8-(4'-nitrophenyl)-4,4-difluoro-4-bora-3a,4a-diaza-s-indacence 1,3,5,7-Tetramethyl-8-(4'-nitrophenyl)-4,4-difluoro-4-bora-3a,4a-diaza-s-indacence{Li, 2004 #11780} (400 mg, 1.08 mmol) and chlorosulfonic acid (144 μl, 2.16 mmol) were reacted according to the general procedure giving an orange powder (630 mg, quant. yield). ^{1}H NMR (300 MHz, D_2O) ḍ8.49 (d, 2H, *J* = 8.5 Hz), 7.70 (d, 2H, *J* = 8.5 Hz), 2.77 (s, 6H), 1.63 (s, 6H); ^{13}C NMR (75 MHz, D_2O) ḍ156.1, 148.8, 144.0, 143.6, 140.5, 132.9, 130.2, 129.6, 125.3, 13.8, 13.0; MS (ESI) calcd for $C_{19}H_{16}BF_2N_3O_8S_2^{2-}$ $(M-2Na)^{2-}$ 263.52 found 263.45; IR (thin film) 1522, 1347, 1190, 1004, 853, 669 cm^{-1}.

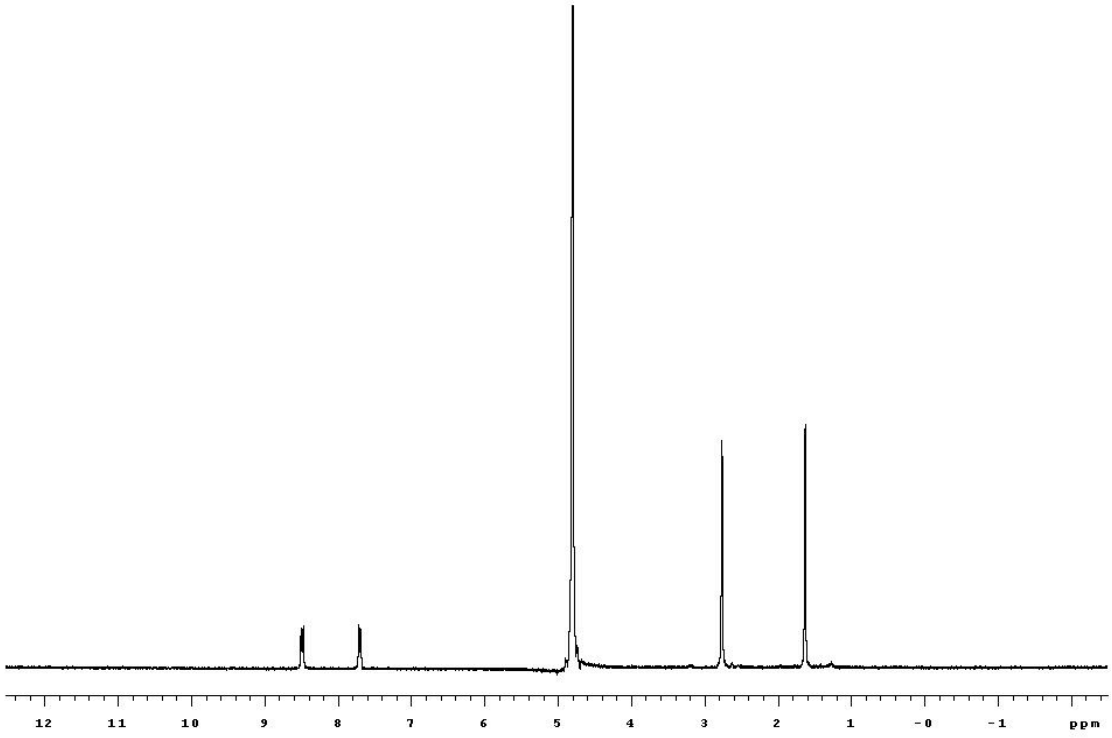

^{1}H NMR (D_2O)

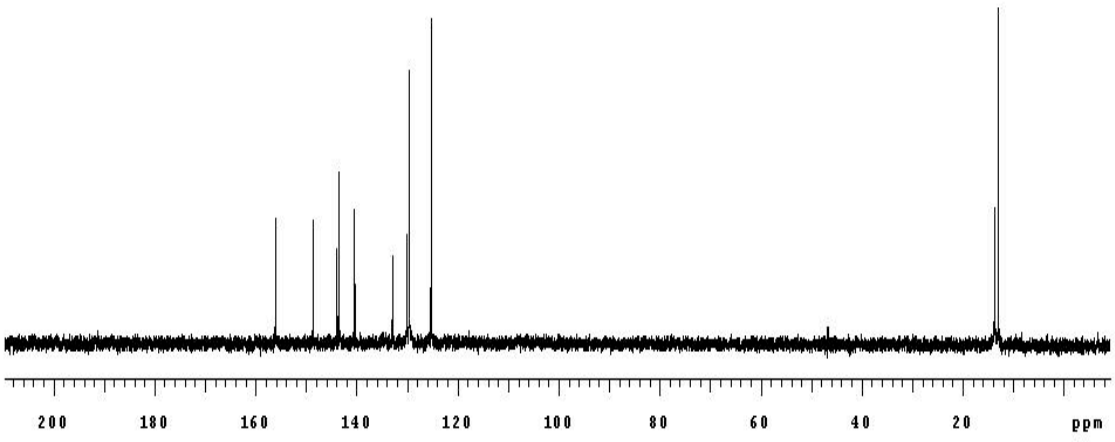

^{13}C NMR (D_2O)

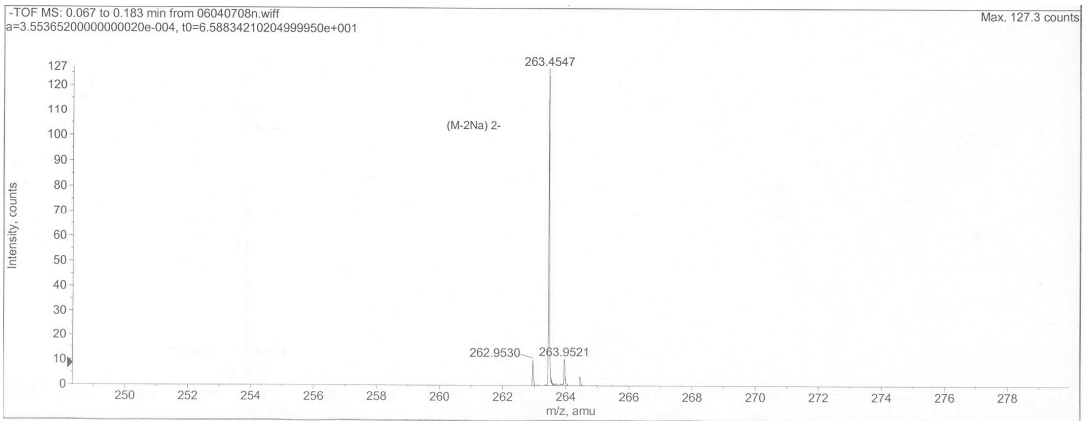
-TOF MS: 0.067 to 0.183 min from 06040708n.wiff
a=3.5536520000000020e-004, t0=6.588342102049995 0e+001
Max. 127.3 counts
263.4547
(M-2Na) 2-
262.9530
263.9521
Intensity, counts
m/z, amu

MS ESI

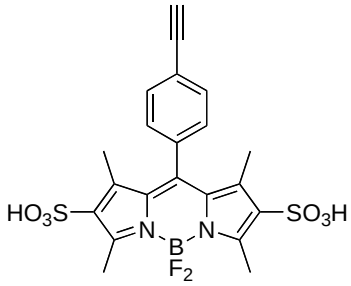

43

1,3,5,7-Tetramethyl-8-(4'-ethynylphenyl)-4,4-difluoro-4-bora-3a,4a-diaza-s-indacence 2,6-disulfonic acid A solution of chlorosulfonic acid (19 µl, 0.276 mmol) in CH_2Cl_2 (2 ml) was added dropwise to a solution of 1,3,5,7-tetramethyl-8-(4'-ethynylphenyl)-4,4-difluoro-4-bora-3a,4a-diaza-s-indacence{Wan, 2003 #11399}[2] (48 mg, 0.138 mmol) in CH_2Cl_2 (5 ml) over 10 min at -40 °C. An orange precipitate was formed as the solution mixture warmed slowly to room temperature. The disulfonic acid was isolated by vacuum filtration giving the disulfonic acid as an orange powder (42 mg, 60%). ^{1}H NMR (300 MHz, D_2O) δ7.66 d, 2H, J = 8.8 Hz), 7.29 (d, 2H, J = 8.5 Hz), 3.48 (s, 1H), 2.63 (s, 6H), 1.54 (s, 6H); MS (ESI) $C_{21}H_{18}BF_2N_2O_6S_2^-$ $(M-H)^-$ 507.07 found 507.08.

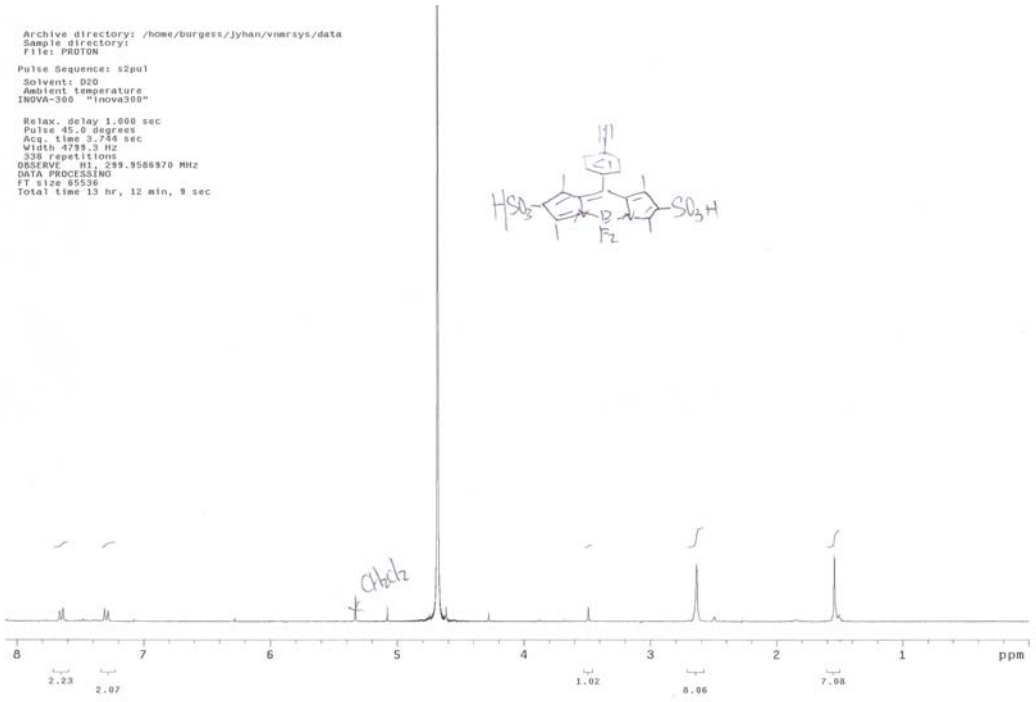

^{1}H NMR (D_2O)

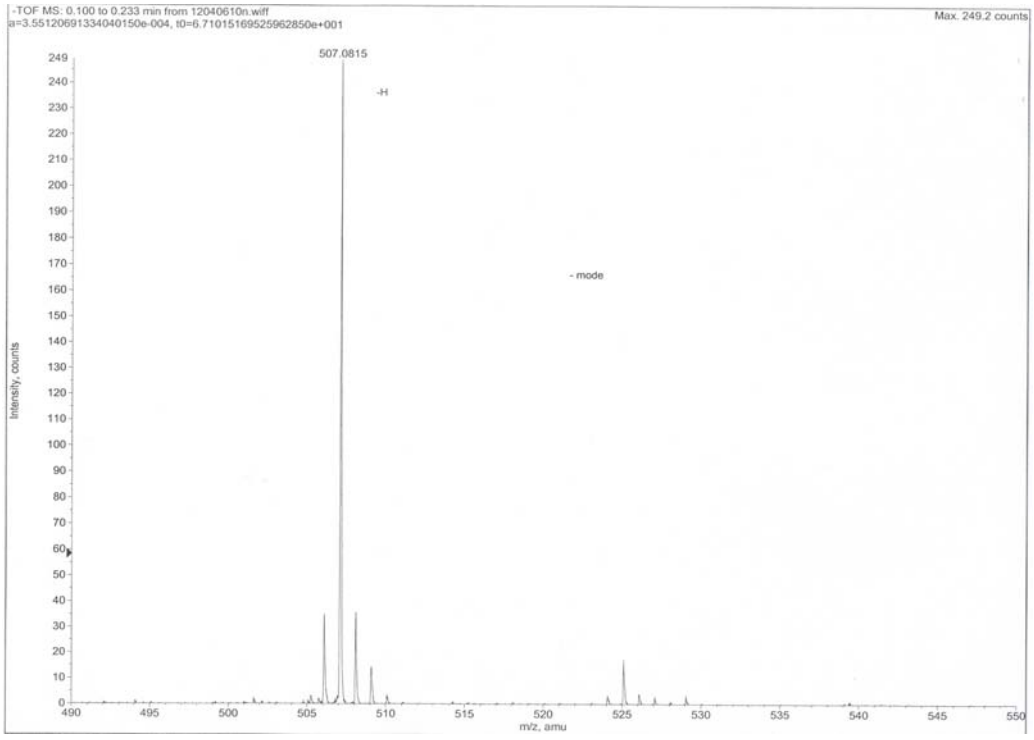

MS ESI

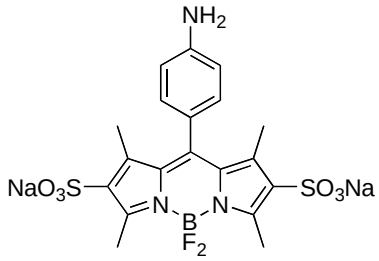

36b

Disodium 2,6-disulfonate-1,3,5,7-tetramethyl-8-(4'-aminophenyl)-4,4-difluoro-4-bora-3a,4a-diaza-s-indacence A solution of **42b** (200 mg, 0.35 mmol) in EtOH (10 ml) was purged with N_2 for 10 min. Hydrazine monohydrate (0.2 ml) and 10% Pd/C (37.1 mg, 0.1 eq) were added. The mixture was refluxed under N_2 for 30 min. Then Pd/C was removed under vacuum filtration. After evaporation the solvent, the residue was dry-loaded onto a silica gel flash column, and eluted using 30% MeOH/CH_2Cl_2 to afford an orange solid (133 mg, 70%). R_f = 0.2 (30% MeOH/CH_2Cl_2). ^{1}H NMR (300 MHz, D_2O) ḍ7.02-6.94 (m, 4H), 2.70 (s, 6H), 1.70 (s, 6H); ^{13}C NMR (75 MHz, D_2O) ḍ154.7, 148.2, 144.1, 132.3, 131.2, 130.0, 123.9, 117.1, 117.0, 13.0 (2); MS (ESI) $C_{19}H_{19}BF_2N_3Na_2O_6S_2^+$ $(M+H)^+$ 544.0572 found 544.0557; IR (thin film) 3346, 2854, 1608, 1519,1197, 1032, 655 cm^{-1}.

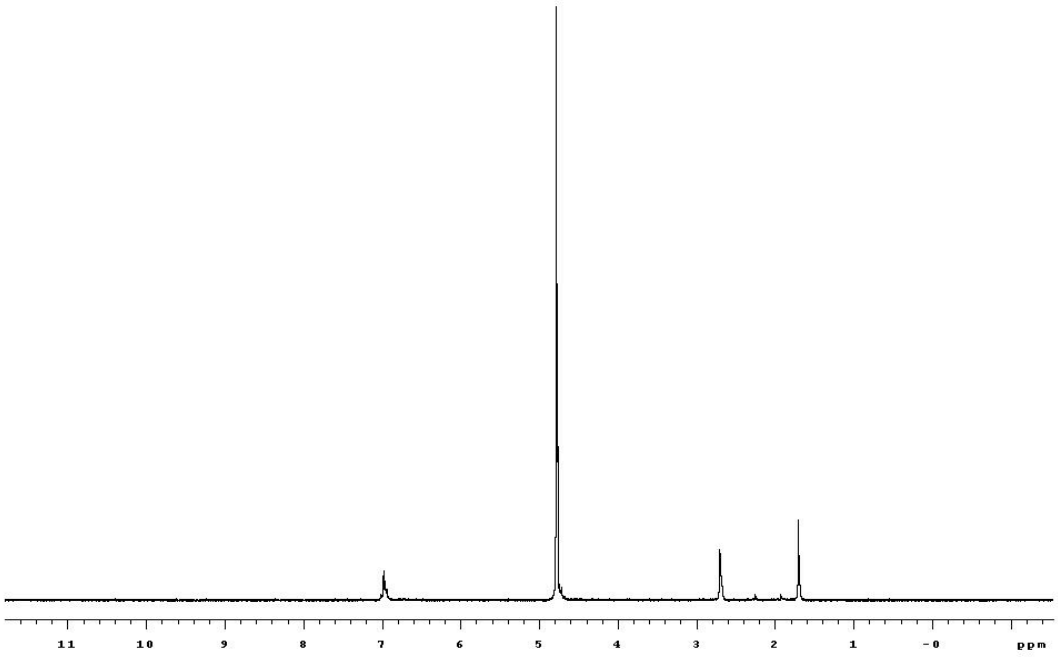

^{1}H NMR (D_2O)

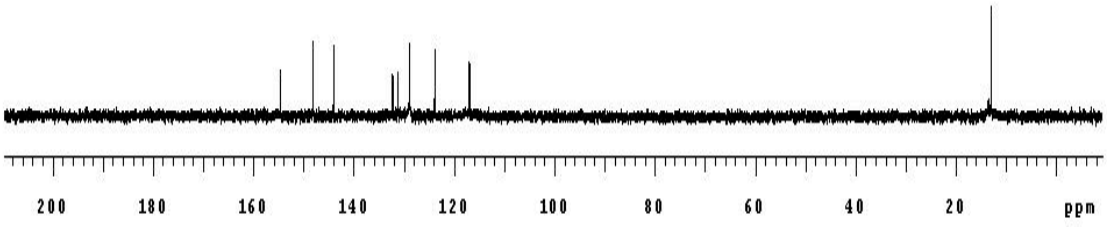

^{13}C NMR (D_2O)

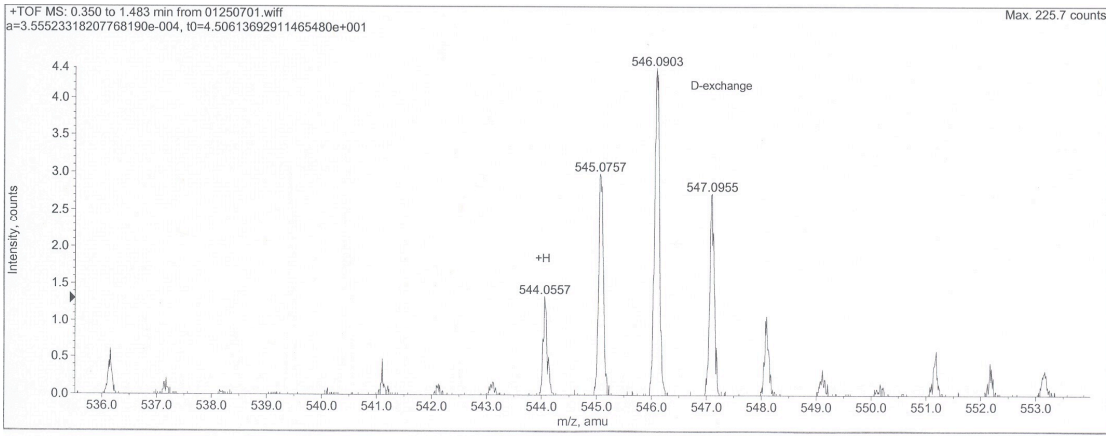
+TOF MS: 0.350 to 1.483 min from 01250701.wiff
a=3.5552331820776819e-004, t0=4.5061369291146548e+001
Max. 225.7 counts
Intensity, counts
m/z, amu
546.0903
D-exchange
545.0757
547.0955
+H
544.0557

MS ESI

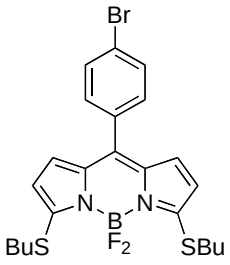

45

A mixture of **41a** (310 mg, 0.75 mmol), n-butane thiol (0.17 mL, 1.55 mmol), Et_3N (0.22 mL, 1.58 mmol) was dissolved in try acetonitrile (15 mL), and then the solution was stirred at 85 ^oC for 4 h. The solvent was removed under reduced pressure and the residue was purified by flash column eluting with 3:1 Hexane/ethyl acetate to afford the desired product (365 mg, 99 %) as a purple solid. ^1H NMR (500 MHz, $CDCl_3$), δ 7.61 (d, *J* = 8.8 Hz, 2H), 7.34 (d, *J* = 8.8 Hz, 2H), 6.68 (d, *J* = 4.5 Hz, 2H), 6.39 (d, *J* = 4.5 Hz, 2H); 3.06 (t, *J* = 7.5 Hz, 4H), 1.80-1.74 (m, 4H), 1.55-1.47 (m, 4H), 0.95 (t, 6H). ^{13}C NMR (125 MHz, $CDCl_3$), δ 157.3, 146.8, 135.4, 132.9, 131.8, 131.6, 128.8, 124.2, 116.5, 32.5, 31.0, 21.9, 13.6. MS (MALDI) calcd for $C_{23}H_{26}BBrFN_2S_2^+$ (M-F), 503.08, found, 503.08. TLC (1:1 EtOAc-Hexane), R_f = 0.80.

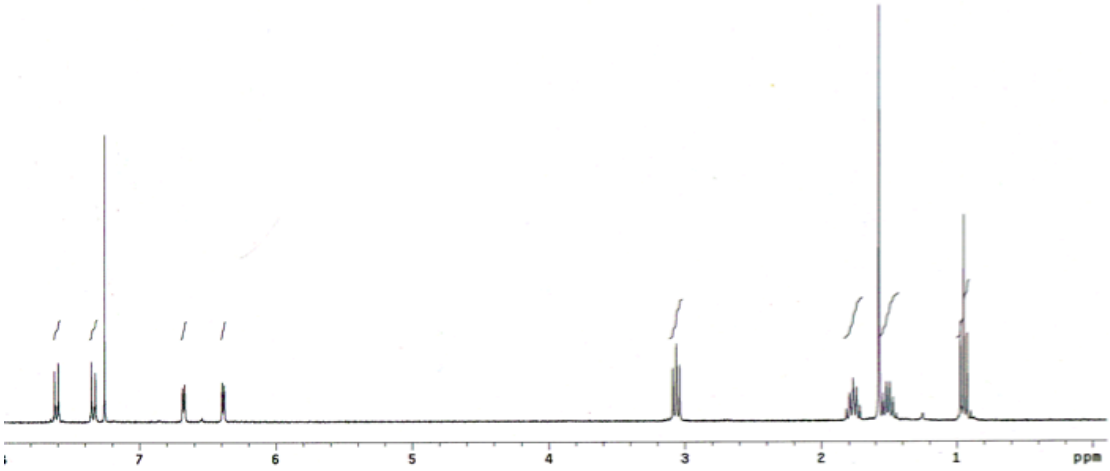

^{1}H NMR ($CDCl_3$)

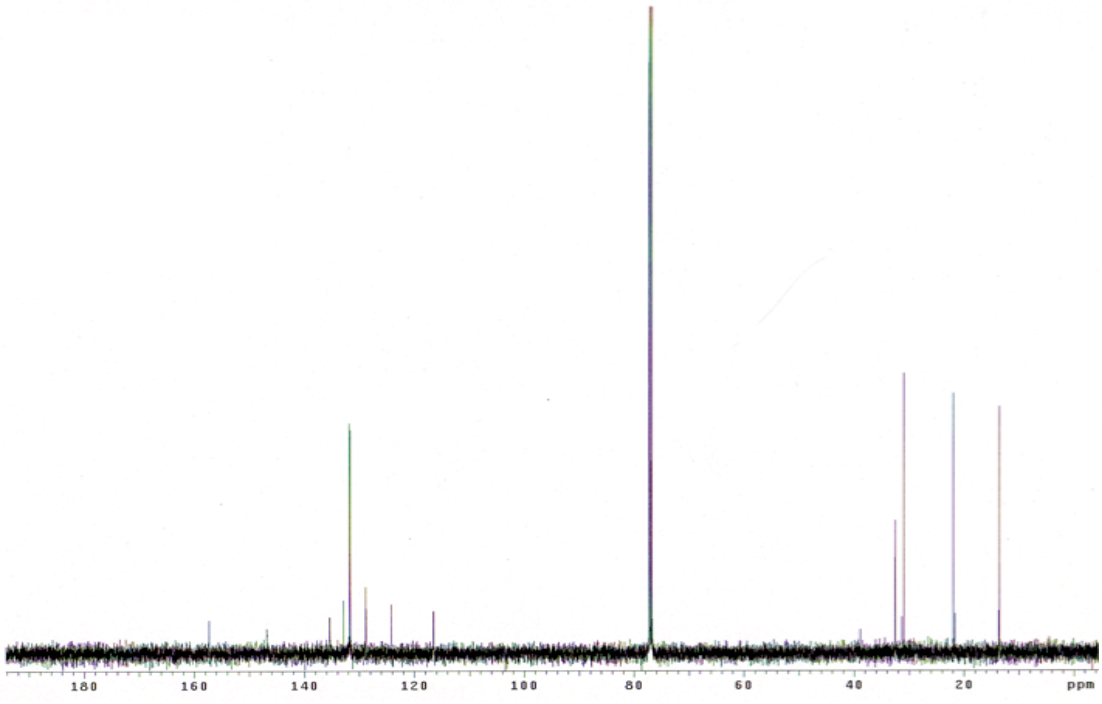

^{13}C NMR ($CDCl_3$)

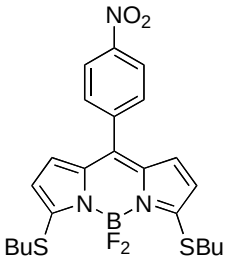

48

A mixture of **41b** (257 mg, 0.67 mmol), n-butylthiol (0.17 mL, 1.55 mmol), Et_3N (0.28 mL, 2.02 mmol) was dissolved in dry acetonitrile (15 mL), and then the solution was stirred at 85 ^oC for 4 h. The solvent was removed under reduced pressure and the residue was purified by flash silica gel column eluting with 3:1 hexane/ethyl acetate to afford the desired product (326 mg, 99 %) as a purple solid. ^1H NMR (300 MHz, $CDCl_3$) δ 8.34 (d, *J* = 8.7 Hz, 2H), 7.65 (d, *J* = 8.7 Hz, 2H), 6.62 (d, *J* = 4.4 Hz, 2H), 6.41 (d, *J* = 4.4 Hz, 2H); 3.08 (t, *J* = 7.4 Hz, 4H), 1.82-1.72 (m, 4H), 1.57-1.45 (m, 4H), 0.95 (t, *J* = 7.4 Hz, 6H). ^{13}C NMR (125 MHz, $CDCl_3$), δ 158.3, 148.5, 140.5, 135.1, 133.3, 131.2, 128.5, 123.5, 116.8, 32.5, 30.8, 21.9, 13.6. MS (ESI) calcd for $C_{23}H_{26}BF_2N_3O_2S_2^-$ (M^-), 489.15, found 489.28.

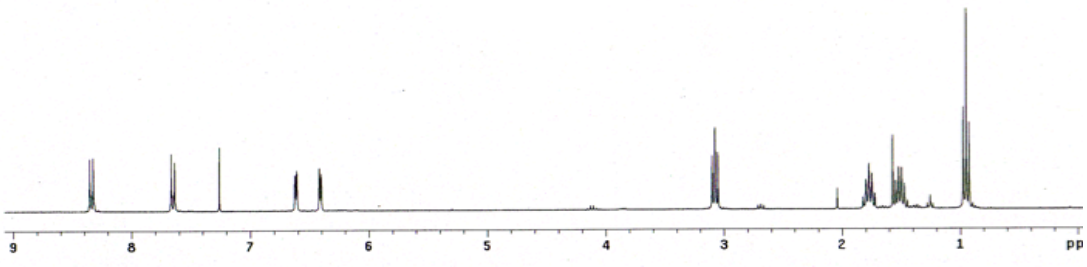

^{1}H NMR ($CDCl_3$)

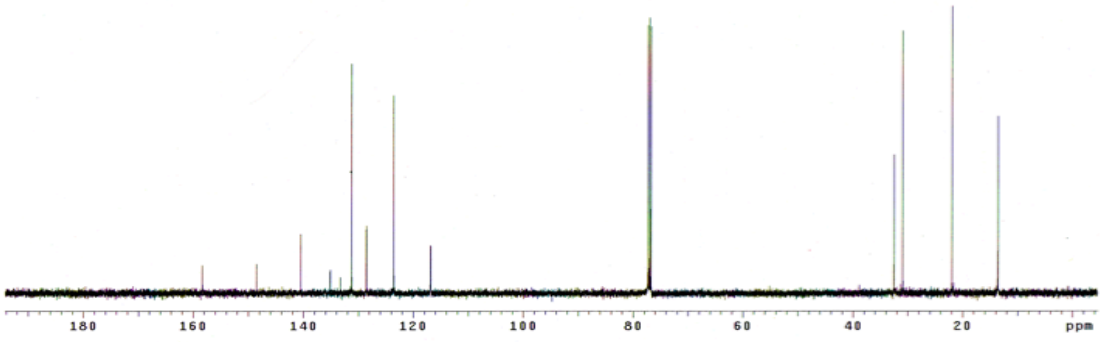

^{13}C NMR ($CDCl_3$)

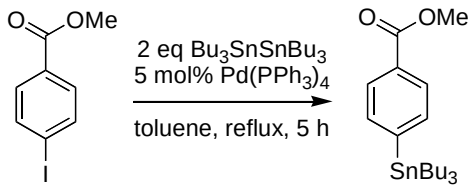

49

Methyl 4-iodobenzoate (300 mg, 1.15 mmol), bistributyltin (1.15 mL, 2.29 mmol) and $Pd(PPh_3)_4$ (70 mg, 0.06 mmol) was degassed by vaccum/nitrogen cycles (three times), then degassed toluene (12mL) was added into the flask. The reaction mixture was heated to 120 ^oC for 5 h. The solvent was removed under reduced pressure and the product was purified by silica gel chromatography eluting with 50:1 hexane/EtOAc to afford the product as colorless oil (330 mg, 70 %). ^1H NMR (500 MHz, $CDCl_3$), δ 7.96 (d, *J* = 8.0 Hz, 2H), 7.56 (d, *J* = 8.0 Hz, 2H), 1.57 - 1.51 (m, 6H), 1.37 - 1.30 (m, 6H), 1.10 - 1.07 (t, *J* = 9.0 Hz, 6H), 0.88 (t, *J* = 7.0 Hz, 9H). ^{13}C NMR (75 MHz, $CDCl_3$), δ 167.5, 149.6, 136.4, 129.5, 128.3, 52.0, 29.0, 27.3, 13.6, 9.6. HRMS (ESI) calcd for $C_{20}H_{34}BO_2SnLi^+$ $(M+Li)^+$, 433.16, found, 433.09. TLC (1:4 EtOAc/Hexane), R_f = 0.80.

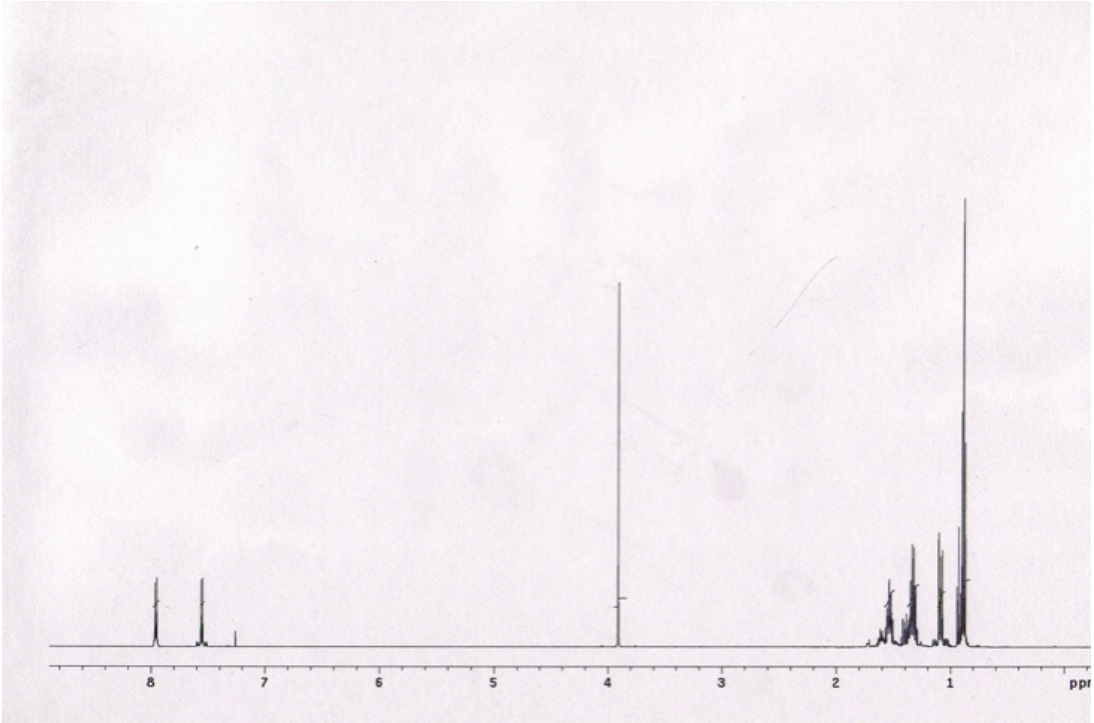

^{1}H NMR ($CDCl_3$)

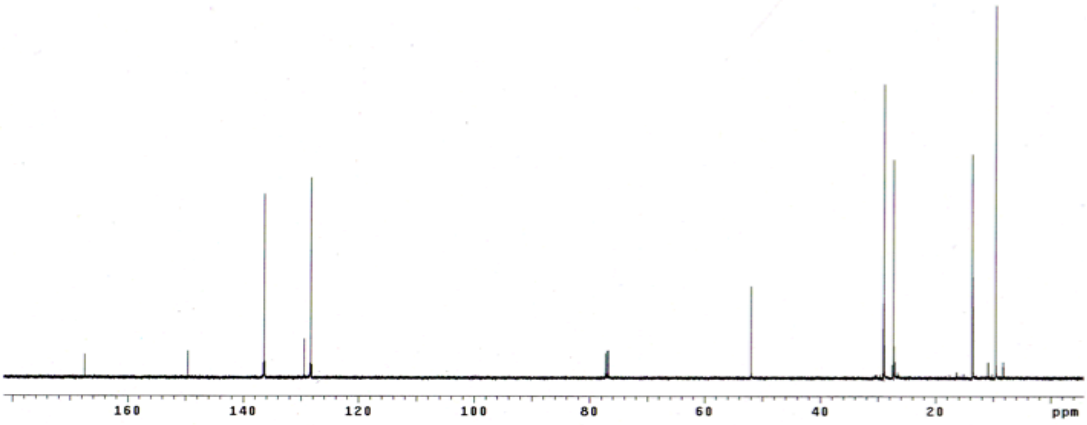

^{13}C NMR ($CDCl_3$)

General Procedure for the Liebeskind-Srogl Coupling

The BODIPY substrate (1 eq), organotin reagent (3-6 eq) or organoboron compound (4 eq), CuMeSal (4 eq) and $Pd(PPh_3)_4$ (5 mol %) were added to a round bottom flask. After 3 vacuum/nitrogen cycles, degassed THF was added into the flask. The mixture was stirred for 16 h at 55 ^{o}C under nitrogen and the reaction was monitored by TLC. After completion, the solvent was removed under reduced pressure and ethyl acetate was added. The mixture was filtered, and the filtrate was concentrated in *vacuo*. The residue was purified by silica gel flash column eluting with a mixture of hexane and ethyl acetate.

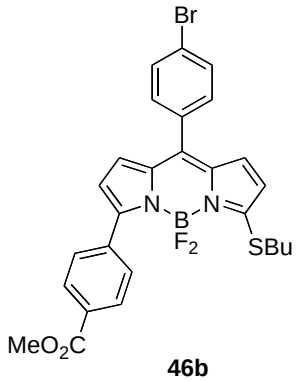

46b

Purple solid (26 %). ^{1}H NMR (300 MHz, $CDCl_3$), δ 8.11 (d, *J* = 8.6 Hz, 2H), 7.96 (d, *J* = 8.6 Hz, 2H), 7.66 (d, *J* = 8.1 Hz, 2H), 7.40 (d, *J* = 8.1 Hz, 2H), 6.87 (d, *J* = 4.7 Hz, 1H), 6.71 (d, *J* = 4.2 Hz, 1H), 6.61(d, *J* = 4.2 Hz, 1H), 6.51 (d, *J* = 4.7 Hz, 1H), 3.94 (s, 3H), 3.09 (t, *J* = 7.2 Hz, 2H), 1.82-1.72 (m, 2H), 1.56-1.44 (m, 2H), 0.95 (t, *J* = 7.2 Hz, 3H). ^{13}C NMR (75 MHz, $CDCl_3$), d 166.9, 162.5, 154.0, 138.4, 137.2, 136.1, 135.8 132.9, 131.9, 131.7, 131.4, 130.0, 129.5, 129.2, (t, J = 15.5 Hz), 127.9, 124.6, 119.3, 118.2, 52.2, 32.4, 30.9, 21.9, 13.5. MS (ESI) calcd for $C_{27}H_{25}BBrF_2N_2O_2S$ $(M+H)^+$ 568.08, found, 569.09, 571.08. ^{19}F NMR (282 MHz, $CDCl_3$), 32.1 (q, *J* = 33.6 Hz). TLC (1:1 EtoAc/Hexane) R_f = 0.50.

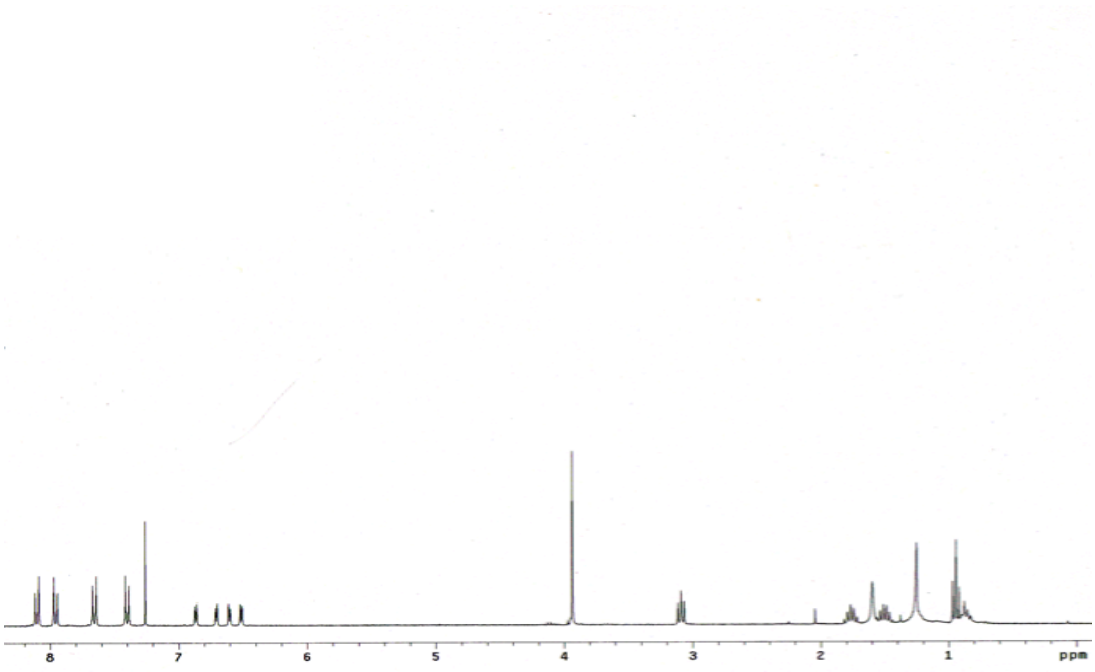

^{1}H NMR ($CDCl_3$)

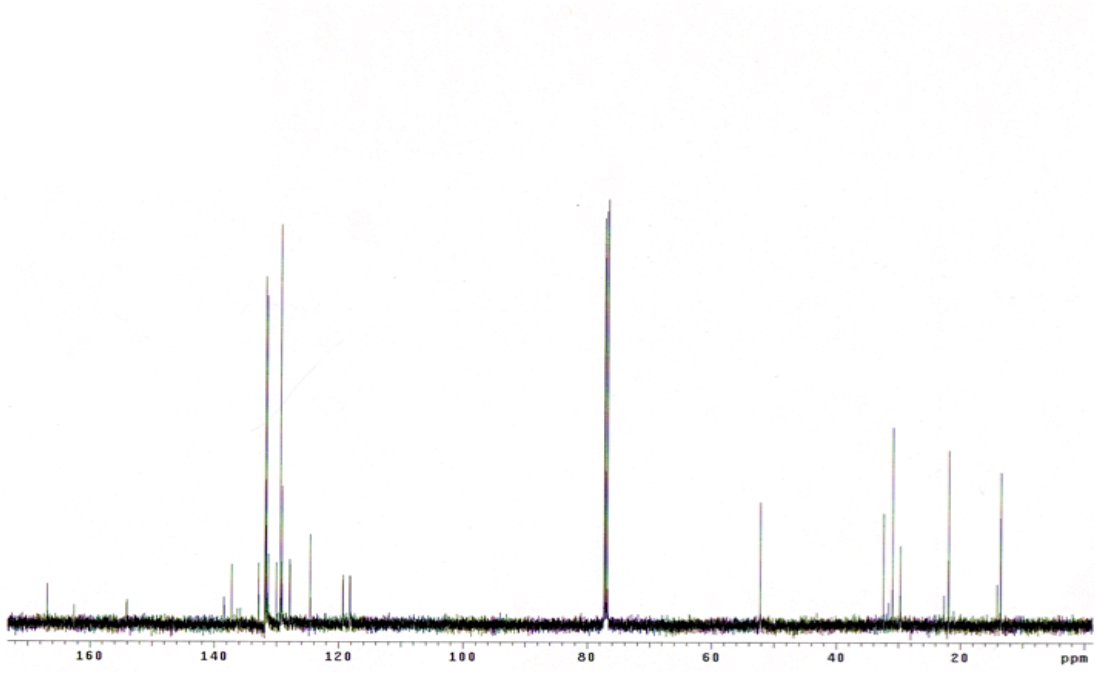

^{13}C NMR ($CDCl_3$)

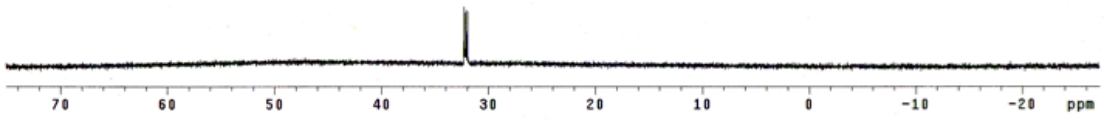

^{19}F NMR ($CDCl_3$)

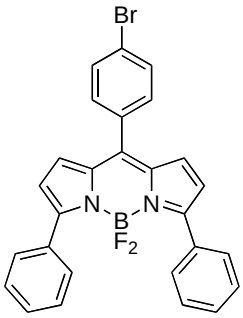

47a

Red solid (85 %) ^{1}H NMR (500 MHz, $CDCl_3$), δ 7.87 (dd, *J* = 7.5 Hz, 2.3Hz, 4 H), 7.69 (d, *J* = 9.0 Hz, 2H), 7.47 (d, *J* = 9.0 Hz, 2H), 7.44-7.41 (m, 6H), 6.86 (d, *J* = 4.3 Hz, 2H), 6.64 (d, *J* = 4.3 Hz, 2H), ^{13}C NMR (125 MHz, CDCl3), δ 159.3, 142.3, 136.2, 133.2, 132.4, 132.0, 131.6, 130.6, 129.6, 129.4 (t, *J* = 17.0 Hz), 128.2, 124.7, 121.2. ^{19}F NMR (282 MHz, $CDCl_3$), 40.5 (q, *J* = 50.2 Hz), MS (ESI) calcd for $C_{27}H_{18}BBrF_2N_2Li^+$ $(M+Li)^+$, 505.07, found, 505.08, 507.08. TLC (1:2 EtOAc/Hexane), R_f = 0.80.

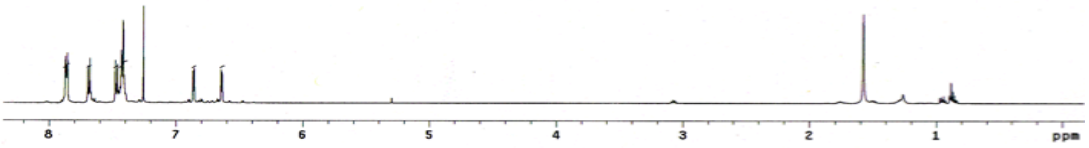

^{1}H NMR ($CDCl_3$)

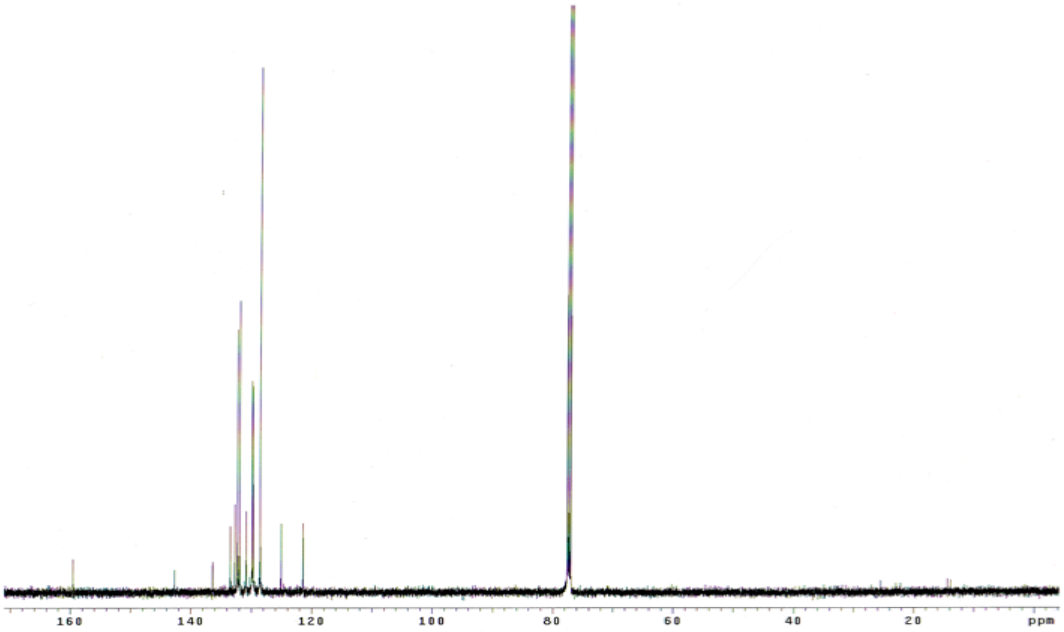

^{13}C NMR ($CDCl_3$)

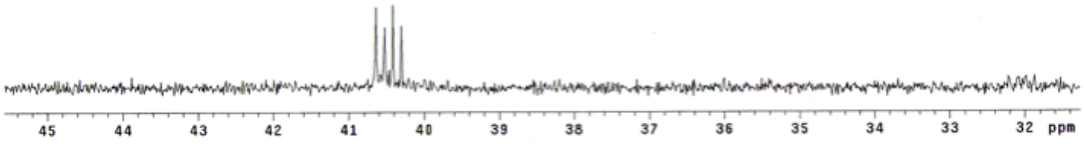

^{19}F NMR ($CDCl_3$)

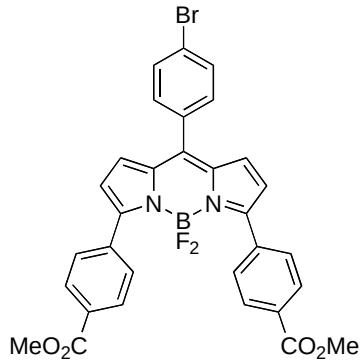

47b

Red-purple solid (62%). ^{1}H NMR (500 MHz, $CDCl_3$), δ 8.09 (d, *J* = 9.0 Hz, 4H), 7.92 (d, *J* = 9.0 Hz, 4H), 7.71 (d, *J* = 8.5 Hz, 2H), 7.47 (d, *J* = 8.5 Hz, 2H), 6.92 (d, *J* = 4.5 Hz, 2H), 6.70 (d, *J* = 4.5 Hz, 2H), 3.93 (s, 6H), ^{13}C NMR (125 MHz, $CDCl_3$), δ 166.6, 158.1, 143.8, 136.5, 132.8, 132.0, 131.8, 131.1, 130.8, 129.5, 129.4 (t, *J* = 15.0 Hz), 125.1, 121.4, 52.2. MS (MALDI) calcd for $C_{31}H_{22}BBrF_2N_2O_4Na$ $(M + Na)^+$, 637.08 found 637.24, 639.24. TLC (1:3 EtOAc/Hexane), R_f = 0.35.

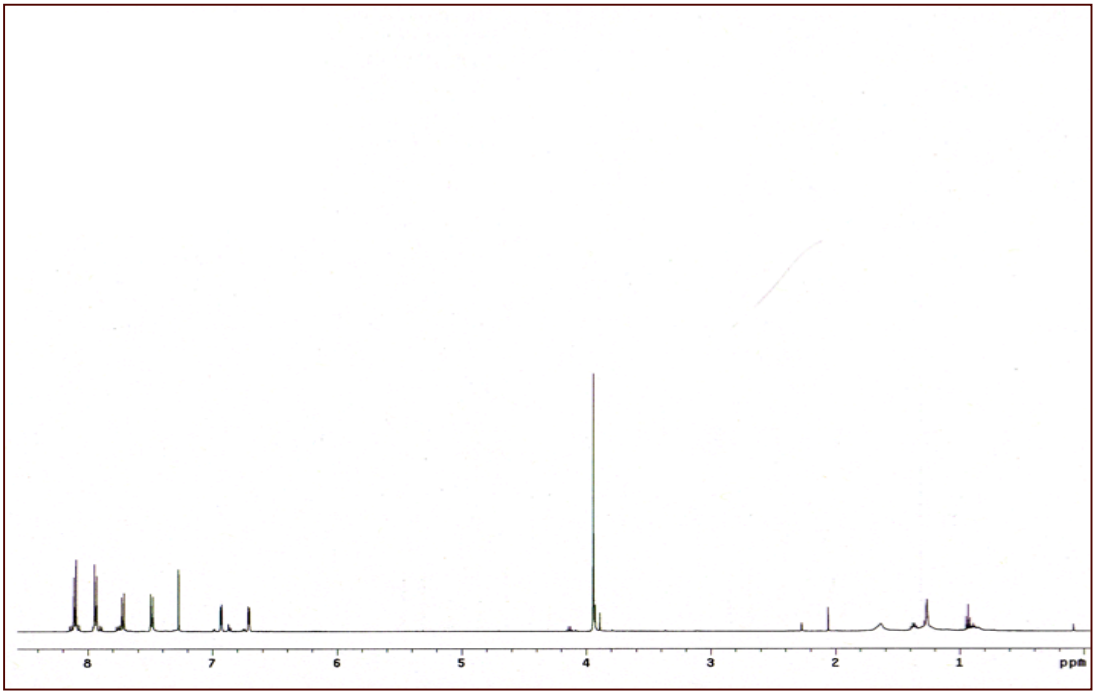

^{1}H NMR ($CDCl_3$)

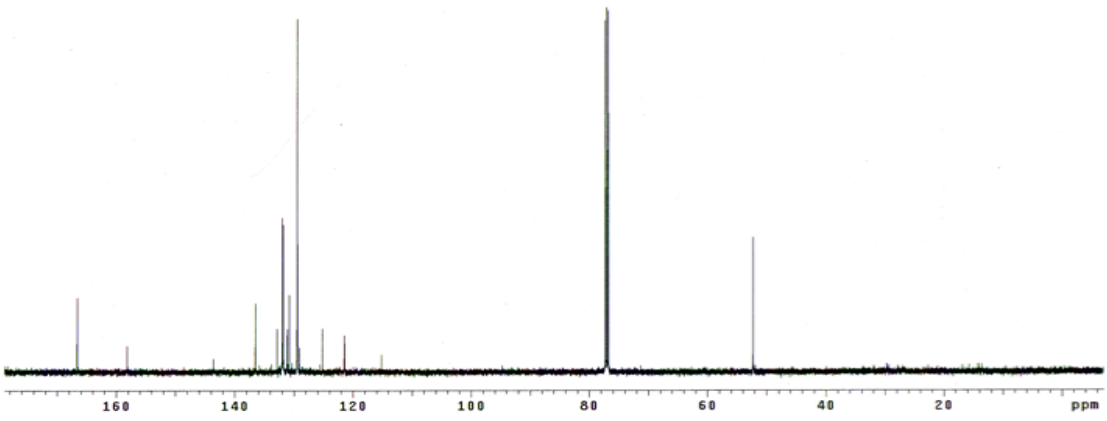

^{13}H NMR ($CDCl_3$)

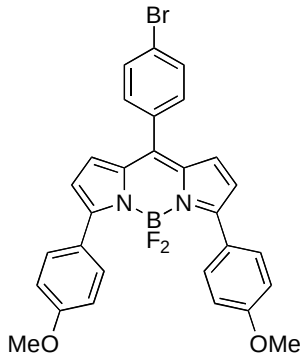

47c

Purple solid (72 %) ^{1}H NMR (300 MHz, $CDCl_3$), δ 7.88 (d, *J* = 9.0 Hz, 4 H), 7.67 (d, *J* = 8.4 Hz, 2H), 7.45 (d, *J* = 8.4 Hz, 2H), 6.96 (d, *J* = 9.0 Hz, 4 H), 6.81 (d, *J* = 4.5 Hz, 2H), 6.62 (d, *J* = 4.5 Hz, 2H), 3.85 (s, 6H), ^{13}C NMR (125 MHz, CDCl3), δ 160.8, 158.6, 140.6, 135.9, 133.4, 132.0, 131.5, 131.1 (t, *J* = 18.0 Hz), 130.1, 125.0, 124.4, 120.7, 113.8, 55.3. ^{19}F NMR (282 MHz, $CDCl_3$), 20.1 (q, *J* = 32.5 Hz), MS (ESI) calcd for $C_{29}H_{23}BBrF_2N_2O_2^+$ $(M+H)^+$, 559.09, found, 559.15, 561.15. TLC (1:3 EtOAc/Hexane), R_f = 0.25.

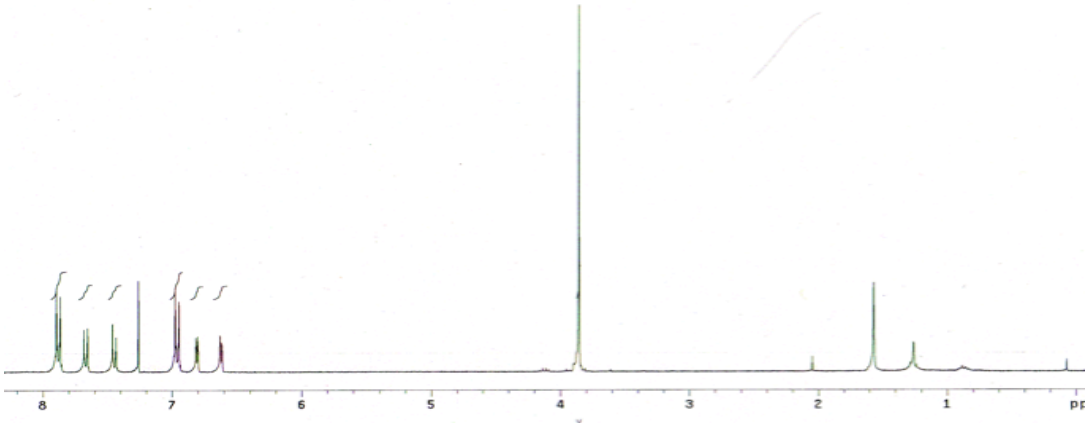

^{1}H NMR ($CDCl_3$)

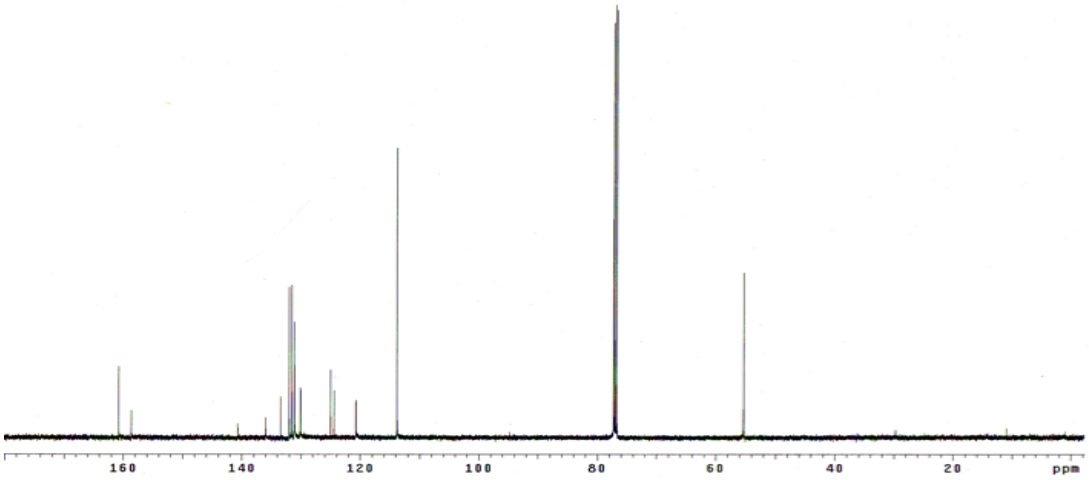

^{13}C NMR ($CDCl_3$)

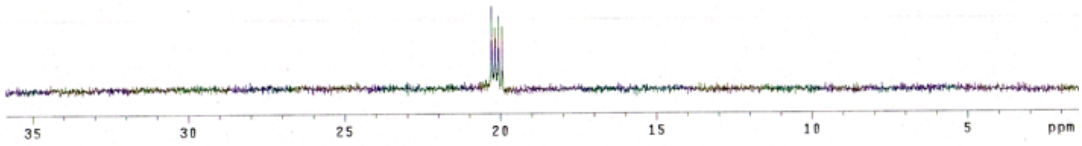

^{19}F NMR ($CDCl_3$)

Purple solid (17 %). ^{1}H NMR (500 MHz, $CDCl_3$), δ 8.38 (d, *J* = 8.5 Hz, 2H), 8.11 (d, *J* = 8.5 Hz, 2H), 7.96 (d, *J* = 8.3 Hz, 2H), 7.71 (d, *J* = 8.3 Hz, 2H), 6.80 (d, *J* = 4.5 Hz, 1H), 6.64 (d, *J* = 4.5 Hz, 1H), 6.62 (d, *J* = 4.0 Hz, 1H), 6.55 (d, *J* = 4.5 Hz, 1H), 3.94 (s, 3H), 3.11 (t, *J* = 7.0 Hz, 2H), 1.80-1.74 (m, 2H), 1.54-1.47 (m, 2H), 0.95 (t, *J* = 7.5 Hz, 3H). ^{13}C NMR (125 MHz, $CDCl_3$), δ 166.8, 163.9, 154.6, 148.7, 140.4, 136.9, 136.3, 136.1, 135.4, 131.3, 131.0, 130.2, 129.5, 129.2 (t, *J* = 16.0 Hz), 127.6, 123.6, 119.7, 118.7, 52.2, 32.5, 30.9, 21.9, 13.5. MS (ESI) calcd for $C_{27}H_{24}BF_2N_3O_4SLi^+$ $(M+Li)^+$, 542.15, found, 542.15. TLC (1:3 EtOAc/Hexane), R_f = 0.45.

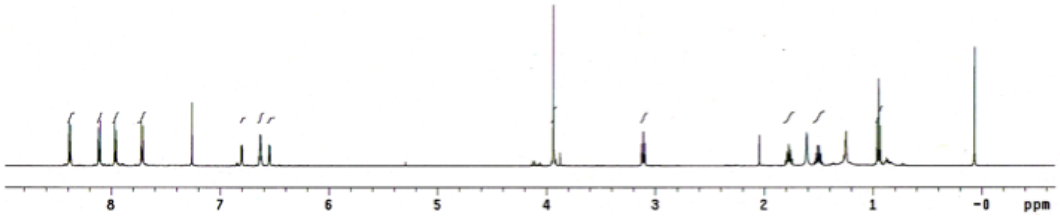

^{1}H NMR ($CDCl_3$)

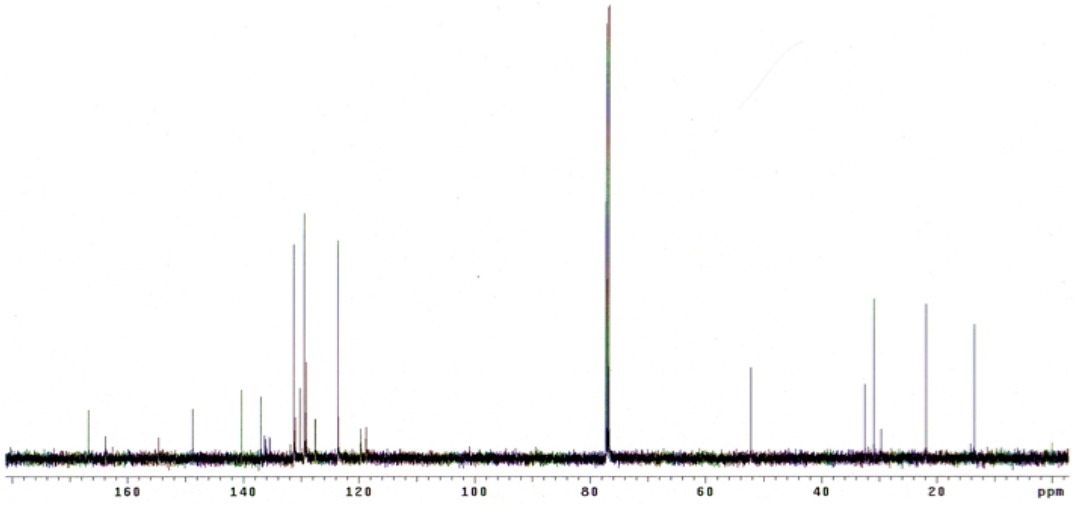

^{13}C NMR ($CDCl_3$)

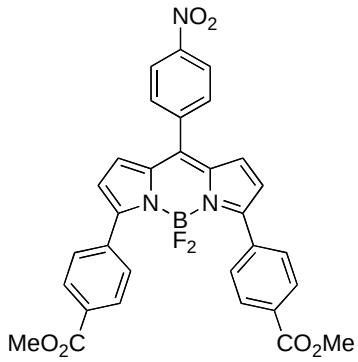

50b

Purple solid (68%). ^{1}H NMR (500 MHz, $CDCl_3$), δ 8.44 (d, *J* = 8.5 Hz, 2H), 8.11 (d, *J* = 8.5 Hz, 4H), 7.94 (d, *J* = 8.5 Hz, 4H), 7.80 (d, *J* = 8.5 Hz, 2H), 6.85 (d, *J* = 4.3 Hz, 2H), 6.73 (d, *J* = 4.3 Hz, 2H), 3.94 (s, 6H). ^{13}C NMR (125 MHz, $CDCl_3$), δ 166.5, 158.9, 148.9, 140.7, 140.2, 136.2, 136.1, 131.4, 131.0, 130.8, 129.5, 129.4 (t, *J* = 15 Hz), 123.6, 121.9, 52.3. ^{19}F NMR (282 MHz, $CDCl_3$), 40.9 (q, *J* = 33.6 Hz). MS (ESI) calcd for $C_{31}H_{22}BF_2N_3O_6Li^+$ $(M+Li)^+$, 588.16, found, 588.18.

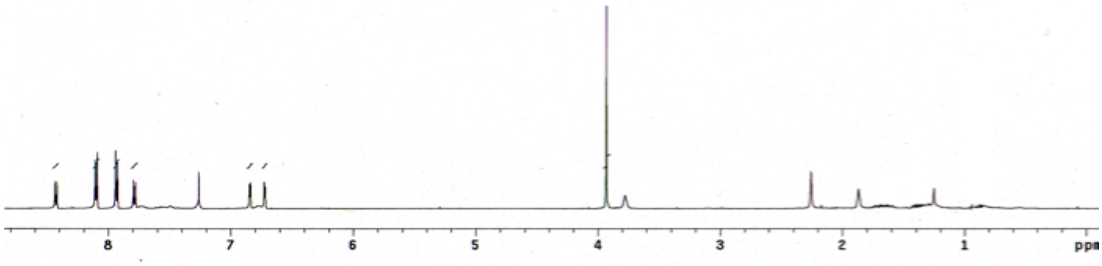

^{1}H NMR ($CDCl_3$)

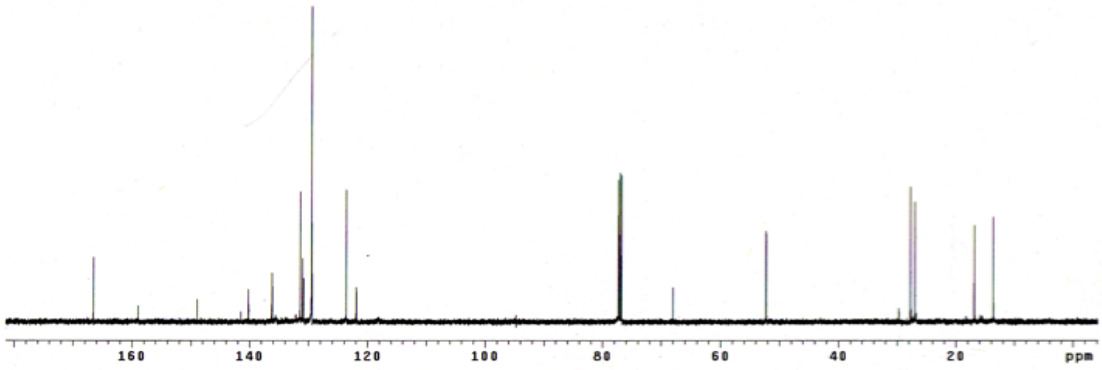

^{1}H NMR ($CDCl_3$)

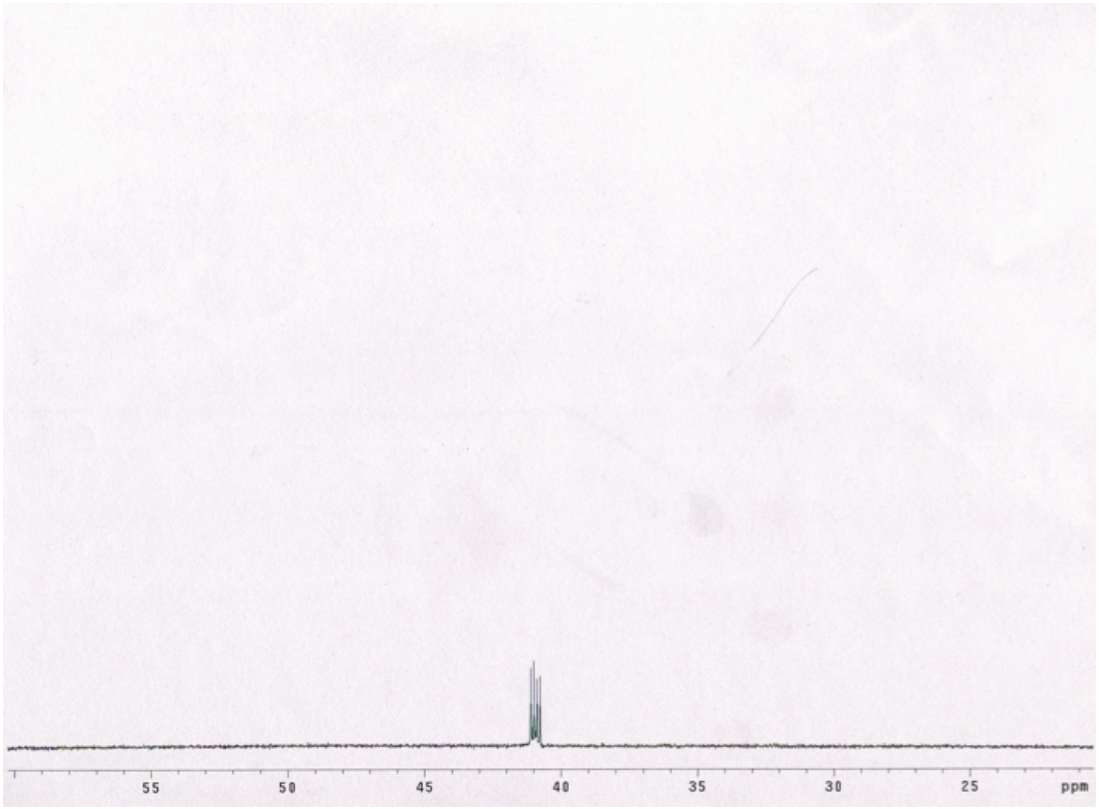

^{19}F NMR ($CDCl_3$)

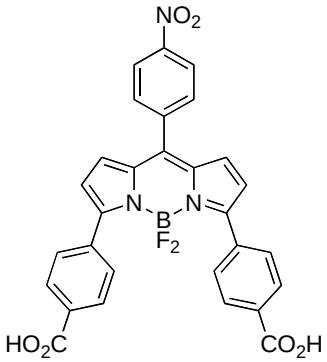

51

Dimethyl ester **50b** (32 mg, 0.06 mmol) was dissolved in 3 mL THF at room temperature. Then potassium trimethylsilanolate (30 mg, 0.23 mmol) was added to the reaction mixture. The reaction was complete in 6 h as indicated by TLC. Aqueous HCl (0.1 M, 10 mL) was added and the product was extracted out of water with 1:2 isopropyl alcohol/CH_2Cl_2 (10 mL x 2). The organic solvent was dried over $MgSO_4$ and then removed under reduced pressure to afford the desired product as a red solid (29 mg, 95 %). ^{1}H NMR (300 MHz, CD_3OD), δ 8.42 (d, J = 8.9 Hz, 2H), 7.98 (d, J = 8.4 Hz, 4H), 7.85 (d, J = 8.4 Hz, 4H), 7.81 (d, J = 8.9 Hz, 2H), 6.84 (d, J = 4.5 Hz, 2H), 6.71 (d, J = 4.5 Hz, 2H). ^{19}F NMR (282 MHz, CD_3OD), 43.8 (q, J = 30.6 Hz). HRMS (ESI) calcd for $C_{29}H_{17}N_3O_6^-$ $(M-H)^-$ 552.1178, found 552.1174. This compound is not very soluble in organic solvent, so ^{13}C could not be obtained. 1:2 Hexane/EtOAc, R_f = 0.75.

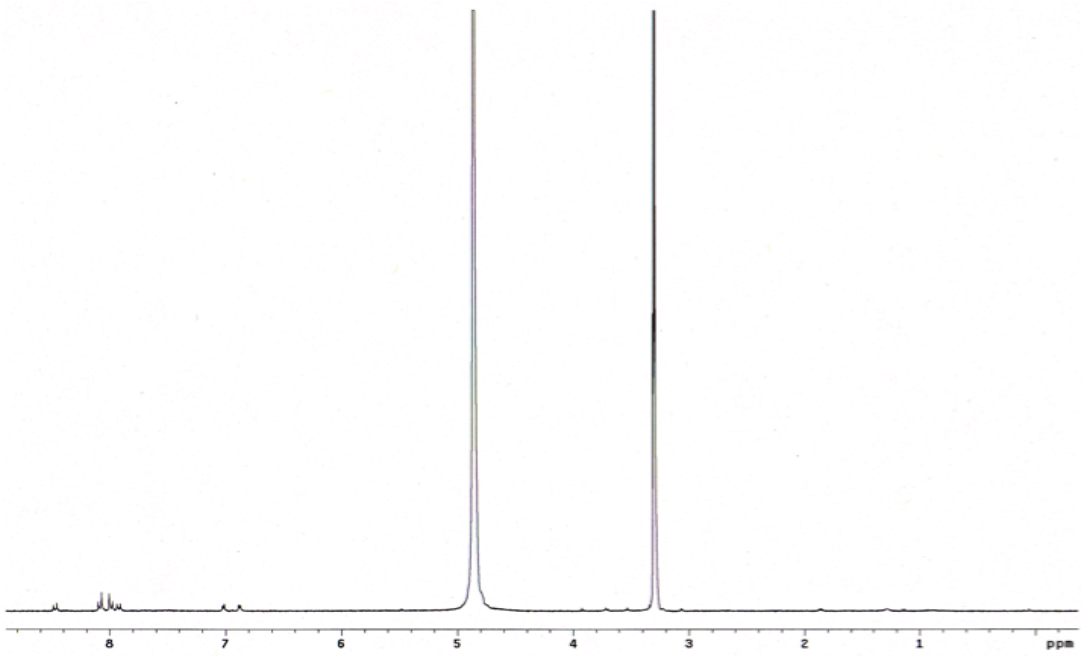

^{1}H NMR ($CDCl_3$)

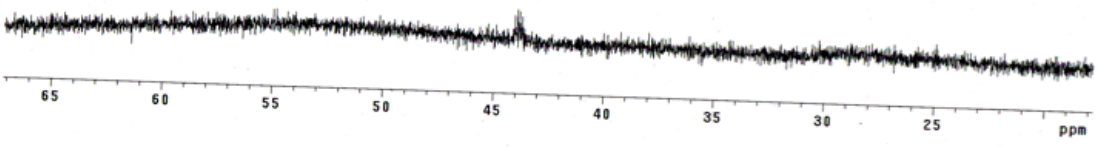

^{19}F NMR ($CDCl_3$)

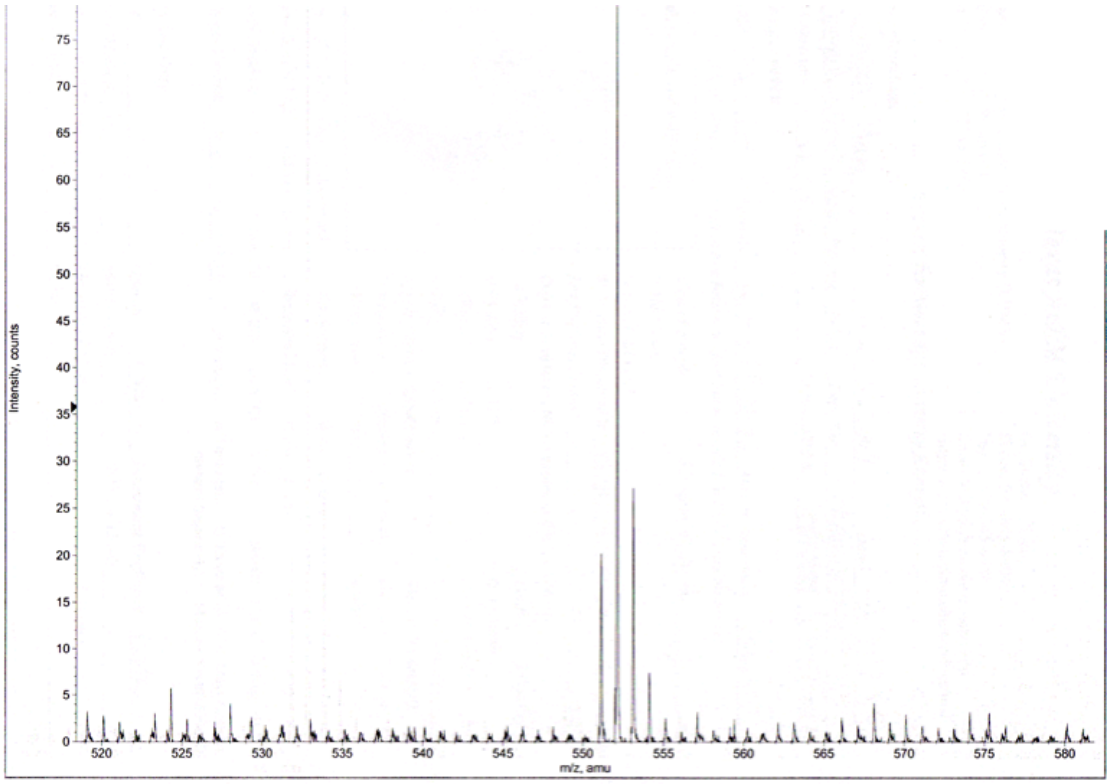
Intensity, counts
m/z, amu
0
5
10
15
20
25
30
35
40
45
50
55
60
65
70
75
520
525
530
535
540
545
550
555
560
565
570
575
580

MS ESI

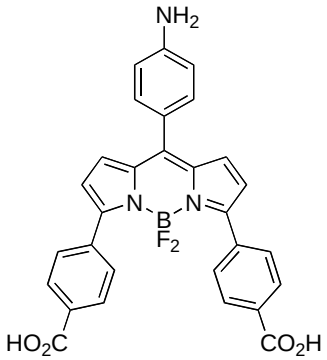

52

The crude product obtained above **51**, Pd/C (5 mg, 0.005 mmol) and hydrazine monohydrate (0.05 mL) were suspended in ethanol (2 mL). The reaction mixture was heated to 82 ^{o}C for 25 min. The reaction solution was passed through celite, and the solvent was removed under reduced pressure to afford desired product as a dark red solid 26 mg (95 %). ^{1}H NMR (300 MHz, CD_3OD 1:2), δ 7.98 (d, J = 8.9 Hz, 4H), 7.85 (d, J = 8.9 Hz, 4H), 7.43 (d, J = 8.4 Hz, 2H), 7.06 (d, J = 4.4 Hz, 2H), 6.83 (d, J = 8.4 Hz, 2H), 6.75 (d, J = 4.4 Hz, 2H). ^{13}C NMR (125 MHz, $CDCl_3$), δ 180.2, 158.1, 153.2, 137.5, 136.0, 134.2, 133.0, 131.8, 130.0, 129.9, 129.7, 123.9, 121.5, 115.1. ^{19}F NMR (282 MHz, $CDCl_3$), 43.8 (q, J = 30.5 Hz). HRMS (ESI) calcd for $C_{29}H_{19}N_3O_4^-$ $(M - H)^-$ 522.1437, found 522.1434.

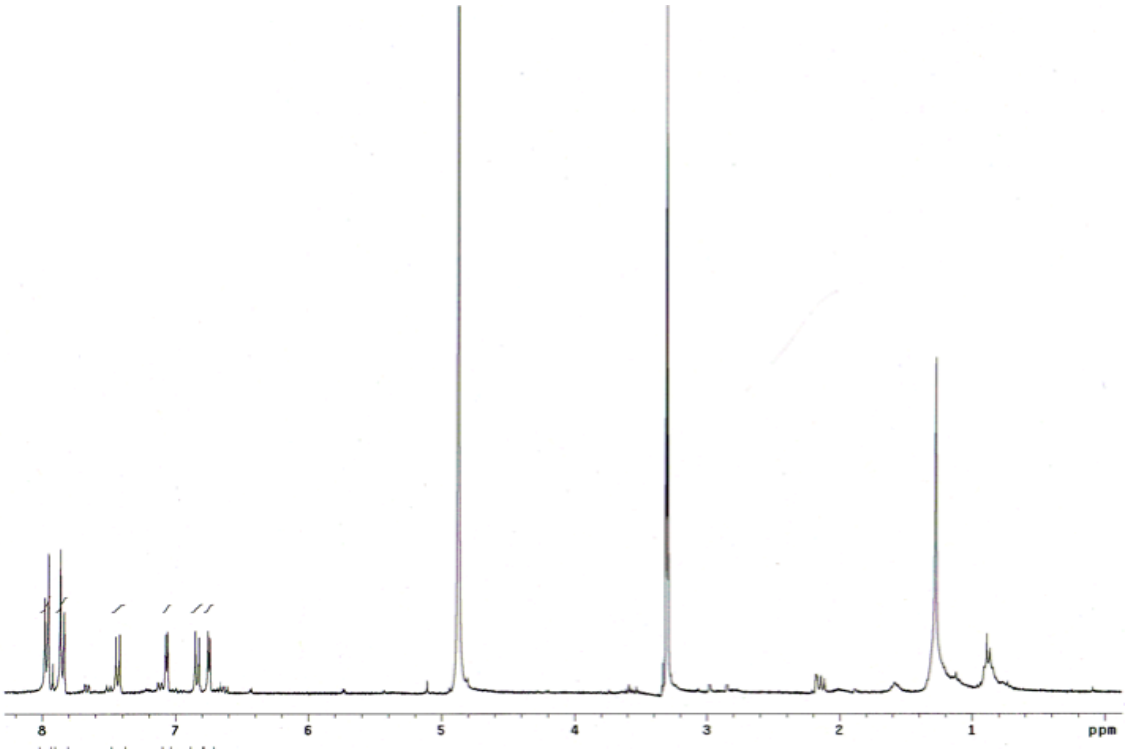

^{1}H NMR (CD_3OD)

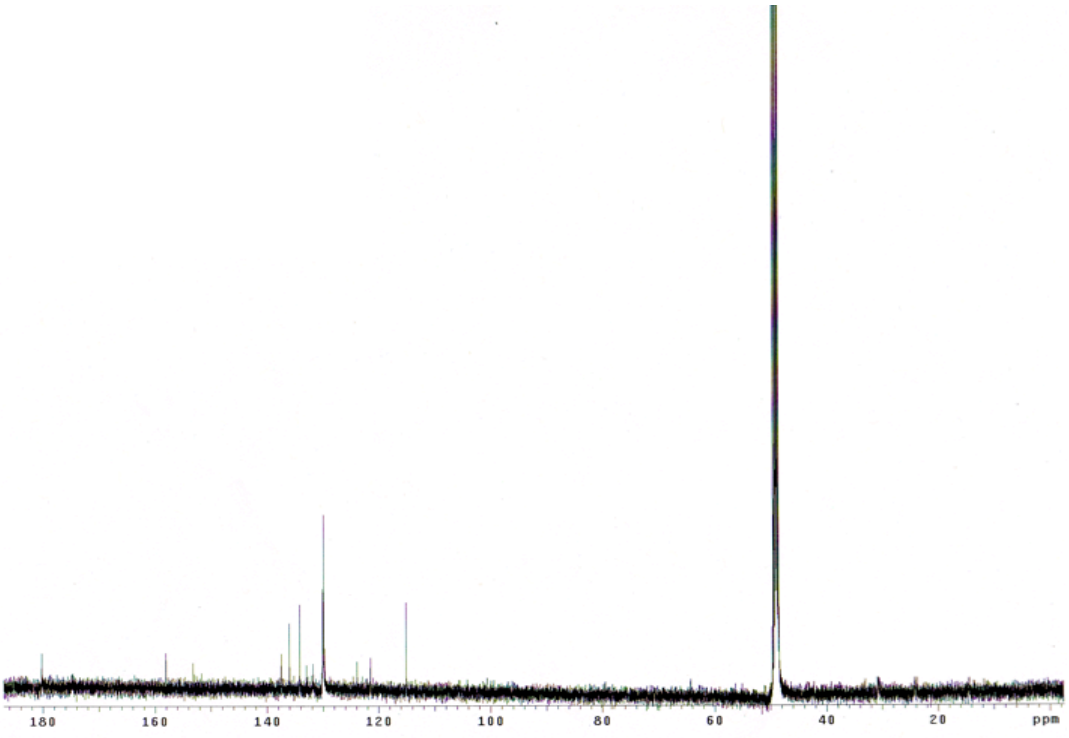

^{13}C NMR (CD_3OD)

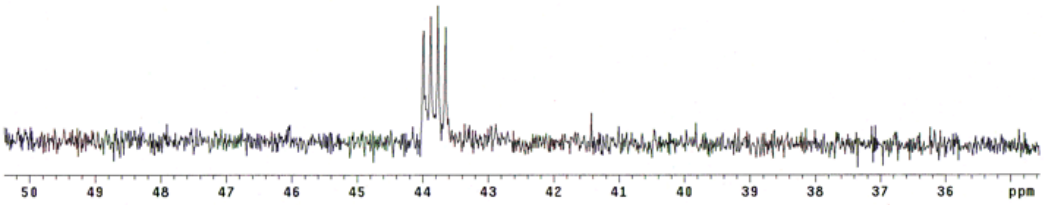

^{19}F NMR (CD_3OD)

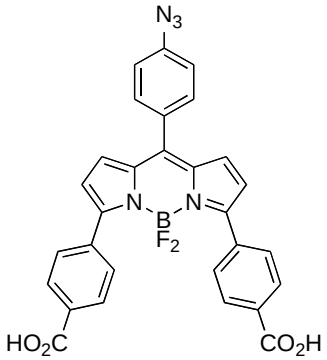

53

A solution of **52** (18 mg, 0.034 mmol) in HCl (0.1 M, 2.5 mL) and HTF (2.5 mL) was cooled to 0 ^{o}C. A solution of $NaNO_2$ (5 mg, 0.072 mmol) in H_2O (0.25 ml) was added slowly and the mixture was kept at 0 ^{o}C with stirring for 30 min. A solution of NaN_3 (21 mg, 0.34 mmol) in H_2O (0.35 mL) was then added dropwise to the mixture. Stirring was continued at room temperature for 16 h after completion of the addition. The reaction mixture was acidified with HCl (0.1 M) carefully, then the product was extracted out of the water using 1:2 ^{i}PrOH/CH_2Cl_2. The product was achieved after removing the solvent under reduced pressure as a red solid (14 mg, 75 %). ^{1}H NMR (500 MHz, 2:1 $CD_3OD/CDCl_3$), δ 8.06 (d, J = 8.5 Hz, 4H), 7.91 (d, J = 8.5 Hz, 4H), 7.65 (d, J = 8.5 Hz, 2H), 7.25 (d, J = 8.5 Hz, 2H), 6.99 (d, J = 4.0 Hz, 2H), 6.74 (d, J = 4.0 Hz, 2H), ^{19}F NMR (282 MHz, 2:1 $CD_3OD/CDCl_3$), δ 44.6 (q, J = 33.6 Hz). HRMS (ESI) calcd for $C_{29}H_{17}BF_2N_5O_4^-$ $(M - H)^-$, 548.1342, found 548.1339.

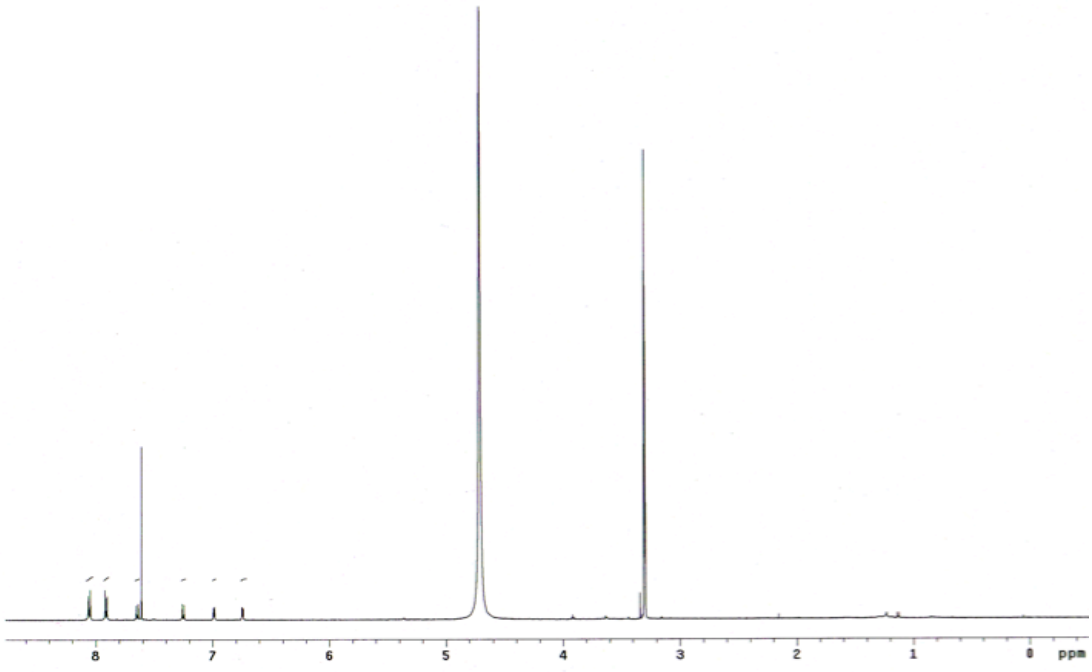

^{1}H NMR (CD_3OD)

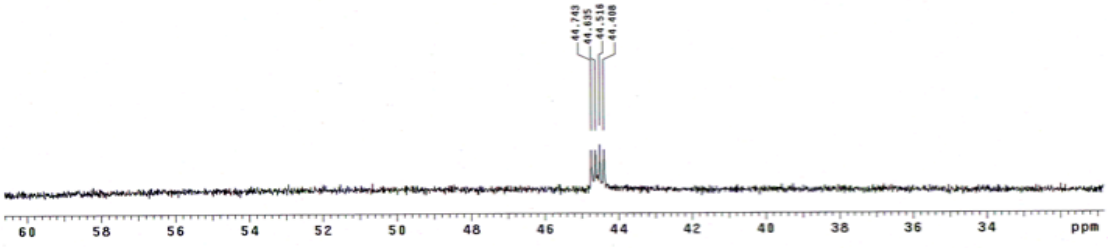

^{19}F NMR (CD_3OD)

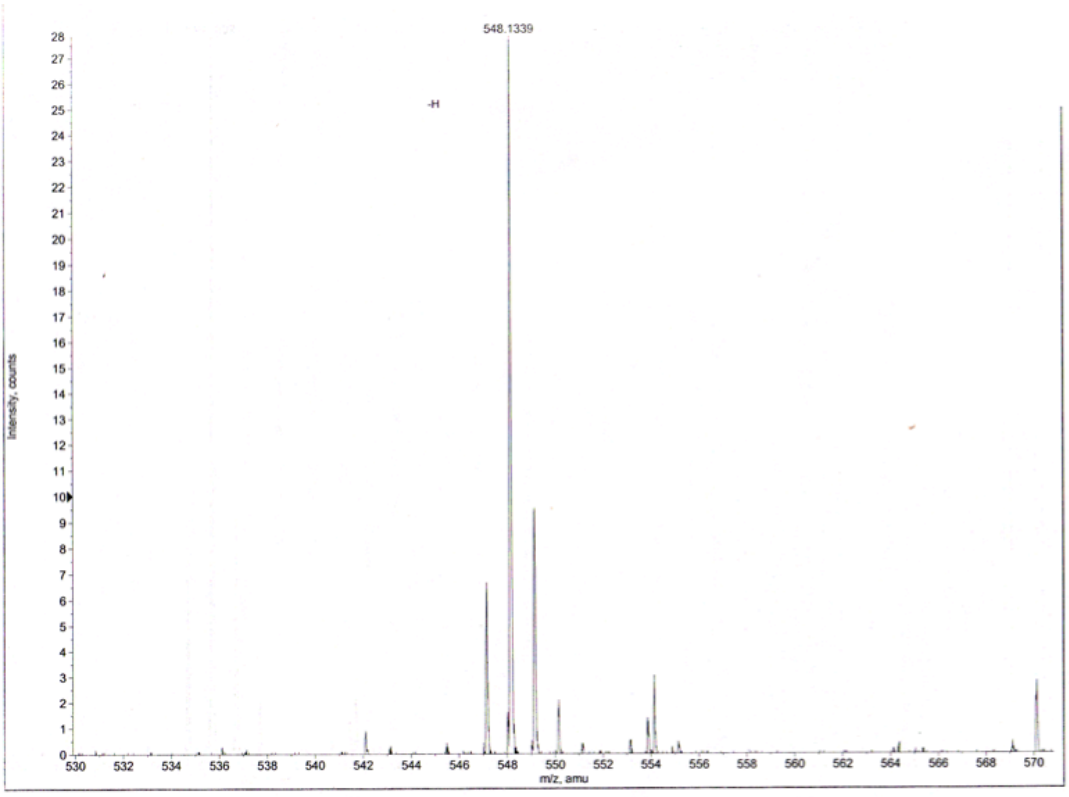

MS ESI

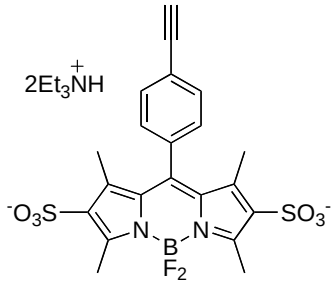

54

A solution of chlorosulfonic acid (23 μL, 0.35 mmol) in 2.0 mL of dry CH_2Cl_2 was added dropwise to a solution of BODIPY **Q** (50 mg, 0.14 mmol) in dry CH_2Cl_2 over 10 min under N_2 at -40 ^oC. The solution was slowly warmed to room temperature and an orange precipitate was formed. The disulfonic acid was neutralized with triethylamine (48 μL, 0.35 mmol) and the solvent was removed under reduced pressure. The resulting salt was purified by reverse phase preparative-HPLC (gradient: 5% solvent B to 95% solvent B, 25 min) to afford the desired product as an orange solid (45 mg, 60 %). ^1H NMR (500 MHz, CD_3OD), δ 7.69 (d, *J* = 8.5 Hz, 2H), 7.38 (d, *J* = 8.5 Hz, 2H), 3.68 (s, 1H), 3.19 (q, *J* = 7.5 Hz, 12H), 2.78 (s, 6H), 1.69 (s, 6H), 1.29 (t, *J* = 7.5 Hz, 18H), ^{13}C NMR (125 MHz, $CDCl_3$), δ 156.9, 145.7, 143.2, 136.3, 136.1, 134.2, 131.5, 129.7, 125.3, 83.5, 80.6, 47.8, 14.5, 13.6, 9.2. MS (ESI) calcd for $C_{21}H_{17}BBrF_2O_6S_2^{2-}$ $(M - 2Et_3NH)^{2-}$, 253.02, found 253.02.

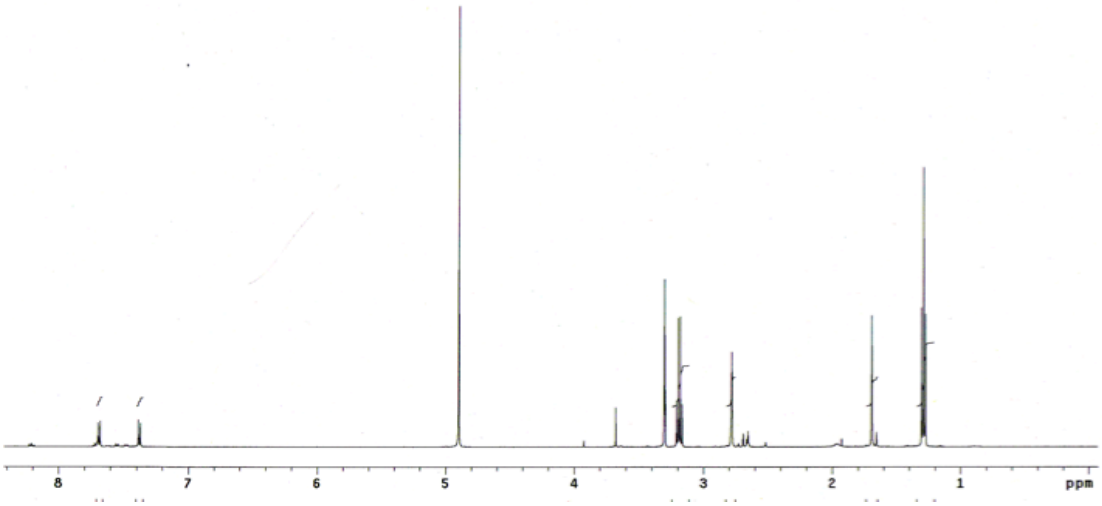

^{1}H NMR ($CDCl_3$)

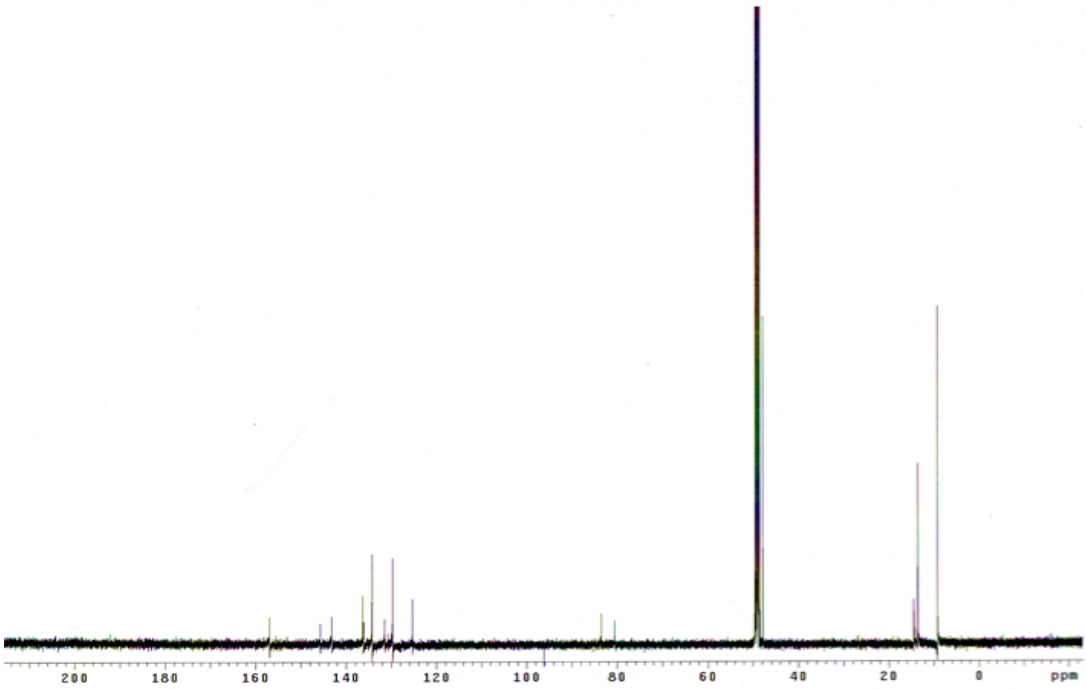

^{13}C NMR (CD_3OD)

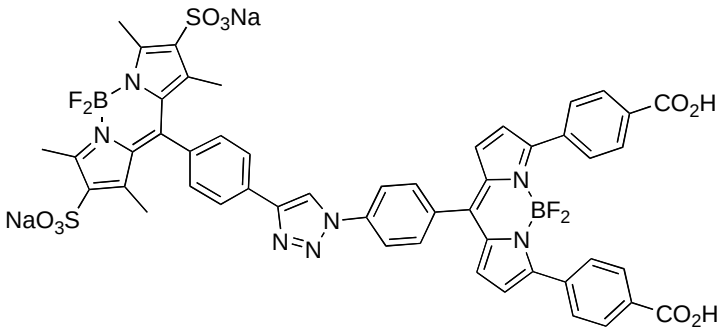

55

Copper (1 mg, 0.02 mmol) and $CuSO_4 \cdot 5H_2O$ (2 mL, 1 M, 0.002 mmol) were added to a solution of **53** (11 mg, 0.019 mmol) and **54** (12 mg, 0.07 mmol) in 1:1 THF/H_2O (2 ml). The reaction mixture was stirred at room temperature for 48 h, and then was evaporated to dryness. The residue was purified by reverse phase prep-HPLC (gradient: 10% solvent B to 90% solvent B, 25 min) to afford a red solid with retention time at 17 min (6 mg, 30%). ^{1}H NMR (500 MHz, CD_3OD), δ 9.28 (s, 1H), 8.28-8.27 (m, 4H), 8.12 (d, J = 8.5 Hz, 4H), 8.03 (d, J = 8.5 Hz, 4H), 7.96 (d, J = 8.0 Hz, 2H), 7.56 (d, J = 6.5 Hz, 2H), 7.16 (d, J = 4.0 Hz, 2H), 6.93 (d, J = 4.5 Hz, 2H), 2.83 (s, 6H), 1.81 (s, 6H). MS (ESI) calcd for $C_{50}H_{33}B_2F_4N_7O_{10}S_2$ $(M\text{-}2Na\text{-}2H)^{4-}$, 263.25, found 263.28.

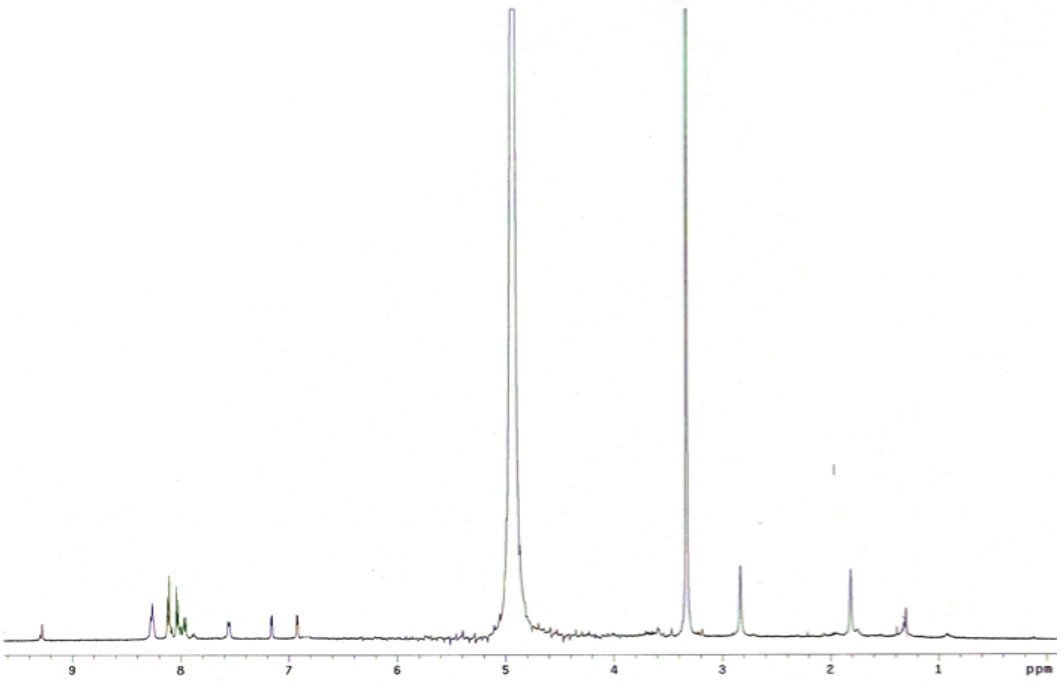

^{1}H NMR (CD_3OD)

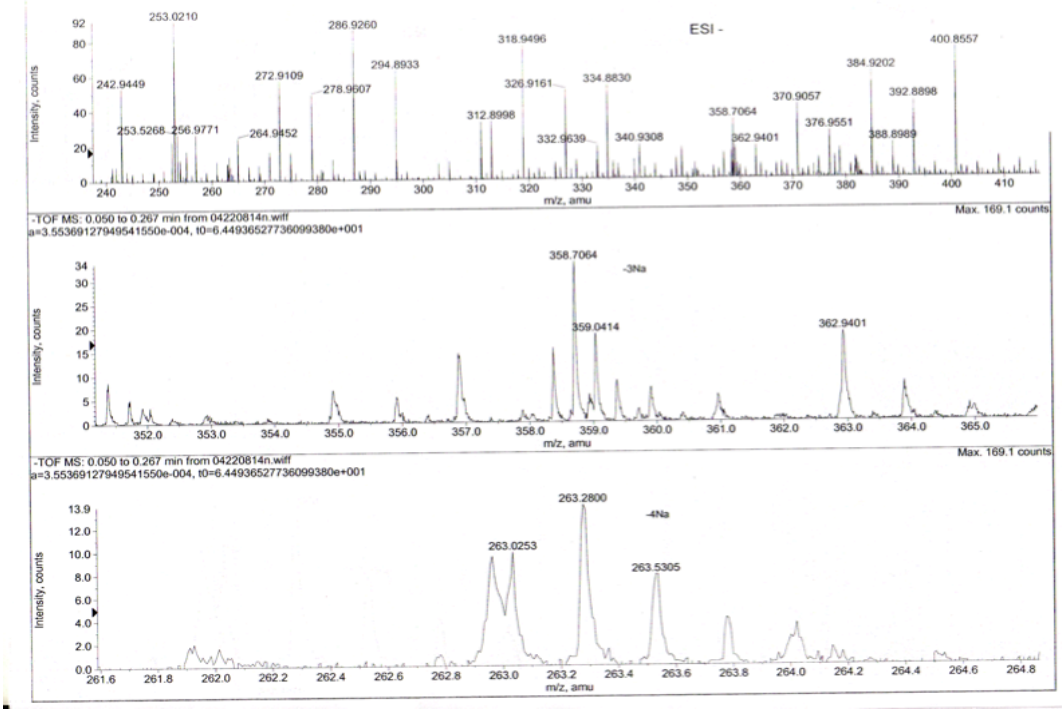

MS ESI

APPENDIX C
EXPERIMENTAL DATA FOR CHAPTER IV

General Experimental Procedures

NMR spectra were recorded on a VXP-300 MHz and Inova-500 MHz spectrometers (^{1}H at 300 MHz or 500 MHz, and ^{13}C at 75 or 125 MHz) at room temperature unless other mentioned. Chemical shifts of ^{1}H NMR spectra were recorded and chemical shifts are reported in ppm from the solvent resonance ($CDCl_3$ 7.26 ppm, CD_3OD 3.30 ppm, CD_3SOCD_3 2.49 ppm). Data are reported as follows: chemical shift, multiplicity (s = singlet, bs = broad singlet d = doublet, t = triplet, q = quartet, br = broad, m = multiplet), coupling constants, and number of protons. Proton decoupled ^{13}C NMR spectra were also recorded in ppm from tetramethylsilane resonance ($CDCl_3$ 77.0, CD_3OD 49.1, DMSO-d_6 39.5 ppm). Analytical thin layer chromatography (TLC) was performed on EM Reagents 0.25 mm silica-gel 60-F plates, and visualized with UV light. Flash chromatography was performed using silica gel (230–600 mesh). UV/Visible and fluorescence (1.0×10^{-6} M) spectra of compound **56** were taken in aqueous Ph = 10 buffer solution (Na_2CO_3, $NaHCO_3$). Absorption and fluorescence spectra of compound **57** were taken in dry DMF. HPLC analysis of samples was preceded by subjecting the sample to reverse phase analytical HPLC [C18, 5:95 (CH_3CN/H_2O)] unless other mentioned. MS were measured (Thermofinnigan LC-Q Deca spectrometer) under ESI, MALDI or APCI conditions. IR spectra were recorded on Bruker (Tensor 27). The total chemiluminescence intensity was calculated by

integrating the decay curve between the point of adding sample and the point where signal decays to the background level. The background signal has been subtracted from the total chemiluminescence intensity during the calculation. THF was distilled over Na/benzophenone. DMF and Et_3N were distilled from CaH_2. Other solvents and reagents were used as received.

Methods for Measuring the Chemiluminescence Spectra and Quantum Yields

Instrument

A confocal microscope was used with a sample cell volume of ~ 200 μl made by gluing a plastic cylinder on a clean microscope cover glass; this was used to hold samples and serves as the reaction chamber. The sample cell was mounted on an inverted, epi-illumination microscope (Nikon, Diaphot 300). A Nikon FLUOR X40, 1.3 numerical aperture objective was used to collect the chemiluminescence. The 670DCSP or 830DCSP dichroic filters (Chroma Technology) were used in the experiments depending on the emission wavelength. A single-photon counting avalanche diode (APD) was used to collect time dependent chemiluminescent signal. The chemiluminescence spectra of samples were obtained by means of a monochromator (Acton Research) equipped with a back-illumination liquid-nitrogen-cooled CCD camera (Princeton Instruments, Trenton, NJ). This CCD array detector allows detection of spectrally resolved signals simultaneously, which is useful for obtaining a dynamical spectrum, such as chemiluminescence which decays as function of time and its spectrum is not accessible by conventional scanning methods.

Materials

The sample solutions of luminol and luminol-fluorescein cassette (LFC) **56** at different concentrations were prepared by dissolving a luminol and LFC in pH=10 buffer solution (Na_2CO_3 and $NaHCO_3$). A second solution containing 1.5x 10^{-3} M $CuSO_4$ and 2x 10^{-3} M H_2O_2 was also prepared and used to react with sample solutions to generate light. The sample solution of luminol-Nile Red cassette **57** (1.0 x 10^{-4} M) was prepared in dry DMF. A second solution of 0.01M potassium tert-butoxide in dry THF was used to react with the sample solution of **57**.

Experiment

Either 30 μl or 15 μl of the second solution containing 1.5x 10^{-3} M $CuSO_4$ and 2x 10^{-3} M H_2O_2 was first added into sample cell and the spectra collected by CCD or the total emission signal by APD, both as function of time. When the computer started collecting data, a 100 μl of sample solution was added to the sample cell, which immediately reacts with H_2O_2 and emits lights. The intensity of light decays as the concentration of reactants decreases. Data collection was stopped when the intensity of signal decayed to the background level.

Spectrum of 2 was taken in dry DMF when adding 10 μl (0.01 M) potassium tert-butoxide solution in dry THF to a sample cell containing 150 μl sample 2 (1 x 10^{-4}M).

Estimation of Quantum Yield of LFC

In principle, the quantum yield of LFC was estimated by preparing two sample solutions containing equal amounts of luminol and LFC, and measuring the total chemiluminescence intensity under the same experimental conditions. The quantum

yields of LFC at different concentrations have been calculated by simply dividing the total intensity of luminal chemiluminescence by that of the sample chemiluminescence, assuming the quantum yield of luminol is 100%.

Calculation of the Overlap Integral $J_{(\lambda)}$, the Föster Distance R_0, and the Energy Transfer Efficiency E.

The degree of spectral overlap between donor emission and acceptor absorption expressed by the overlap integral $\mathbf{J_{(\lambda)}}$. It can be calculated according to the equation derived from classical and quantum mechanic considerations:

$$J(\lambda) = \int \mathbf{F_{D(\lambda)}}\varepsilon_{A(\lambda)}\lambda^4 d\lambda = \frac{\int \mathbf{F_{D(\lambda)}}\varepsilon_{A(\lambda)}\lambda^4 d\lambda}{\int \mathbf{F_{D(\lambda)}} d\lambda} \qquad (1)$$

The overlap integral $\mathbf{J_{(\lambda)}}$ is in units of $M^{-1}cm^{-1}(nm)^4$. $\mathbf{F_{D(\lambda)}}$ is the corrected normalized fluorescence intensity of the donor. $\boldsymbol{\varepsilon_{A(\lambda)}}$ is the extinction coefficient of the acceptor at λ. The Föster Distance $\mathbf{R_0}$ in angstroms, is expressed by

$$\mathbf{R_0 = 0.211[\kappa^2 n^{-4} Q_D J_{(\lambda)}]^{1/6}} \qquad (2)$$

$\boldsymbol{\kappa^2}$ is the orientation factor, which describes the orientation of the transition dipoles of the donor and acceptor. **n** is the refractive index of the medium, which is 1.40 in aqueous solution and 1.43 in DMF. $\mathbf{Q_D}$ is the fluorescence quantum yield of the emitter generated from donor through chemiluminescent reactions in the absence of acceptor.

The efficiency of the energy transfer (**E**) is the fraction of photons generated by the donor that are transferred to the acceptor. If the energy transfer rate is much faster than the decay rate of the donor, then much transfer will occur and FRET will be

efficient. If the transfer rate is slower that the decay rate, then energy transfer will be inefficient. The energy transfer efficiency E is given by:

$$\mathbf{E} = \frac{\mathbf{R_0}^6}{\mathbf{R_0}^6 + \mathbf{r}^6} \qquad (3)$$

r is the distance between donor and acceptor.

Table S2. Calculated R_0 values for FRET and Energy Transfer efficiency **E**. $\mathbf{R_0}$ was calculated using n = 1.4 (H_2O), 1.43 (DMF), $Q_D = 2.0 \times 10^{-4}$ (data from reference 6 in the text) and $\kappa^2 = 1/4$

Compounds	$\mathbf{J_{DA}}$ ($M^{-1}cm^3(nm)^4$)	$\mathbf{R_0}$ (Å)	**r** (Å)	**E** (%)
56	1.15×10^{15}	10.47	11.3	39
57	6.95×10^{14}	9.50	10.0	42

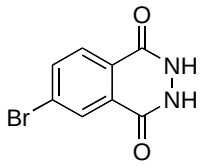

58

6-Bromo-2, 3-dihydrophathalazine-1, 4-dione 5-Bromophthalic anhydride (11.8 g, 52 mmol) and 40 ml acetic acid were added into a 250 mL round bottom flask. The mixture was heated to 125 ^{o}C. After 1h, the mixture was cooled to 25 ^{o}C. Hydrazine monohydrate (2.65 mL, 54.6 mmol) was added dropwise into the flask, and then the mixture was refluxed at 125 ^{o}C for 30 min. The mixture was cooled to room temperature again and white solid precipitated out from the solvent. The white solid was separated by filtration. The crude product was dissolved in 5% NaOH (30 mL), acidified with AcOH (3 mL), and white solid precipitated out. The solid was washed with a large amount of water and then MeOH to afford 11.9 g **58** (95 %) as colorless powder. ^{1}H NMR (300 MHz, DMSO), δ11.72 (s, 2H), 8.16 (d, *J* = 1.8 Hz, 1H), 8.05 (dd, *J* = 8.4 Hz, 1.8 Hz, 1H), 7.98 (d, *J* = 8.4 Hz, 1H); ^{13}C NMR (125 MHz, DMSO), δ153.9 (bs), 135.6, 128.7, 127.7, 127.5, 126.4, 126.1. HRMS (ESI) calcd for $C_8H_4BrN_2O_2Na$ $(M-H)^-$ 238.9462, found 238.8779, 240.8754. mp 358-361 ^{o}C.

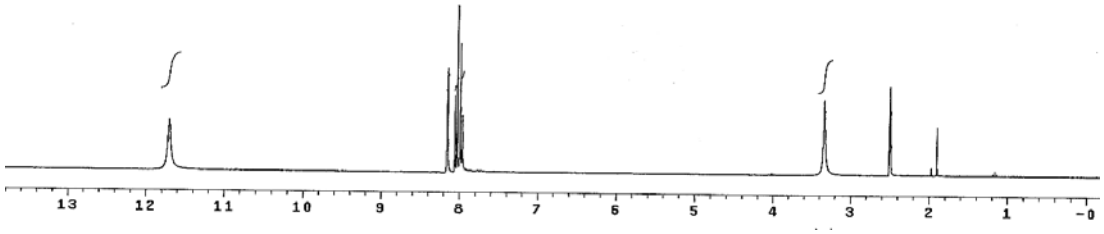

^{1}H NMR (DMSO-d$_6$)

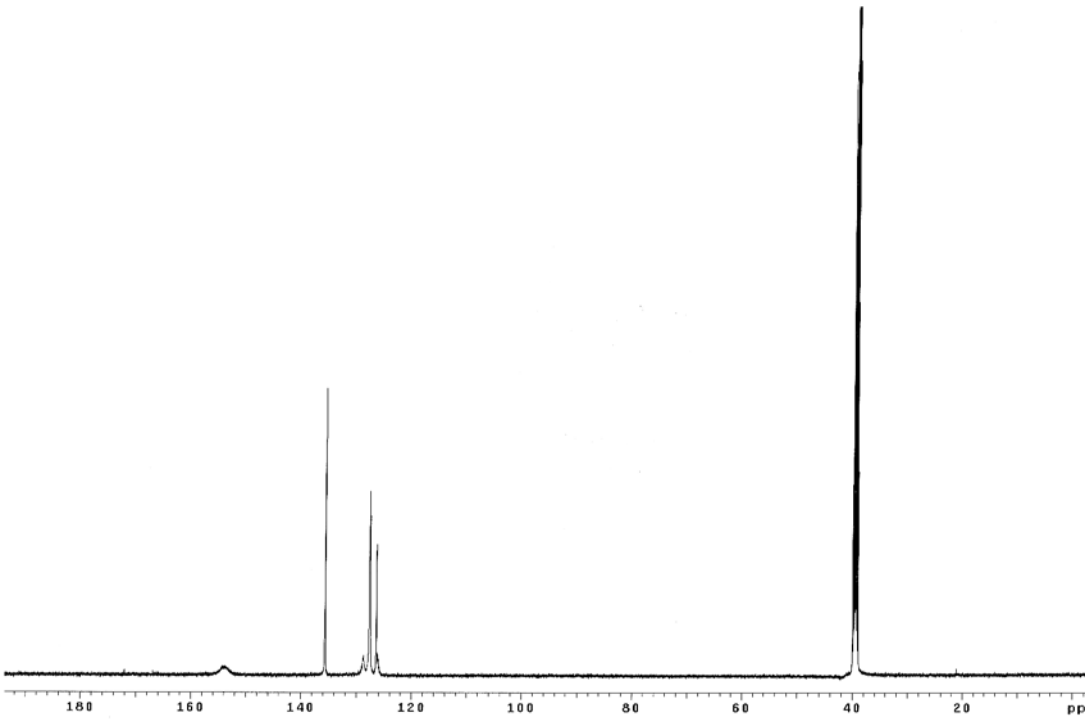

^{13}C NMR (DMSO-d$_6$)

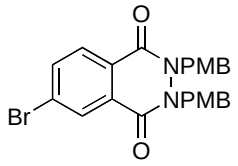

59a

6-Bromo-2, 3-bis(4-methoxybenzyl)-2, 3-dihydrophathazine-1, 4-dione A mixture of 6-bromo-2, 3-dihydrophathalazine-1, 4-dione **3** (526 mg, 2.18 mmol) and dry DMF (15 mL) in a 100 mL flask were cooled to 0 ^{o}C, then NaH (183 mg, 4.58 mmol) was added. The mixture was stirred for 30 min, and then PMBCl (0.63 mL, 4.58 mmol) was added into the flask dropwise. The reaction mixture was warmed up to 25 °C slowly and stirred for 14 h. Water (100 mL) was added to the reaction mixture, and the product was extracted from water with ethyl acetate (50 mL x 3). The combined organics were concentrated under reduced pressure, and the resulting crude product was purified by flash chromatography eluting with hexane and ethyl acetate (10:1) to give 430 mg (41%) **59a** as a colorless solid. FTIR (neat) 2832, 1726, 1650 cm^{-1} . ^{1}H NMR (300 MHz, $CDCl_3$), δ 8.54 (bs, 1H), 7.81 (m, 2H), 7.41 (d, *J* = 8.7 Hz, 2H), 7.36 (d, *J* = 8.7 Hz, 2H), 6.90 (d, *J* = 8.4 Hz, 2H), 6.85 (d, *J* = 8.7 Hz, 2H), 5.22(s, 2H), 5.22 (s, 2H), 3.83 (s, 3H), 3.79 (s, 3H). ^{13}C NMR (125 MHz, $CDCl_3$), δ 159.6, 159.2, 157.1, 149.22, 135.9, 130.5, 130.3, 130.1, 130.1, 129.1, 128.2, 126.7, 125.3, 123.4, 113.9, 113.8, 68.5, 55.3, 55.2, 53.6. HRMS (ESI) calcd for $C_{24}H_{22}BrN_2O_4^+$ $(M+H)^+$, 481.0763, found, 481.0757, 483.0741. TLC (50 % EtOAc-Hexane) R_f = 0.78.

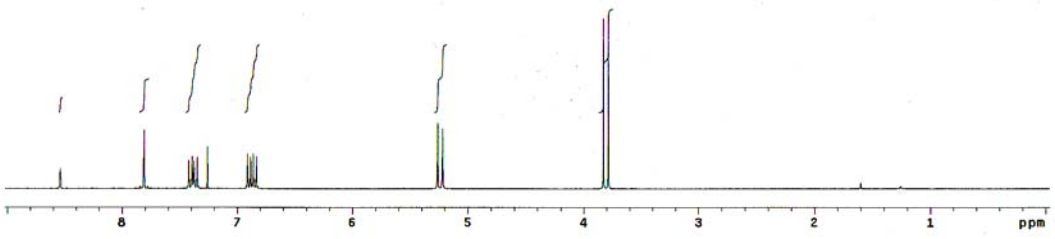

^{1}H NMR ($CDCl_3$)

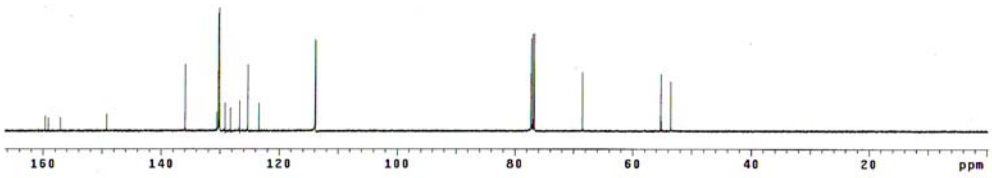

^{13}C NMR ($CDCl_3$)

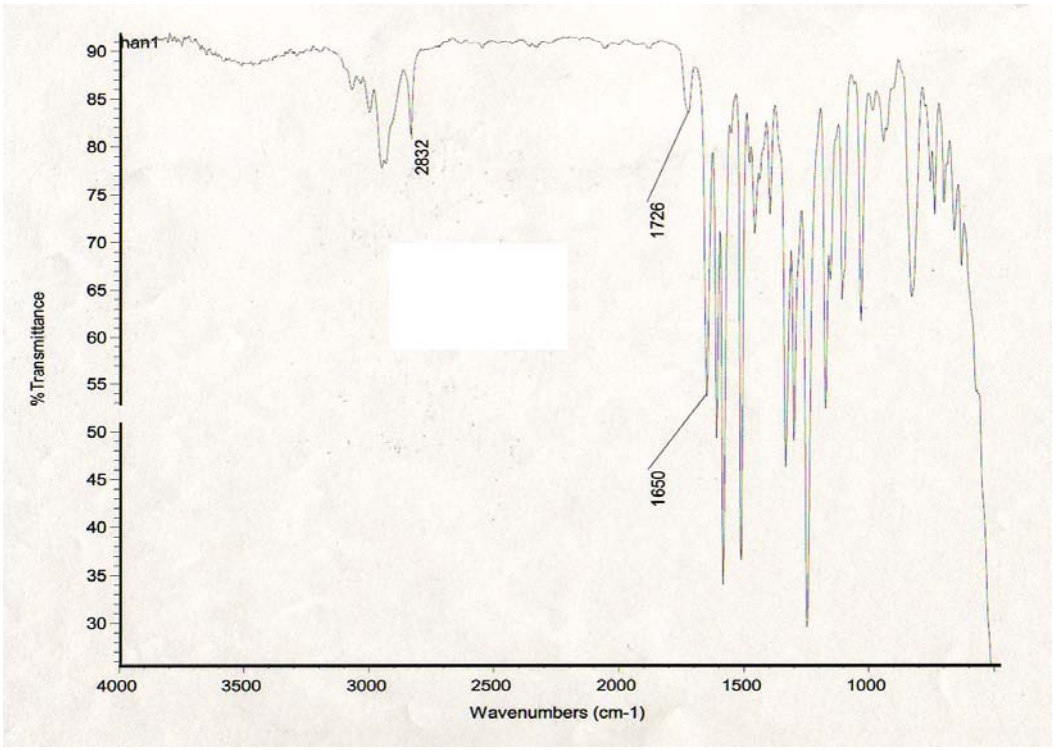
han1
%Transmittance
Wavenumbers (cm-1)
2832
1726
1650
90
85
80
75
70
65
60
55
50
45
40
35
30
4000
3500
3000
2500
2000
1500
1000

IR

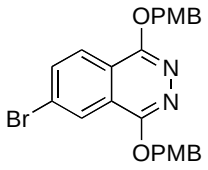

59b

6-Bromo-1, 4-bis (4-methoxybenzyloxy) phathalazine The same procedure above for preparing **59a** also afforded **59b** (471 mg, 45%) at the same time. FTIR (neat) 2832, 1650, 1609 cm^{-1}. ^1H NMR (300 MHz, $CDCl_3$), δ 8.24 (d, *J* = 8.2 Hz, 1H), 8.08 (d, *J* = 2.0 Hz, 1H), 7.81 (dd, *J* = 8.2 Hz, 2.0 Hz, 1H), 7.41 (d, *J* = 8.4 Hz, 2H), 7.37 (d, *J* = 8.5 Hz, 2H), 6.91 (d, *J* = 8.2 Hz, 2H), 6.86 (d, *J* = 8.4 Hz, 2H), 5.26 (s, 2H), 5.21(s, 2H), 3.81 (s, 3H), 3.60 (s, 3H). ^{13}C NMR (125 MHz, $CDCl_3$), δ 159.5, 159.0, 157.7, 148.1, 134.9, 130.1, 130.0, 129.0, 128.9, 128.0, 127.8, 127.7, 126.1, 125.9, 113.8, 113.7, 68.5, 55.1, 55.1, 53.4. TLC (50 % EtOAc-Hexane) R_f = 0.52.

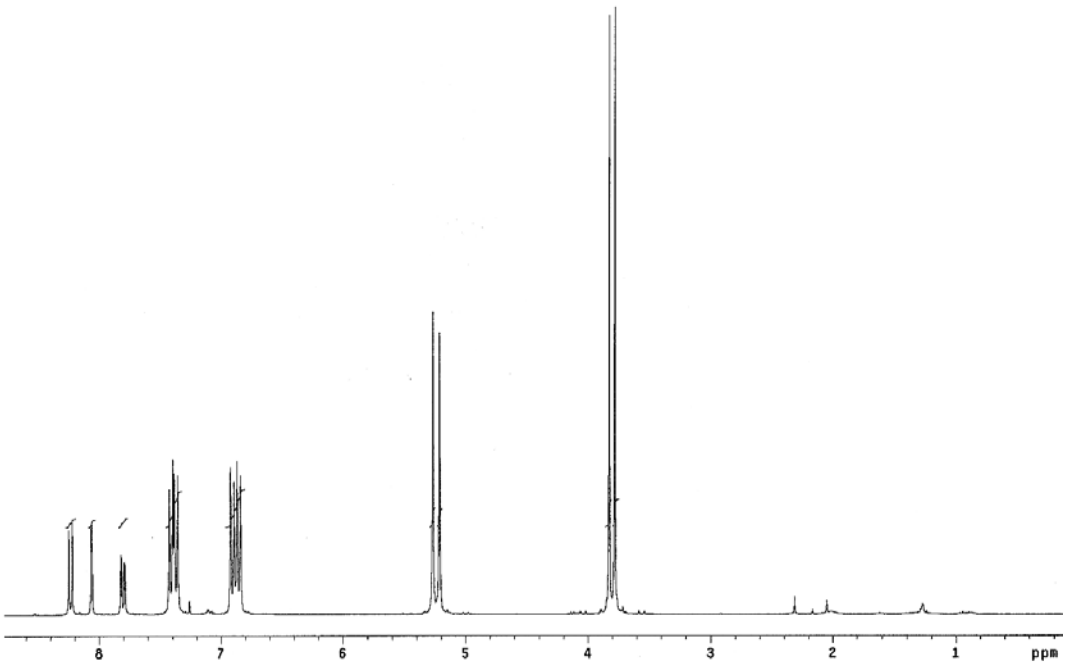

^{1}H NMR ($CDCl_3$)

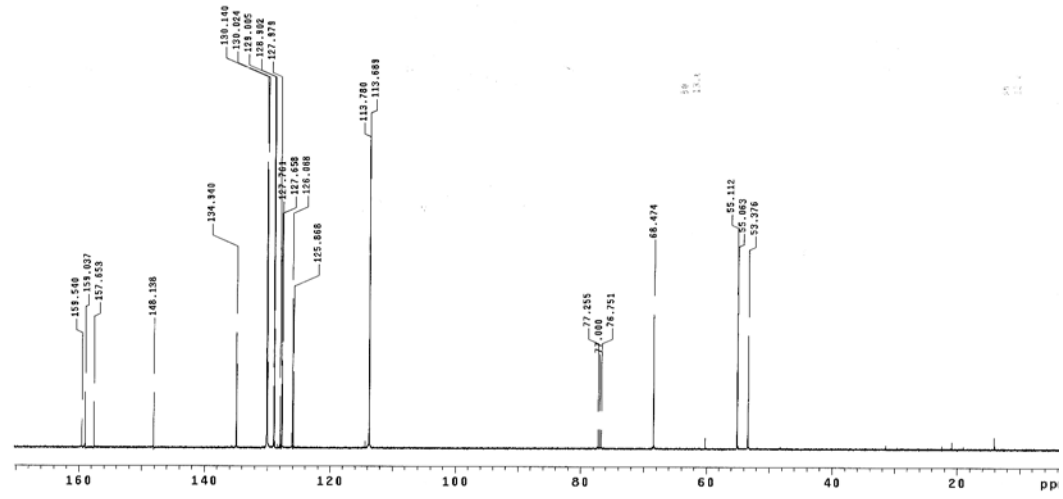

^{13}C NMR ($CDCl_3$)

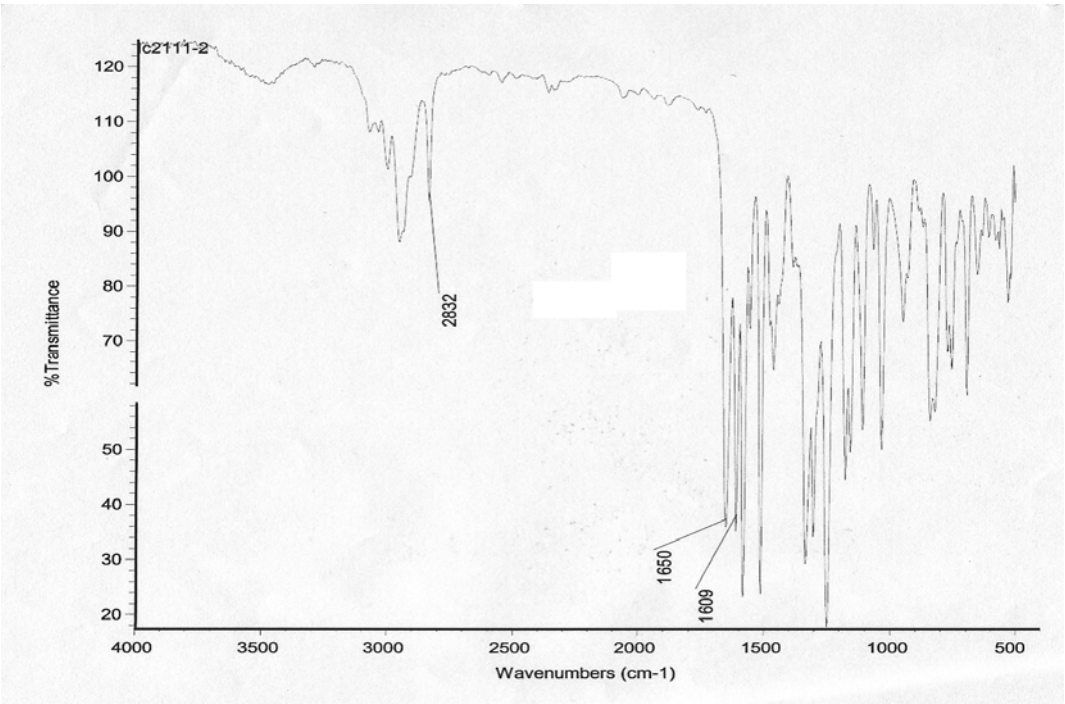
c2111-2
%Transmittance
120
110
100
90
80
70
50
40
30
20
2832
1650
1609
4000
3500
3000
2500
2000
1500
1000
500
Wavenumbers (cm-1)

IR

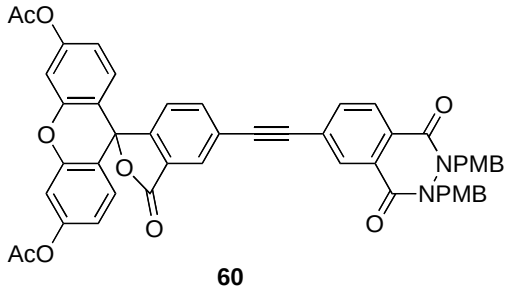

60

5-((2,3-Bis(4-methoxybenzyl)-1,4-dioxo-1,2,3,4-tetrahydrophthalazin-6-yl)ethynyl)-3-oxo-3H-spiro[isobenzofuran-1,9'-xanthene]-3',6'-diyl diacetate

Compound **59a** (103 mg, 0.215 mmol), 5-ethynyl-3-oxo-3*H*-spiro[isobenzofuran-1,9'-xanthene]-3',6'-diyl diacetate **C** (104 mg, 0.236 mmol), $PdCl_2(PPh_3)_2$ (8 mg, 0.02 mmol), CuI (4 mg, 0.04 mmol), Et_3N (0.3 mL, 2.15 mmol), and THF 2.0 mL were added to a sealed microwave tube. This tube was subjected to microwave irradiation at 120°C for 20 min. The solvent was removed under reduced pressure. The crude product was purified by flash chromatography over silica gel eluting with hexane/ethyl acetate (2:1) to give **60** (104 mg, 58 %) as a colorless solid. ^{1}H NMR (300 MHz, $CDCl_3$), δ 8.57 (d, *J* = 0.9 Hz, 1H), 8.18 (m, 1H), 7.96 (d, *J* = 8.4 Hz, 1H), 7.86 (dd, *J* = 5.4 Hz, 1.8 Hz, 1H), 7.83 (dd, *J* = 5.1 Hz, 1.5 Hz, 1H), 7.42 (d, *J* = 8.7 Hz, 2H)), 7.36 (d, *J* = 8.7 Hz, 2H), 7.20 (dd, *J* = 8.1 Hz, 0.3 Hz, 1H), 7.11 (m, 2H), 6.84-6.92 (m, 8H), 5.29 (s, 2H), 5.25 (s, 2H), 3.83 (s, 3H), 3.79 (s, 3H), 2.32 (s, 6H). ^{13}C NMR (75 MHz, $CDCl_3$), δ 168.8, 168.1, 159.6, 159.1, 157.6, 152.5, 152.1, 151.5, 149.2, 138.4, 135.2, 130.6, 130.3, 130.1, 129.3, 129.2, 128.9, 128.3, 126.6, 126.0, 125.0, 124.3, 124.2, 123.8, 117.9, 115.9, 113.9, 113.8, 110.5, 90.3 (2C), 68.5, 55.3, 55.2, 53.5, 21.1. HRMS (MALDI) calcd for $C_{50}H_{36}N_2O_{11}^+$ $(M+H)^+$, 841.2397, found, 841.2381. TLC (50 % EtOAc-Hexane) R_f = 0.60.

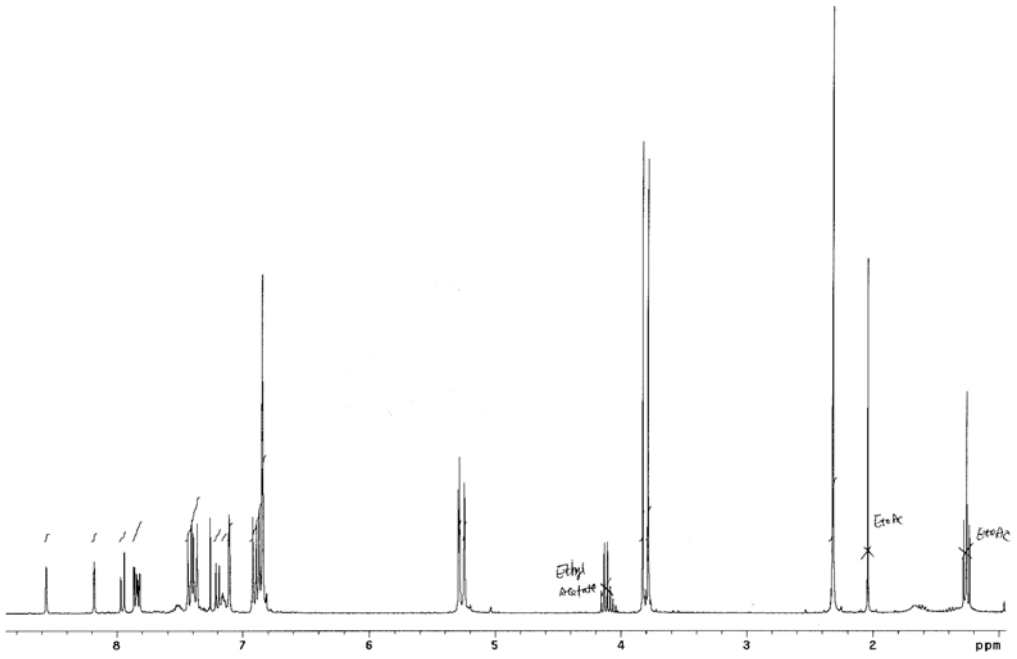

^{1}H NMR ($CDCl_3$)

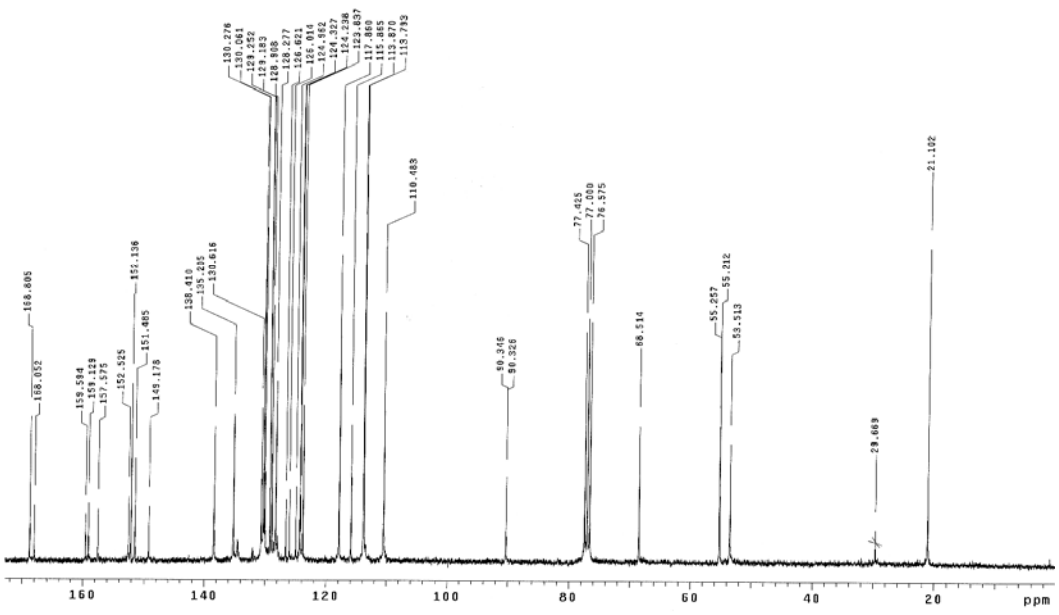

^{13}C NMR ($CDCl_3$)

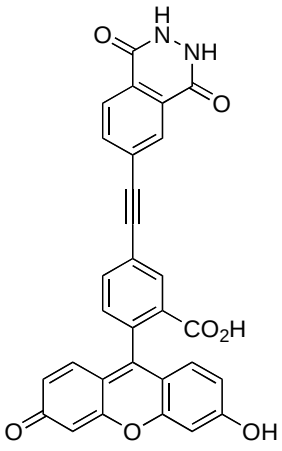

56

5-((1,4-Dioxo-1,2,3,4-tetrahydrophthalazin-6-yl)ethynyl)-2-(6-hydroxy-3-oxo-3*H*-xanthen-9-yl)benzoic acid 5-((2,3-Bis(4-methoxybenzyl)-1,4-dioxo-1,2,3,4-tetrahydrophthalazin-6-yl)ethynyl)-3-oxo-3*H*-spiro[isobenzofuran-1,9'-xanthene]-3',6'-diyl diacetate **60** (45 mg, 0.055 mmol) and TFA 5 mL were added to a 25 mL flask. The mixture was heated to 70 ^{o}C for 1h. The solvent was removed under reduced pressure. The crude product was dissolved in 1 mL NaOH (1M), acidified with one drop of concentrated HCl, then a yellow solid precipitated out. The crude product was separated by filtration, washed with 5 mL water and 10 mL ethyl acetate to afforded 24 mg (88%) desired product. IR (neat) 3428, 1638 cm^{-1}. ^{1}H NMR (500 MHz, DMSO), δ 8.26 (s, 1H), 8.23 (s, 1H), 8.11 (d, *J* = 8.0 Hz, 1H), 8.00 (d, *J* = 7.5 Hz, 1H), 7.92 (d, *J* = 8.5 Hz, 1H), 7.31 (d, *J* = 8.0 Hz, 1H), 6.65 (d, *J* = 9.0 Hz, 2H), 6.58 (s, 2H), 6.50 (d, *J* = 8.0 Hz, 2H), HRMS (ESI) calcd for $C_{30}H_{15}N_2O_7^-$ $(M-H)^-$, 515.0885, found, 515.0873. Reverse phase analytical HPLC: R. T. = 5.533 min (UV detector), 5.483 min (fluorescence detector).

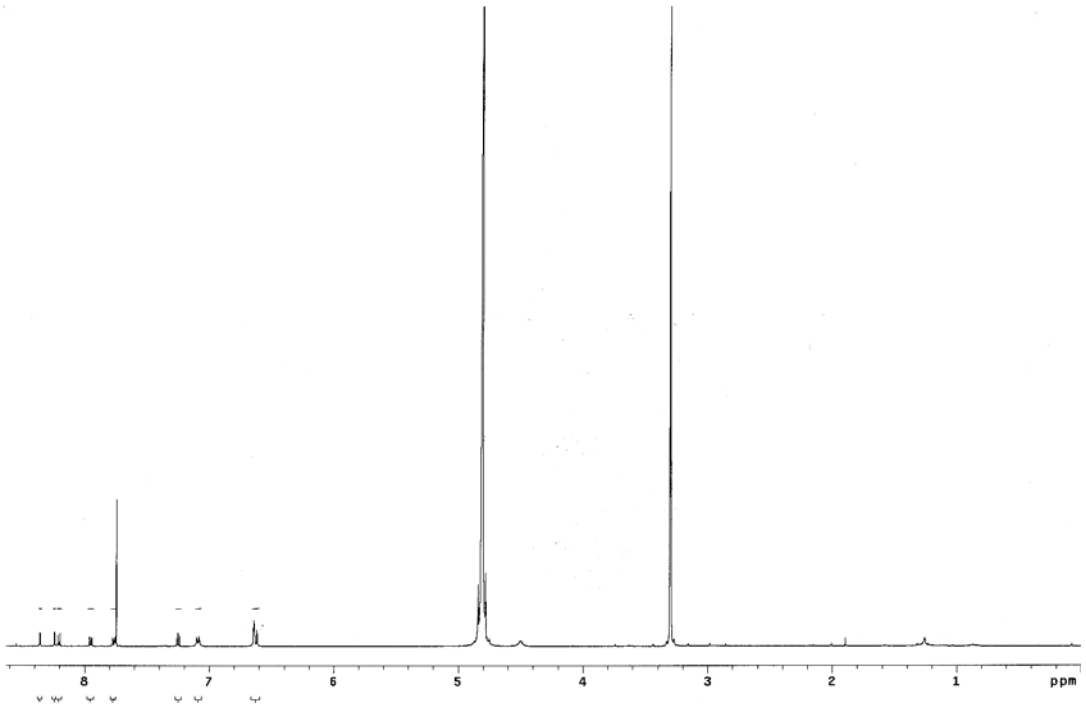

^{1}H NMR ($CDCl_3$)

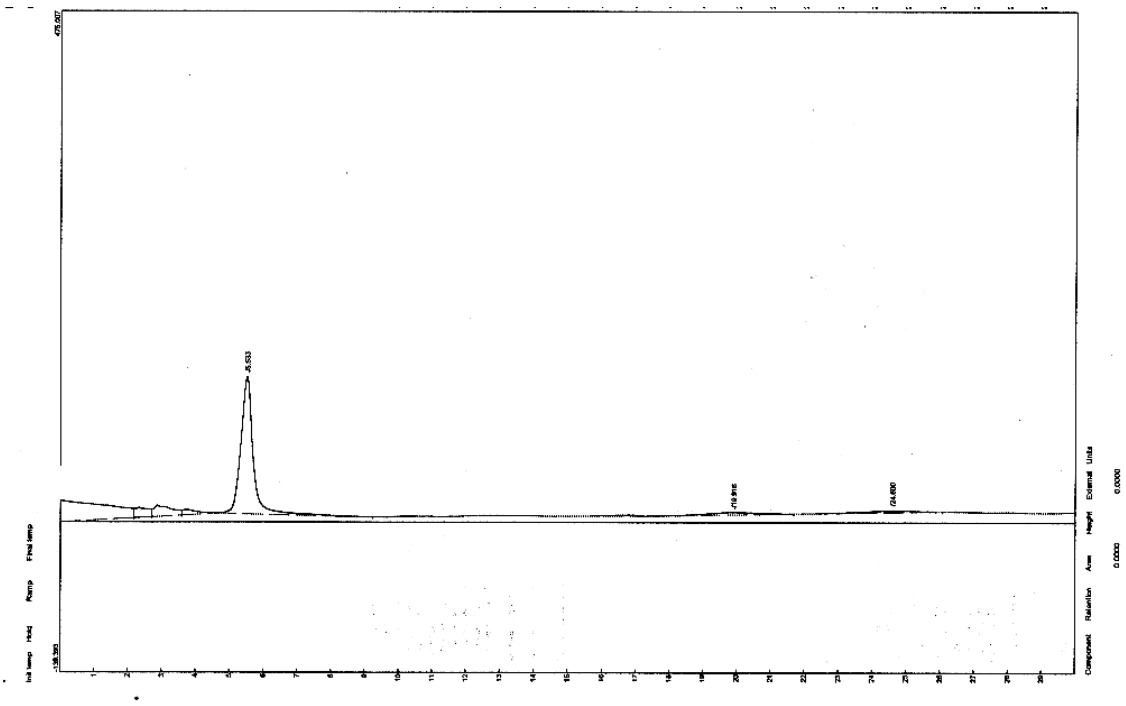

HPLC (UV detector)

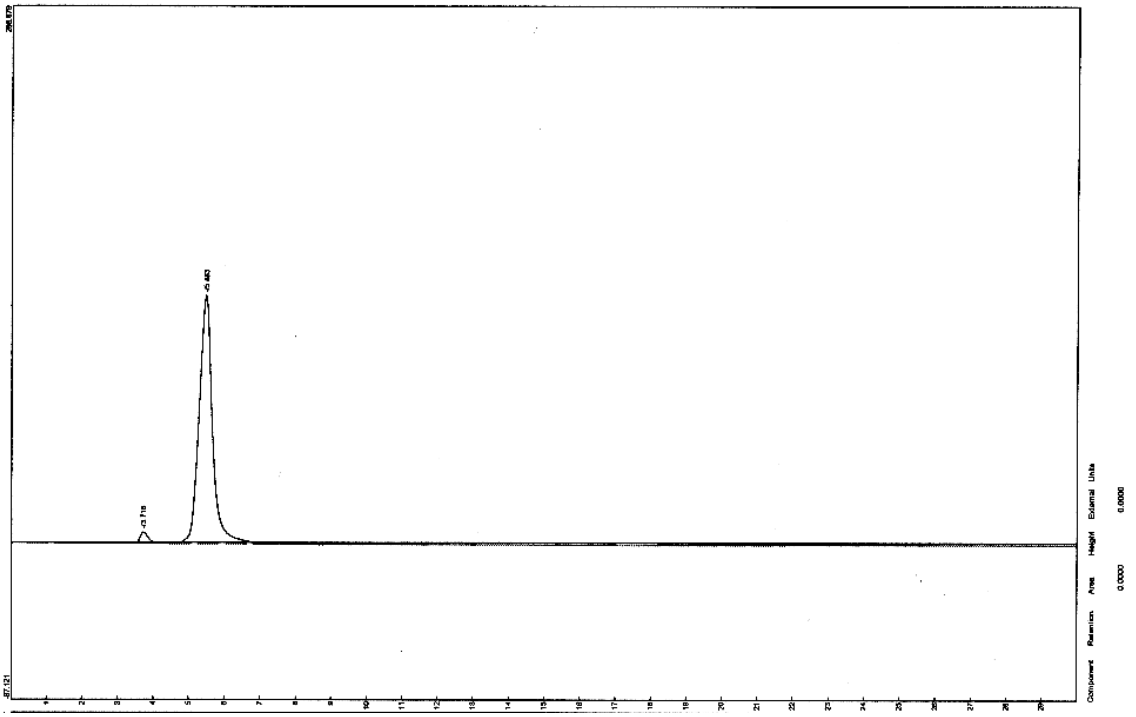

HPLC (fluorescence detector)

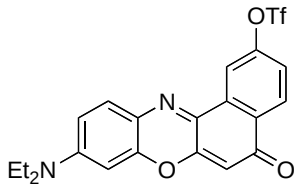

61

9-(Diethylamino)-5-oxo-5*H*-benzo[a]phenoxazin-2-yl trifluoromethanesulfonate. A mixture of compound **Q** (230 mg, 0.689 mmol), *N*-phenyltrifluoromethane sulfonamide (615 mg, 1.72 mmol) and Et_3N (0.24 mL, 1.72 mmol) was stirred at 20 ^oC in dry THF for 1 d. The reaction solvent was removed under reduced pressure to afford dark red solid. The crude product was purified by flash column eluting with 3% MeOH: CH_2Cl_2 to give the desired product as a dark red solid 240 mg (75%). FTIR (neat) 3077, 2985, 1642, 1622, 1589 cm^{-1}. ^1H NMR (300 MHz, $CDCl_3$), δ 8.54 (d, *J* = 2.7 Hz, 1H), 8.41 (d, *J*= 8.4 Hz, 1H), 7.66 (d, *J* = 9.3 Hz, 1H), 7.50 (dd, *J* = 8.7, 2.4 Hz, 1H), 6.72 (dd, *J* =9.0, 2.7 Hz, 1H), 6.50 (d, *J* = 2.7 Hz, 1H), 6.41 (s, 1H), 3.50 (q, 4.5 Hz, 4H), 1.29 (t, *J* = 4.5 Hz, 6H), ^{13}C NMR (75 MHz, $CDCl_3$), δ 181.9, 152.6, 151.5, 151.5, 147.2, 137.8, 134.3, 131.7, 131.1, 128.7, 125.2, 122.2, 116.6, 110.3, 109.8, 105.5, 96.2, 45.2, 12.6. ^{19}F NMR (300 MHz, $CDCl_3$), δ -73.1. HRMS (ESI) calcd for $C_{21}H_{18}F_3N_2O_5S$ $(M+H)^+$ 467.0889, found, 467.0873. TLC (50 % EtoAc-Hexane) R_f = 0.50.

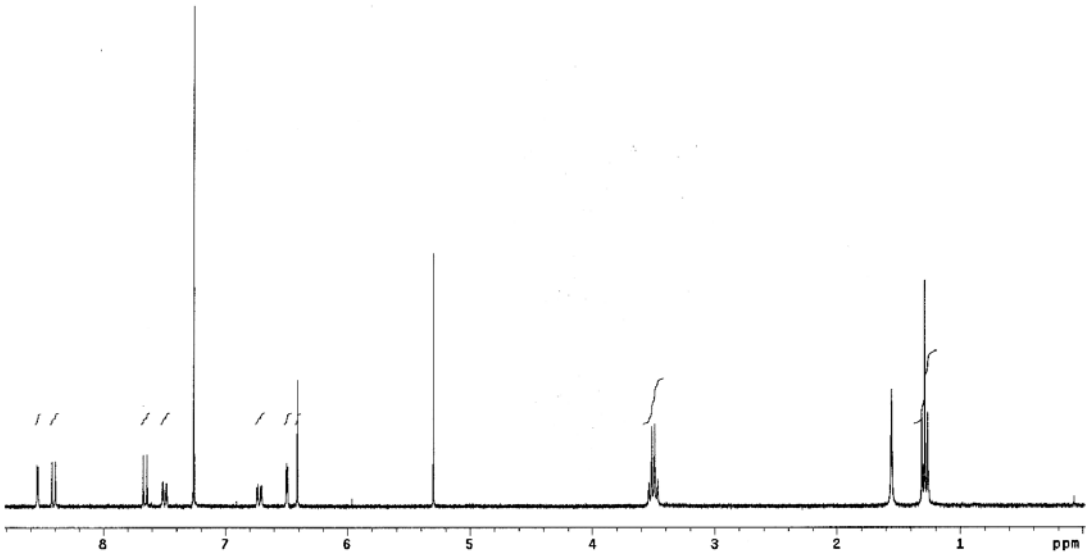

^{1}H NMR ($CDCl_3$)

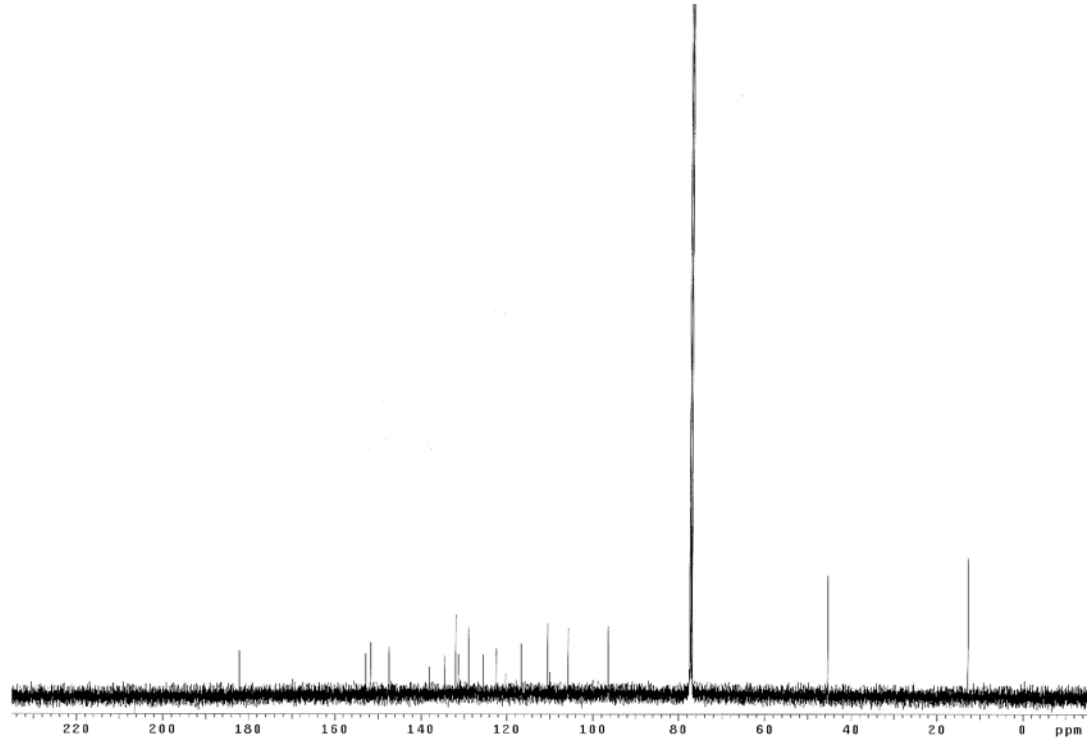

^{13}C NMR ($CDCl_3$)

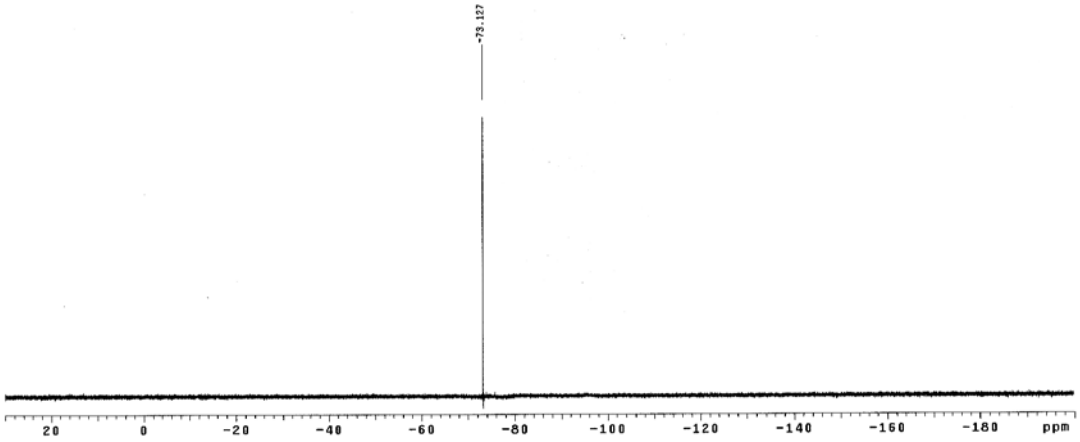

^{19}F NMR ($CDCl_3$)

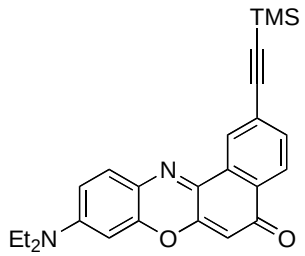

62

9-(Diethylamino)-2-((trimethylsilyl)ethynyl)-5*H*-benzo[*a*]phenoxazin-5-one.

A mixture of compound **61** (190 mg, 0.408 mmol), trimethylsilylacetylene (0.58 mL, 4.08 mmol), Et_3N (0.57 mL, 4.08 mmol), $Pd(PPh_3)_4$ (47 mg, 0.041 mmol), CuI (16 mg, 0.082 mmol) were dissolved in 4.0 mL dry DMF. After degassed three times via the freeze-thaw method, the mixture was heated up to 80°C for 4 h. The reaction solvent was removed under reduced pressure and the crude product is purified by flash column eluting with 50% hexane : ethyl acetate to give the desired product as a dark red solid 145 mg (80%). ^{1}H NMR (300 MHz, $CDCl_3$), δ 8.70 (d, *J* = 1.5 Hz, 1H), 8.21 (d, *J* = 8.1 Hz, 1H), 7.67 (dd, *J* = 8.1 Hz, 1.5 Hz, 1H), 6.57 (d, *J* = 9.3 Hz, 1H), 6.63 (dd, *J* = 9.3 Hz, 3.0 Hz, 1H), 6.41 (d, *J* = 2.7 Hz, 1H), 6.35 (s, 1H), 3.43 (q, *J* = 7.2 Hz, 4H), 1.25 (t, *J* = 7.2 Hz, 6H), 0.30 (s, 9H), ^{13}C NMR (75 MHz, $CDCl_3$), δ 182.9, 152.2, 150.9, 146.8, 138.9, 132.7, 131.9, 131.2, 130.9, 127.3, 126.1, 125.6, 125.0, 109.9, 105.8, 104.5, 97.1, 96.2, 45.1, 12.6, -0.1. HRMS (ESI) calcd for $C_{25}H_{27}N_2O_2Si$ $(M+H)^+$, 415.1842, found 415.1795. TLC (50 % EtOAc-Hexane) Rf = 0.73.

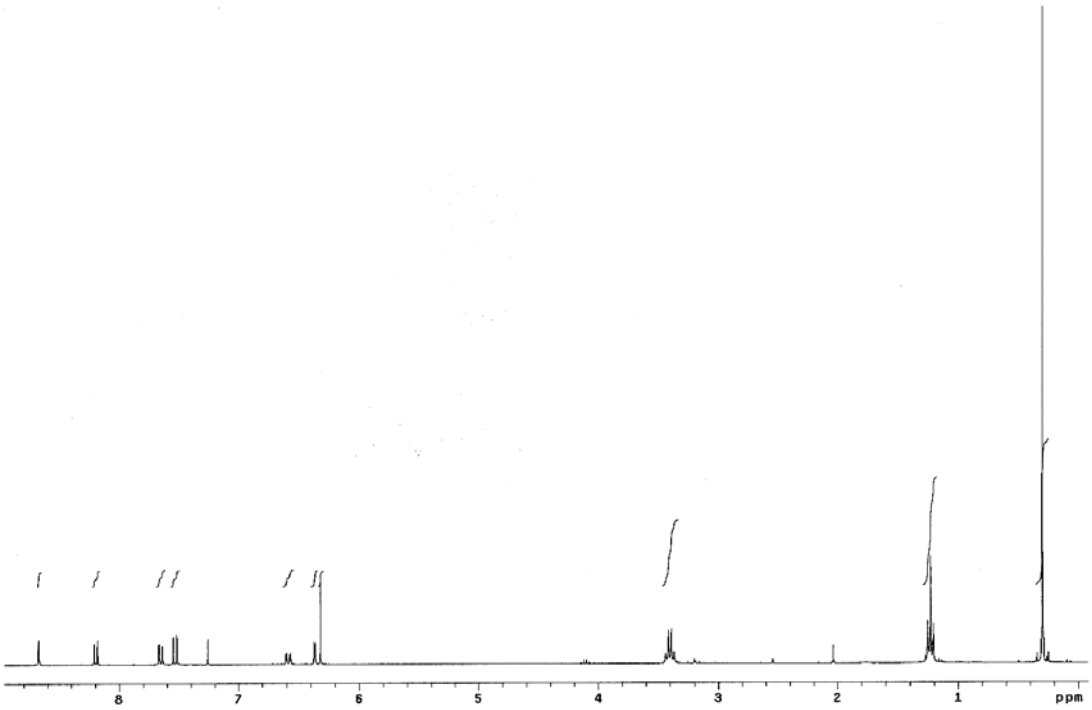

^{1}H NMR ($CDCl_3$)

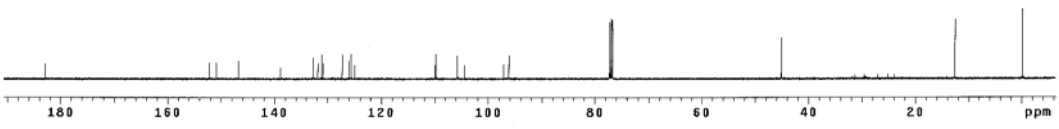

^{13}C NMR ($CDCl_3$)

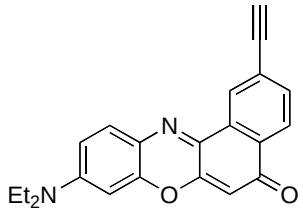

63

9-(diethylamino)-2ethynyl-5*H*-benzo[*a*]phenoxazin-5-one. Compound **62** (130 mg, 0.313 mmol) was dissolved in 6mL dichloromethane at room temperature. TBAF (0.63 mL, 0.1M) in THF was added dropwise to the reaction mixture. The reaction was complete in 5 min. The solvent was removed under reduced pressure and the crude product was purified by flash column eluting with 50% hexane : ethyl acetate to provide dark red solid 102 mg (95%). FTIR (neat) 3095, 2974, 1622, 1597, 1580 cm^{-1}. ^{1}H NMR (500 MHz, $CDCl_3$), δ 8.75 (d, *J* = 1.5 Hz, 1H), 8.24(d, *J* = 8.1 Hz, 1H), 7.70 (dd, *J* = 8.1 Hz, 1.5 Hz, 1H), 7.57 (d, *J* = 9.3 Hz, 1H), 6.65 (dd, *J* = 9.3 Hz, 3.0 Hz, 1H), 6.43 (d, *J* = 3.0 Hz, 1H), 6.36 (s, 1H), 3.45 (q, *J* = 7.2 Hz, 4H), 3.26 (s, 1H), 1.26 (t, *J* = 7.2 Hz, 6H). ^{13}C NMR (125 MHz, $CDCl_3$), δ 182.9, 152.3, 151.0, 146.8, 138.8, 132.8, 132.0, 131.3, 131.3, 127.7, 125.8, 125.1, 125.0, 109.9, 105.8, 96.2, 83.2, 79.5, 45.1, 12.6. HRMS (ESI) calcd for $C_{22}H_{19}N_2O_2$ $(M+H)^+$ 343.1447, found 343.1441. mp 203-206 ^{o}C. TLC (33 % EtOAc-Hexane) R_f = 0.32.

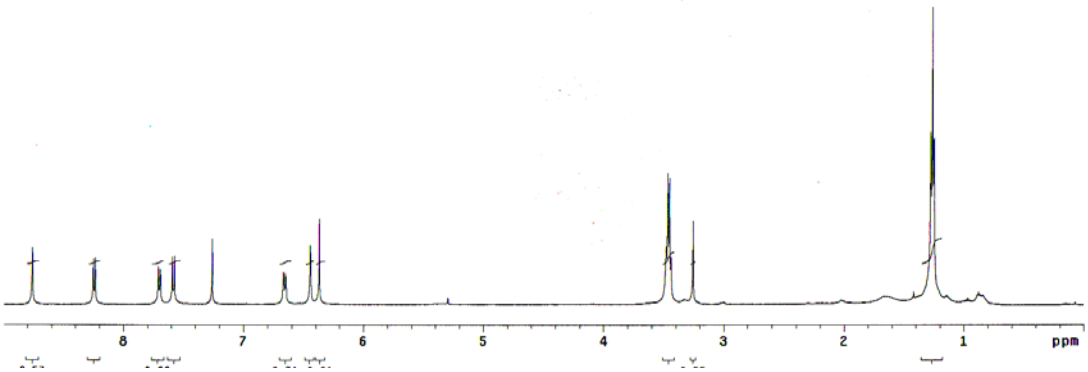

^{1}H NMR ($CDCl_3$)

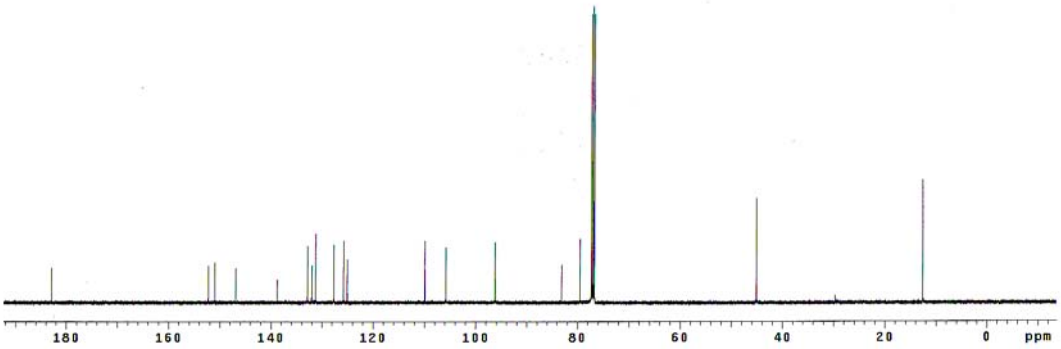

^{13}C NMR ($CDCl_3$)

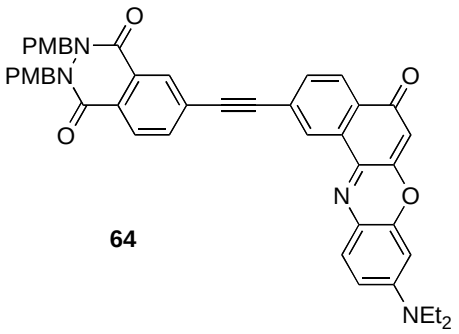

64

6-((9-(Diethylamino)-5-oxo-5*H*-benzo[*a*]phenoxazin-2-ethynyl)-2,3-bis(4-methoxybenzyl)-2,3-dihydrophthalazine-1,4,-dione. A mixture of compound **63** (55 mg, 0.161 mmol), **59a,** (70 mg, 0.146mmol), Et_3N (0.22 mL, 1.61 mmol), $Pd(PPh_3)_4$ (19 mg, 0.016 mmol), CuI (6 mg, 0.032 mmol) were dissolved in 8 mL 25% DMF:THF. After the solution was degassed three times via the freeze-thaw method, the mixture was heated to 80 ^oC for 4 h. The reaction solvent was removed under reduced pressure and the crude product was purified by flash column eluting with 50% hexane:ethyl acetate to give the desired product as a dark red solid 75 mg (69%). ^1H NMR (300 MHz, $CDCl_3$), δ 8.83 (d, J = 1.8 Hz, 1H), 8.61 (d, J = 1.5 Hz, 1H), 8.31 (d, *J* = 8.1 Hz, 1H), 7.97 (d, *J* = 8.1 Hz, 1H), 7.89 (dd, J = 8.1 Hz, 1.5 Hz, 1H), 7.78 (dd, *J* = 8.1 Hz, 1.5 Hz, 1H), 7.65 (d, *J* = 9.3 Hz, 1H), 7.46 (d, J = 8.7 Hz, 2H), 7.41 (d, *J* = 8.4 Hz, 2H), 6.94 (d, *J* = 8.4 Hz, 2H), 6.89 (d, *J* = 8.4 Hz, 2H), 6.70 (dd, *J* = 9.0 Hz, 2.4 Hz, 1H), 6.46 (d, *J* = 2.4 Hz, 1H), 6.41 (s, 1H), 5.30 (s, 2H), 5.28 (s, 2H), 3.86 (s, 3H), 3.82 (s, 3H), 3.49 (q, *J* = 7.2 Hz, 4H), 1.29 (t, *J* = 7.2 Hz, 6H), ^{13}C NMR (75 MHz, $CDCl_3$), δ 182.8, 159.6, 159.1, 157.6, 152.2, 151.0, 149.2, 146.8, 138.7, 135.2, 132.3, 132.0, 131.3, 131.2, 130.5, 130.3, 130.0, 129.3, 129.2, 128.3, 127.4, 126.6, 125.9, 125.3, 125.1, 123.9, 123.7, 113.9, 113.8, 110.0, 105.8, 96.1, 92.3, 90.4, 68.4, 55.3, 55.2, 53.4, 45.1, 12.6. MALDI

MS calcd for $C_{46}H_{38}N_4O_6$ $(M+H)^+$ 743.2864, found 743.3370. TLC (67 % EtOAc-Hexane) Rf = 0.70.

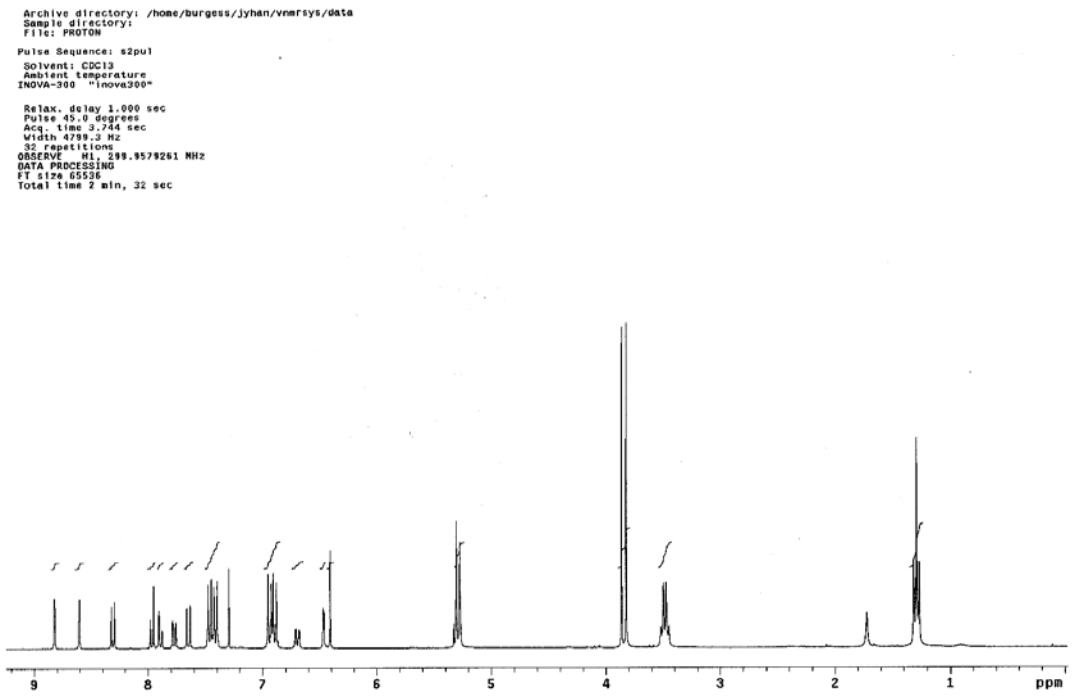

^{1}H NMR ($CDCl_3$)

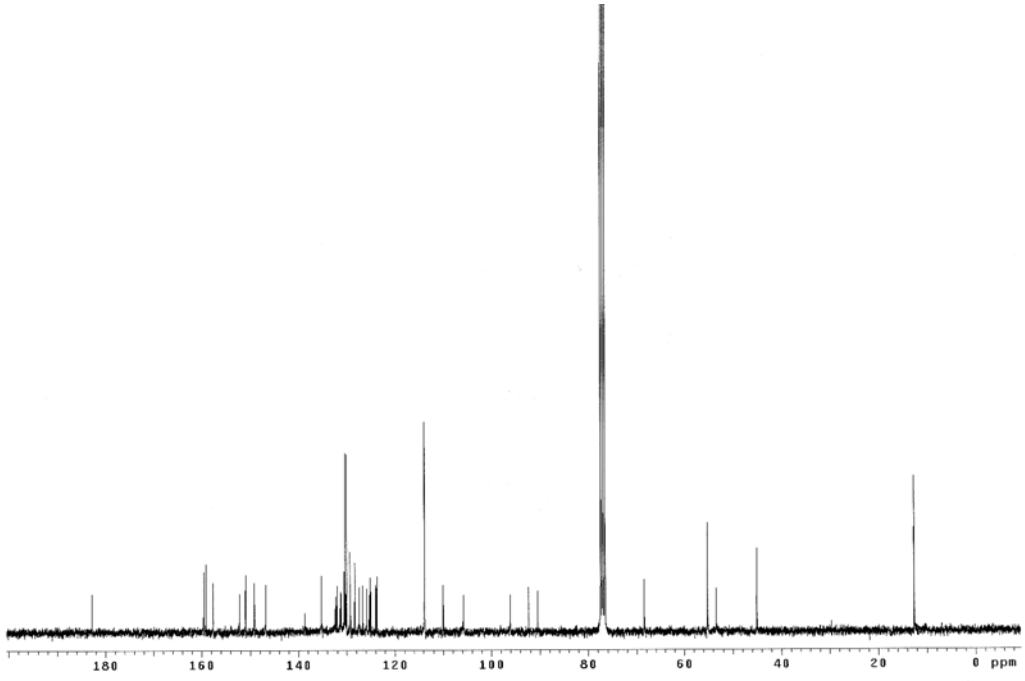

^{1}H NMR ($CDCl_3$)

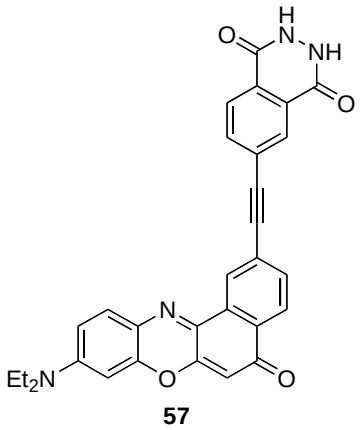

57

6-((9-(Diethylamino)-5-oxo-5H-benzo[*a*]phenoxazin-2-yl)ethynyl)-2,3-dihydrophthalazine-1,4-dione. Compound **64** (45 mg, 0.061 mmol) and 2 mL TFA were added to a 25 mL flask. The mixture was heated to 70 ^{o}C for 1 h. The solvent was removed under reduced pressure, and the crude product was recrystalized from AcOH (1.5 mL) to afford dark red solid 25 mg (82%). ^{1}H NMR (500 MHz, DMSO, 80 ^{o}C), δ 8.73 (s, 1H), 8.26 (s, 1H), 8.17 (d, *J* = 8.5 Hz, 1H), 8.12 (d, *J* = 8.5 Hz, 1H), 8.06 (d, *J* = 8.0 Hz, 1H), 7.87 (d, *J* = 8.5 Hz, 1H), 7.67 (d, *J* = 9.0 Hz, 1H), 6.86 (dd, *J* = 9.5 Hz, 2.0 Hz, 1H), 6.65 (d, *J* = 2.0 Hz, 1H), 6.30 (s, 1H), 3.53 (q, *J* = 7.0 Hz, 4H), 1.20 (t, *J* = 7.0 Hz, 6H). ^{13}C NMR (125 MHz, DMSO, 80 ^{o}C), δ 180.6, 151.7, 151.0, 146.2, 137.1, 134.5, 131.9, 131.7, 131.5, 130.9, 130.5, 128.0, 127.8, 126.2, 125.5, 125.2, 125.3, 124.3, 110.6, 104.7, 104.4, 96.5, 95.8, 95.3, 91.3, 90.1, 44.1, 12.0. HRMS (ESI) calcd for $C_{30}H_{23}N_4O_4$ $(M+H)^+$ 503.1719, found 503.1687. TLC (10 % MeOH-CH_2Cl_2) Rf = 0.57.

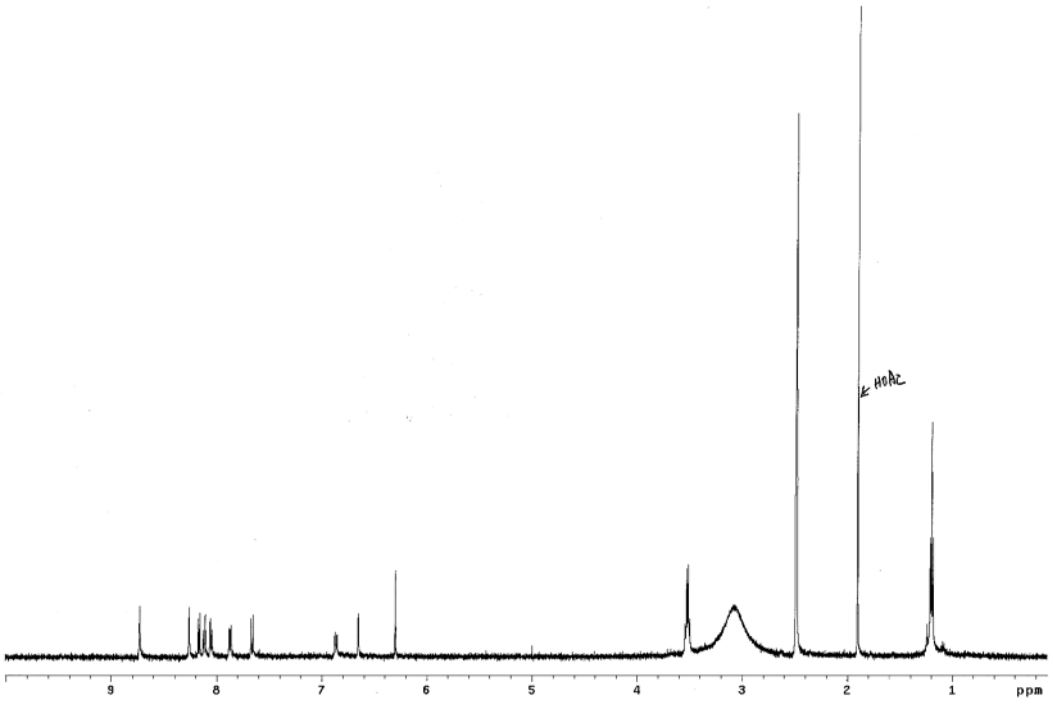

^{1}H NMR (DMSO-d_6 at 80 ^{o}C)

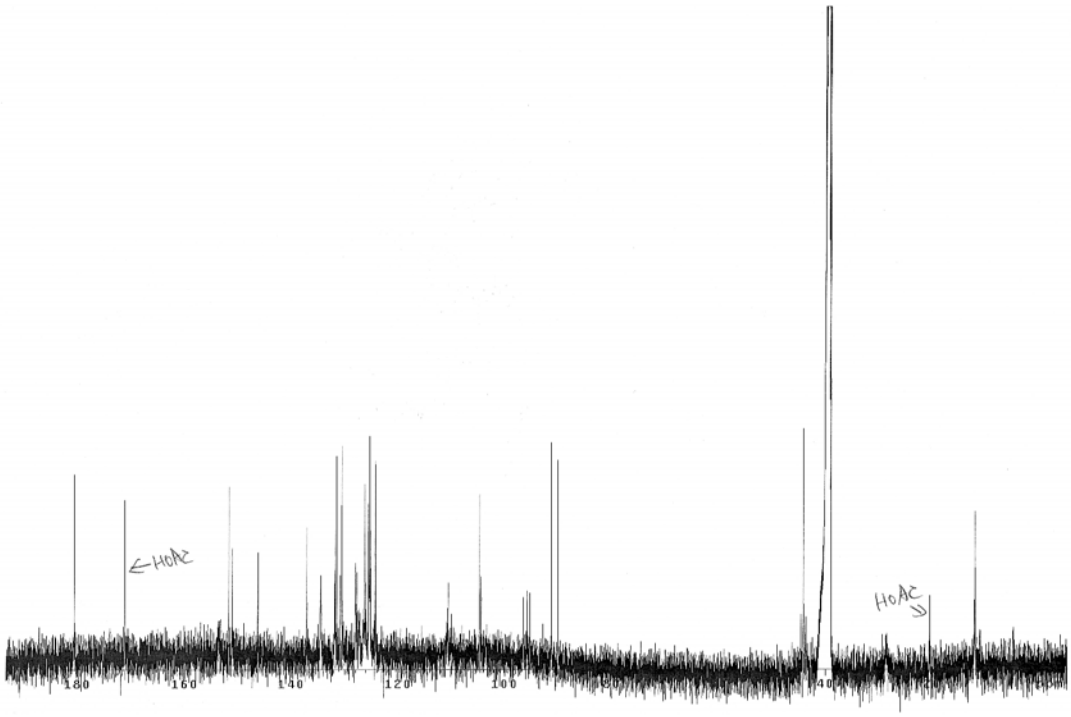

^{13}C (DMSO-d_6 at 80 ^{o}C)

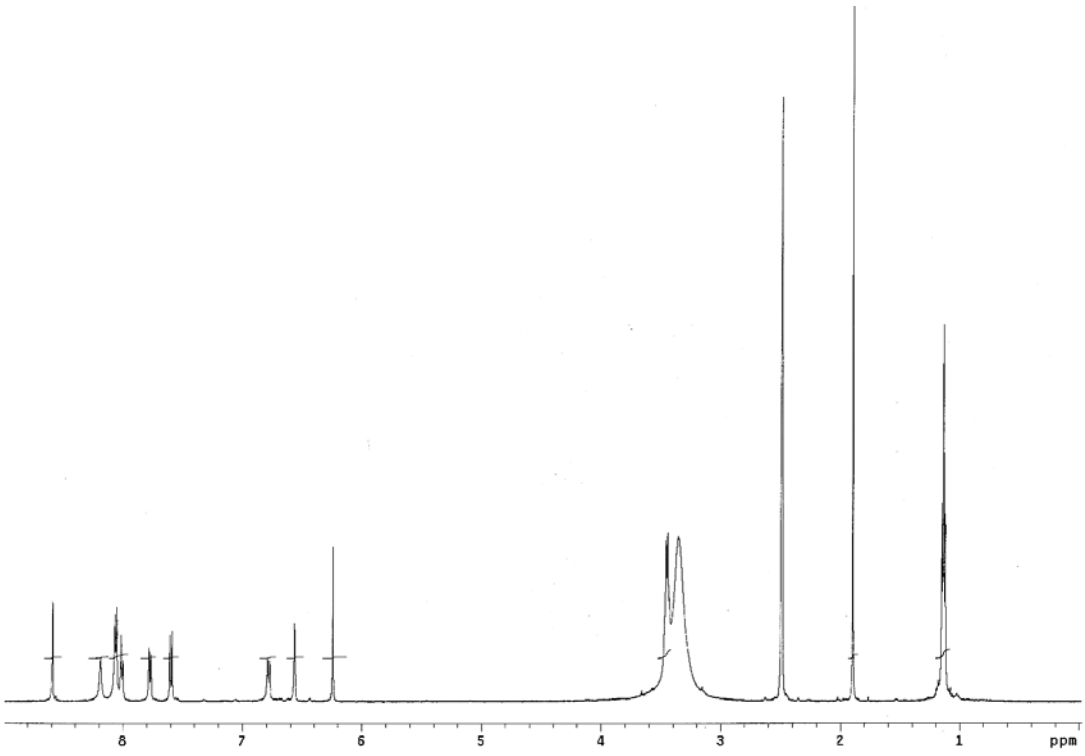

^{1}H NMR (DMSO-d_6 at 22 ^{o}C)

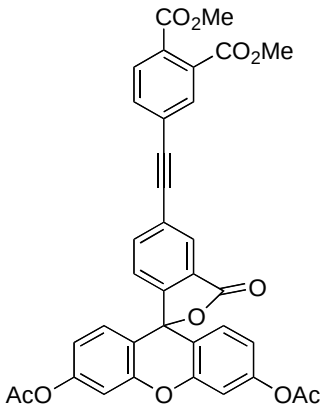

65

Dimethyl 4-((3', 6'-bis(ethanoyloxy)-3-oxo-3H-spiro[isobenzofuran-1,9'-xanthene]-5-yl)ethynyl)benzene-1,2-dicarboate. Dimethyl 4-bromobenzene-1,2-dicarboate (29 mg, 0.107 mmol), 5-ethynyl-3-oxo-3*H*-spiro[isobenzofuran-1,9'-xanthene]-3',6'-diyl diacetate **C** (52 mg, 0.118 mmol), $PdCl_2(PPh_3)_2$ (7 mg, 0.01 mmol), CuI (4 mg, 0.02 mmol), Et_3N (0.15 mL, 1.07 mmol), and THF 1.0 mL were added to a sealed microwave tube. This tube was subjected to microwave irradiation at 120 ^oC for 30 min. The solvent was removed under reduced pressure. The crude product was purified by flash chromatography over silica gel eluting with hexane/ethyl acetate (3:1) to give (40 mg, 60 %) as a colorless solid. ^1H NMR (300 MHz, $CDCl_3$), δ 8.19 (m, 1H), 7.92 (m, 1H), 7.84 (dd, *J* = 8.1 Hz, 0.9 Hz, 1H), 7.80 (d, *J* = 8.1 Hz, 1H), 7.73 (dd, *J* = 8.1 Hz, 0.9 Hz, 1H), 7.22 (d, *J* = 7.8 Hz, 1H), 7.13 (m, 2H)), 6.87 (d, *J* = 0.9 Hz, 4H), 3.96 (s, 3H), 3.95 (s, 3H), 2.34 (s, 6H). ^{13}C NMR (75 MHz, $CDCl_3$), δ 168.8, 168.0, 167.3, 167.2, 152.6, 152.2, 151.5, 138.3, 133.9, 132.6, 132.0, 131.4, 129.2, 128.8, 128.3, 126.6, 125.7, 124.9, 124.3, 117.9, 115.9, 110.5, 90.3, 89.8, 81.8, 52.8, 52.8, 21.1. HRMS (ESI) calcd for $C_{34}H_{25}O_{11}^+$ $(M+H)^+$, 633.1397, found, 633.1379. TLC (50 % EtOAc-Hexane) R_f = 0.68.

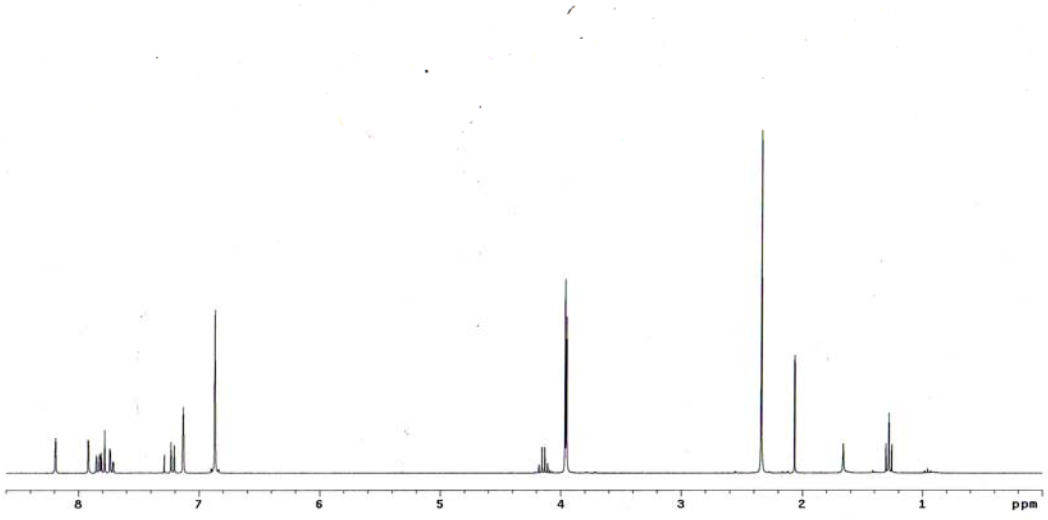

^{1}H NMR ($CDCl_3$)

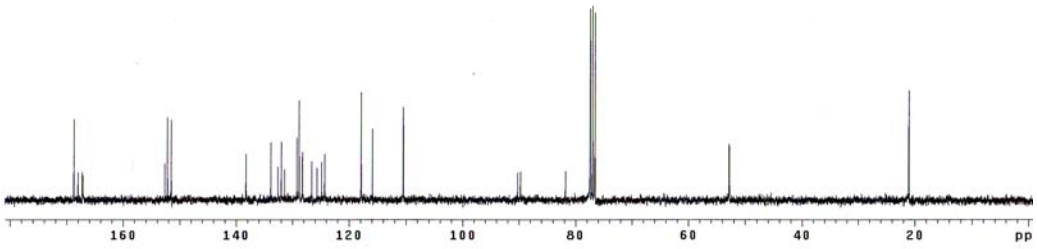

^{13}C NMR ($CDCl_3$)

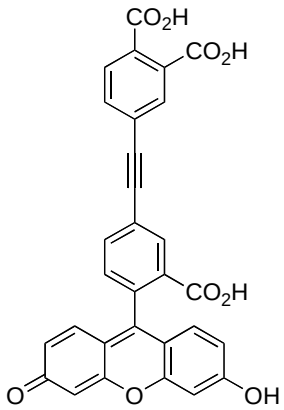

66

4-((3-Carboxy-4-(6-hydroxy-3-oxo-3H-xanthen-9-yl)phenyl)ethynyl)benzene -1,2-dicarboic acid. Compound **65** (35 mg, 0.055 mmol) was dissolved in 2 mL THF at room temperature. Potassium trimethylsilanolate (140 mg, 1.11mmol) was added to the reaction mixture. The reaction was complete in 15 h. The solvent was removed under reduced pressure. The crude product was dissolved in 2 mL water, acidified with two drops of concentrated HCl, then a yellow solid precipitated out. The crude product was separated by filtration, washed with 5 mL water and 10 mL ethyl acetate to afforded 26 mg (90%) desired product as an orange solid. ^{1}H NMR (500 MHz, CD_3OD), δ 8.19 (s, 1H), 7.93 (d, *J* = 8.5 Hz, 1H), 7.92 (s, 1H), 7.81 (d, *J* = 7.5 Hz, 1H), 7.78 (dd, *J* = 8.0 Hz, 1.3 Hz 1H), 7.26 (d, *J* = 8.0 Hz, 1H), 6.73 (d, *J* = 2.0 Hz, 1H), 6.68 (d, *J* = 9.0 Hz, 1H), 6.60 (dd, *J* = 9.0 Hz, 2.0 Hz, 1H). ^{13}C NMR (125 MHz, CD_3OD), δ 170.5, 170.5, 170.4, 162.0, 154.5, 153.5, 139.5, 135.0, 134.9, 133.9, 132.9, 130.5, 130. 5, 129.3, 129.1, 126.8, 126.3, 126.2, 126.0, 114.2, 111.3, 103.7, 91.2, 90.5. LRMS (ESI) calcd for $C_{30}H_{17}O_9$ $(M+H)^+$ 521.1, found 521.1.

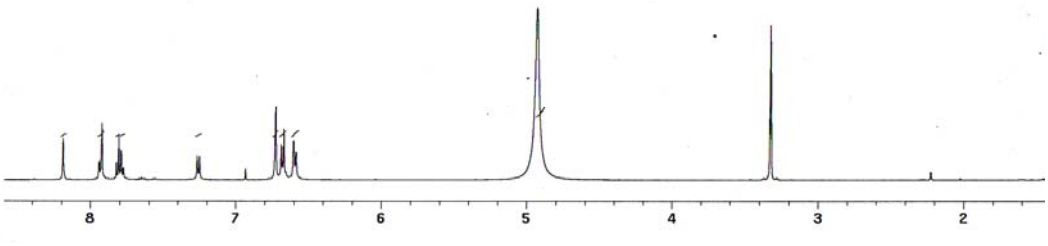

^{1}H NMR (CD_3OD)

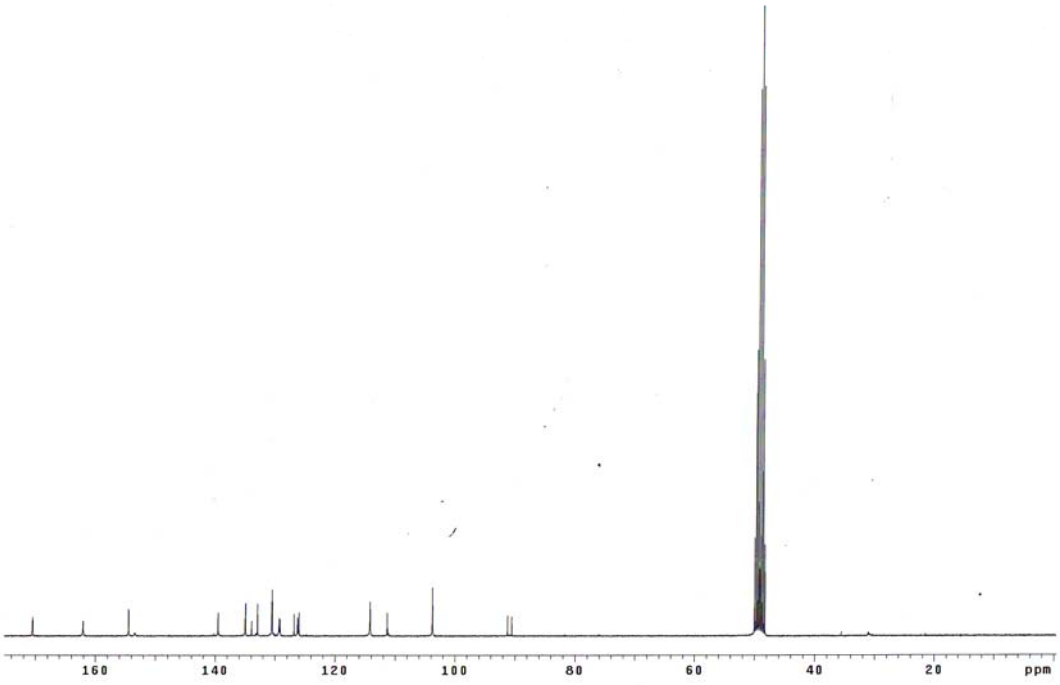

^{13}C NMR (CD_3OD

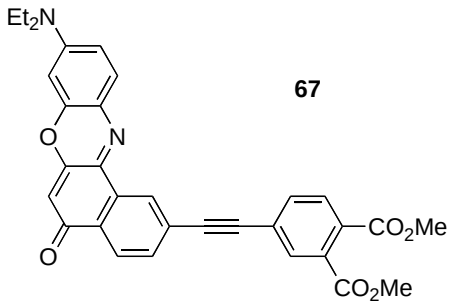

67

Dimethyl 4-(2-(9-(diethylamino)-5-oxo-5*H*-benzo[a]phenoxazin-2-yl)ethynyl)benzene-1,2-dioate. A mixture of compound **63** (47 mg, 0.137 mmol), dimethyl 4-bromobenzene-1,2-dicarboate (34 mg, 0.125 mmol)**,** Et_3N (0.17 mL, 1.25 mmol), $Pd(PPh_3)_4$ (15 mg, 0.013 mmol), CuI (5 mg, 0.026 mmol) were dissolved in 5 mL 25% DMF:THF. After the solution was degassed three times via the freeze-thaw method, the mixture was heated to 80 ^oC for 4 h. The reaction solvent was removed under reduced pressure and the crude product was purified by flash column eluting with 75% hexane : ethyl acetate to give the desired product as a dark red solid 31 mg (49%). FTIR (neat) 3066, 2977, 1728, 1622, 1594, 1580 cm^{-1}. ^1H NMR (500 MHz, $CDCl_3$), δ 8.84 (d, J = 1.5 Hz, 1H), 8.32 (d, J = 8.5 Hz, 1H), 7.94 (d, *J* = 1.5 Hz, 1H), 7.79 (d, *J* = 8.0 Hz, 1H), 7.77 (dd, J = 8.5 Hz, 1.5 Hz, 1H), 7.74 (dd, *J* = 8.0 Hz, 2.0 Hz, 1H), 7.66 (d, *J* = 9.0 Hz, 1H), 6.72 (dd, J = 9.0 Hz, 2.5Hz, 1H), 6.50 (d, *J* = 3.0 Hz, 1H), 6.42 (s, 1H), 3.97 (s, 3H), 3.95 (s, 3H), 3.50 (q, *J* = 7.0 Hz, 4H), 1.29 (t, *J* = 7.0 Hz, 6H). ^{13}C NMR (75 MHz, $CDCl_3$), δ 182.8, 167.4, 167.3, 152.3, 151.0, 146.9, 138.8, 133.8, 132.5, 132.4, 132.0, 131.3, 131.3, 131.0, 129.2, 127.3, 126.3, 126.0, 125.3, 125.1, 110.0, 105.9, 96.2, 94.7, 92.2, 89.8, 52.8, 52.8, 45.2, 12.6. LRMS (ESI) calcd for $C_{32}H_{27}N_2O_6$ $(M+H)^+$ 535.2, found 535.4. mp 233-236 ^oC. TLC (50 % EtoAc-Hexane) R_f = 0.29.

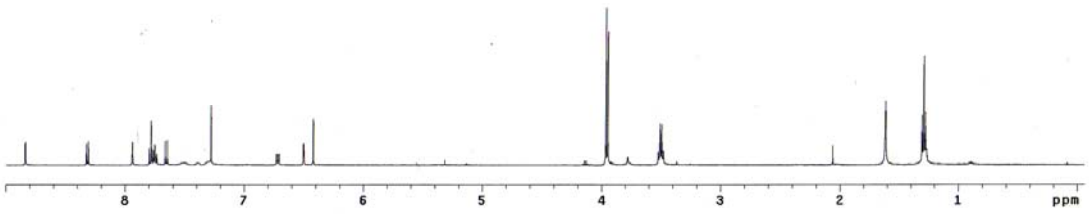

^{1}H NMR ($CDCl_3$)

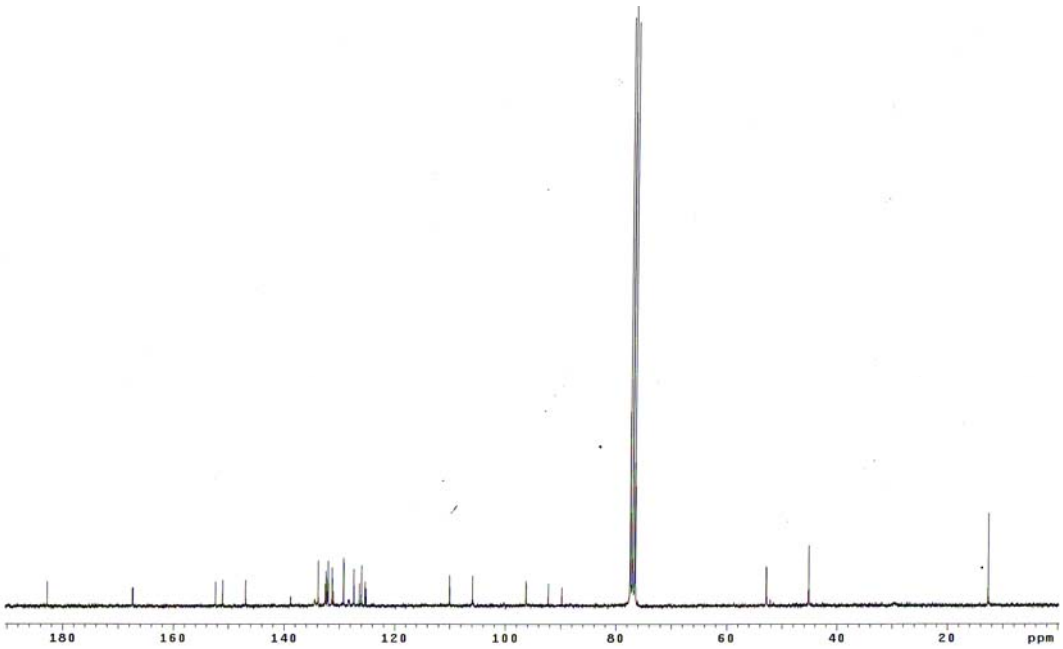

^{13}C NMR ($CDCl_3$)

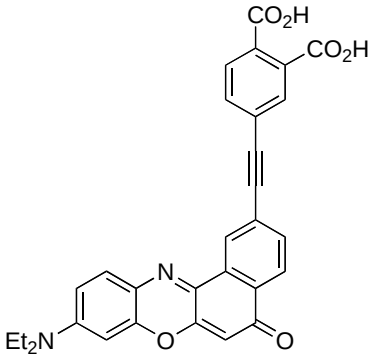

68

4-(2-(9-(diethylamino)-5-oxo-5*H*-benzo[a]phenoxazin-2-yl)ethynyl)benzene-1,2-dioic acid. Dimethyl 4-(2-(9-(diethylamino)-5-oxo-5*H*-benzo[a]phenoxazin-2-yl)ethynyl)benzene-1,2-dioate **67** (15 mg, 0.024 mmol) was dissolved in 2 mL THF at room temperature. Potassium trimethylsilanolate (8 mg, 0.061mmol) was added to the reaction mixture. The reaction was complete in 15 h. The solvent was removed under reduced pressure. The crude product was dissolved in 1 mL water, acidified with 0.2M HCl, then a dark red solid precipitated out. The crude product was separated by filtration, washed with 5 mL water and 10 mL ethyl acetate to afforded 8 mg (65%) desired product as a red solid. ^{1}H NMR (500 MHz, $CDCl_3$), δ 7.79 (d, *J* = 1.5 Hz, 1H), 8.21(d, *J* = 8.0 Hz, 1H), 8.02 (s, 1H), 7.88 (d, *J* = 8.0 Hz, 1H), 7.79 (dd, *J* = 4.5 Hz, 1.5 Hz, 1H), 7.73 (dd, *J* = 4.5 Hz, 1.5Hz, 1H), 7.67 (d, *J* = 9.0 Hz, 1H), 6.80 (dd, *J* = 9.0 Hz, 3.0Hz, 1H), 6.54 (d, 3.0Hz, 1H), 6.38 (s, 1H), 3.52 (q, *J* = 7.0 Hz, 4H), 1.28 (t, *J* = 7.0 Hz, 6H). ^{13}C NMR (125 MHz, $CDCl_3$: CDCl3 = 2:1), δ 184.1, 170.0 (bs), 153.6, 152.4, 147.8, 138.1, 134.2, 133.1, 132.8, 132.7, 132.2, 131.3, 130.4, 129.0, 128.9, 127.8, 126.4, 126.3, 126.3, 126.2, 116.6, 105.5, 96.6, 92.1, 90.8, 45.8, 12.8. HRMS (ESI) calcd for $C_{30}H_{21}N_2O_6$ $(M-H)^-$ 505.1400, found 505.1303. TLC (10 % MeOH-CH_2Cl_2) R_f = 0.38.

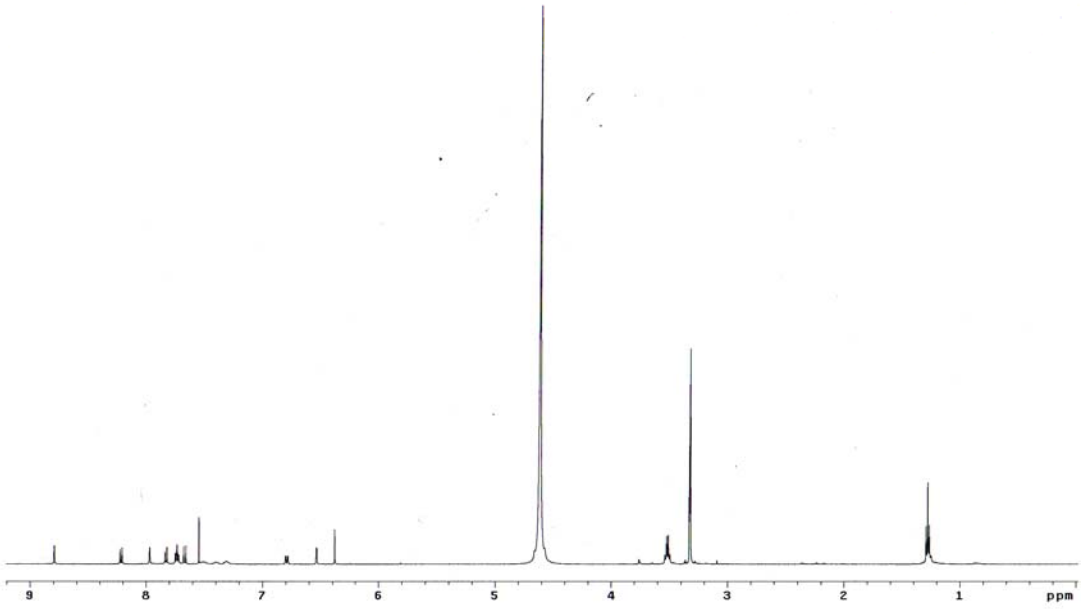

^{1}H NMR (CD_3OD)

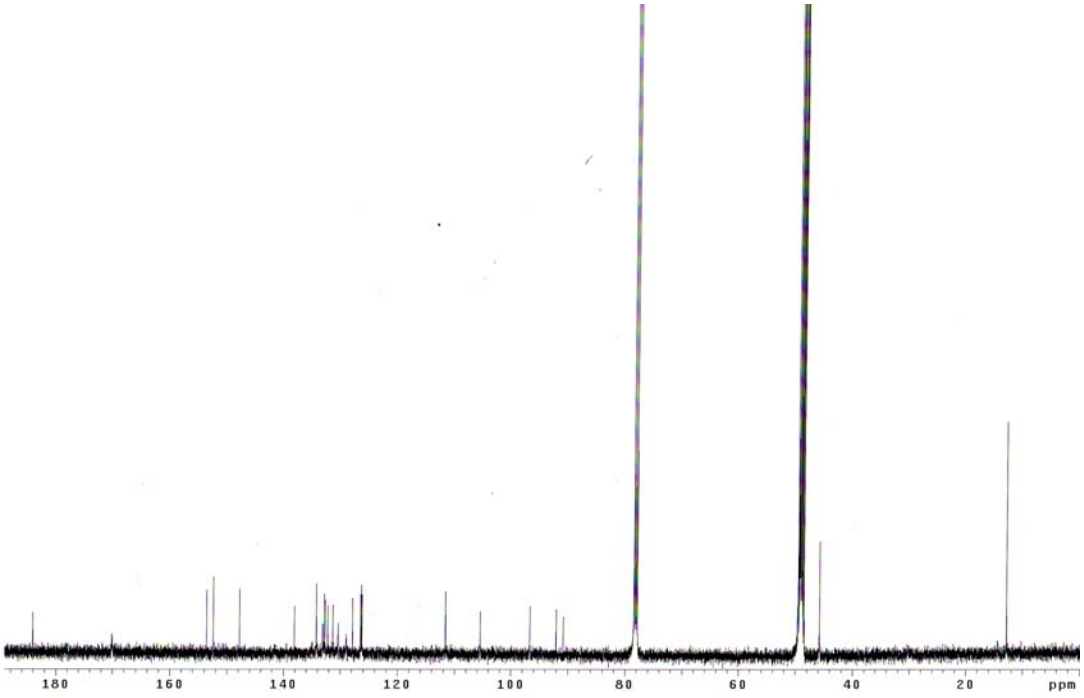

^{13}C NMR (CD_3OD)

APPENDIX D

EXPERIMENTAL DATA FOR CHAPTER V

General Procedures

Anion Exchange Resin, IONAC A-554, Cl^- Form, type II, beads (16-50 mesh) were bought from Sigma-Aldrich. Dry DMF, (< 50 ppm water) was purchased from Acros. THF was dried with molecular sieves and Et_3N was distilled from CaH_2. Other solvents and reagents were used as received. All reactions were carried out under an atmosphere of dry nitrogen. Unless otherwise indicated, common reagents or materials were obtained from commercial source and used without further purification.

NMR spectra were recorded on a VXP-300 MHz and Inova-500 MHz spectrometers (^1H at 300 MHz or 500 MHz, and ^{13}C at 75 or 125 MHz) at room temperature unless other mentioned. Chemical shifts of ^1H NMR spectra were recorded and chemical shifts are reported in ppm from the solvent resonance ($CDCl_3$ 7.26 ppm, CD_3OD 3.30 ppm, CD_3SOCD_3 2.49 ppm). Data are reported as follows: chemical shift, multiplicity (s = singlet, bs = broad singlet d = doublet, t = triplet, q = quartet, m = multiplet), coupling constants, and number of protons. Proton decoupled ^{13}C NMR spectra were also recorded in ppm from tetramethylsilane resonance ($CDCl_3$ 77.0, CD_3OD 49.1, DMSO-d_6 39.5 ppm). Analytical thin layer chromatography (TLC) was performed on EM Reagents 0.25 mm silica-gel 60-F plates, and visualized with UV light or stained with $KMnO_4$. Flash chromatography was performed using silica gel 60 (230–400 mesh). HPLC (Beckman Coulter) analysis of samples was subjected to reverse phase analytical

HPLC column [protein & peptide C18, VYDAC] eluting with solvents CH_3CN (0.1 % TFA) and H_2O (0.1 % TFA). Some compounds were purified using prep HPLC ((Beckman Coulter, X Terra Prep-MS-C18 Column, 5mm, 19 x 160 mm) eluting with solvents A (H_2O, 0.1 % TFA) and B (CH_3CN, 0.1 % TFA). MS were measured under ESI or MALDI conditions.

Experimental

Material and Methods

Pep-1 was obtained from Active Motif. Avidin-Alexa Fluor 488 conjugate, BSA-Alexa Fluor 488 conjugate, FM 4-64, BODIPY TR ceramide complexed to BSA and Hoechst 33342 were purchased from Invitrogen. β-Galactosidase and the recombinant Streptavidin were purchased from Calbiochem and Roche, respectively and labeled with Alexa Fluor 488 5 SDP ester (purchased from Invitrogen) according to the procedure provided by Invitrogen.

Fluorescence Quenching Experiment

The fluorescence intensity of a solution of BSA-F* (1 μM in DMEM) was compared to the fluorescence intensity of a solution of azo-R_8:BSA-F* complexe (1μM BSA-F*:10 μM azo-R_8 in DMEM). Both solution were excited at 488 nm. As a control experiment, the fluorescence quenching of a solution of fluorescein (0.1 μM) with azo-R_8 (1 μM) was also studied.

Cell Culture

COS 7 cells were purchased from the American Type Culture Collection (ATCC) and cultured on 75 cm^2 culture flasks in DMEM supplemented with 10% fetal bovine serum (FBS) in a humidified incubator at 37 ºC with 5% CO_2. Cells grown to subconfluence were plated 2-3 days prior to the experiments in Lab-Tek two well chambered coverglass slides (Nunc).

Fluorescence Microscopy

Subcellular protein localization was measured on living COS7 cells using a Zeiss Stallion Dual Detector Imaging System consisting of an Axiovert 200M inverted fluorescence microscope, CoolSnap HQ digital cameras and Intelligent Imaging Innovations (3I) software. Digital images of Alexa Fluor 488-tagged proteins, FM 4-64 labeled membranes and endosomes, BODIPY TR ceramide complexed to BSA labeled Golgi, and Hoechst 3342-labeled nuclear DNA were captured with a C-APO 63X/1.2 W CORR D=0.28M27 objective with the following filter sets: Exciter BP470/20, Dichroic FT 493, Emission BP 505-530 for Alexa Fluor 488; Exciter BP560/40, Dichroic FT 585, Emission BP 630/75 for FM 4-64 and BODIPY TR ceramide complexed to BSA; and Exciter G 365, Dichroic FT 395, Emission BP 445/50 for Hoechst 3342. Sequential optical sections (Z-stacks) from the basal-to-apical surfaces of the cell were acquired. Digital image acquisition was initiated approximately 1 μm below he basal surface of the cells and optical slices were collected at 0.5 μm steps through the apical surface of the cells with a high numerical objective lens (C-APO 63X/1.2 W CORR D=0.28M27). These wide-field images were subjected to deconvolution using 3I software.

The protein:carrier complexes were pre-formed at room temperature for 30 min by mixing (in a mol:mol ratio) the protein and the carrier in DMEM supplemented with 10% fetal bovine serum (FBS). A 1:10 mol:mol ratio of protein:carrier was used for avidin-F*, BSA-F* and rec. Streptavidin-F*, while a 1:20 mol:mol ratio was used for b-gal-F*. To study the cellular uptake of the proteins, the culture medium was removed, the preformed protein:carrier complex was added, and the cells were incubated for another hour at 4 or 37 ºC. After the incubation period, the cells were washed with phosphate-buffered saline (PBS, pH 7.4) several times before imaging. For experiments at 4 ºC, cells were preincubated at 4 ºC for 30 min before being incubated with the protein solution for 1h. The cells were also co-stained with Hoescht (2 μg/mL), a nuclear marker, and FM-464, an endosome marker.

Endosomal Colocalization

COS7 cells were incubated with the protein:carrier complex for 1h at 37 ºC. After the cells were washed with PBS, FM 4-64 (5 μg/mL) was added and the cells were incubated for 15 min at 37 ºC. The cells were washed again with PBS before imaging.

Note: when the cells were co-incubated with the labeled protein and FM 4-64 for 1h at 37 ºC, predominant labeling of the mitochondria was observed.

Golgi Colocalization

After the protein was loaded into the COS7 cells, the cells were washed. Then fresh DMEM medium was added, and the cells were incubated with 5 μM of BODIPY TR ceramide complexed to BSA for 30 min at 4 ºC. The cells were then rinsed several

with ice-cold medium and incubated in fresh medium for 30 min at 37 ºC. Finally, the cells were washed with PBS before imaging.

Viability Assay

Viability of cells was evaluated by searching for any changes in cellular morphology using Nomarski differential interference contrast (DIC) microscopy during and following analysis of cellular uptake of proteins. Parallel cultures were also evaluated using DIC microscopy along with fluorescence analysis of the cell-impermeant viability indicator ethidium homodimer-1 (EthD-1) (Invitrogen). This high-affinity nucleic acid stain is weakly fluorescent until bound to DNA. Unlike Hoechst 33342, EthD-1 can only penetrate cells in which the plasma membrane is compromised. Viability assessment was conducted by incubating cells at 4ºC for 1 h with a 1:10 mol ratio of protein:carrier, followed by washing cells with PBS with Ca^{2+} before imaging of proteins. Following image capture of proteins, EthD-1 (1 μM final concentration) was added and images were recorded at 5, 10, 20 and 30 min using the 630/75 BP filter and revealed no EthD-1 fluorescence. Cultures were returned to the incubator at 37ºC for 17 hr before viability was again evaluated by EthD-1 staining. Morphology of cells monitored by DIC and Hoechst 33342 staining was normal and no EthD-1 uptake into cell nuclei was detected. Therefore, no cytotoxic effects of protein:carrier combinations were detected for up to 24 h of cell treatments.

Flow Cytometry

Protein internalization was measured by flow cytometry on living cells. COS 7 cells were cultured as subconfluent monolayers on 25 cm^2 cell culture plate with vent

caps in DMEM supplemented with 10% fetal bovine serum (FBS) in a humidified incubator at 37 ºC with 5% CO_2. Carrier/protein complexes were formed in 1 mL DMEM at a molar protein/carrier ratio of 1:10 for avidin and BSA and 1:20 for β-galactosidase and incubated for 30 min at room temperature. Cells grown to 60-70% confluency were then overlaid with the preformed complexes and incubated for 1 h at 37 or 4 ºC. For experiments at 4 ºC, the cells were preincubated at 4 ºC for 30 min before addition of the protein/carrier complex.

After 1h incubation, the cells were washed with PBS, and treated with trypsin (2 min) and heparin (0.5 mg/mL in PBS, 3 x 5 min) to remove extracellular bound protein. Samples were resuspended in 500 μL PBS and transferred to sterile tubes. Cells were analyzed on a FACSCalibur (Becton Dickinson Immunocytometry Systems, San Jose, CA) flow cytometer, equipped with a 15 mW air-cooled argon laser, using CellQuest (Becton Dickinson) acquisition software.. Green fluorescence from Alexa Fluor 488 or fluorescein was collected through a 530/30-nm bandpass filter. List mde data were acquired on a minimum of 10,000 cells or beads defined by forward and side light scattering light scatter properties. Data analysis was performed in FlowJo (Treestar, Inc., Ashland, OR), using forward and side light scatter to gate on cells or single beads. The Calibrated Parameter platform of FlowJo was used to determine the molecules of equivalent soluble fluorescein (MESF). Data are expressed as the median MESF.

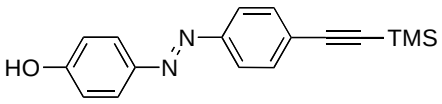

69

(*E*)-4-((4-((Trimethylsilyl)ethynyl)phenyl)diazenyl)phenol. (*E*)-4-((4-iodophenyl)diazenyl)phenol **T** (257 mg, 0.793 mmol), which was prepared by the coupling reaction of phenol and 4-iodophenyl diazonium salt, trimethylsilyl acetylene (1.12ml, 7.93 mmol), $PdCl_2(PPh_3)_2$ (28 mg, 0.04 mmol), CuI (15 mg, 0.08 mmol), Et_3N (1.1 ml, 7.93 mmol) and 8 ml THF were added into a 50 mL round bottom flask. After degassed three times via the freeze-thaw method, the mixture was stirred at r.t. for 12 h. The reaction solvent was removed under reduced pressure and the crude product was purified by flash column eluting with 30% hexane : ethyl acetate to give the desired product as a red solid 115 mg (49%). ^{1}H NMR (300 MHz, $CDCl_3$), d 7.89 (d, J = 9.0 Hz, 2H), 7.82 (d, J = 8.1 Hz, 2H), 7.59 (d, J = 8.1 Hz 2H), 6.96 (d, J = 6.3 Hz, 2H), 0.27 (s, 9H).

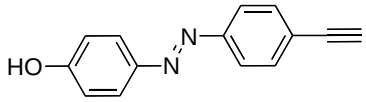

70

(*E*)-4-((4-Ethynylphenyl)diazenyl)phenol. Compound **69** (78 mg, 0.265 mmol) was dissolved in methanol (20 mL) in a 50 mL flask. Then potassium carbonate (110 mg, 0,796 mmol) was added to the solution and the mixture was stirred at r.t. until the reaction went to completion. The solvent was removed under reduced pressure. And the product was dissolved in CH_2Cl_2 (50 mL), which was then washed with water (25 mL x 2). The organic phase was dried with $MgSO_4$ and the product was achieved as a pure orange solid after removing the organic solvent under reduced pressure. ^{1}H NMR (300 MHz, CD_3OD), d 7.81 (d, *J* = 9.0 Hz, 2H), 7.78 (d, *J* = 8.5 Hz, 2H), 7.57 (d, *J* = 8.5 Hz, 2H), 6.91 (d, *J* = 9.0 Hz, 2H); ^{13}C NMR (125 MHz, CD_3OD), d 162.6, 153.8, 147.6, 134.0, 126.3, 125.5, 123.6, 116.9, 84.2, 80.8. MS (ESI) calcd for $C_{14}H_{11}N_2O$ $(M+H)^+$ 223.25, found 223.24.

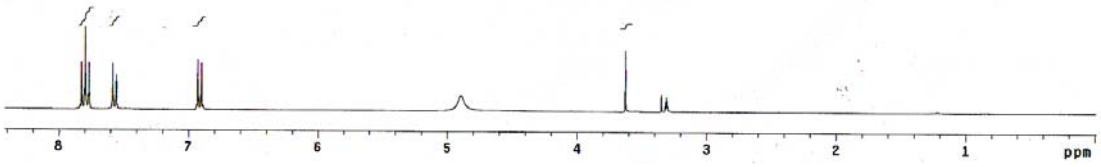

^{1}H NMR ($CDCl_3$)

^{13}C NMR ($CDCl_3$)

71

***tert*-Butyl 4-(azidomethyl)piperidine-1-carboxylate.** A mixture of *tert*-butyl 4-((methylsulfonyloxy)methyl)piperidine-1-carboxylate **U** (2.90 mg, 0.1 mol), NaN_3 (1.95g, .0.3 mol) and dry DMF (100 mL) in a 250 mL flask were stirred at 60 ^oC until the reaction went to completion. Water (200 mL) was added to the reaction mixture, and the product was extracted from water with ethyl acetate (50 mL x 3). The combined organics were washed with water (50 ml x 3), and then dried over MgSO4. The crude product after removing the organic solvent under reduced pressure was purified by flash chromatography eluting with hexane and ethyl acetate (4:1) to give desired product (2.37 g, 99%) as colorless oil. ^1H NMR (300 MHz, $CDCl_3$), d 4.13 (bs, 2H), 3.19 (d, J = 6.3 Hz, 2H), 2.69 (bs, 2H), 1.73-1.66 (m, 3H), 1.45 (s, 9H), 1.24-1.10 (m, 2H). ^{13}C NMR (125 MHz, $CDCl_3$), d 154.6, 79.3, 56.9, 43.7, 42.9, 36.4, 29.5, 28.3. MS (ESI) calcd for $C_{11}H_{21}N_4O_2^+$ $(M+H)^+$, 241.17, found, 241.16. TLC (1:1 EtOAc:hexane) R_f = 0.78.

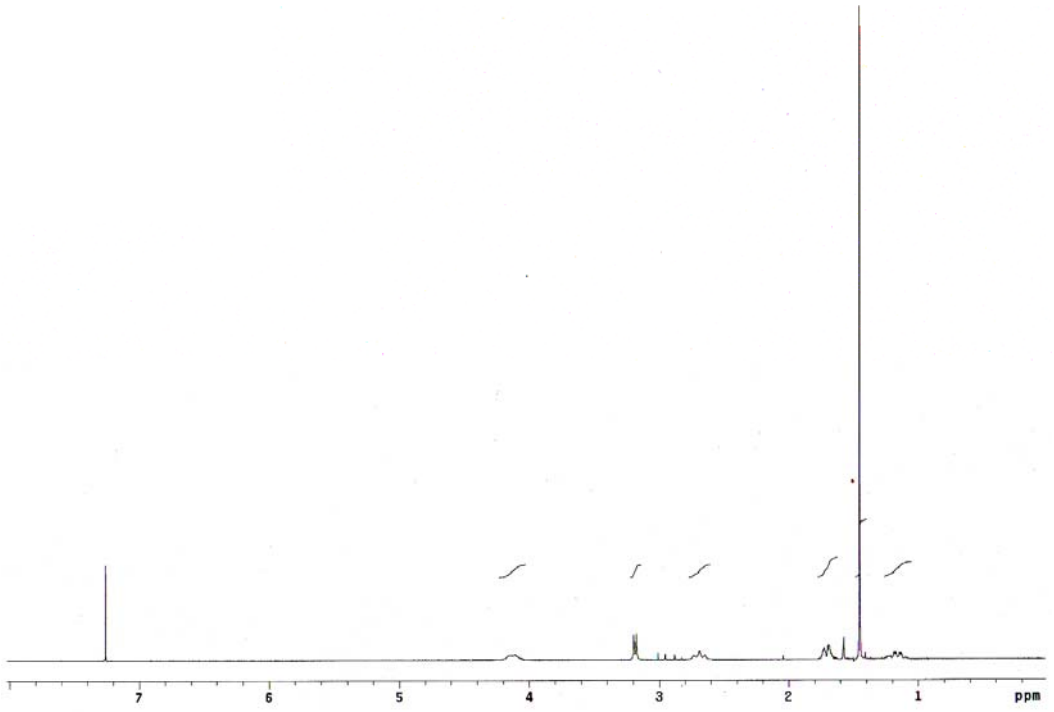

^{1}H NMR ($CDCl_3$)

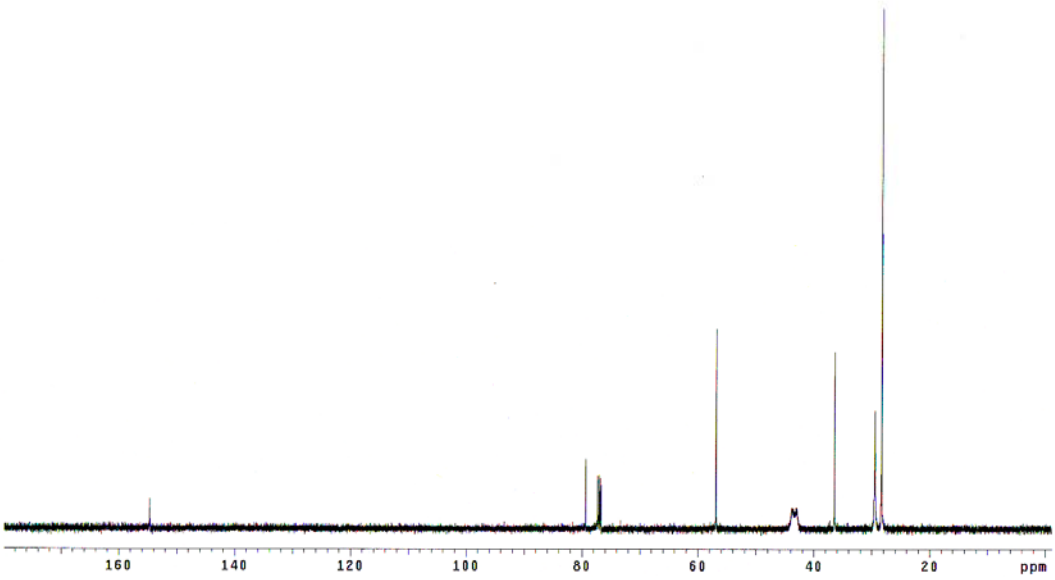

^{13}C NMR ($CDCl_3$)

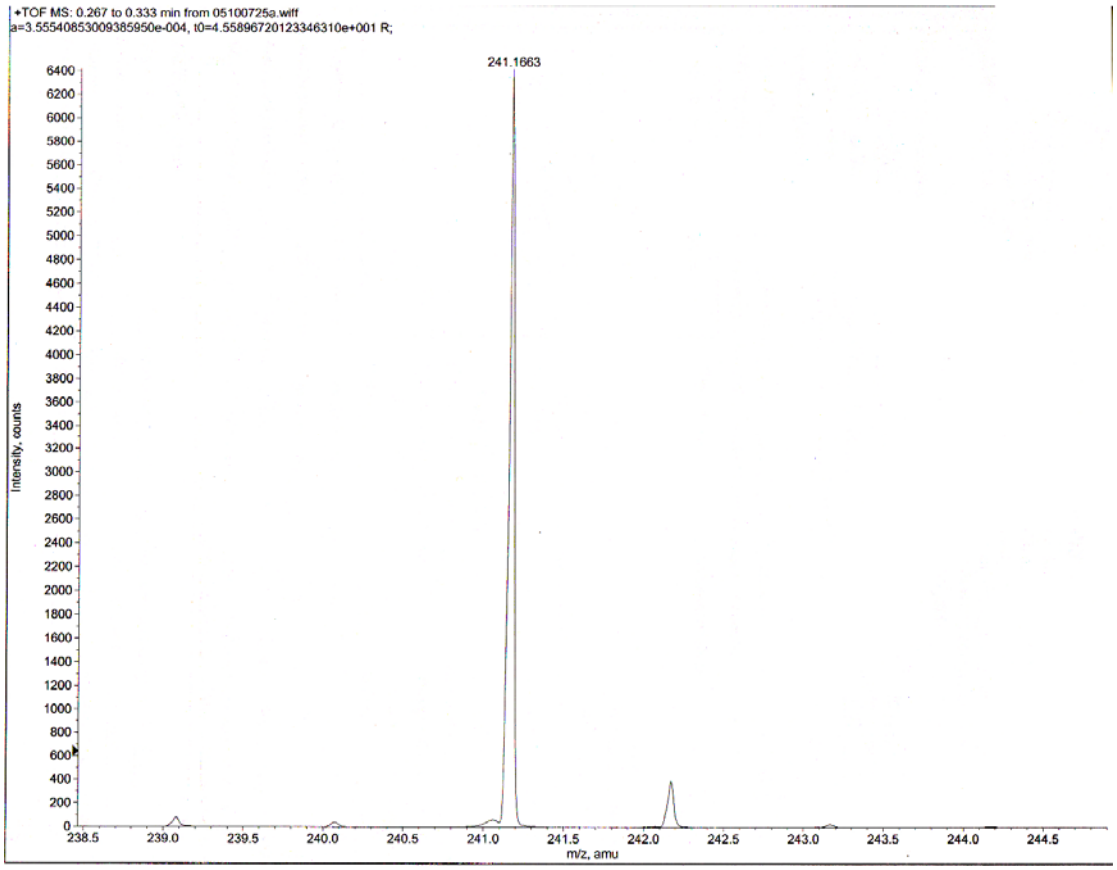
+TOF MS: 0.267 to 0.333 min from 05100725a.wiff
a=3.5554085300938595e-004, t0=4.558967201233463 10e+001 R;
241.1663
Intensity, counts
m/z, amu

MS ESI

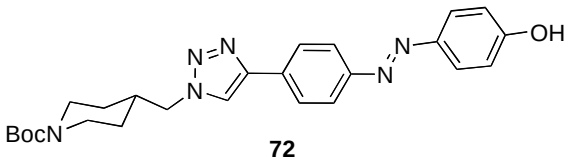

72

(*E*)-*tert*-Butyl 4-((4-(4-((4-hydroxyphenyl)diazenyl)phenyl)-1*H*-1,2,3-triazol-1-yl)methyl)piperidine-1-carboxylate. A mixture of terminal alkyne **70** (100 mg, 0.455 mmol), organic azide **71** (110mg, 0.455 mmol), Cu (29mg, 0.455 mmol) and $CuSO_4$ (0.046 mL, 1M) in THF/H_2O (1:1, 10 mL) was stirred in a flask for overnight. The product was isolated pure as an orange solid by filter out of Cu and other impurity through celite. ^{1}H NMR (500 MHz, CD_3OD), d 8.19 (s, 1H), 7.92 (d, *J* = 9.0 Hz, 2H), 7.88 (d, *J* = 9.0 Hz, 2H), 7.81 (d, *J* = 9.0 Hz, 2H), 6.90 (d, *J* = 9.0 Hz, 2H), 4.32 (d, *J* = 7.5 Hz, 2H), 4.10 (bs, 1H), 4.07 (bs, 1H), 2.71 (bs, 2H), 2.18-2.09 (m, 1H), 1.63 (bs, 1H), 1.60 (bs, 1H), 1.42 (s, 9H), 1.27-1.08 (m, 2H), ^{13}C NMR (125 MHz, CD_3OD), d 161.4, 155.8, 153.1, 147.7, 146.9, 132.6, 126.9, 125.6, 123.7, 122.5, 116.4, 80.8, 60.6, 56.1, 37.8, 30.0, 28.6. MS (ESI) calcd for $C_{25}H_{31}N_6O_3^+$ $(M+H)^+$, 463.25, found, 463.15. TLC (1:1 EtOAc-Hexane) R_f = 0.30.

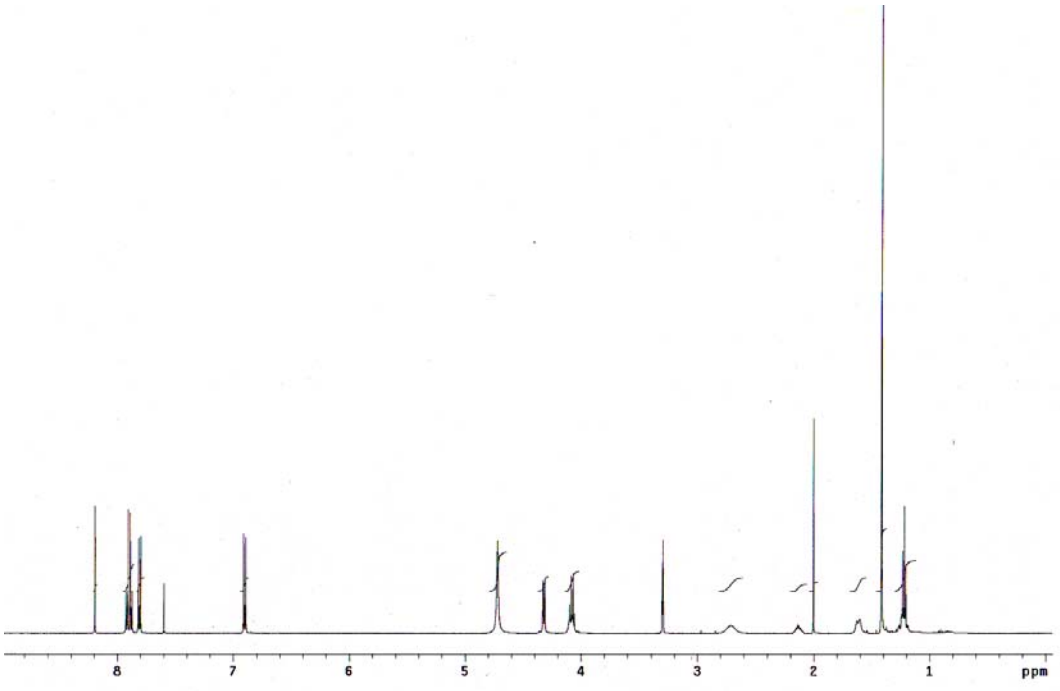

^{1}H NMR ($CDCl_3$)

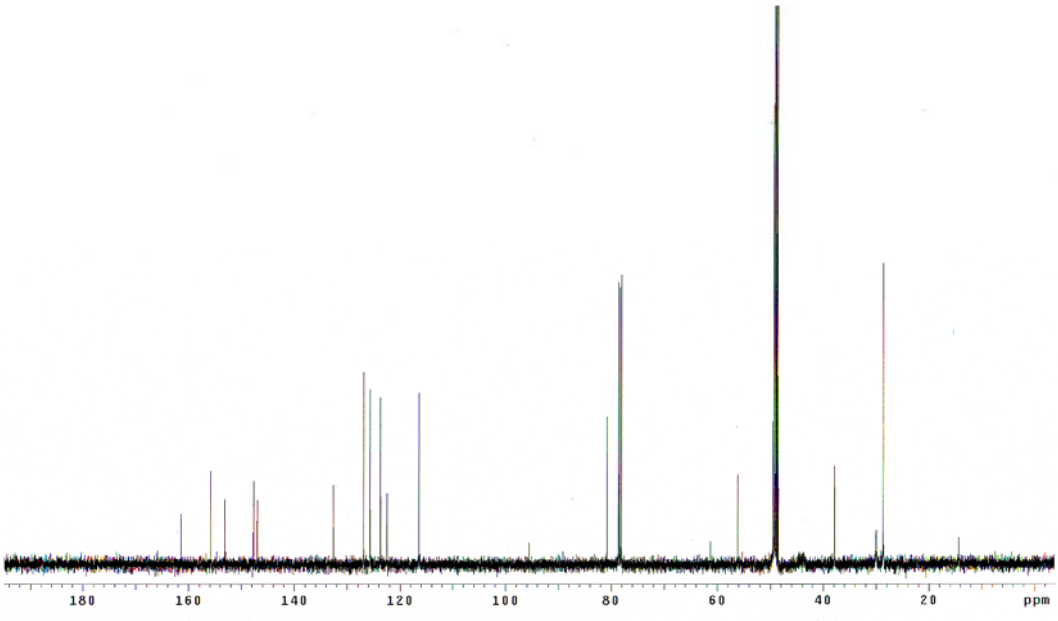

^{13}C NMR ($CDCl_3$)

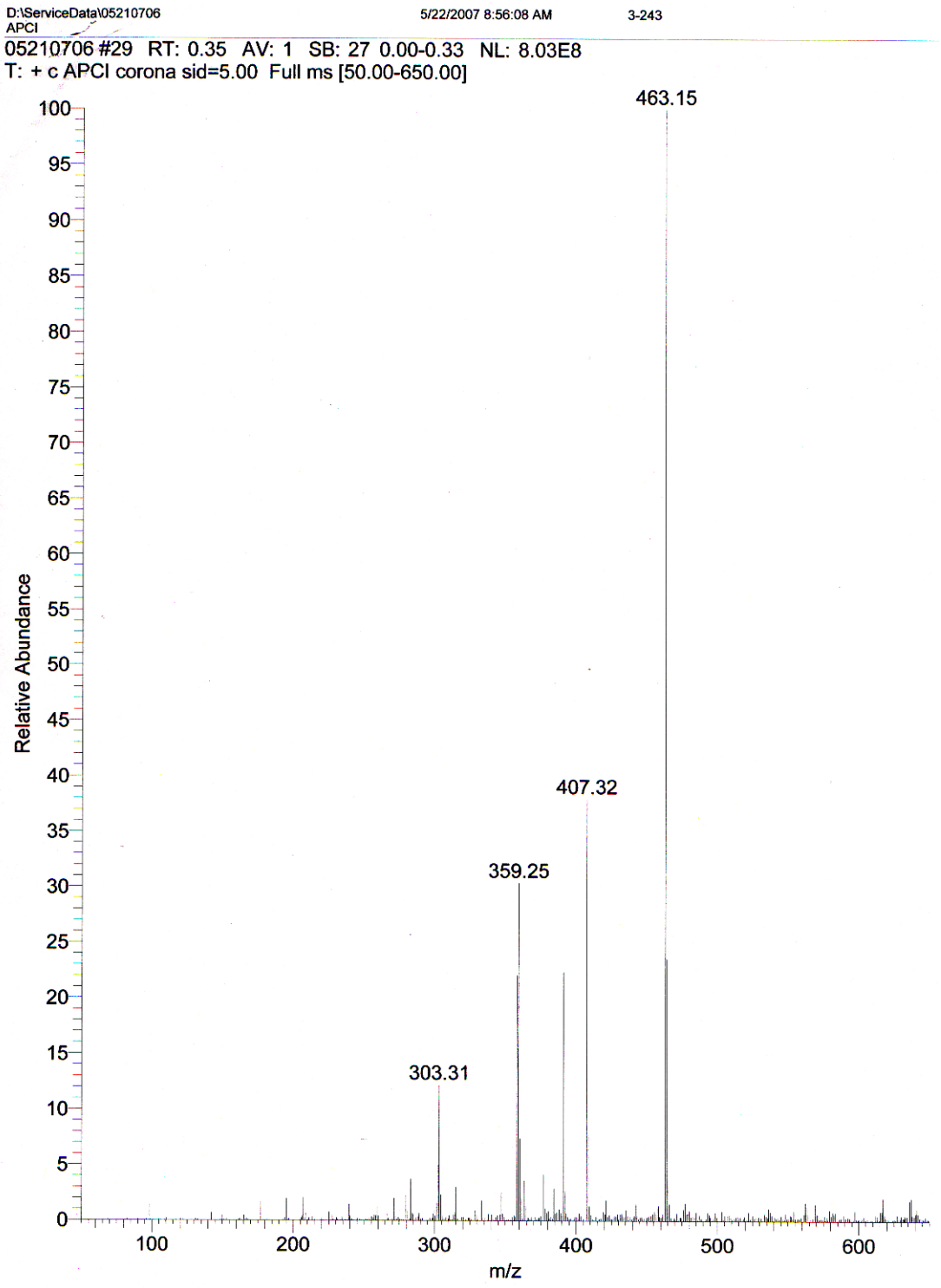
D:\ServiceData\05210706
APCI
5/22/2007 8:56:08 AM
3-243
05210706 #29 RT: 0.35 AV: 1 SB: 27 0.00-0.33 NL: 8.03E8
T: + c APCI corona sid=5.00 Full ms [50.00-650.00]
463.15
407.32
359.25
303.31
Relative Abundance
m/z
100
95
90
85
80
75
70
65
60
55
50
45
40
35
30
25
20
15
10
5
0
100
200
300
400
500
600

MS ESI

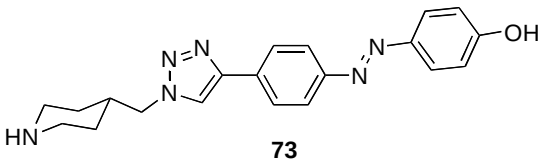

73

(***E***)**-4-((4-(1-(Piperidin-4-ylmethyl)-1*H*-1,2,3-triazol-4-yl)phenyl)diazenyl)-phenol.** BOC protected compound **72** (157 mg, 0.339 mmol), and one drop of triisopropylsilane (TIS) was dissolved in CH_2Cl_2/TFA (1:1, 20 mL) and the mixture was stirred for 5 h at room temperature. The solvent was removed under reduced pressure. Then the residue was washed with ether (10 ml x 1) to provide the desired product as a yellow solid (117 mg, 95%). ^{1}H NMR (500 MHz, CD_3OD), d 8.44 (s, 1H), 7.97 (d, *J* = 8.5 Hz, 2H), 7.91 (d, *J* = 8.5 Hz, 2H), 7.83 (d, *J* = 8.5 Hz, 2H), 6.92 (d, *J* = 9.0 Hz, 2H), 4.45 (d, *J* = 7.0 Hz, 2H)), 3.42 (d, *J* = 13 Hz, 2H), 3.00 (td, *J* = 13 Hz, 2.5Hz, 2H), 2.37-2.29 (m, 1H), 1.90 (d, *J* = 14Hz, 2H), 1.59-1.50 (m, 2H). ^{13}C NMR (75 MHz, $CDCl_3$), d 162.4, 153.8, 147.5, 133.3, 127.3, 126.1, 124.1, 123.5, 123.5, 116.8, 55.6, 44.7, 36.0, 27.4. MS (ESI) calcd for $C_{20}H_{23}N_6O^+$ $(M+H)^+$, 363.19, found, 363.19.

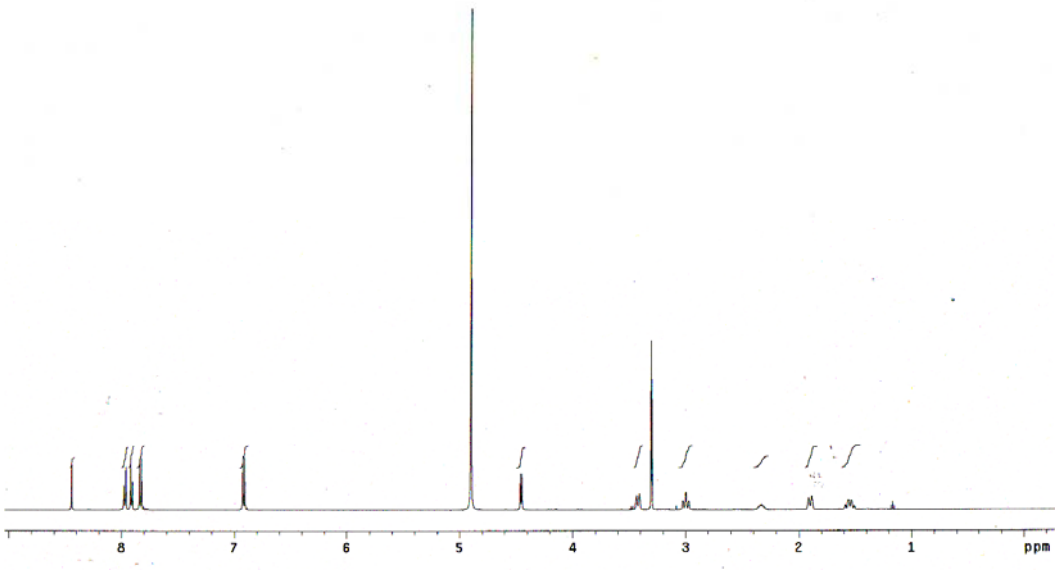

^{1}H NMR ($CDCl_3$)

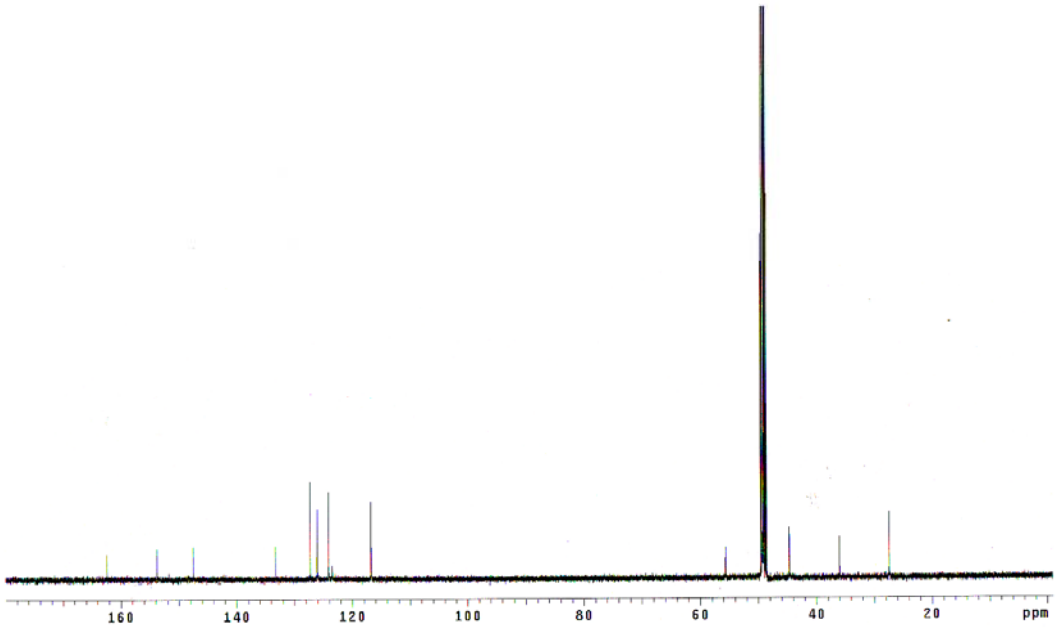

^{13}C NMR ($CDCl_3$)

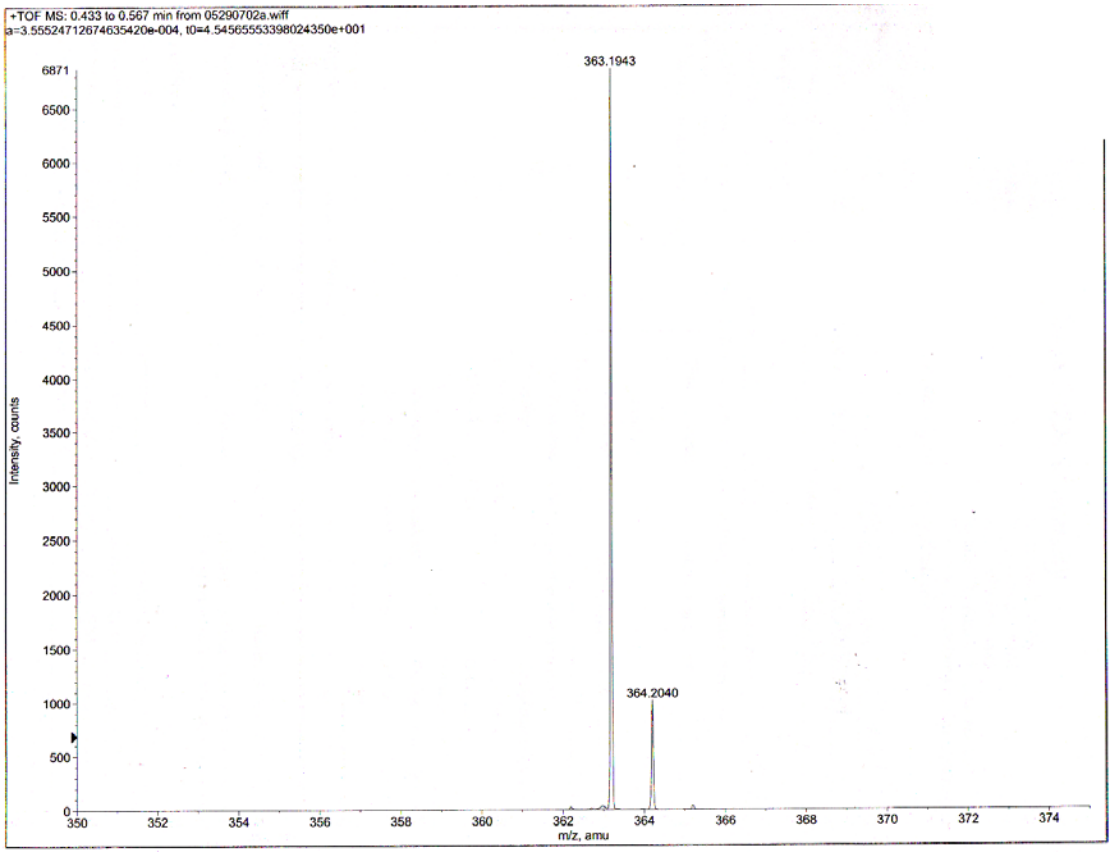
+TOF MS: 0.433 to 0.567 min from 05290702a.wiff
a=3.5552471267463542e-004, t0=4.5456555339802435e+001
363.1943
364.2040
Intensity, counts
m/z, amu
6871
6500
6000
5500
5000
4500
4000
3500
3000
2500
2000
1500
1000
500
0
350
352
354
356
358
360
362
364
366
368
370
372
374

MS ESI

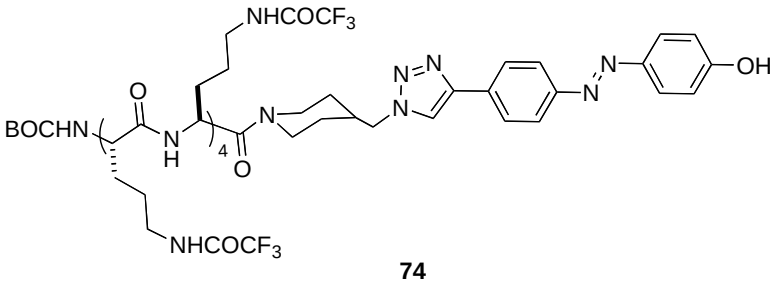

74

BocNH-(OrnNHCOCF$_3$)$_8$-azo. To a 25 mL flask was added the known compound BocNH-(OrnNHCOCF$_3$)$_8$-CO$_2$H **W** (324 mg, 0.18 mmol), AZO compound **73** (86 mg, 0.18 mmol), 1-ethyl-3-(3'-dimethylaminopropyl)carbodiimide (EDC, 52 mg, 0.27 mmol),1-hydroxybenzotriazol (HOBt, 26 mg, 0.189 mmol), and CH_2Cl_2/DMF (5:1, 6 mL). The mixture was stirred at 0 ^oC for 10 min, then N-methyl morpholine (NMM, 0.038 ml, 0.54 mmol) was added to the reaction mixture dropwise, which was then slowly warmed to r.t., and kept stirring for overnight. The reaction mixture was treated with 100 mL CH_2Cl_2. The organic solution was washed with $NaHCO_3$ (1M, 50 mL x 3), and then washed with $NaHSO_4$ (1M, 50 mL x 3). At last, the dichloromethane phase was washed with brine (25 ml x 1) and then dried over $MgSO_4$. The product was afforded as a yellow solid (331 mg, 85%, > 90% purity) after removing the organic solvent under reduced pressure. ^{1}H NMR (500 MHz, DMSO), d 8.39 (s, 1H), 7.96 (d, *J* = 8.5 Hz, 2H), 7.90 (d, *J* = 8.5 Hz, 2H), 7.83 (d, *J* = 9.0 Hz, 2H), 6.92 (d, *J* = 9.0 Hz, 2H), 4.61-3.97 (m, 11H), 3.70-3.69 (m, 1H), 3.32-3.30 (m, 16H), 2.68-2.64 (bm, 2H), 2.32-2.24 (m, 1H), 1.87-1.63 (m, 34H), 1.42 (s, 9H), 1.32-1.26 (M, 2H). MS (MALDI) calcd for $C_{81}H_{102}F_{24}N_{22}O_{19}Na^+$ $(M+Na)^+$, 2165.74, found, 2165.94.

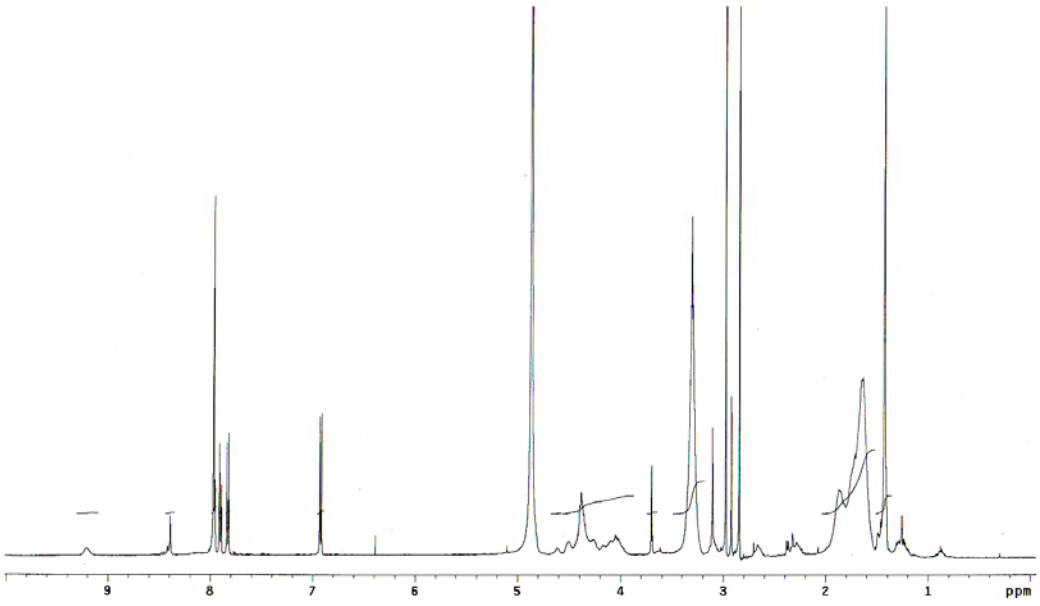

^{1}H NMR ($CDCl_3$)

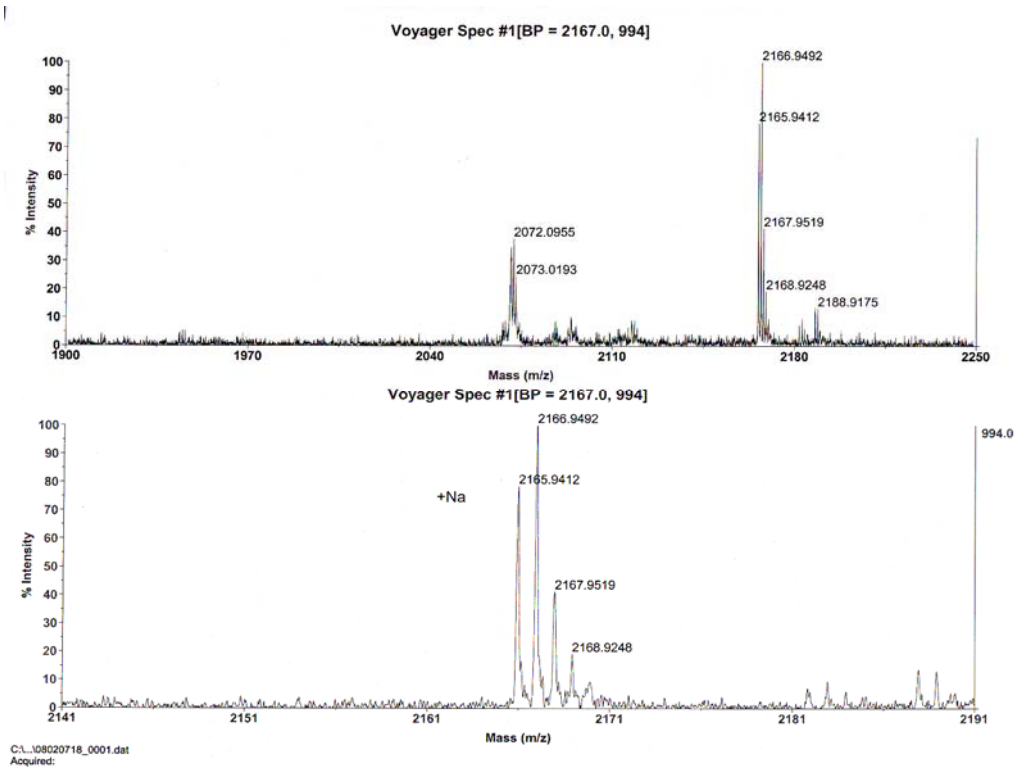

MS MALDI

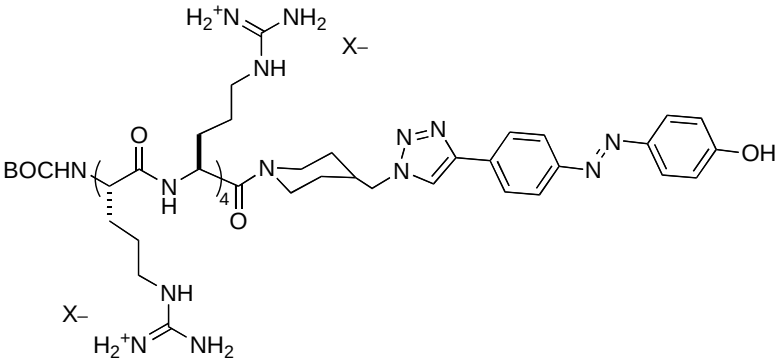

75

BocNH-((Arg)$_8$-azo (8•TFA). A mixture of **74** (24 mg, 0.018 mmol), pyrazole-1-carboxamidine hydrochloride (107 mg, 0.728 mmol), and Na_2CO_3 (77 mg, 0.728 mmol) were dissolved in MeOH/H_2O (8 mL, 1:1). Then the mixture was heated up to 55 ^oC for 48 h. The reaction solvent was removed under reduced pressure and the crude product is purified by RP-prep HPLC (isocratic: 5% solvent B, 5 min; gradient: 5% solvent B to 50% solvent B, 19 min) to give the desired product as a yellow solid (25 mg, 78%, retention time 11 min in analytical HPLC spectra, > 99% pure). MS (MALDI) calcd for $C_{73}H_{127}N_{38}O_{11}$ $(M+H)^+$, 1712.05 found 1712.24.

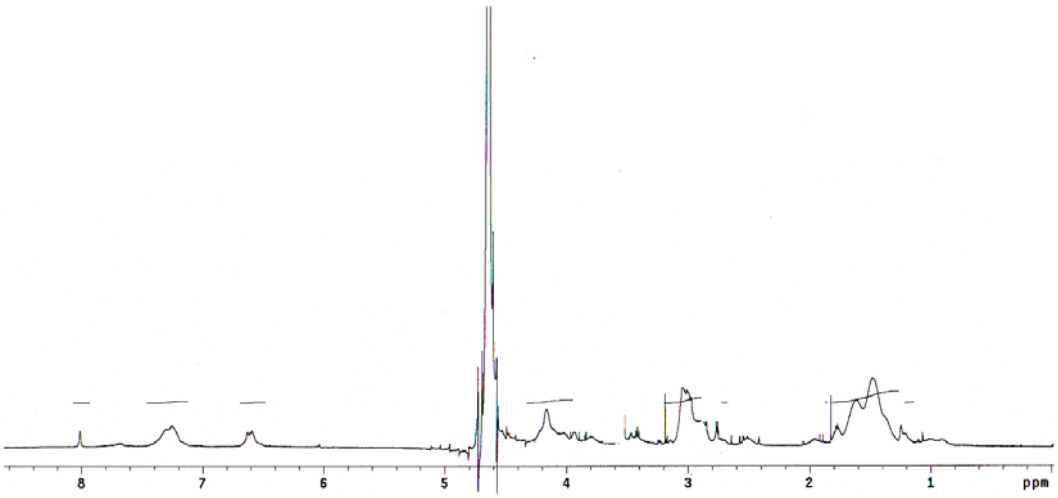

^{1}H NMR (D_2O)

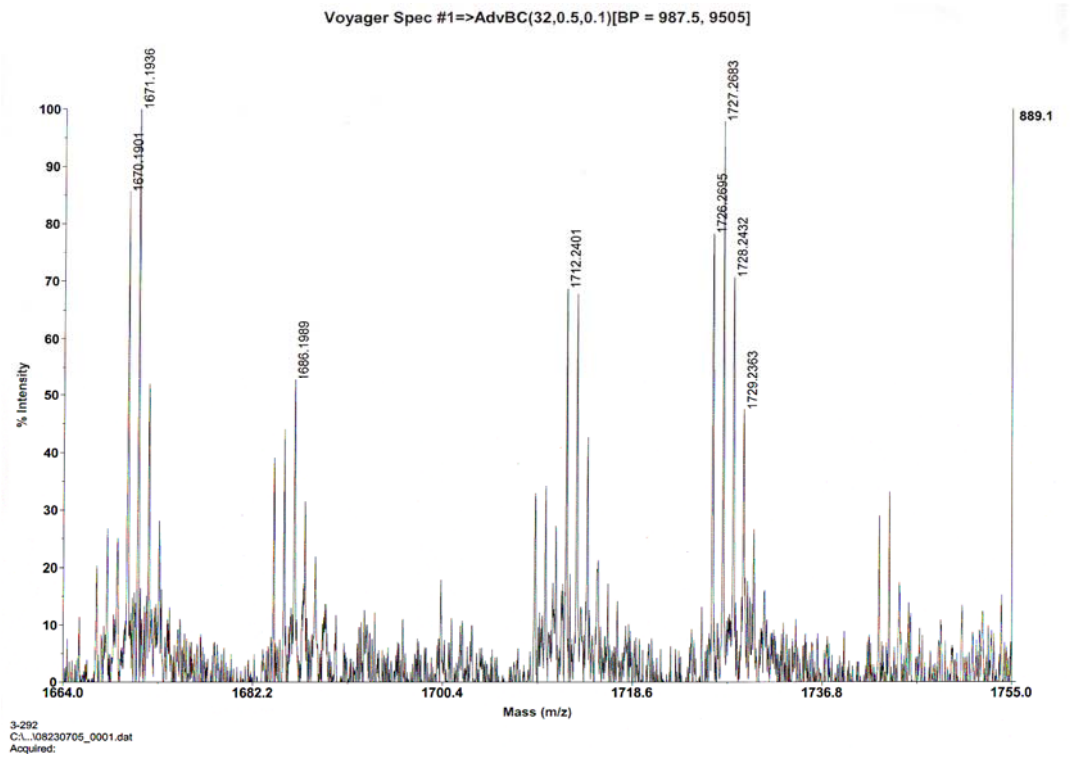

MS MALDI

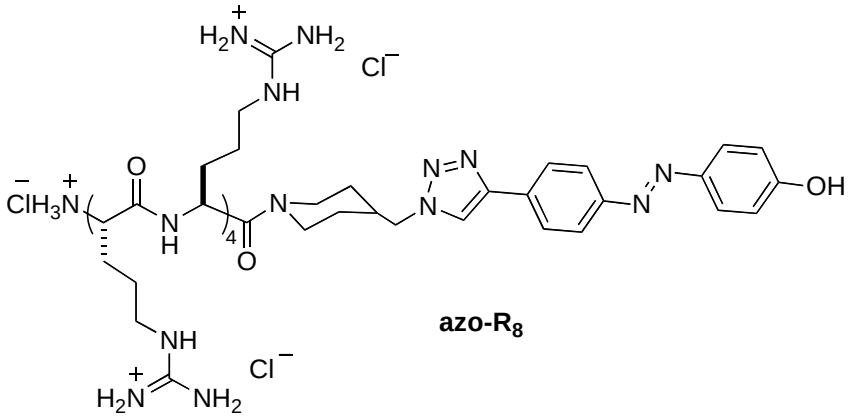

azo-R_8

NH_3-$((Arg)_8$-AZO (9•Cl) (azo-R_8). A solution of **75** (10 mg, 0.0058 mmol) in 1 mL trifluoroacetic acid with one drop of triisopropylsilane (TIS) was stirred at room temperature for 2 h. The solvent was removed under the reduced pressure and the crude product was purified by RP-prep HPLC (isocratic: 5% solvent B, 5 min; gradient: 5% solvent B to 50% solvent B, 19 min) to provide a yellow solid 9 mg (retention time is 11 min, > 99% purity, 90%), which was dissolved in DI water (1 mL). Then 500 mg Cl^- exchange resin was added and the resulting mixture was stirred for 10 h to make sure that the Cl^- and $CF_3CO_2^-$ exchange was complete. The desired product with Cl^- counter anions was achieved after removing the resin by filtration. MS (MALDI) calcd for $C_{69}H_{119}N_{38}O_9$ $(M+H)^+$ 1611.99, found 1612.04.

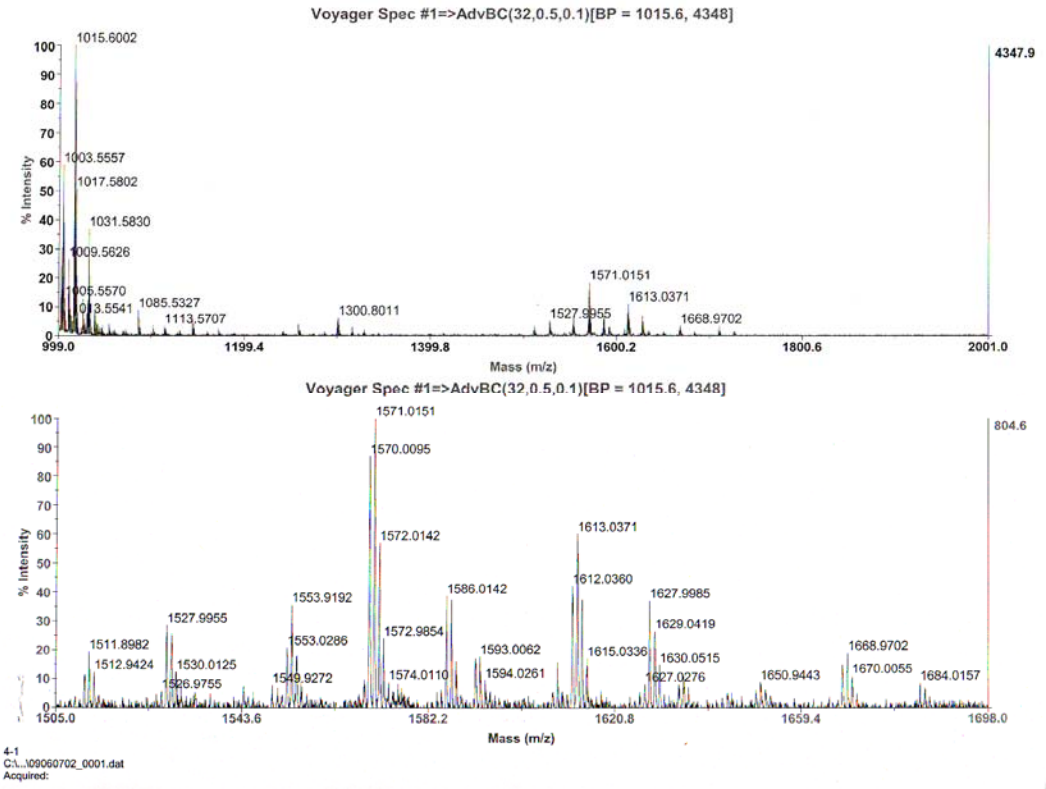

MS MALDI

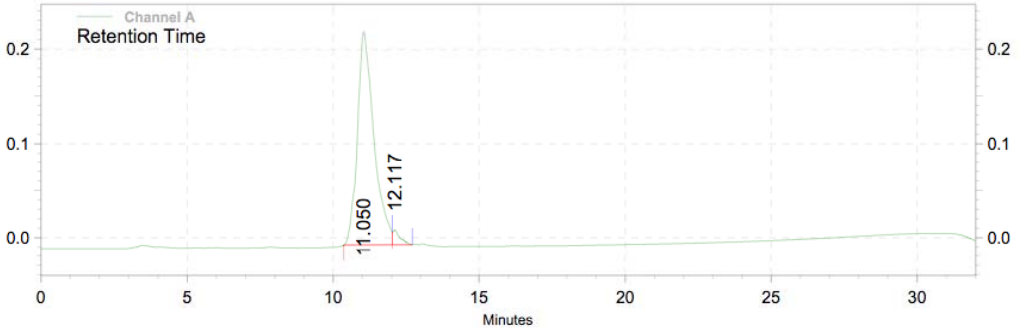

Analytical HPLC of azo-R_8 after purification.

APPENDIX E

DEVELOPMENT OF RATIOMETRIC PH PROBES BASED ON THROUGH-BOND ENERGY TRANSFER CASSETTES

Ratiometric methods, especially dual emission method (excitation at single wavelength and observing emission at two different wavelengths), for determination of pH_i values have many advantages, *e.g.* operation convenience, high sensitivity and accurate results, however there are only limited this type pH probes available in the market, and most of them exhibit the poor photophysical properties. For instance, C.SNARF-1, a commonly used commercialized dual emission ratiometric pH_i probe from Life Technologies, has very low quantum yield, especially in the acidic form ($\phi = 0.03$). Development of dual emission pH_i indicators that have better spectral properties will benefit the biological research related to pH-dependent cell functions.

As mentioned in the first chapter that all three types of benzoxanthene dyes, SNARFs, SNAFLs and SNAFRs, exhibit pH-dependent shifts in their fluorescent emission spectra (see chapter 1, intracellular pH indicators) indicating potential candidates as the ideal pH_i indicators. Benzoxanthene dyes also have desired characteristics for cell imaging including long-wavelength emissions (up to 825 nm), large Stoke's shift between emission maxima of their acidic forms and basic forms (up to 200 nm), high photostability and good water-solubility. The brightness of a dye is dependent on its molar absorptivity at the excitation wavelength and its quantum yield. One common problem when using benzoxanthene dyes as dual emission ratiometric pH

probes is that the small molar absorptivity at single excitation wavelength, which is close to absorbance isobestic point. This usually results in a bigger noise to fluorescence ratio (See Figure S1a). For instance, compared to the maximum absorptivity of its basic form, the absorptivity of C.SNARF-1 at the absorbance isobestic point (534 nm) is only a half of that. The ideal dual emission ratiometric pH probe should have a large pH-independent absoptivity at the excitation wavelength as well as exhibit pH-dependent emission. We would like to design such kind of ideal pH probes based on through-bond energy transfer cassettes, which is composed of a pH-independent donor, *e.g.* a BODIPY, and a pH-dependent benzoxanthene acceptor. The hypothesis of through-bond energy transfer cassettes is that *when donor and acceptor systems are connected via conjugated bonds then rapid and efficient energy transfer from the donor to the acceptor may occur through-bonds*. Through-bond energy transfer (Figure S1b) is mechanistically different from FRET, and there is no known requirement for overlap of the emission of the donor fragment with the absorption of the acceptor part (Figure S1c). Thus, appropriately designed through-bond energy transfer cassettes could absorb photons via a donor part, or parts, at a convenient wavelength (*e.g.* 488 nm: excitation from an Ar-laser), and transfer the energy rapidly through the conjugated linker to the acceptor fragment that emits at a far longer wavelength. Therefore, it is possible to design dyes that absorb strongly at a short wavelength and emit brightly from the acceptor when the overlap between donor emission and acceptor absorbance are changed with variation of pH (Figure S1d). In summary, *through-bond energy transfer cassettes*

have the potential to become dual emission pH_i probes excited by a laser source operating at a single wavelength.

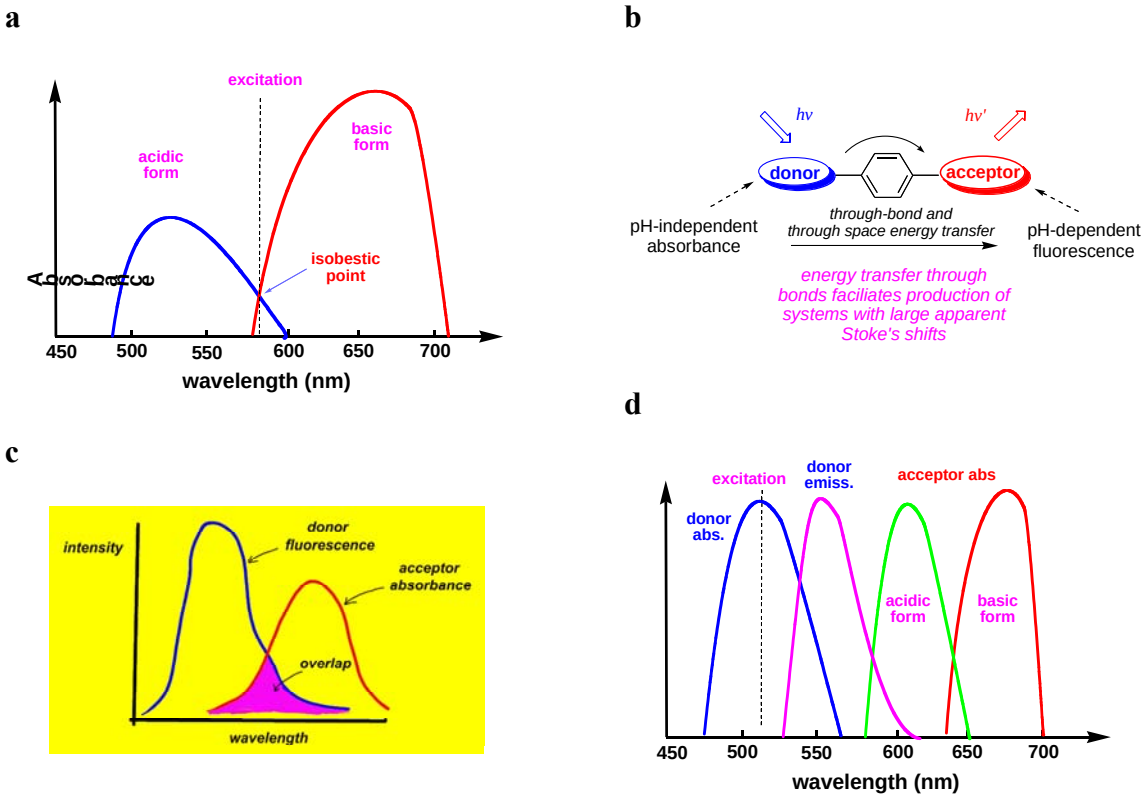

Figure S1. (a) typical excitation of a dual emission pH probe at the isobestic point. (b) Through-bond energy transfer cassettes as a pH indicator with a pH-insensitive donor and a pH-dependent acceptor. (c) FRET-based cassettes only partially alleviate this problem because Förster energy transfer requires overlap of donor emission with the acceptor absorbance. (d) pH-independent absorbance and fluorescence of the donor and pH-dependent absorbance of the acceptor in through-bond energy transfer cassettes-based pH indicators.

As discussed in the first chapter of this dissertation, the pH_i indicator **16,** a through-bond energy transfer cassette, consisting of a pH-dependent donor and a pH-independent acceptor, is able to overcome this issue. Excitation at 488 nm is always close to the absorbance maxima of the donor. However, compound **16** has two

drawbacks that limit its wide application for determination of intracellular pH values. First, the xanthene donor can be photobleached quickly in basic environment. Second, the quantum yield of the donor (0.14) in basic media is quenched by the PeT (See Chapter 1). The ideal pH indicators based on through-bond energy transfer cassette should have the following properties:

1. The donor exhibits a large molar absorptivity that is not pH-dependent.
2. The acceptor should be photostable, and its fluorescence spectrum should be significantly shifted with changing of pH.
3. The acceptor should have a high quantum yield despite of changing of pH.
4. The energy transfer efficiency should always be very efficient even the pHs of the solution is changed.
5. The compound should be water-soluble and have a handle to attach to biomolecules.

BODIPY dyes exhibit excellent photophysical properties, *e.g.* large molar absorptivity and high quantum yields, water-soluble sulfonated BODIPYs are also accessible, and are therefore the ideal donors for the cassettes. Figure S2a shows two typical cassettes having water-soluble BODIPY dyes as the donor. The pKa values of acceptors can be tuned by halogenation of the benzoxanthenes core. And more of the possible acceptor fragments based on benzoxanthene fluorophores are shown in Figure S2b.

a

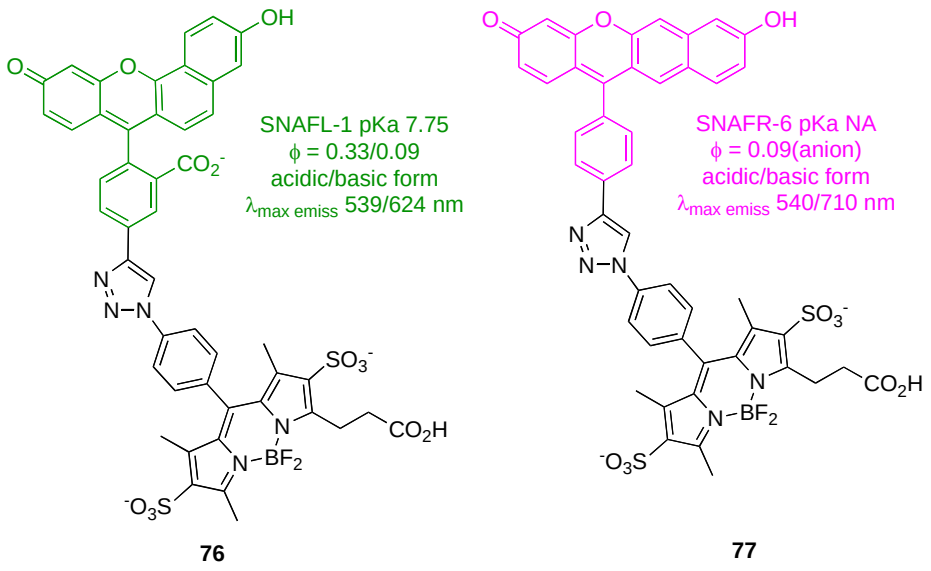

76 **77**

b

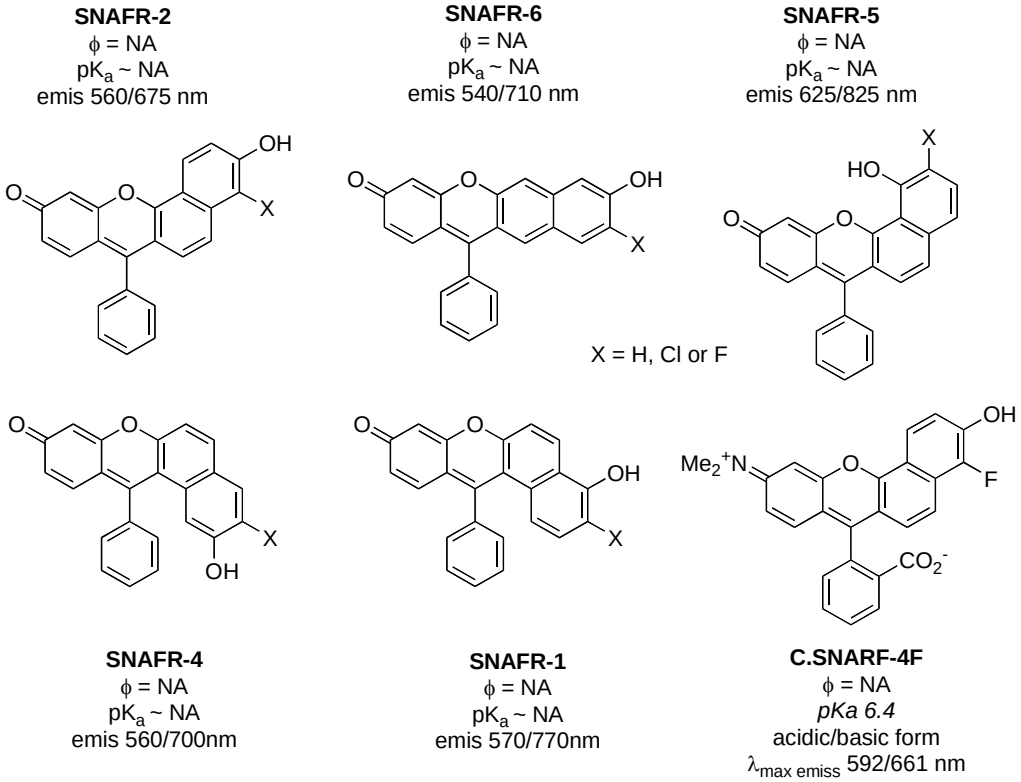

Figure S2. (a) Two typical pH-sensitive cassettes having a water-soluble BODIPY donor; (b) a few of pH-sensitive benzoxanthene acceptors.

All of the cassettes can be synthesized via Cu(I) catalyzed cyclization reaction of the water-soluble BODIPY azide **78** and the acceptor with a terminal alkyne group. Two methods can be used to construct the acceptors, and they are illustrated in Scheme S1b and S1c. First, the acceptor 5'-Br.SNFAL-1 **81** can be synthesized via condensation of 1,6-dihydroxynaphthalene **79** with the appropriately substituted benzophenone derivatives **80**; these in turn were made via coupling of resorcinol or 3-aminophenol with phthalic anhydride derivatives in toluene. Second, lithiated dimethoxynaphthalene **82** can react with a benzophenone derivative **83**, followed by cyclization with BBr_3, to afford 5'-Br.SNAFR-6 **84**. The final alkyne for the click chemistry can be achieved via Sonogashira coupling reaction of aromatic bromide, *e.g.* **81** and **84**, with trimetrylsilylacetylene, followed by removal of the trimethylsilyl group.

Scheme S1. (a) Synthesis of Cassettes via Click chemistry; Ilustrative syntheses of two acceptors (b) 5'-Br.SNAFL-1 **81**; and (c) 5'-Br.SNAFR-6 **84**.

a

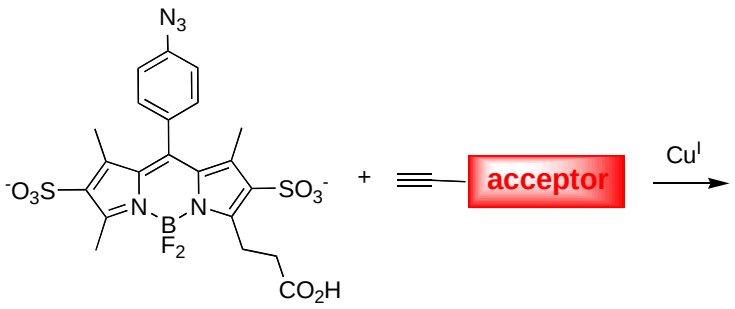

78

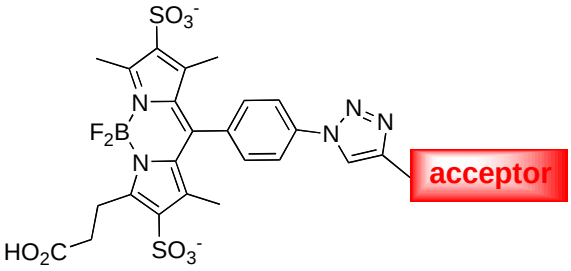

b

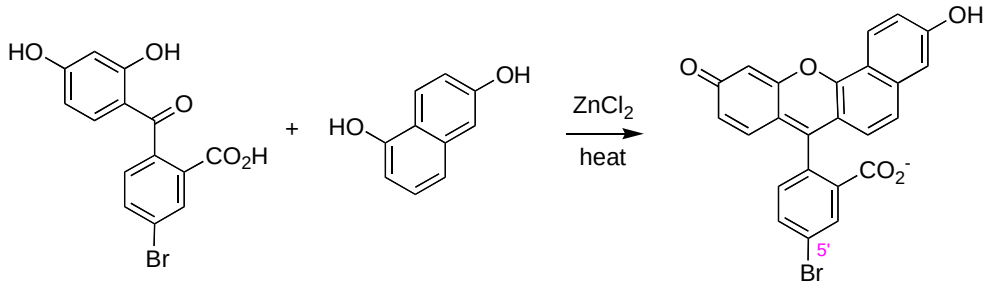

79 **80** **81**

Scheme S1. Continued.

c

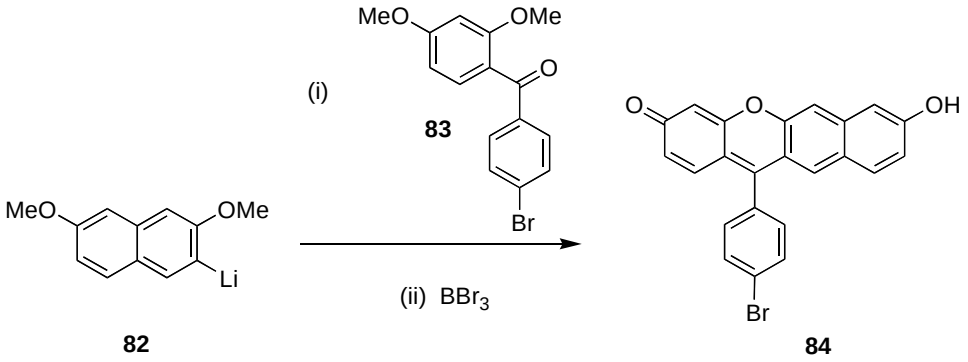

VITA

Name:		Junyan Han
Permanent Address:		Department of Chemistry Texas A&M University College Station, TX 77843-3255
Education:	August 2009	Ph.D., Chemistry Texas A&M University, College Station
	July 1998	B.S., Chemistry, Shandong University, Jinan, Shandong Province, P.R.China